MICELLES FOR OCULAR DRUG DELIVERY

By

Butsabarat Klahan

A dissertation submitted to South East Technological University in fulfilment of the requirements for the degree of Doctor of Philosophy

Prepared under the supervision of Dr. Niall O'Reilly, Prof. Anuj Chauhan, Prof. Hakon Hrafn Sigurdsson, Dr. Satu Mering, and Dr. Laurence Fitzhenry

Ocular Therapeutics Research Group
Pharmaceutical and Molecular Biotechnology Research Centre
Department of Science, South East Technological University Waterford

Submitted to SETU, July 2024

Declaration

I hereby declare that this thesis, which I now submit for assessment, is entirely my own work in fulfilment of the requirements of a Doctor of Philosophy degree. It is based on research carried out in the Department of Science, South East Technological University Waterford in Ireland, the Faculty of Pharmaceutical Sciences, University of Iceland in Iceland, the Department of Chemical and Biological Engineering, Colorado School of Mines in the US, and Experimentica Ltd., Kuopio in Finland.

Butsabarat Klahan

Date: 17/07/24

Acknowledgements

First and foremost, I would like to express my sincere thanks to all my supervisory teams, Larry, Niall, Hakon, Anuj, and Satu, for all their invaluable help, support, mentorship and constant encouragement throughout my PhD journey over the last four years in making this research project successful. I am most grateful to them for their teaching and advice, not only for research methodologies but also for other methodologies in life, which made me a stronger researcher every day. I would not have achieved this far, and this dissertation would not have been completed without the support I have received from them.

I want to give special thanks to my supervisors based in Ireland, both Larry and Niall, for allowing me to try doing several things in research and for their unwavering support throughout my PhD studies at Southeast Technological University (SETU) Waterford, Ireland. Moreover, I would like to express my very great appreciation to Hakon, Anuj, and Satu for a very warm welcome and help when I did the secondment in their countries (Iceland, the US and Finland). Many thanks for the collaboration. I would also like to thank Jenni from Experimentica Ltd. for her input into my project in Chapter 4 and her help with the cell experimental studies during my secondment in Finland.

I would like to extend my heartfelt thanks to my wonderful friends and colleagues, both Ocular Therapeutics Research Group (OTRG) and Pharmaceutical and Molecular Biotechnology Research Centre (PMBRC) research teams at SETU Waterford, for their support and the cherished time spent together in the lab and in social settings throughout the four years of my PhD journey in Ireland. I am especially thankful for all of the OTRG lab members. I appreciated their help, support, friendship, and always being together during my project time away from home.

Additionally, I would like to express my appreciation to all my Thai friends in Ireland for being my lovely friends outside of the lab, providing a listening ear and words of encouragement, and supporting me through thick and thin since I came to Ireland in 2019. Their friendship has been a source of strength and comfort. In addition, I would like to thank all Thai companies whom I met and spent time with during my secondment in each country. It was such a wonderful time. Thank you for all your company.

To my family in Thailand, I most gratefully acknowledge them for all their strong encouragement throughout the period of this PhD research. Thank you for your love and support of me both emotionally and financially throughout my academic journey in Ireland. I always knew that you believed in me and wanted the best for me. Moreover, I would like to thank you for another source of my happiness, my lovely boyfriend in Thailand, Seksung. Thank you for being the best boyfriend in my life, and for your endless love, patience, and support me despite the challenges of a long-distance relationship.

Finally, I extend my sincere appreciation to the European Union's Horizon 2020 research and innovation program under the Marie Sklodowska-Curie Actions (grant agreement-813440) (ORBITAL ITN) scholarship to give me this wonderful opportunity to proceed with my PhD program and support me. This funding has been invaluable in shaping my academic journey. Furthermore, instrumental support from the Department of Sciences (SETU Waterford), the Faculty of Pharmaceutical Sciences (University of Iceland), and Experimentica Ltd. (Finland) are also acknowledged.

With deepest appreciation

Butsabarat Klahan

Micelles for Ocular Drug Delivery

Abstract

Butsabarat Klahan

This research aimed to design polymeric micelles (PMs) that could induce the controlled release of small therapeutic drugs, curcumin (CUR) and fenofibrate (FEB), from the micellar formulation to treat diseases in the posterior segment of the eye.

The initial study evaluated the preparation of a PM system based on Pluronic F127 (PF127), which obtained a critical micelle concentration of approximately 0.21 %(w/v) (DI water) and 0.16 %(w/v) (PBS). Moreover, after CUR loading into the micelles, the study demonstrates that CUR/PF127 micelles prepared by thin-film hydration with a nanometer particle size range (46-78 nm, PDI~0.44-0.61) and negative zeta potential values exhibited a high CUR encapsulation efficiency (EE) of 97% at a 1:140 ratio of drug-to-polymer. The *ex vivo* permeation study revealed a 2.5-fold higher CUR retention in porcine cornea compared to the free CUR as a control group (8 ng/mg of tissue).

Consequently, the study explored the combination system between micelles and cyclodextrins (CDs) for ocular drug delivery of FEB. The Soluplus®/PF127/CD poly(pseudo)rotaxanes (PPRs), a type of molecular assembly in which polymer chains are threaded through the cavity of CDs with only non-covalent bonds, enhanced the water solubility of FEB (0.00034 mg/mL) up to 0.31 mg/mL, demonstrating the potential for increased drug bioavailability. In addition, an *ex vivo* permeation study demonstrated that FEB-loaded PPRs efficiently permeated through the porcine sclera, highlighting their potential to enhance drug absorption and permeation in ocular tissues.

A mathematical model was thereafter applied to explain the *ex vivo* permeation study of FEB-loaded micelles and PPRs, predicting drug delivery across scleral tissue. The calculation showed no significance in diffusivity values across the different FEB PPRs (1-15x10^{-3} cm^2/h), supporting PPR formulations to help FEB transportation across the porcine sclera. The study also investigated the use of PF127 micelles and chitosan as

positively charged micelles for FEB drug loading, resulting in bimodal particle size distributions (17-52 nm and 169-661 nm, PDIs~0.6-0.8) and low %EE (6-13% EE), indicating another potential nanocarriers for drug delivery.

Keywords: micelles; Pluronic F127; Pluronic F127/CH; curcumin micelles; cyclodextrins; fenofibrate micelles; poly(pseudo)rotaxanes

Table of Contents

List of abbreviations

2-HPβCD	2-hydroxypropyl-β-cyclodextrin
6-CF	6-carboxyfluorescein
AMD	Age-related macular degeneration
APA	Acid phosphatase colorimetric
APEG	Allyl polyethylene glycol
API	Active pharmaceutical ingredients
BLG	γ-benzyl-L-glutamate
BZ	Brinzolamide
CAC	Critical aggregation concentration
CD	Cyclodextrin
CE	Complexation efficiency
CG	Cow ghee
CH	Chitosan
CMC	Critical micelle concentration
CMCE	Carboxylmethyl cellulose
CMD	Consolidated micellar dispersion
CMT	Critical micelle temperature
Cou6	Coumarin-6
CsA	Cyclosporine A
CSO-SA	Chitosan oligosaccharide-stearic acid
Ctf	Centrifugation speed
CU	Ultracentrifugation
CUR	Curcumin
CVS	Chitosan oligosaccharide-valylvaline-steric acid
CXB	Celecoxib
D	Diffusivity
D-Dex	Dendrimer-cyanine 5 conjugated dexamethasone
DAF	5-dodecanoylaminofluorescein
DAPI	4’,6-diamidino-2-phenylindole

DCM	Dichloromethane
DDS	Drug delivery system
DEX	Dexamethasone
DI	Deionized
DIC	Diclofenac
DL	Drug loading
DLS	Dynamic light scattering
DMF	Dimethylformamide
DMβCD	Dimethyl-β-cyclodextrin
DOX	Doxorubicin
DR	Diabetic retinopathy
DSC	Differential scanning calorimetry
DSC	Differential scanning calorimetry
EE	Encapsulation efficiency
Evr	Everolimus
FA	Fluocinolone acetonide
FEB	Fenofibrate
FT-IR	Fourier transform infrared
GX	Gatifloxacin
HCE-T	Human corneal epithelial
HPLC	High-performance liquid chromatography
HPMC	Hydroxypropyl methylcellulose
HPγCD	Hydroxypropyl γ-cyclodextrin
IM-HCEpi	Immortalized human corneal epithelial
Int%	Intensity percentage of the particle size distribution
IOP	Intraocular pressure
IR	Infrared spectroscopy
IVT	Intravitreal
LDH	Lactate dehydrogenase
LOD	Limit of detection

LOQ	Limit of quantification
ME	Microemulsion
MET	Molecular envelope technology
mPEG	Methoxy polyethylene glycol
MS	Microsphere
NCA	N-carboxyanhydride
NE	Nanoemulsion
NIPAM	*N*-isopropylacrylamide
NP	Nanoparticle
OcDD	Ocular drug delivery
P19	Pluripotent
P_{app}	Apparent permeability coefficient
PBS	Phosphate buffered saline
PC12	Rat pheochromocytoma
PCL	Polycaprolactone
PDI	Polydispersity index
PEG	Polyethylene glycol
PEO	Poly(ethylene oxide)
PF103	Pluronic P103
PF127	Pluronic F127
PG	Progesterone
PIGF	Placental growth factors
PIC	Polyion complex
PLA	Poly(lactic acid)
PLGA	Poly (lactic-co-glycolic) acid
PM	Polymeric micelle
PPARα	Peroxisome proliferator activated receptor α
PPO	Poly(propylene oxide)
PPR	Poly(pseudo)rotaxane
PQ	Paraquat

PSED	Posterior segment eye disease
Pt	Pterostilbene
Pt	Pterostilbene
PTFE	Polytetrafluoroethylene
PTX	Paclitaxel
PVA	Polyvinyl alcohol
PVP	Polyvinylpyrrolidone
RA	Rebaudioside A
Rh	Tetramethylrhodamine-5-carbonyl azide
Rho-B	Rhodamine B
ROS	Reactive oxygen species
RP-HPLC	Reversed-phase high-performance liquid chromatography
RPE	Retinal pigment epithelium
SASP	Salazosulfapyridine
SBECD	Sulfobutylether β-cyclodextrin
SC	Subconjunctival
SCL	Soft contact lense
SD	Standard deviation
SDS	Sodium dodecyl sulfate
SEM	Scanning electron microscope
SN	Sonication
TA	Triamcinolone acetonide
TAC	Tacrolimus
TEM	Transmission electron microscopy
TPGS	D-α-tocopheryl polyethylene glycol succinate
TQ	Thymoquinone
VEGF	Vascular endothelial growth factors
Vol%	Volume percentage of the particle size distribution
VV	Valylvaline
XRD	X-ray powder diffraction

ZP	Zeta potential
α-CD	α-cyclodextrin
β-CD	β-cyclodextrin
γ-CD	γ-cyclodextrin

Chapter 1

Introduction

1.1 Global trends in blindness and vision impairment

The majority of information humans obtain from the environment depends on the ability to see. Therefore, loss of sight affects not only activities in everyday life but also reduces the quality of life. As such, scientists and medical professionals exert a continued effort to minimize the impact of conditions that can affect vision. The plot in Figure 1.1, measured in millions of people affected, illustrates the estimated number of people from 1990 to 2050 who have moderate or severe vision impairment and blindness.[1]

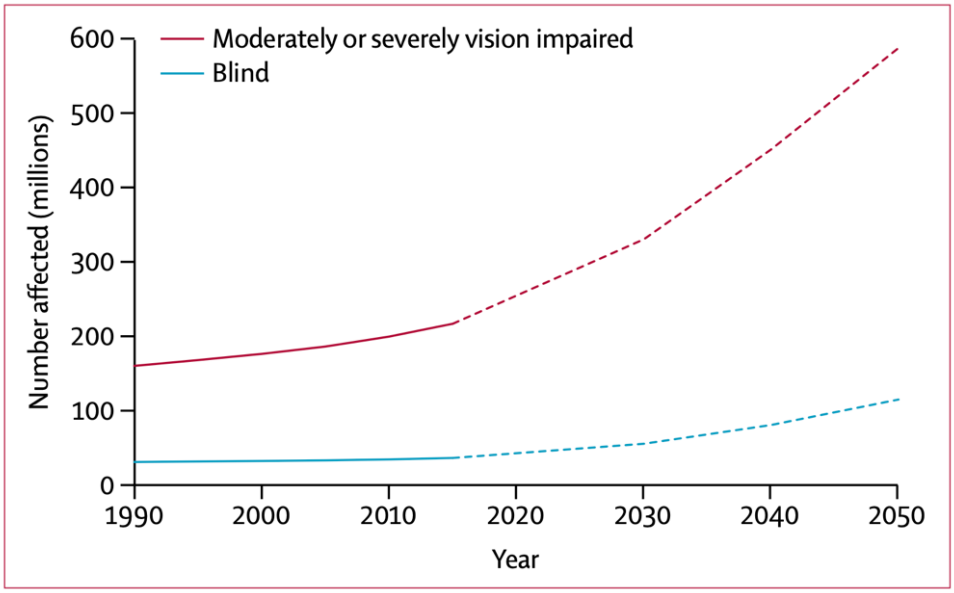

Figure 1.1: Global trends and predictions of the number of people who are blind or moderately and severely vision impaired from 1990 to 2050.[1]

The statistical review, as shown in Figure 1.1, suggests that the trend of both problems has increased over the period from 1990 to 2024. Specifically, in 2024, the total number of people visually impaired in the world was over 250 million, with around 40 million

blind and 280 million having moderate to severe vision impairment.[2] Furthermore, these numbers are expected to continue to rise up to the year 2050, in part owing to global population growth and a rapidly ageing population. Such statistics highlight the impact of blindness and visual impairment throughout the world.

To demonstrate the complexity of the eye, Figure 1.2 shows the main components of this organ. This schematic depicts both the front (anterior segment) and the back (posterior segment) of the eye and will be used as a reference for the following sections.

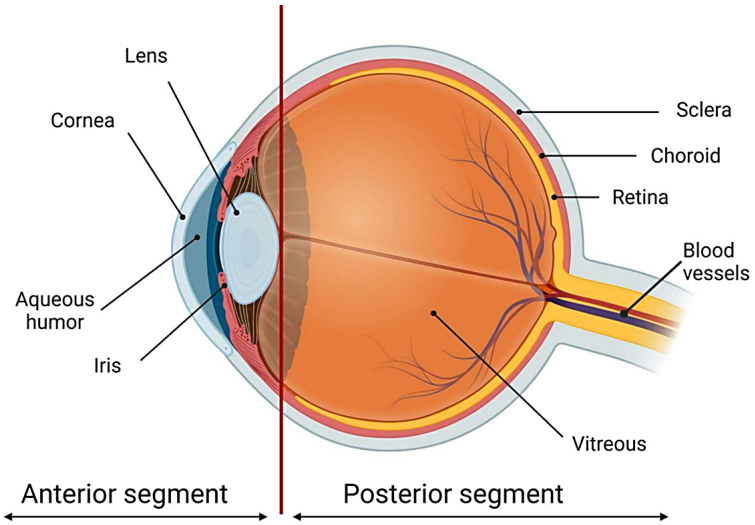

Figure 1.2: Schematic diagram of the anatomy of the eye in the anterior and posterior segments.[3]

As shown in Figure 1.2, the eyeball is composed of three basic layers. The sclera and cornea are on the outside, the retina is on the inside, and the uvea, which is composed of the iris, ciliary body, and choroid, is in between.[4] As depicted (Figure 1.2), the anterior mainly consists of light focusing elements, such as the cornea, the iris, and the lens, as well as the aqueous humor and conjunctiva. Whereas the posterior contains the retina, the optic nerves, the vitreous humor, the choroid, and the sclera.[5]

1.2 Diseases of the eye

As previously mentioned, the impact of vision loss and blindness on people worldwide leads to significant studies of the eye diseases and conditions that cause those problems.

Substantial numbers of both anterior and posterior eye disorders exist, which has led to different disease treatment strategies for both parts of the eye.[6–9]

1.2.1 Anterior segment diseases of the eye

Regarding the anterior segment or the front of the eye, several common diseases affect this part, including cataracts, uveitis, conjunctivitis, iris nodules, and dry eye disease.[6] Dry eye disease is one of the most common diseases affecting the anterior part of the eye, affecting 350 to 700 million people worldwide.[10] Figure 1.3 presents some factors involved and some signs of dry eye disease.

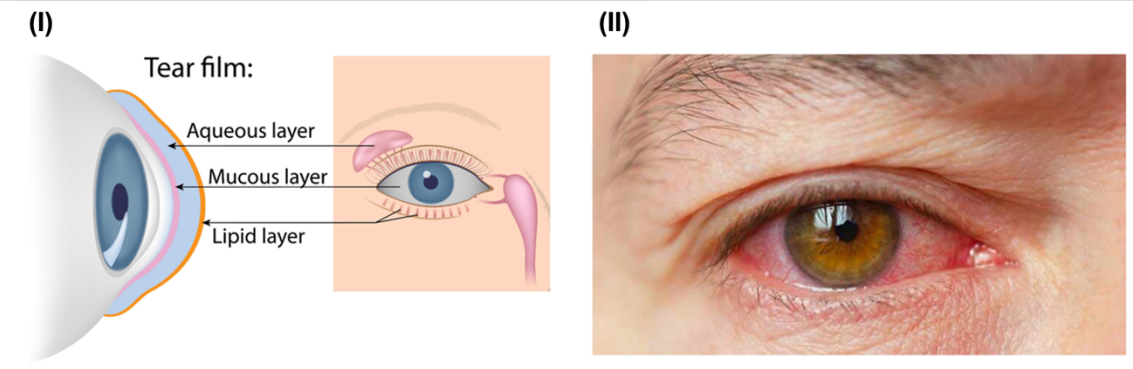

Figure 1.3: An illustration of (I) the structure of the tear film and (II) an example of the physical impact of dry eyes.[11,12]

Dry eye is caused by a lack of adequate tears to lubricate the surface of the eye (Figure 1.3(I)). Basically, tears are composed of water, fatty oils, and mucus that combined, make the surface of the eye smooth and clear.[10] If there is an imbalance in tear composition, it can lead to redness, burning, and stinging and can result in blurred vision for patients (Figure 1.3(II)).[13] In terms of dry eye treatment, topical administration in the form of eye drops is considered a primary therapy for dry eye, as this strategy both increases aqueous tear volume on the eye surface and keeps the eye surface moist.[14]

Cataracts are another important cause of low vision in people in the world, mostly the elderly.[15] They are a type of anterior segment eye disease affecting the lens, which is responsible for refracting light to be focused on the retina.[16] The effect of the cataract on

the eye and the comparison of the sight between people with normal vision and people who have cataracts are shown in Figure 1.4.

Figure 1.4: An illustration of (I) the effect of cataracts on the appearance of the eye in people who have cataracts, a comparison between (II) people with normal vision, and (III) the effect on the vision of people living with cataracts.[17]

The cataract occurs owing to the gradual accumulation of the molecular modification of the crystalline lens, which contains a protein inside the lens.[16] Since the proteins in the crystalline lens break down, the lens can no longer maintain the protein or chemical process that keeps the lens transparent. As a result, the lens starts to create a cloudy or opaque area (Figure 1.4(I)), which leads to blurred vision in the eyes of people who have cataracts (Figure 1.4(III)) compared to people with normal vision (Figure 1.4(II)).

1.2.2 Posterior segment diseases of the eye

There are also many prominent diseases affecting the posterior segment or the back of the eye, such as diabetic macular oedema (DME),[18] diabetic retinopathy (DR),[19] and age-related macular degeneration (AMD).[5]

1.2.2.1 Diabetic retinopathies

Diabetic retinopathy (DR) is an eye disease that impacts vision loss in approximately 35% of people who have diabetes. The longer the patient has diabetes, the more likely it is that they can develop DR since high blood sugar levels cause DR. Currently, DR is a significant cause of vision impairment. Globally, 451 million people were living with DR in 2017 and this number is expected to reach 693 million by 2045.[20–22] A comparison

between people with full vision and the vision of those living with DR is shown in Figure 1.5.

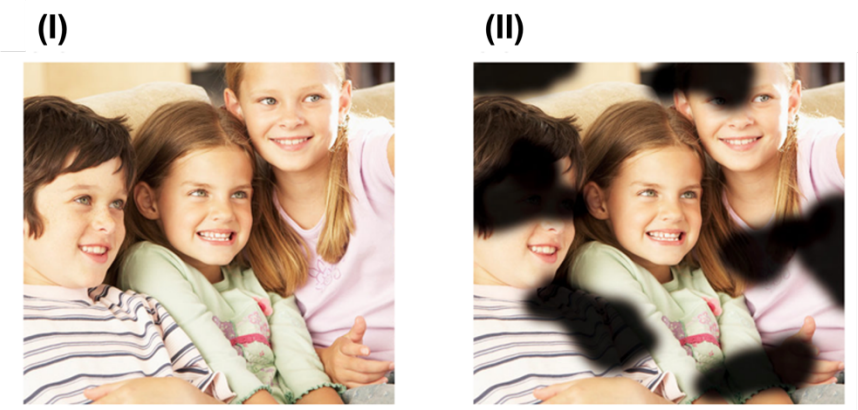

Figure 1.5: An illustration of a comparison of (I) full vision and (II) vision with DR.[23,24]

DR is caused by damage to the blood vessels of the light-sensitive tissue at the retina due to an excess amount of sugar level in the blood. It thereafter results in blurred vision of patients. People who live with DR notice symptoms such as seeing an increasing number of floaters and seeing black or dark areas in their field of vision (Figure 1.5(III)).

To overcome this problem, innovative drug development strategies are essential for protecting against sight loss. There are several intraocular treatment strategies for DR at present, such as laser photocoagulation, intravitreal injections of anti-vascular endothelial growth factor (VEGF) and steroid agents, and vitreoretinal surgery.[19,25]

1.2.2.2 Age-related macular degeneration

Age-related macular degeneration (AMD) is another eye disease that can cause blindness, mostly in elderly populations. Figure 1.6 shows an example of vision loss in people living with AMD.

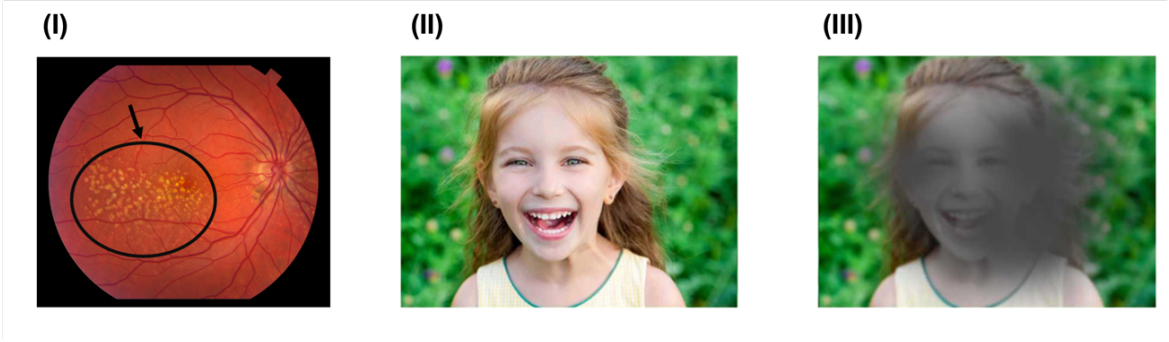

Figure 1.6: An illustration of (I) drusen in dry AMD and to present a visualization of the difference in sight between (II) people with normal vision and (III) people living with AMD in the centre point.[26–28]

AMD is an abnormality of the retinal pigment epithelium (RPE) that affects the photoreceptor in the macula. This is the part of the retina responsible for clear vision, and as such, this results in the loss of the central vision of people who have AMD (Figure 1.6 (I)).[29] A comparison of the ability to see straight ahead between people with full vision and people with vision loss from AMD is demonstrated in Figure 1.6. People with full vision can see clearly in the central part of their visual fields, whereas people living with AMD are affected by an accumulation of small dark spots at the central vision due to damaged macular, resulting in blurry central vision (Figure 1.6(III)). In comparison, the side or peripheral vision remains unaffected.

Conventionally, there are two types of AMD: dry macular degeneration (dry AMD) and wet macular degeneration (wet AMD).[30] Dry AMD is caused by an abnormality of blood vessels that leak fluid or blood into the macula and make the macula swell, leading to the destruction of central vision, whereas wet AMD is a chronic, progressive degeneration of the macula that causes severe loss of vision. Moreover, dry AMD is responsible for the majority of cases of severe vision loss in patients with AMD. Specifically, dry AMD occupies about 90% of the total cases of AMD, while only 10-20% of severe vision loss in patients with AMD comes from wet AMD.[31] Although there is no treatment to prevent AMD at present, there are many clinical trials in progress. Furthermore, there are some treatments available for people with wet AMD. The most common treatment doctors use to slow vision loss from wet AMD is the use of anti-VEGF injections.

1.2.3 Ophthalmic drugs for diabetic retinopathy and age-related macular degeneration treatments

There is a wide variety of anti-VEGF agents that have proven effective for the management of DR and wet AMD, as summarized in Table 1.1.

Table 1.1: Properties of ophthalmic therapeutic agents intended for the management of posterior segment eye diseases (PSEDs). Anti-VEGF agents for the treatment of *AMD and **DR.

Drugs	mw	Route of administration and dosage regimen	Mechanism of action	Reported side effects
Bevacizumab (Avastin®)*, **	149 kDa	IVT, 1.25 mg every 4 weeks[32]	Block all VEGF-A isoforms from binding to endothelial cell receptors (VEGFR-1 and VEGFR-2), thereby decreasing VEGF activity, inhibiting angiogenesis[33]	Blurred vision, vitreous floaters, and swelling of the cornea[32]
Ranibizumab (Lucentis®)*, **	48 kDa	IVT, 0.3 or 0.5 mg every 4 weeks[34]	Inhibit all VEGF-A isoforms from binding to endothelial cell receptors, thereby reducing the growth of VEGF and neovascularization[35]	Endophthalmitis, vitreous floaters, and eye pain[34]
Aflibercept (Eylea®)*, **	115 kDa	IVT, 2 mg at weeks 0, 4, and 8 then every 8 weeks[36]	Bind to VEGF-A, VEGF-B, and PIGF to protect them from binding to endothelial cell receptors, thereby preventing endothelial proliferation, vascular permeability[37]	Conjunctival hemorrhage, eye pain, vitreous detachment and floaters, and ocular hypertension[36]
Brolucizumab (Beovu®)*, **	26 kDa	IVT, 6 mg every 12 weeks[38]	Bind specifically to VEGF-A to block its from binding to endothelial cell receptors, thereby blocking from neovascularization and vascular leakage[38,39]	Blurred vision, cataract, conjunctival hemorrhage, vitreous floaters, and eye pain[38,40,41]
Conbercept (Lumitin®)*, **	142 kDa	IVT, 0.5 mg at weeks 1, 4, 12 and 24[42]	Bind VEGF-A, VEGF-B, and PIGF to protect them from binding to endothelial cell receptors, thereby suppressing vascular leakage[43]	Eye pain, intraocular pressure, and conjunctival haemorrhage[43,44]
Curcumin Supplement	368.38 g/mol	Oral administration, 500-2000 mg twice a day[45]	-Has antioxidant property that scavenges reactive oxygen species (ROS) and reduces oxidative stress, which can protect retinal cells from oxidative damage -Inhibit proinflammatory cytokines and mediators (e.g., TNF-α, IL-6, and COX-2), thereby reducing inflammatory effect and helping to protect renical celles from damage[46]	A pigmented compound, low solubility and poor bioavailability of drug[46,47]
Fenofibrate (Tricor®)	360.83 g/mol	Oral administration, 48-160 mg once a day[48]	Activate PPAR-α, thus leading to : -A decrease in the production of pro-inflammatory cytokinases (e.g., TNF-α and IL-6) that causes a promotion of VEGF expression in the retina -A decrease in triglycerides and LDL cholesterol levels which causes DR[49]	The low solubility of drug and clearance from the vitreous[50]

*VEGF-Vascular Endothelial Growth Factors: a signalling protein involved in the formation of new blood vessels (angiogenesis), PIGF-Placental Growth Factors: a member of VEGF family involved in promoting the growth of new blood vessel, IVT-Intravitreal, PPAR-α-Peroxisome proliferator activated receptor α: a transcription factor that is involved in lipid metabolism, COX-2-cyclooxygenase-2, TNF-α-tumor necrosis factor-α, IL-6-interleukin-6.

Anti-VEGF treatments such as bevacizumab, ranibizumab, and aflibercept can prevent the growth of aberrant arteries caused by VEGF, which is present in wet AMD or DR. Therefore, the development and use of anti-VEGF medication have been extensively researched.

Bevacizumab, a full-length recombinant humanized antibody, was first investigated as a systemic intravenous injection for cancer treatment and then as an intravitreal (IVT) injection for wet AMD.[32] A study focusing on IVT injections of bevacizumab to 79 patients who had subfoveal neovascular AMD illustrated that no significant ocular or systemic side effects were observed at 1 month (1.25 mg dose of bevacizumab), and more than 55% of those patients had a reduction in baseline retinal thickness after one week of injection. Regarding aflibercept, a dimeric glycoprotein, several scholars have pointed out that a 2 mg dose of aflibercept via IVT injections monthly or every 2 months displayed similar efficacy and safety outcomes as a 0.5 mg monthly dose of ranibizumab.[36] Moreover, most of the clinical research on ranibizumab, a recombinant humanized monoclonal antibody fragment, suggests the effectiveness of IVT ranibizumab for treating eye disease is similar to bevacizumab and aflibercept. Ranibizumab 0.5 mg IVT injection enhances visual acuity (34%) of people who have neovascular AMD (n=176).[34] Nowadays, numerous scholars have turned their attention to finding new and longer lasting drugs for treating patients with wet AMD instead of bevacizumab, aflibercept, and ranibizumab, described above, which need to be injected in the eye every 4-8 weeks. Hence, recent studies have explored the use of brolucizumab and conbercept, the novel FDA approved anti-VEGF agents, for the treatment of AMD and DR, as these drugs could help reduction in eye damage associated with a number of injections (Table 1.1). Brolucizumab is a humanized single-chain antibody fragment, which is the smallest functional unit of an antibody. This allows its delivery in a greater molar dose compared

to large molecules. Additionally, it can prolong the duration of action due to more effective tissue penetration of the small molecule drug.[40,51,52] In addition, brolucizumab offers both greater fluid resolution, a longer duration of therapeutic action vs aflibercept, and the ability to maintain eligible wet AMD patients on a three-month dosing interval immediately after a three-month loading phase, leading to patient care improvement in wet AMD.[38,51] A laboratory-based study comparing brolucizumab and aflibercept for neovascular AMD found that brolucizumab was not inferior in mean best corrected visual acuity change and central subfield thickness reductions compared to aflibercept.[38] In another study, by Pravin *et al*. it was revealed that brolucizumab showed better fluid control and resolution in the retina compared to aflibercept at week 40.[51] Furthermore, a number of studies on conbercept (Table 1.1), a recombinant fusion protein, have also shown promise for the drug's ability to treat neovascular AMD since conbercept has a higher binding affinity of a ligand to VEGF-A (Kd=0.5 pM) than ranibizumab and bevacizumab, resulting in greater bimolecular interactions between the target molecule and the ligand.[43,53] Besides, the IVT half-life of conbercept in the vitreous (4.2 days) is longer than ranibizumab (2.9 days), which can lead to a more effective inhibitory effect against VEGF.[54–57] Gao *et al*. found that intravitreal conbercept injection reduces central retinal thickness in patients with exudative AMD.[56] Similarly, Bai *et al.* found that 83.3% of eyes experienced disease regression after receiving intravitreal conbercept injection once, indicating its effectiveness for retinopathy of prematurity.[57]

In addition, the last few years have seen an increased interest in developing nanocarriers for ocular drug delivery (OcDD) to address posterior segment eye diseases (PSEDs), including those for delivery of curcumin (CUR) and fenofibrate (FEB). CUR is an antioxidant that displays a wide range of physiological and pharmaceutical properties, such as antioxidant, anti-inflammatory, and anti-VEGF properties.[46] In terms of ophthalmology, CUR could treat some forms of retinopathy by inhibiting the expression of VEGF in rats.[47] Moreover, it inhibits the proliferation of human lens epithelial cells, protects retinal cells, suppresses oxidative stress, inflammation and angiogenesis formation, resulting in VEGF reduction.[46] For example, Kim *et al*. investigated the antioxidant protectant efficacy of rosmarin and CUR in the retinal epithelial cells by

forming nanospheres with bovine serum albumin (BSA).[58] They found that antioxidant-containing nanoformulations (~30-50 μM of drug) provided a higher drug solubility and decreased reactive oxygen species (ROS) production in the retinal epithelial cell. Fenofibrate, a fibric acid derivatives, can be used for treating DR and AMD due to its antiangiogenic and anti-inflammatory activities.[50,59] In addition, FEB displays some advantages over anti-VEGF agents, such as low cost, fewer side effects, and neuroprotective effects.[50] Rats were given FEB (50 mg/kg) for 6 h after brain injury and then neurological assessment was examined at 24 h. The results showed that FEB promoted neurological recovery by reducing matrix metalloproteinase-9, cyclooxygenase-2, and VEGF-caused traumatic brain injury, including a decrease in oxidative stress.[50]

Therefore, these results, as mentioned previously, indicate the efficacy of ophthalmic therapeutic agents as novel VEGF inhibitors for the treatment of PSEDs, especially AMD and DR, due to their longer duration of action and reduced need for injections.

1.3 Routes of ocular drug administration

A wide range of drug administration routes have been developed to treat conditions such as those discussed in the preceding sections. Figure 1.7 presents a schematic of various drug delivery routes for treating ocular diseases.

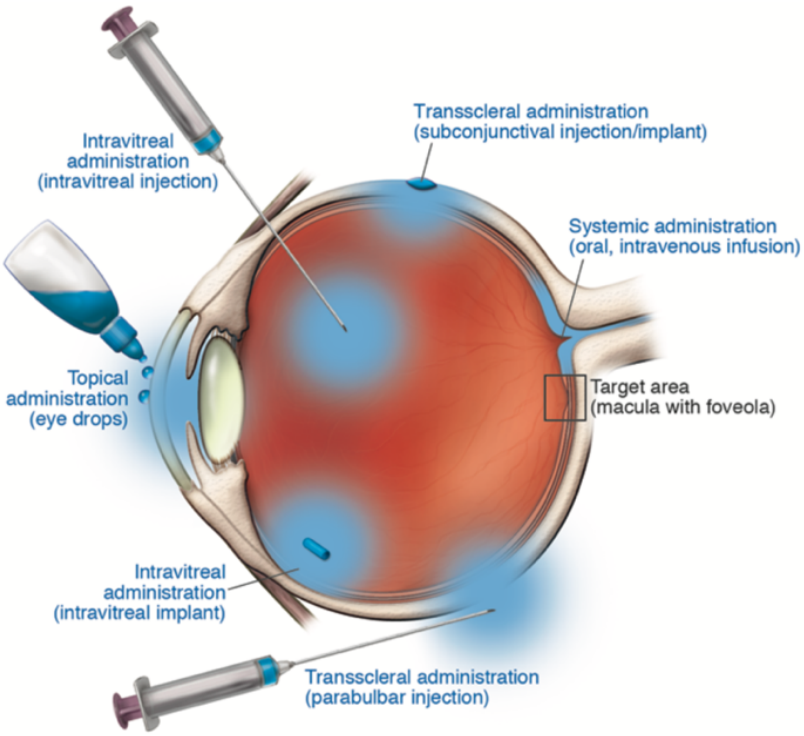

Figure 1.7: Method of ocular drug administration and delivery routes to both anterior and posterior eye segments.[60]

As shown in Figure 1.7, the primary route for drug delivery for the anterior segment is topical administration. In this technique, drugs can be administered topically to the surface of the eye in the form of eye drops, gels and ointments. Additionally, transscleral administration (subconjunctival and parabulbar injections) are another method used for both anterior and posterior ocular treatment. For these methods, drugs are administered by injection underneath the conjunctiva to the target area. In addition, in terms of posterior segment, IVT injection is the most commonly used as a clinical option in the treatment of posterior segment diseases. Specifically, drugs are injected directly into the vitreous humor for the IVT route.[61] Finally, systemic administration can also be used for drug delivery in the posterior segment by oral or intravenous infusion.[62]

Nevertheless, ophthalmic drug administration has presented a major challenge to scientists and clinicians alike, owing to the intricate, unique anatomical and physiological barriers in the eye.[61] Static barriers to drug transport include different eye sections such

as the cornea, sclera, retina, and blood retinal barriers. Furthermore, dynamic barriers include choroidal and conjunctival blood flow, tear dilution, and lymphatic clearance.[63] All of these barriers diminish drug absorption through the ocular tissues before reaching the target site, especially the posterior segment of the eye.[64,65]

Hence, each route of drug administration presents different barriers that act as a permeation membrane, allowing only molecules with certain characteristics to pass through by diffusion.

1.3.1 Topical administration

In terms of topical administration, this mode of drug delivery is used to treat anterior segment diseases affecting the ocular surface, such as dry eye disease or infections. Additionally, this route is characterized by applying the drug product to the ocular surface, where it mixes with the lacrimal fluid. Hence, in order to treat dry eyes by targeting the ocular surface, the drug needs to be kept within the site of action or absorbed by the cornea or conjunctiva for the treatment of dry eye disease.[66] Furthermore, in the case of intraocular target tissues, such as the iris or ciliary body, the drug must permeate across the cornea and/or conjunctiva to reach these tissues in the aqueous humor.[67] The main barrier of the topical route is the cornea, as shown in Figure 1.8

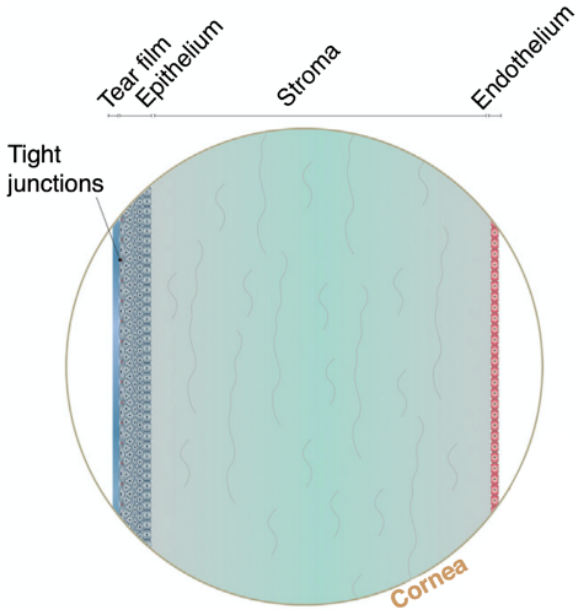

Figure 1.8: Cross section of the barrier for drug penetration after topical installation.[68]

Basically, the cornea consists of three main layers, including the epithelium, stroma, and endothelium, in which each layer presents a different characteristic for drug permeation (Figure 1.8).[67] The corneal epithelium is lipophilic in nature, which leads to the limitation of the permeation of hydrophilic molecules, whereas the corneal stroma acts as a permeability barrier to lipophilic drug molecules. Specifically, the innermost layer of the cornea is the corneal endothelium, which is a monolayer of hexagonal endothelial cells that adjust water influx into the cornea and act as a barrier between the cornea and aqueous humor.[69,70] Apart from that, other factors, such as dosage spill-over, nasolacrimal drainage, blinking, tear film, and tear mucin, as well as low corneal permeability, all lead to unsuccessful transportation of drugs to the target site in the eye.[63,71,72]

In the case of eye drops, for example, once the drops are administered to the ocular surface, they are suddenly diluted by an ocular tear film. Healthy eyes with a tear volume of 7-10 μL have a turnover rate of the administered eye drop around 0.5-2.2 μL/min, and excess volume spills over the eyelids and cheek by blinking or drains into the nasolacrimal duct.[73] As a result, only a small percentage (<10%) of the applied dose can reach ocular tissues, leading to frequent administration to achieve the desired therapeutic effect. For instance, Timolol eye drops should be administered with a recommended dosage of 0.25 %(w/v) solution twice daily, to achieve the desired therapeutic effect.[74] Furthermore, it creates issues for patient compliance and has a negative impact on therapeutic efficacy in terms of disease control.[61]

In conclusion, although there are various strategies to extend the duration of cornea contact time, such as adding viscosity enhancing polymer and gelling agents to the eye drops for slow elimination from the eye structure, these formulations still affect patient sight with blurred vision due to unclear solution, and matted eyelids, and have a frequent dose requirement.[75–78] Therefore, the topical routes still face several problems that limit their success in achieving the desired drug concentrations at the target tissue and do not typically result in effective concentrations in the posterior segment. In other words, the ocular barriers such as the cornea, sclera and blood-aqueous barriers could restrict the penetration of the drugs administered topically to the deeper layers of the eye.[72,79,80]

1.3.2 Subconjunctival administration

Subconjunctival (SC) injection is a type of periocular injection for OcDD. In terms of injection route, current formulations for the SC injection are in the form of solutions or suspension, and the injection can be given under the conjunctival membrane, which is the transparent tissue covering the sclera (Figure 1.7). Several SC barriers for OcDD are illustrated in Figure 1.9.

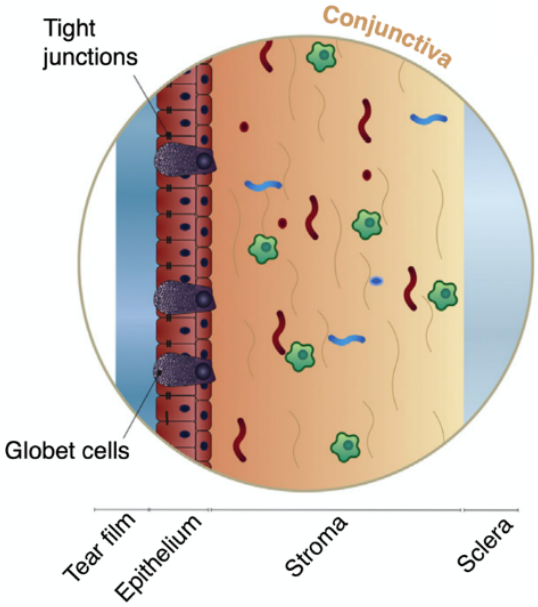

Figure 1.9: Cross section of the conjunctival barriers in ocular drug delivery.[68]

Conventionally, the SC route can be used to deliver drugs to both anterior and posterior segments of the eye.[72] In terms of anterior segment drug delivery, part of the subconjunctivally injected drug distributes from the SC space across the sclera deeper into the eye. SC injection presents an advantage over the topical route by providing higher drug bioavailability in the aqueous humor because injection underneath the conjunctiva allows small molecule drugs to bypass the epithelium, which is one of the main barriers limiting drug entry (Figure 1.9).[65,66,68]

For the treatment of PSEDs, drug injection by this method can bypass the sclera as the posterior part of the eye without penetration into the conjunctiva, which is a significant rate-limiting barrier for water-soluble drugs (Figure 1.9).[81,82]

On account of substantial barriers, as previously mentioned, high drug clearance from the choroid and retina is a major problem for drug bioavailability in the system.[82,83] For example, retinal bioavailability after SC injection is very low, with as little as 0.1% of the total amount of drug injected accessing the target site due to several barriers between the injection site and retina, resulting in more frequent dosing. Therefore, it indicates that the SC route is a mode of OcDD more suitable for the treatment of anterior segment eye diseases.

Different approaches have been developed to enhance the penetration of drugs injected through the route into the sclera for PSED treatments.[84,85] One such technique is transscleral iontophoresis, a non-invasive method that uses a low electric current to enhance the penetration of pharmaceutical compounds across the sclera into the intraocular tissues. The pharmaceutical compounds can be ophthalmic drugs such as corticosteroids, antibiotics, non-steroidal anti-inflammatory drugs and immunosuppressants, as highlighted in the reviews by Myles *et al*.[86] Nevertheless, the procedure itself may cause discomfort or irritation to the eye, especially due to the presence of the electric current and the need for prolonged contact with the eye during drug delivery. Patients may experience side effects related to the iontophoresis process, such as irritation, redness, or burning in the eye.[86]

Thus, the SC routes are effective for delivering therapeutic agents to the eye, but several challenges, such as poor drug retention and infection risk, necessitate further research and innovation to improve efficacy and safety in SC administration.

1.3.3 Intravitreal administration

The limitations of both topical and SC administration often necessitate the adoption of invasive measures, including IVT injections, to clinically deliver medications to reach the posterior part of the eye.[68,72] In a statistical analysis studying clinical IVT injection treatment of 556 patients with AMD, those patients were treated in a total of 1524 injection cycles.[87] The result showed that there were 1418 successful cycles, which were not interrupted and did not result in side effects for patients. However, 106 injection cycles disturbed patients after treatment through many effects, such as decreased vision

in the injected eye, decreased vision in those patients, and irritation in the non-injected eye.

Relating to the IVT route, several forms, such as solution, suspension, or depot formulation, are directly injected into the vitreous humor, which then diffuses in various directions to the retina. Additionally, drug targets depend on the disease and drug type, as mentioned in Section 1.1. Currently, the most effective treatment for AMD disease is using this method.[25] Furthermore, this method of drug delivery presents advantages over the topical route. The IVT route not only sustains drug levels in the patient but also delivers the drug directly to the site of action in the posterior segment.[63,72] For example, anti-VEGF agents can reach the retina to treat AMD by permeation through only one barrier, the vitreous humor, instead of multiple barriers, as is the case for topical delivery (Figure 1.8).[88]

Although IVT injection presents substantial advantages in drug delivery to the posterior segment, there still remain some limitations to drug permeation to the back of the eye, including vitreous humor and retinal barriers, as illustrated in Figure 1.10.

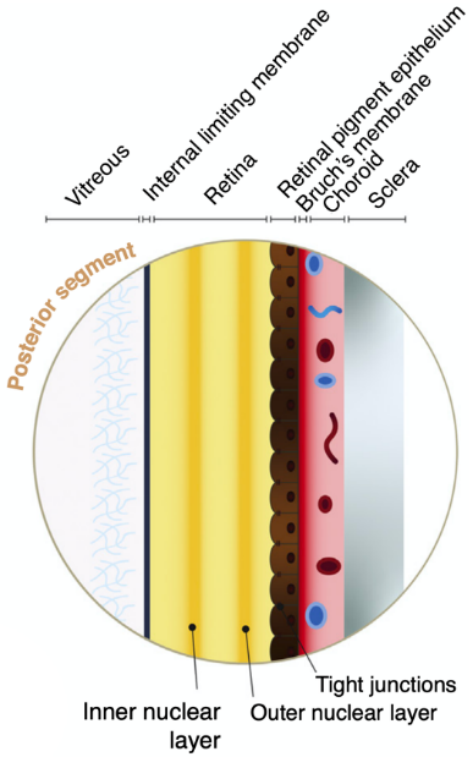

Figure 1.10: Schematic cross section of the barriers to drug penetration after IVT injection.[68]

Barriers to drug penetration in the eye following IVT injection can hinder the delivery of drugs to the posterior segment of the eyes (Figure 1.10). During IVT injection, drugs intended for transportation to the posterior segments of the eye must encounter several barriers such as vitreous humor, retinal layers and blood-retinal barriers to reach their to reach and treat the specific target sites in the back of the eye effectively.

One example of the barriers for IVT injection, presented in Figure 1.11, is the position of the vitreous humor in the eye (Figure 1.11(I)) and the composition within the vitreous humor (Figure 1.11(II)).

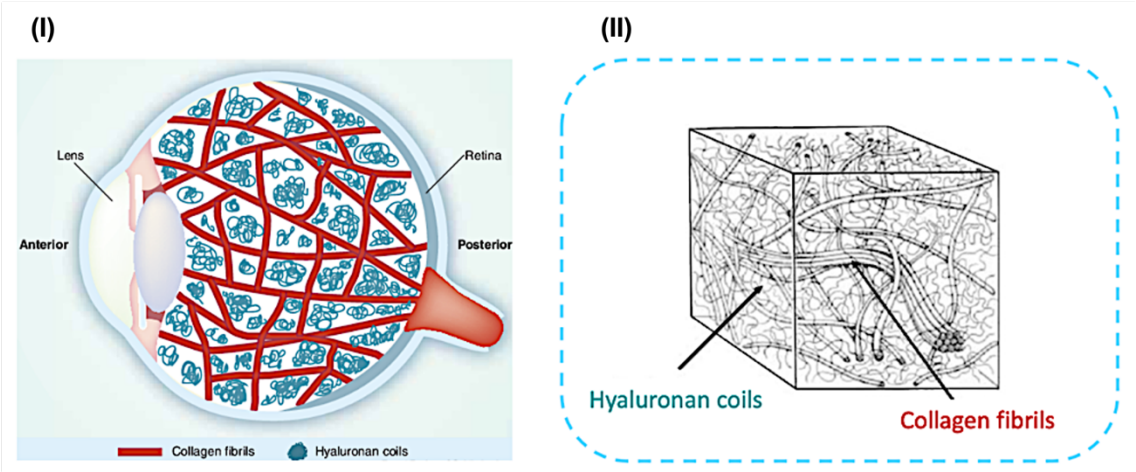

Figure 1.11: Schematic diagram of (I) the vitreous humor in the eye and (II) a picture of the cooperation between two networks of the gel structure inside the vitreous humor.[89]

The vitreous humor is an isotonic clear gel and contains collagen, hyaluronic acid, proteoglycans, and some hyalocyte cells (Figure 1.11(II)). For that reason, owing to the viscous gel in the vitreous humor, the diffusion of molecules from the vitreous humor to the retina is greatly limited. Both large and charged molecules are difficult to transport to the retina since the positive charge of the molecules can react with the negative charge of the gel structure in the vitreous humor (Figure 1.11(II)), resulting in aggregation of the molecules in the vitreous humor before reaching the retina.[90] Apart from that, other obstacles, such as the pathophysiological condition of diseases, the molecular weight of

administered drugs, also majorly impact the distribution of drug molecules in the vitreous humor to the retina.[91]

In clinical practice, as described previously in Table 1.1, IVT injections are injected directly into the vitreous cavity by a skilled specialist. As a consequence, it is important to consider the risks associated with this invasive procedure and take necessary precautions during the IVT administration.[92] These precautions include avoiding contact with the retina or lens, and making a small incision for the injection to minimize the risk of eye infections and vitreous hemorrhage in the patients. Furthermore, it is crucial to plan a follow-up visit between the patients and the expert for repeated IVT administration, especially for chronic diseases (DR and AMD), since this IVT repetition is the only alternative way to administer drugs (anti-VEGF, steroids and antibiotics) to treat diseases affecting the posterior segment of the eyes.[93]

1.3.4 Topical drug delivery to the posterior eye segment

The typical management of anterior as well as posterior eye diseases involves the use of local ophthalmic drug delivery. As mentioned above, the eye offers multiple potential entry routes through which ocular drugs may be delivered. Moreover, posterior segment delivery can be achieved in several ways, including topically, as per Section 1.3.1. Briefly, topical administration refers to the application of medication to the surface of the tear film of the eye, and this route is widely used for drug delivery to treat eye diseases in the anterior segment. Nonetheless, it remains a major challenge to deliver drugs topically for treating posterior segment diseases such as AMD and DR.[67] Therefore, a considerable amount of research has focused on using this mode of drug delivery to deliver drugs to the back of the eye. For these reasons, various ocular drug delivery strategies, namely nanoparticles and nanomicelles which will be described in Section 1.4.2, have been investigated, and several methods of ocular drug administration to posterior segments of the eye have been developed, as highlighted in the review literature by Wang *et al*.[94] Among the various ocular drug delivery routes, topical administration might be the best approach to overcoming several drawbacks since drugs can be administered noninvasively to the surface of the eye.[95,96] This overcomes substantial issues with drug administration via injections or implants, which are invasive approaches,

such as desegmentation of the implant, accidental injection into the crystalline lens, and migration of the implant into the anterior chamber.[97] In addition, most available topical ocular preparations are in the form of aqueous ophthalmic formulations.[98] Although topically applied drugs such as commercial eye drops are commonly used by patients due to their ease of usage, low interference with vision, and non-invasiveness, overusing eye drops in the long term can put your eye health at risk, leading to several drawbacks, namely eye redness, irritation, and dry eye. In some cases, this can cause glaucoma due to eye drops containing steroids, with consequent vision loss and blindness.[75,99] Thus, careful design of non-irritant and non-toxic topical ophthalmic preparations that do not interfere with long-term eye physiology is crucial.

In conclusion, as reported in several studies, novel routes for drug delivery that can bypass these barriers have been developed by researchers and tested by ophthalmologists.[100–103]Several novel approaches for topical drug absorption in the form of eye drops or suspensions of hydrogels, polymeric colloidal nanocarriers and cyclodextrin-based nanocarriers for OcDD will be presented in Section 1.4.2 to 1.4.4.

1.4 Emerging drug delivery systems for ocular routes

According to the routes of administration, types of disease, complexity of the structure, and nature of the eyes, as already pointed out in Sections 1.2 and 1.3, these aspects pose a challenge for drug delivery to formulation scientists. Therefore, innovative and new drug delivery systems (DDS) and devices have been investigated by many researchers over a long period of time to overcome the limitations associated with these parameters.[104–106] In this section, a brief account of the ideal drug release profiles will be given. After this, various novel strategies for drug delivery to both anterior and posterior eye segments will be presented.

1.4.1 Characteristics of an ideal drug delivery system

Taking into account the drug release profile, an ideal DDS should deliver the drug only to the target tissue and maintain a therapeutic concentration for a specified period of time.[72] Figure 1.12 shows the line graph of drug concentration over time in different release profiles.[107]

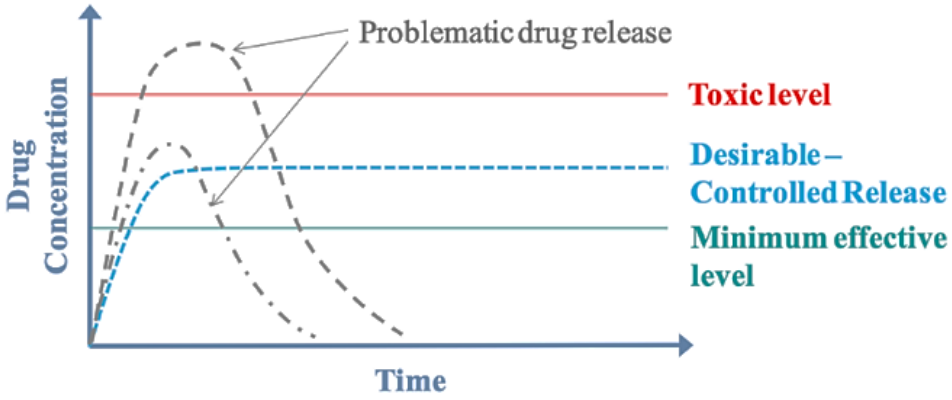

Figure 1.12: Release drug concentration over time. The red and green lines indicate the toxic and minimum effective levels of the drug, respectively. Whereas the blue and grey lines indicate a desirable-controlled release and two cases of problematic drug release, respectively.[107]

As illustrated in Figure 1.12, a key aspect in biomedical applications is the ability for sustained and controlled release of drug molecules over time, both below the toxic level and above the minimum effective level at the same time. Subrizi *et al.* highlighted that an appropriate OcDD system must be able to show the sustained release of the drug in the target tissues for a long time under suitable therapeutic drug concentrations.[68] Similarly, Mark *et al*. emphasized that the critical factors of DDS were to deliver the drug to the "right area, at the right time and the right concentration".[107] However, some limitations that affect drug release profiles are increasingly apparent. Rinda and colleagues mentioned that factors such as low drug solubility, environmental or enzymatic degradation, and inability to cross biological barriers lead to a decrease in drug delivery efficiency.[61]

For OcDD applications, many approaches have been successful in transporting drugs to the target site with a controlled release profile. These include contact lenses, nanocarriers, and hydrogels.[108–110] Ciolino *et al.* demonstrated that poly (lactic-co-glycolic) acid (PLGA)-co-poly (2-hydroxyethyl methacrylate) contact lens presented a prolonged and controlled drug release of ciprofloxacin for four weeks longer than topical eye drops.[108]

In terms of nanomedicine applications, in their review, Jo and coworkers state that nanocarriers such as nanoparticles, liposomes, and dendrimers were suitable for OcDD systems, as they prolonged residence time and controlled drug delivery at the ocular surface of the eye after installation, resulting in a reduction of the dose administered and installation frequency.[109] Also, the work of Zhaoliang *et al.* demonstrated a new formulation of a micellar supramolecular hydrogel, which is a novel class of 3D cross-linked polymer material developed by incorporating drug-loaded micelles within a self-assembled supramolecular network structure using noncovalent interactions. Thus, the presence of a 3D network in the supramolecular hydrogel (95% within 216 h) could provide a physical barrier that hinders the diffusion of drug-loaded micelles that could extend the release of diclofenac (DIC) longer than a micellar drug formulation (95% within 6 h).[110]

Thus, several controlled drug delivery strategies could benefit patients by maintaining the amount of drug at the target site for a long time, leading to a reduction in treatment frequency. As a result, it is of great importance to develop various controlled release systems for OcDD.

1.4.2 Hydrogels

Within the field of OcDD, several studies have shown that OcDD in the form of eye drops can show higher ocular biodistribution. However, approximately 75% of the total volume of the eye drops is lost from the precorneal area of the eye within 2-6 min after instillation owing to several factors such as blinking, nasolacrimal drainage, and systemic absorption by the conjunctiva.[111] Thus, hydrogel formulations have gained significant interest for effective OcDD to overcome these obstacles.

Hydrogels are a network of monomers and multifunctional linkers that react to form flexible, water-laden structures. The network formation is achieved with hydrophilic monomers that would be solubilized in a non-crosslinked form. Importantly, crosslinkers are the compounds that make the overall hydrogel structure insoluble and retain a high water capacity.[112] Furthermore, the three-dimensional network makes hydrogels capable of absorbing large quantities of water or biological fluids, leading to potential advantages for biomedical applications. In addition, other properties, namely, stimuli-responsiveness

to heat, pH, and light, can be altered with the monomers and crosslinkers used.[113] Hence, these properties make hydrogels extremely useful for drug loading and controllable drug release systems. Clinical studies have shown the potential of micellar supramolecular hydrogel-based OcDD systems to achieve higher drug penetration across cornea surfaces in rabbits compared with plain micellar formulations. For example, during the study of Zhaoliang *et al.,* low molecular weight mPEG, PCL, and DIC were copolymerized via host-guest interaction to form micelles. DIC/mPEG-PCL micelles and α-cyclodextrin (α-CD) aqueous solutions were then mixed in different concentrations to form a hydrogel.[110] Figure 1.13 presents drug release profiles over time of DIC/mPEG-PCL micelles and DIC/α-CD/mPEG-PCL micelles supramolecular hydrogels in different conditions.

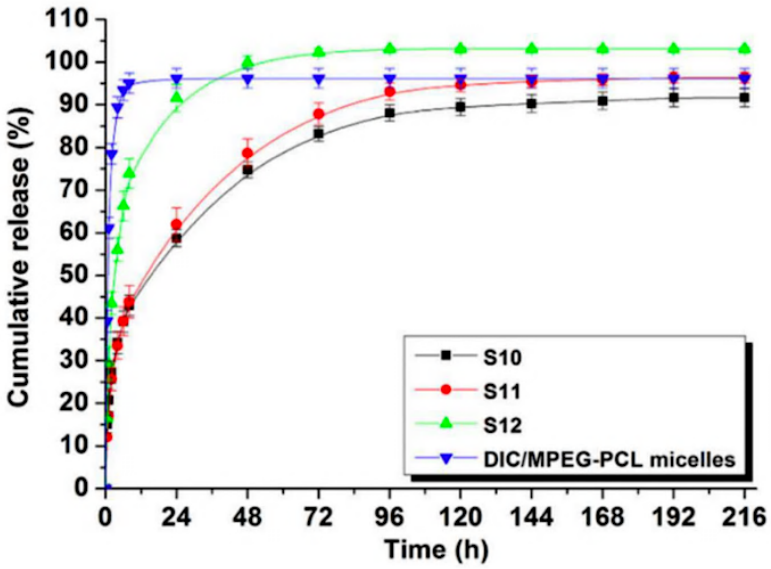

Figure 1.13: *In vitro* drug release profiles of DIC from the DIC/mPEG-PCL micelles and DIC/α-CD/mPEG-PCL micellar supramolecular hydrogels in different concentrations of α-CD. The α-CD concentration (%w/v) of S10, S11, and S12 samples are 7.5, 5, and 2.5 %(w/v), respectively.[110]

According to Figure 1.13, the formulation in the form of micellar supramolecular hydrogel enhanced the percentage cumulative drug release profile. Specifically, the micellar supramolecular hydrogel with α-CD (S10, S11, and S12) presented sustained DIC release over 216 h with cumulative drug release of 91%, 96%, and 103% from S10,

S11 and S12, respectively. Conversely, the DIC/mPEG-PCL micelles without α-CD showed a burst release of DIC to around 95% within 12 h. Interestingly, the DIC release from the supramolecular hydrogel was controlled by the α-CD concentration since higher α-CD concentration influenced the crosslink density and strength of the hydrogel. As a result, the α-CD concentration affected the release behavior of DIC inside the hydrogel. Also, in another study, Zhang *et al.* demonstrated that significant drug levels could be achieved in anterior ocular segment tissues after sustained drug release from drug-loaded supramolecular hydrogels derived from succinated dexamethasone (DEX-SA).[114]

To sum up, these findings support the new approach of using supramolecular hydrogels to control the release profile of drugs over time.

1.4.3 Polymeric colloidal nanocarriers

Polymeric colloidal nanocarriers could be a promising strategy to deliver drugs to the target site of the eye. Encapsulation of the drugs inside the nanocarriers by this strategy can avoid not only blood-ocular barriers but also drug degradation before reaching the target site.[121,122] Thus, each colloidal system presents different properties, including drug modification strategy and preparation methods, which affect the drug release profile.[123] In this section, polymeric micelles, micro/nanoemulsions, and nanoparticles will be discussed.

1.4.3.1 Polymeric micelles

Polymeric micelles (PMs) are nano-sized colloidal carriers (10-200 nm) formed through the self-aggregation of amphiphilic block or graph copolymer in aqueous solutions.[115] Basically, PMs consist of a hydrophobic core and a hydrophilic shell, as shown in Figure 1.14, and their properties are influenced by factors such as the mass and composition of the copolymer backbone, the concentration of the polymer chains and the properties of drug encapsulation.[116]

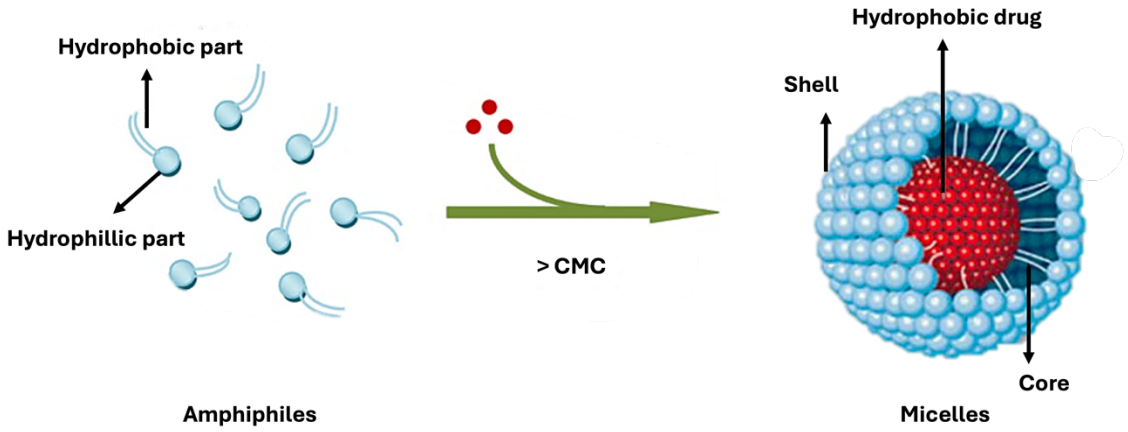

Figure 1.14: Schematic illustration of drug-loaded micelles formation in solution (CMC-critical micelle concentration).[117]

As depicted in Figure 1.14, drugs can be encapsulated within the hydrophobic core via aggregation of amphiphilic molecules or block copolymers. In contrast, the hydrophilic outer shell is in contact with the external aqueous environments. They become micelles when the concentration of polymer chains adsorbed at the interface of the aqueous solution is over the critical micelle concentration (CMC), which is the minimum polymer concentration required to form micelles.[118]

As indicated earlier, PMs have been introduced as one of the most promising drug delivery platforms to manage ocular diseases in both anterior (dry eye) and posterior (AMD, DR, and glaucoma) segments of OcDD.[119] To that end, feasibility studies on using a topical DDS to the posterior segment of the eye have been investigated.[64] Figure 1.15 shows an example of the penetration of PMs in the form of an eye drop via the topical route for delivery to the posterior segment of the eye.

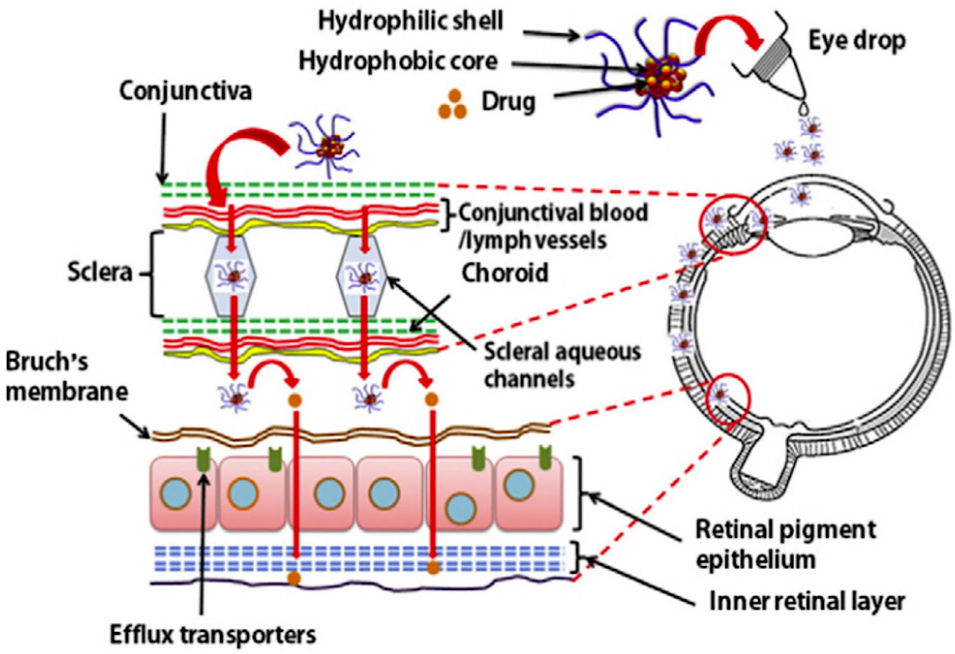

Figure 1.15: A schematic illustration of polymeric micelles reaching the posterior segment of the eye via topical ocular administration.[120]

PMs are self-assembled core-shell nanostructures suspended in an aqueous solution, which can produce clear aqueous solutions, leading to a suitable application in the form of eye drops without any vision interference. As depicted in Figure 1.15, the drug could penetrate the posterior segment of the eye via either the cornea or the conjunctival-scleral route after topical installation.[64] Due to the encapsulation of hydrophobic drugs inside the hydrophobic core of micelles, it enables drug-loaded micelles to cross the hydrophilic stroma barrier in the cornea and thereafter penetrate through the cornea and/or the conjunctival-scleral pathway.[64] Finally, the conjunctival-scleral surface area allows sideways diffusion of PMs to reach the posterior segment of the eye.[121] Xu *et al.* designed chitosan oligosaccharide-valylvaline-steric acid (CVS) micelles formulated in eye drops for topical drug delivery of dexamethasone (DEX) to the posterior segment of the eye.[122] The synthesis of CVS polymers composed of two steps, which were copolymerization of chitosan oligosaccharide-stearic acid (CSO-SA) and valylvaline (VV) conjugation by freeze-drying, followed by DEX loading into CVS polymer solution to form the micelles via probe-type ultrasonic and dialysis methods. Owing to the larger conjunctival-scleral

surface area, it allows lateral diffusion of CVS micelles to reach the posterior part effectively.[123] Approximately 100 nm sized CVS micelles with a zeta potential (ZP) of +33 mV and encapsulation efficiency (EE) of 99% illustrated the *in vivo* permeation of DEX (200 ng/g) to the scleral-choroid-retina in rabbits within 2 h. Indeed, owing to the nanoscale size with hydrophilic property of the CVS micelles, it could diffuse through the sclera's porous structure via transscleral route, as previously stated, facilating the drug transport to come across ocular barriers and reach targeted drug delivery in the back of the eye. Additionally, due to the incorporation of VV and SA with the ratio 5:4 to the CSO micelles, the *in vitro* studies in simulated tear fluid demonstrated 60% of DEX release after 6 h, whilst CSO micelles had only 40% of drug release over the same period of time. Furthermore, the *in vitro* cytotoxicity studies in human corneal epithelial primary cells and human conjunctival epithelial primary cell systems revealed that the cell viability of DEX-loaded CVS micelles remained above 80% after 12 h, showing no significant cytotoxicity. Thus, the CVS micelles modification presented sustained release, biocompatibility, and penetration enhancing properties that would be suitable for nanocarriers for OcDD to the posterior segment of the eye.[122]

In addition, micelle DDS through the scleral pathway can overcome the clearance mechanism from the conjunctival blood circulation and lymphatic effects, which limit the transport of drug-loaded micelles to treat retinal disease. Subsequently, PMs may be taken into the RPE cells by endocytosis to generate therapeutic concentrations in posterior ocular tissues.[124] Laibin *et al.* studied fluorescently labelled PMs of poly (ethylene oxide)-block-polycaprolactone (PEO-*b*-PCL) conjugating tetramethylrhodamine-5-carbonyl azide (Rh) to the end of PCL block for enhancing the internalization of the micelles into the cell by endocytosis.[125] A block copolymer mixture (PEO-*b*-PCL/PEO-*b*-PCL-Rh, molar ratio 19/1) was dissolved in dimethylformamide (DMF) before adding the water into the mixture to obtain Rh-labeled micelles. The aqueous solution was then dialyzed against water for one day, followed by dilution of the solution to get Rh-labeled micelles with 0.67 %(wt) of the polymer and 67 μM of Rh. A size range of 25 nm allowed the Rh-labeled micelles to internalize into the pluripotent (P19) cells for up to 24 h. Moreover, the fluorescent intensity of Rh in the P19 cells increased when the concentration of Rh

increased (from 0.74-6.7 μM). Similarly, the study of Radoslav Savic *et al*., investigating PEO-*b*-PCL block copolymer micelles with rhodamine in rat pheochromocytoma (PC12) cells, found that the fluorescent-labeled PEO-*b*-PCL micelles could be internalized mainly into the cytoplasm.[126] Approximately 0.4-0.6 μg per million cells of polymer was detected in the cytoplasmic compartment of PC12 cells. They also studied spectrophotometric measurements, and 5-dodecanoylaminofluorescein (DAF) was used to label the plasma membrane selectively. The result demonstrated that the Rh-PEO-*b*-PCL micelles incorporated in DAF presented greater cellular content than that of free DAF, with almost 600% of DAF detected in the cells from DAF incorporated in the PEO-*b*-PCL micelles.[126]

To conclude, these approaches suggest that PMs not only increase the amount of drug delivered to the target cells but also enhance the internalization of the drug into the cell. Hence, the micelles could be an effective carrier for lipophilic drug transportation to treat a range of diseases in the posterior segment of the eye via topical or transscleral drug delivery.

In terms of modification strategies, the structure of polymeric micelles is divided into three categories: polymer-drug conjugates, drug-encapsulated carriers, and polyion complex micelles.[115]

1.4.3.1.1 Polymer-drug conjugates

Polymer-drug conjugates represent a novel approach to drug delivery. This method is developed through the chemical bonding of functional groups between polymers and a drug molecule, as shown in Figure 1.16.[127]

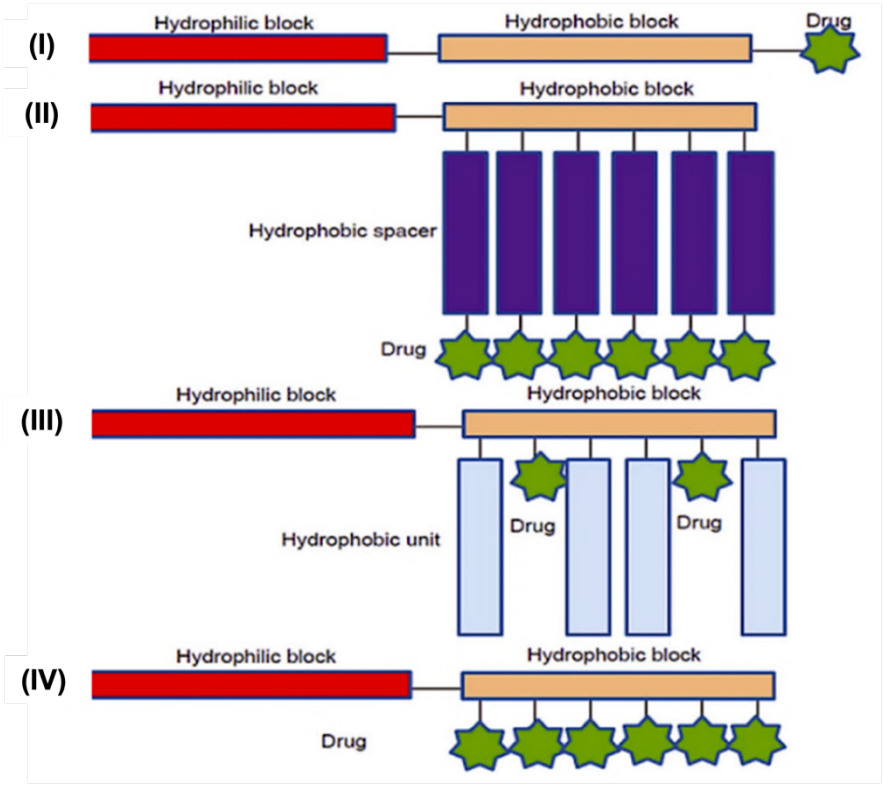

Figure 1.16: Different designs and models for micelle-forming drug-block copolymer conjugates.[115]

Drugs can be conjugated to various polymers through different conjugation linkages and spacers, both onto the polymer backbone and side chains (Figure 1.16).[127] Additionally, this type of PMs is beneficial in the field of chemotherapeutic delivery systems, which lead to a chemical change in response to an external stimulus such as pH and temperature.[127,128] Polyethylene glycol (PEG) and PEO are the most common compounds used as hydrophilic copolymers due to their high aqueous solubility, high mobility, and low toxicity.[129,130] So far, PEO-*b*-poly(ester) and PEO-*b*-poly(amino acid) are the most conjugated block copolymers for drug delivery applications.[131–135] On the one hand, conjugation of drugs to the end of the polymer backbone is commonly found in block copolymers between PEO/PEG and poly(ester) since the terminal hydroxyl group of poly(ester) can react with the reactive group on the drugs (Figure 1.16(I)).[106] Zhang *et al.* investigated the *in vivo* micellar integrity of PEG-PCL PMs after intravenous injection using NBD-X and MS735 as fluorescence donors and acceptors, respectively.[136] To synthesize PEG-PCL-NBD-X (donor) and MS735 (acceptor), PEG-PCL-OH was

modified to bear amino terminated (PEG-PCL-NH_3Cl) and alkyne terminated (PEG-PCL-alkyne) groups. Then, the NBD-X (D) and MS735 (A) were separately conjugated to the termination of the block polymers. Finally, the PEG-PCL block copolymers with donors and acceptors were prepared via dialysis to obtain the micelles. Their findings showed that *in vivo* micellar integrity studies in mouse blood revealed that around 60% of the micelles$_{D+A}$ (8% donor and 5% acceptor, size~42 nm) were intact in plasma for 72 h after intravenous injection with 30 μL of micelle$_{D+A}$ at a dose of 40 mg polymer per kg of mice. This demonstrated that most of the micelles remained intact during blood circulation.

On the other hand, due to several functional groups consisting in the poly (amino acid) structure in block copolymers, including PEO/PEG, this provides substantial sites for drug conjugation to one polymer chain of the hydrophobic block copolymer of poly(amino acid) (Figure 1.15(II)-(IV)).[130–132,134,137] According to the work of Sang *et al.,* pH and thermal dual stimuli-responsive PMs between doxorubicin (DOX) and block copolymers were prepared using a hydrazone bond to link between drug and polymer chains for anticancer drug delivery.[138] Preparation of pH/thermo sensitive PMs consisted of three steps. First, copolymerization of allyl polyethylene glycol (APEG) and *N*-isopropylacrylamide (NIPAM) were synthesized in the presence of 2-aminoethanethiol. Then, P-(NIPAM-*co*-APEG) was copolymerized with γ-benzyl-L-glutamate and N-carboxyanhydride (BLG-NCA) via ring opening polymerization to form P(NIPAM-*co*-APEG)-*b*-PBLG micelles. Finally, DOX, as a model drug, was covalently conjugated into the core of PMs via a hydrazone bond. A scanning electron microscope (SEM) image of the copolymer micelles is shown in Figure 1.17(I).

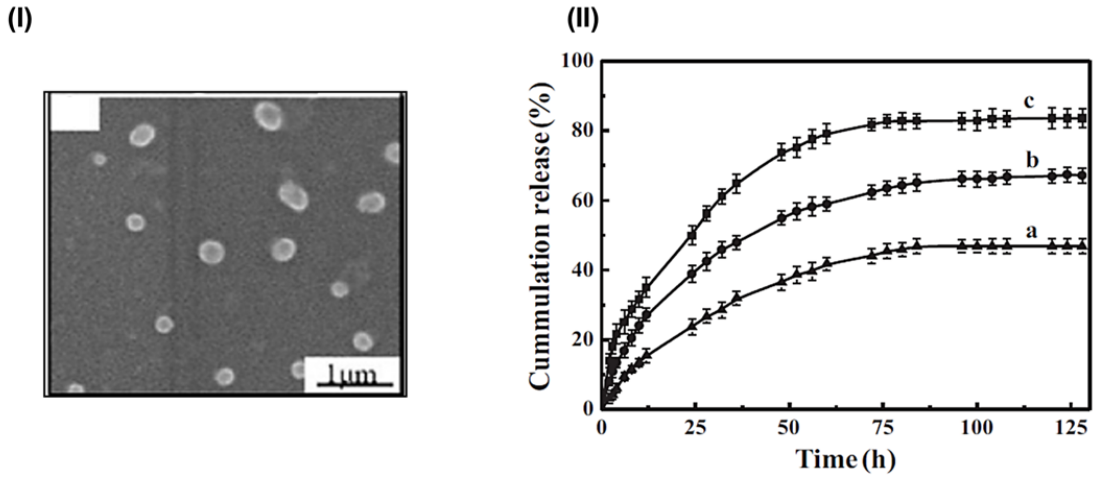

Figure 1.17: Physical characterization and *in vitro* release study of P(NIPAM-*co*-APEG)-*b*-PBLG micelles; (I) SEM image of P(NIPAM-co-APEG)-b-PBLG micelles after drug loading; (II) The effect of temperature on the release of doxorubicin (DOX) from drug-loaded micelles pH=4.0: (a) 25°C, (b) 37°C, (c) 45°C.[138]

Following this strategy, the DOX-loaded micelles with a hydrodynamic diameter of 368 nm exhibited a good drug EE (79.8%) and drug release profile. An *in vitro* drug release study showed that the cumulative DOX release from the copolymer micelles at pH 4.0 increased to 62% over 72 h. Moreover, because of the thermo-sensitive PNIPAM segment, the cumulative DOX release reached 74% at 45°C within 48 h, whereas only 55% of the drug was released at 37°C (Figure 1.17(II)). Aside from pH-responsive stimulus, hydrolysis is another typical reaction for the cleavage of polymer-drug conjugates.[139,140]

Taken altogether, while there has been a great deal of research on the advantages of using polymer-drug conjugates for OcDD, some studies highlighted that accession of the drug to water molecules outside is limited owing to the phase separation between the inner core and outer shell structures of the PMs, resulting in low drug release by cleavage of a chemical bond following this technique.[141,142]

1.4.3.1.2 Drug-encapsulated carriers

Physical entrapment techniques are an alternative approach to preparing PMs and overcoming problems such as complex molecular design, multistep synthesis processes, and toxic side effects after drug release from polymer-drug conjugates (Figure 1.18).[143,144]

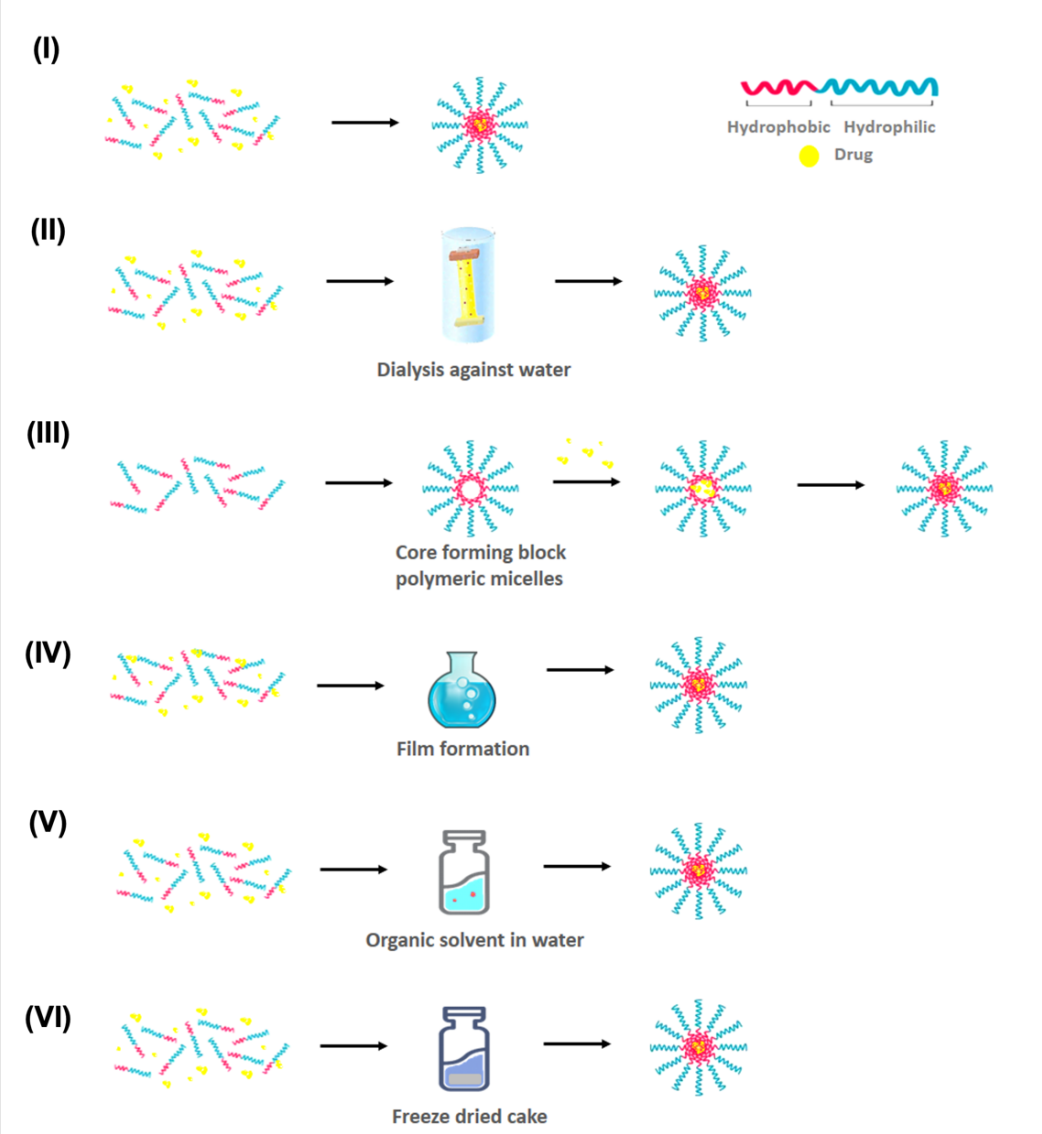

Figure 1.18: Physical methods of drug encapsulation inside PMs: (I) direct dissolution, (II) dialysis, (III) oil-in-water (o/w), (IV) emulsion, (V) solvent evaporation and (VI) freeze-drying methods.

As illustrated in Figure 1.18, the micelles are formed in the aqueous medium using various physical methods to encapsulate drugs inside PMs. Each technique is described in more detail below.

Direct dissolution

Direct dissolution (Figure 1.18(I)) is the simplest technique for preparing drug-loaded PMs. It involves physically mixing copolymers and drugs in water.[143] Micellar structures are then formed when the concentration of surfactant is above the CMC.[145,146]

Several studies have demonstrated the successful formation of drug-loaded PMs using the direct dissolution technique. For example, Pepic *et al.* reported the preparation of DEX-loaded Pluronic F127 (PF127)/CH micelles (~28 nm, ZP=9-18 mV) following a direct dissolution method by adding CH solution at different concentrations to the PF127 copolymer solution, obtaining high drug loading of 0.52%.[155] Similarly, Terreni *et al.* developed cyclosporine (CsA)-loaded assembling surfactants-mucoadhesive polymer nanomicelles (~14 nm) using the direct dissolution method. Mixing Vit-E/D-α-tocopheryl polyethylene glycol succinate (TPGS) with octylphenoxy poly(ethyleneoxy)ethanol and CsA drug, followed by the addition of hyaluronic acid before filtration, could enhance CsA solubilization up to 0.1 %(w/w) and achieve sustained the *in vitro* drug release over 30 h.[147]

Dialysis method

The dialysis method (Figure 1.18(II)) involves dialysis of a solution consisting of polymers, drugs, and organic solvents, such as N, N dimethylformamide, and triethylamine, against water. Replacing the organic solvent with water during the dialysis process enhances the self-association of block copolymers and drug entrapment.[148]

Oil-in-water emulsion method

An oil-in-water emulsion is a mixture in which the copolymers are dispersed in either the aqueous or organic phase (Figure 1.18(III)). Drugs are dissolved in a water-immiscible organic solvent (such as chloroform and methylene chloride), followed by the addition of this organic phase to the aqueous phase, leading to an oil-in-water emulsion. Lastly, the organic solvent is removed by solvent evaporation, and the PMs are formed.[149,150]

Solvent evaporation method

Regarding the solvent evaporation method (Figure 1.18(IV)), the drug and polymer are dissolved in a volatile organic solvent. After the organic solvent evaporates, a thin film of polymer/drug is formed, which is then resuspended in aqueous solution to form the

PMs.[151,152] Wang *et al*. reported the preparation of CUR-loaded Soluplus®/Solutol®HS15 PMs (~83 nm) via thin-film hydration method, achieving a high drug EE of 92% and sustained drug release over 50 h.[152] In a similar study, Mehra *et al*. developed everolimus (Evr)-loaded Soluplus® PMs using the thin-film hydration method.[153] The Soluplus® and Evr was mixed with ethanol before evaporating using rotary evaporation and resuspending in deionized (DI) water afterwards to obtain a clear solution of Evr-PMs (size~66 nm, 97% EE). Their study found that Evr-PMs (70%) enhanced drug release compared to the drug suspension (30%) within 36 h.

Co-solvent evaporation method

In connection with the co-solvent evaporation method (Figure 1.18(V)), the preparation is similar to the solvent evaporation method, but the organic solvent changes to a volatile water-miscible organic solvent before the aqueous solvent is added to produce the PMs.[154–156] Safwat *et al.* prepared triamcinolone acetonide (TA)-loaded PEG-*b*-PCL micelles following the co-solvent evaporation technique.[156] TA and each polymer were solubilized in 2 mL of acetone before adding dropwise into 4 mL of DI water under magnetic stirring in a glass vial. The mixture was kept stirring for 24 h to remove acetone and form the drug-loaded micelles. Their results demonstrated that TA aqueous solubility was increased by 5-fold after loading into the PEG-*b*-PCL micelles at a low polymer concentration of 0.5 mg/mL. Additionally, 64 nm-sized TA-loaded PEG-*b*-PCL micelles could sustain the drug release at 40% over 180 h in phosphate buffered saline (PBS) pH 7.4 at 37°C, whereas the burst release (100%) was obtained from the drug solution formulations within 60 h.

Freeze-drying method

The freeze-drying method (Figure 1.18(VI)) is used to produce PMs by mixing them with a freeze-dryable organic solvent such as tert-butanol. Polymers and drugs are dissolved in the freeze-dryable organic solvent, and DI water is subsequently added. The polymer/drug solution is then freeze-dried and reconstituted with isotonic aqueous media.[157]

Due to the small-sized performance (20-100 nm), amphiphilic properties, and hydrophilic nature of PMs, these features benefit drug-loaded polymer micelles in overcoming the ocular barriers and delivering the drug to the target site. For example, the previous study of Ghezzi *et al.* reported up to 15% permeated of the CsA to the scleral tissue of the pig eye from the 13 nm-sized CsA-loaded TPGS micelles.[158] Nevertheless, the limitations of drug-encapsulated micelles, including low drug loading (DL) and EE, as well as poor stability of the micelles, are increasingly apparent.[159] For that reason, the hydrophilicity of the block copolymers and chemical interactions between the polymeric core segment and the drug need to be modified to improve the stability of the drug.[99,160–163]

1.4.3.1.3 Polyion complex micelles

Polyion complex (PIC) micelles are used to deliver charged macromolecular drugs such as DNA, peptides, and enzymes.[164,165] The formation of PIC micelles is schematically shown in Figure 1.19.

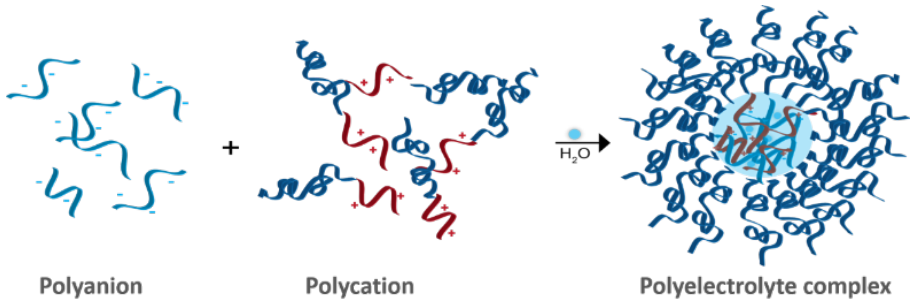

Figure 1.19: Schematic illustration of the formation of PIC micelles.

The method to produce PMs via this technique is the combination of opposite charges between polymers and drugs via electrostatic interactions in an aqueous medium, which acts as a driving force of PM formation (Figure 1.19).[166] In addition to hydrophobic and electrostatic interactions of this type of PM, it can be applied to the DDS that respond to specific stimuli to release the drug from PMs.[165,167–169]

Overall, a number of studies presented here provide evidence that PMs have been developed so far. Due to the small size and hydrophilic nature of micelles, they can efficiently permeate through several ocular barriers in both the anterior and posterior segments as well as enhance drug permeation to the target sites. Moreover, according to

the Masayuki and Hongyan Xu reviews, the amphiphilic diblock copolymers of micelles present substantial benefits as carriers for DDS, such as prolonged drug release, enhanced stability, targetability, and bioavailability, which benefit in OcDD.[170,171] Therefore, these benefits and all examples previously mentioned in section 1.4.2.1 clearly indicate the potential of PMs as drug delivery carriers for the efficient treatment of eye diseases.

1.4.3.2 Micro/nanoemulsions

Recent studies have explored the use of microemulsions (MEs) (10-100 nm) and nanoemulsions (NEs) (20-500 nm) as new DDS. MEs or NEs are composed of an oily phase, an aqueous phase, and a combination of surfactant and/or co-surfactant, to form spontaneously on a combination of those three components. To be specific, a ME is a transparent, thermodynamically stable mixture of oil, water and surfactant that forms spontaneously without the need of external energy (e.g. heat, mechanical agitation, ultrasonication). Whereas, a NE requires external energy to form and maintain the small droplet.[172] This strategy is an alternative to conventional ophthalmic dosage forms due to their long-term stability, low toxicity, and ease of preparation, including the advantage in terms of incorporating water-soluble and lipophilic drugs.[173]

Current studies appear to support the notion that ocular MEs/NEs are an interesting formulation since both present good spreading onto the ocular surface due to their low viscosity (less blurring of vision in patients) as well as enhancement of drug distribution to tissues. As a consequence, the topical delivery of various drugs into the eye can be achieved by using ocular MEs and NEs. In a promising study, Mahboobian *et al.* prepared oil-in-water ocular NEs involving brinzolamide (BZ), an intraocular pressure (IOP) reducing agent with low bioavailability, to reduce IOP over a prolonged time.[174] In their study, they applied the NEs onto rabbit eyes and measured the IOP level using a rebound tonometer, which works by analyzing the rebound behavior of a small probe when contacting the cornea and bouncing back due to IOP. To prepare the NEs, triacetin or capryol 90 were used as the oil phase, Brij 35, cremophor RH40, labrasol or tyloxapol as surfactants, and transcutol as a co-surfactant to evaluate their efficacy in delivering BZ. The average droplet size of NEs ranged between 7.5 and 42.4 nm. BZ-loaded NEs illustrated high formulation stability under freeze-thawing at temperatures from -2°C to

+25°C and heating-cooling rates between 4°C and 40°C as well as centrifugation at 13,000 rpm for 30 mins. Furthermore, *in vitro* drug release studies exhibited more than 90% release of BZ from NEs within 360 min. The percentage of drug released decreased with increasing surfactant, which led to the lower thermodynamic activity of BZ. Also, it was confirmed that NE-loaded BZ (oil:surfactant mixture=5:30) penetrated the corneal tissue successfully and exhibited the maximum reduction in IOP (area under the dose-response curve $(AUC)_{0\text{-}6h}$=130) in comparison to commercial product ($AUC_{0\text{-}6}$=98), resulting in higher therapeutic efficacy *in vivo* of BZ NEs. A similar study by Gohil *et al*. using MEs of BZ in goat eyes demonstrated no ocular irritation for 8 h, again indicating its safety and efficacy for ophthalmic use without causing unwanted side effects.[175]

Another area of interest amongst researchers is ocular MEs and NEs for anti-inflammatory ocular conditions.[176] A more recent study by Gupta *et al.* designed ME systems (size~64-84 nm) composed of lauroglycol as the oil phase, labrasol as the surfactant, and transcutol as a co-surfactant for fluocinolone acetonide (FA) administration in the posterior segment of the eye.[177] Summary results are shown in Figure 1.20.

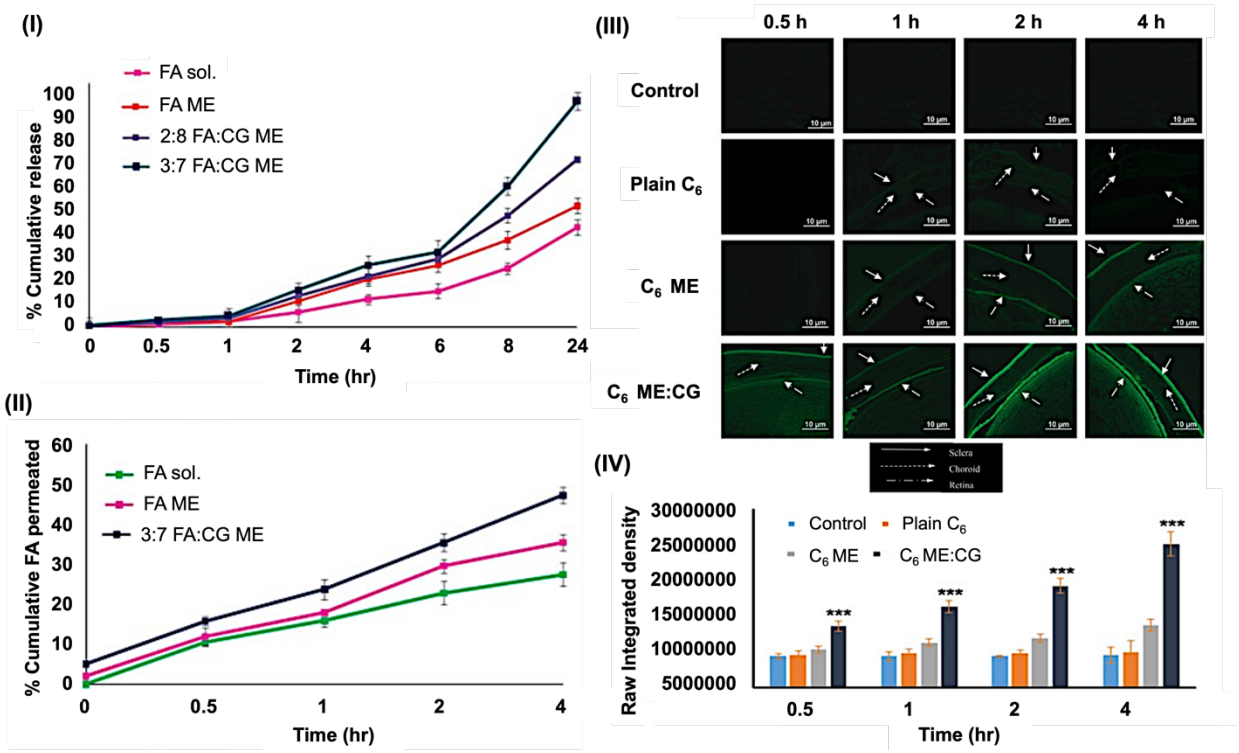

Figure 1.20: (I) *In vitro* FA release from FA solution, FA ME, 2:8 FA:CG ME, and 3:7 FA:CG ME throughout 24 h, (II) *Ex vivo* FA permeation through goat cornea, %cumulative FA permeated, (III) representative images of fluorescence (10x magnification) observed under fluorescence microscope from the sectioned eyes of Sprague Dawley rats treated with different formulations (normal saline solution, plain C6, C6 ME, and C6:ME CG) and enucleated at different time points (30 min, 1 h, 2 h, and 4 h). (IV) analysis of observed fluorescence by ImageJ software, values in the mean ± SD (n=3). Arrows were indicating the sclera, choroid, and retina. The presence of fluorescence in those regions suggested the reach of the instilled dose.[177]

In this study, they were interested in utilizing cow ghee (CG) as a permeation enhancer in the development of topical ocular MEs. It was reported that the optimized condition of FA-loaded MEs fortified with CG (oil:surfactant:co-surfactant:water=4:23:23:50) had a droplet size ranging between 63.92 and 83.56 nm. The MEs prolonged the stability at three different temperatures (4°C, 25°C, and 40°C) for 3 months without changing the particle size, PDI, ZP, pH, and %DL. Furthermore, the result obtained from *in vitro* drug release studies demonstrated the highest percent drug release for FA ME fortified with CG at a 3:7 ratio (93%) compared to a FA solution (40%) and other formulations within

24 h (Figure 1.20(I)). This study clearly proved the efficiency of MEs in increasing the drug diffusion capability of the drug in comparison to the drug solution alone. In addition, *ex vivo* corneal permeation studies displayed higher permeation of the MEs (48%) through goat cornea compared to FA solution (25%) within 4 h (Figure 1.20(II)). Also, *in vivo* pharmacokinetic studies exhibited retention of CG fortified ME in the posterior rat eye, confirmed by the fluorescence microscopy shown in Figure 1.20(III)-(IV).

Hence, as mentioned previously, either MEs or NEs can play a major role in ocular disease treatment due to their unique characteristics, ease of preparation, and cost-effectiveness.

1.4.3.3 Nanoparticles

A nanoparticle (NP) is a small particle that has a diameter in the range between 1 to 100 nm. Moreover, NPs can exhibit significantly different physical and chemical properties owing to the materials used for preparation. As a result, numerous scholars have examined the role of biodegradable and non-biodegradable NPs in treating anterior and posterior segment ocular diseases.

Guo *et al.*, in their study of controlled release TA-loaded methoxy PEG (mPEG)-PLGA NPs for the treatment of autoimmune uveitis, found that 82 nm-sized TA-loaded NPs with 77% TA entrapment efficiency could maintain drug release (80%) for more than 45 days.[178] Additionally, TA-loaded NPs had higher anti-inflammatory effects than TA alone after pathological examination, resulting in decreased IL-17 and elevated IL-10 levels in both the aqueous humor and serum. A similar study by Alverez-Trabado and coworkers prepared CsA-loaded hyaluronic acid-coated sorbitan ester NPs, which demonstrated an enhanced ocular tissue penetration into the cornea stroma compared to the commercial formulation, again proving its better bioavailability.[179]

1.4.4 Cyclodextrin-based nanocarriers

Previous sections have clearly demonstrated that hydrogels and polymeric colloidal nanocarriers can substantially improve drug permeation and *in vivo* biodistribution, leading to enhanced accumulation at the target sites. Recent years have seen a surge in interest in cyclodextrins (CDs), cylindrical oligosaccharides with hydrophilic and

lipophilic surfaces, which can form inclusion complexes with hydrophobic drugs (Figure 1.21).

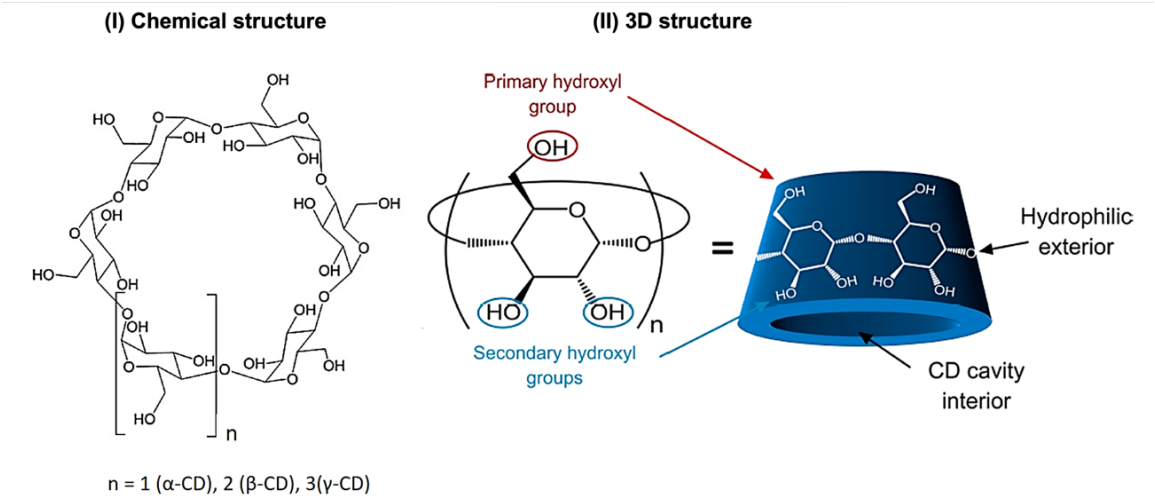

Figure 1.21: A schematic of (I) CD structures and (II) the native CD molecule in the 3D form.[180]

As shown in Figure 1.21, CDs are cyclic oligosaccharides of glucopyranose, consisting of six to eight glucose units linked by β-1, 4-glucosidic bonds (Figure 1.21(I)). There are three types: α-CD with 6, β-CD with 7, and γ-CD with 8 glucopyranose units. Moreover, CDs can form complexes with lipophilic drugs due to the lipophilic inner surface of CDs (Figure 1.21(II)). As a result, CDs are enabled to enhance the drug adsorption across biological barriers and to deliver the drug to the targeted site.[180]

1.4.4.1 Cyclodextrin-based nanoparticles

The combination of drug complexation with CDs and complex incorporation into different types of nanocarriers is a strategy to enhance EE by increasing aqueous solubility and therapeutic activity. Tang *et al*. studied dimethyl-β-CD/salazosulfapyridine (DMβCD/SASP) inclusion complex loaded into chitosan (CH) NPs for drug delivery (Figure 1.22).[181]

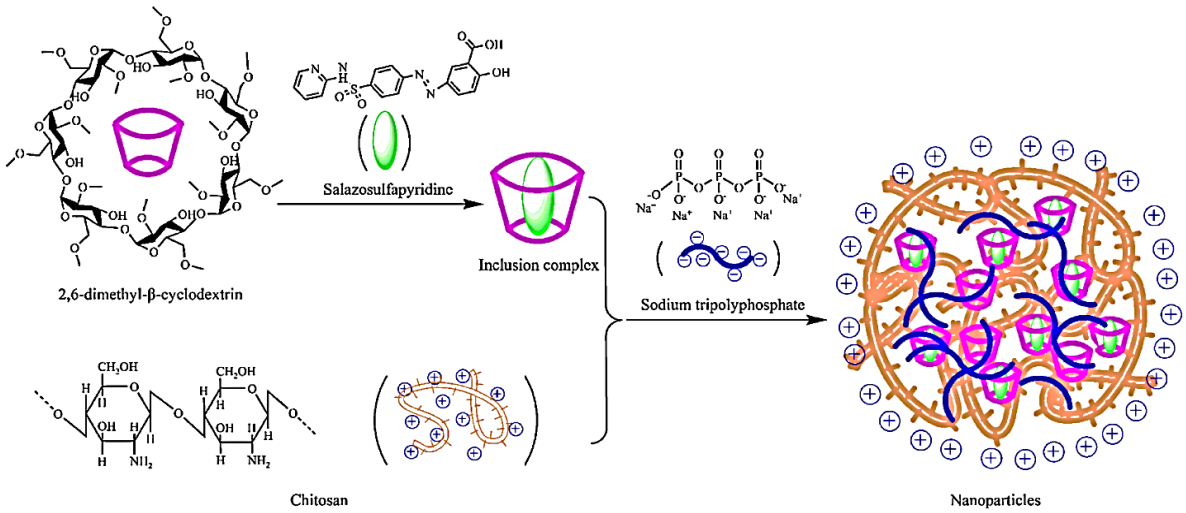

Figure 1.22: The formation of DMβCD/SASP inclusion complex loaded CH nanoparticles.[181]

In their study, they prepared an inclusion complex of SASP and DMβCD, which was incorporated into CH to form DMβCD/SASP/CH NPs with an average size of 90 nm (ZP=+35.4 mV). These NPs showed higher EE (91%) and sustained drug release than SASP/CH NPs (18% EE). *In vitro* cytotoxicity studies showed no apoptotic cells and minor inhibition against the HK-2 cell line, reducing hepatotoxicity and nephrotoxicity. Thus, CD inclusion complex-loaded CH NPs could be applied for hydrophobic drug delivery. Moreover, many previous studies on polymeric NPs have focused on developing PLGA NPs together with CD complexes to enhance the solubility of hydrophobic drugs.[182–185] Similarly, Guo *et al*. developed an anti-cancer drug formononetin-2-hydroxypropyl-β-CD (2-HPβCD) inclusion complex-loaded PLGA nanoparticles using a solid/oil/water technique, resulting in increased *in vitro* drug release and reduced cytotoxicity in Hela and MCF-7 cells.[186]

In ocular applications, CDs may serve as carriers for lipophilic active pharmaceutical ingredients (APIs) transportation, facilitating their passage across eye barriers like the corneal barrier (Figure 1.23).

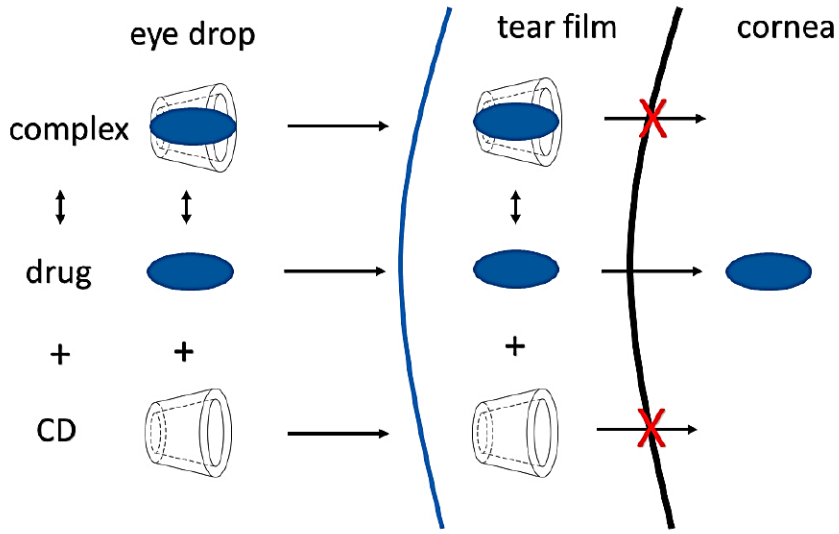

Figure 1.23: A picture represents the cyclodextrin drug permeability enhancer attributes in the corneal tissue.[187]

After eye drop administration, the cornea, a major barrier, prevents the APIs from reaching the target site in the anterior eye segment (Figure 1.23). In contrast, drugs containing CDs in the form of inclusion complexes can enhance APIs permeation across the cornea, while hydrophilic CDs are eliminated through the nasolacrimal pathway. Table 1.2 provides a summary of recent methods for using CDs in ophthalmic formulation.

Table 1.2. The approaches to use CDs in ophthalmic formulations as eye drops.

CDs type	Carriers	Loaded drug/disease	Comments
HPβCD	N-Trimethyl CH NPs	Flurbiprofen, treatment of bacterial conjunctivitis	The particle size was 201 nm with a ZP of +13.9mV and 11% EE demonstrated a sustained drug release for up to 12 h, with 75% and 45% of drug release from flurbiprofen-HPβCD loaded CH and N-trimethyl CH NPs, respectively[188]
HPβCD HPγCD	CD/polymer nanoaggregates of PVP, PVA, CMCE and tyloxapol	Nepafenac, treatment of inflammation associated with cataract surgery	-The particle size of HPβCD and HPγCD were in the range from 220 to 332 nm -HPβCD performed best in terms of solubilization, whereas HPγCD performed best in terms of enhancing nanoaggregate formation -The addition of a second solubilizing agent to a drug/CD complex improved the solubility of the drug and make the formulation more cost effective by allowing the use of lower concentrations of CDs[189]
HPβCD SBECD	Drug/CDs/HPMC to form mucoadhesive type ocular film	Amlodipine, anti-inflammatory activity	-*In vitro,* drug release and ocular permeation were enhanced by the HPMC and SBECD film formation[190]
HPβCD HPγCD	Drug/CDs hydrogel formulations	Dexamethasone acetate, treatment of corneal inflammation	-The cumulative drug release reached 90% and 60% within 2 h from mixed gel containing HPβCD and HPγCD, respectively[191]

*PVP:polyvinylpyrrolidone, PVA:polyvinyl alcohol, CMCE:carboxylmethyl cellulose, HPγCD:hydroxypropyl γ-cyclodextrin, SBECD:sulphobutyl-ether-β-cyclodextrin; HPMC:hydroxypropyl methylcellulose

1.4.4.2 Cyclodextrin-based micelles

In addition to the CD-based inclusion complexation bridged biodegradable self-assembly micelles for OcDD, CDs are often added to increase the solubility of the drug in PMs and thus efficiently enhance permeation and reduce cytotoxicity when in contact with the cornea of the eye.[192] Lorenzo-Veiga *et al*. studied encapsulating natamycin in micelles

and poly(pseudo)rotaxanes (PPRs) for fungal treatment.[193] They prepared Soluplus® and Pluronic P103 dispersions, observed micelles ranging from 90-100 nm, and found that combining copolymers and CDs increased drug solubility. Ocular tolerance studies showed non-irritant formulations, and *ex vivo* corneal and sclera permeability studies showed increased natamycin accumulation, indicating an enhancement of ocular permeability. Similar results were observed by the work of Sayed and colleagues in the development of β-CD consolidated micellar dispersions (CMDs) to solubilize hydrophobic drug itraconazole.[194] The CMD was prepared using a melt dispersion technique, resulting in a 204 nm-sized formulation with a 4% solubilization efficiency. The optimized formulation showed 90% itraconazole release within 24 hours and a two-fold higher permeation in rabbit corneas compared to the drug suspension (0.30 mg/cm^2) over 26 h. Also, the optimized CMD formulation reduced fungal colony count in rat eyeballs, with an 82% reduction compared to untreated eyes. Hence, their optimized CMD formula, found to be safe, stable, mucoadhesive, and efficient for transcorneal delivery of lipophilic drugs, including antifungals, was found to be promising.

Taken altogether, the utilization of CD-based micelle formulations represents a promising strategy to enhance the permeability of hydrophobic drugs for the treatment of eye diseases, especially the anterior segment. Moreover, the ability of CD-based micelles to interact with cell membranes and modulate drug release kinetics offers additional advantages in overcoming barriers to drug penetration within the eye. These formulations hold great promise for the treatment of a wide range of ocular diseases, where conventional DDS may fall short.

1.5 Research objective

To address the challenges in OcDD outlined in Sections 1.3 and 1.4, the main goal of this project is to develop novel drug-loaded nanomaterials for controlled release of therapeutic drugs to the target site in posterior eye segments to treat AMD and other PSEDs. In addition, the aim is to take advantage of recent advances in novel delivery platforms that could greatly improve patient comfort and outcomes by negating or reducing the need for ocular injections. Research and experimental work will involve the synthesis,

characterization, and evaluation of novel nano-enhanced delivery systems capable of attenuating the release profile as dictated by the clinical need.

Within the program of work, the thesis is comprised of 6 chapters, and brief details of the study in each chapter are as follows:

Chapter 1 reviews a recent line of research studies in the field of OcDD for the treatment of both anterior and PSEDs. Different routes of ocular administration and various types of emerging DDS for ocular routes are discussed, including their advantages and disadvantages are outlined.

Chapter 2 describes the formation and preparation method of micellar solutions of PF127 solution. Several strategies to improve micelle stability were evaluated. This is an initial step to focus on the design of micelle formulations, which will become a drug carrier for us to explore various treatment options for OcDD.

Chapter 3 presents several strategies for preparing CUR-loaded PF127 micelles. Multiple parameters were optimized to enhance the drug's EE into the PF127 micelles, followed by *in vitro* drug release and *ex vivo* permeation studies of drug-loaded micelles.

Chapter 4 discusses the development of CD-based PF127 micelles, mixed PF127/Soluplus® micelles and PPR formulations (PF127/Soluplus®/CD) as a DDS to enhance the solubility and bioavailability of FEB drugs. Multiple characterizations were performed to confirm the formation of PPRs. Also, *in vitro* cytotoxicity and *ex vivo* permeation studies of the prepared formulations were tested to prove the bioavailability and permeability efficiency of the formulations for OcDD.

Chapter 5 uses a mathematical model to prove the hypothesis of the permeation of the prepared formulations to come across the cornea and sclera tissues of the porcine eyes according to *ex vivo* permeation study from Chapter 4

Chapter 6 describes the formation and preparation method of micellar solutions of mixed PF127/CH systems to encapsulate the FEB drug. Moreover, this chapter also highlights the recommendations for future work based on the research study.

Chapter 2

Development of micellar solutions of Pluronic F127 systems

2.1 Introduction

Numerous research groups, as highlighted in the review by Gorantla *et al.*, have considered the implications of current ocular drug delivery (OcDD) approaches in terms of prolonging the contact of the drug delivery system (DDS) with the ocular surface, sustaining the release of drugs, and potentially enhancing barrier permeability.[195] As Chapter 1 outlines, one potential option is the use of nanosystems (such as nanoparticles and nanomicelles) in the form of an aqueous solution or suspension, since the drug can be encapsulated within the nanocarrier to facilitate crossing multiple barriers in the eye to reach the target site, potentially even the posterior segment of the eye.[158,196,197] Additionally, it is necessary to consider the side effects and limitations of different routes of administration. For example, intravitreal (IVT) administration is an invasive treatment potentially damaging to the retina, resulting in endophthalmitis and irritation for patients with aged-related macular degeneration (AMD), as discussed in detail in Chapter 1.[87] Moreover, fast elimination due to tear turnover and the impermeability of the drugs to the multi-layered structure of the cornea are potential barriers to the efficacy of commercial topical eye drops.[61] Despite these drawbacks, previous research, as reviewed by Yang *et al*., has supported the hypothesis that topical OcDD in the form of eye drops is the most convenient and compliant drug administration route for patients, owing to their ease of use and low interference with vision, including the simplicity of scaling up production of the pharmaceutical product in the form of a homogeneous solution.[198] For this reason, this study was conducted to investigate the hypothesis: whether topically applied drugs in the form of eye drops can reach the back of the eye, with the first step being the development of a potential micellar nanocarrier, as outlined in this chapter.

Current studies indicate that polyoxyethylated nonionic surfactants could be useful materials in OcDD since they can enhance drug permeability to the ocular surface.[199,200]

From other commercially available triblock copolymers, Pluronic F127 (PF127) has been chosen for this investigation owing to its useful aggregation behavior.[201] PF127 is an amphiphilic triblock copolymer composed of hydrophobic poly(propylene oxide) (PPO) and hydrophilic poly(ethylene oxide) (PEO), which can, in appropriate systems, self-assemble to form micelles with increasing copolymer concentration. Therefore, numerous scholars have demonstrated the use of PF127 as a micellar DDS to improve the bioavailability of poorly water-soluble drugs.[146,199,202] For example, the study of Bao *et al.* focused on preparing micelles based on PF127 polymers to enhance corneal permeability.[203] In their research, celecoxib (CXB), a non-steroidal anti-inflammatory drug, was loaded in PF127 micelles prepared via the thin film hydration method.[203] By varying the drug/polymer feed ratios, the mean diameter and the drug loading capacity of the formed micelles ranged from 22-29 nm and 4-16%, respectively. *In vitro* studies indicated a sustained release of CXB-loaded micelles, with 90% of CXB release within 70 h at pH 7.4. In addition, the CXB micelles exhibited a 4-fold increase in corneal permeability of the CXB drug compared to the CXB suspension (0.3 µg) at 6 h as measured by *in vitro* corneal permeability of rabbits.

Herein, this research aimed to prepare micelles using PF127 copolymers. The chosen experiments in this chapter are critical for designing nanomaterial formulations with potential use as efficient OcDD systems in pharmaceutical applications. A suitable concentration for micelle formation and the stability of the micelles after freeze-drying and sonication processes were examined. Therefore, several characterizations to confirm the formation and stability of micelles, such as surface tension, dynamic light scattering (DLS) measurement, and the effect of both freeze-drying and sonication on the micelle sizes, were investigated.

2.2 Materials and methods

2.2.1 Materials

Pluronic F127 triblock copolymer (PF127, mw:12600 g/mol) and acetone (purity≥99.9%, HPLC grade) were purchased from Sigma Aldrich (Arklow, Ireland). Deionized (DI) water (specific conductivity<1 µS cm^{-1}, pH 6-7) was used for the

preparation of all solutions. Phosphate buffered saline (PBS) tablets (pH 7.4) from Sigma Aldrich (Arklow, Ireland) were used for the preparations of phosphate buffer solutions. One tablet was dissolved in 200 mL of DI water to prepare the PBS solution to yield 0.01 M phosphate buffer, 0.0027 M potassium chloride and 0.137 M sodium chloride, pH 7.4, at 25°C.

2.2.2 Surface tension measurement of micelle systems

Surface tension measurements were performed using contact angle measurement to measure the surface tension value of the micelles. Surface tension values (σ) as a function of concentration (mol/L) were determined by the pendant drop method at room temperature.[204] Each PF127 solution was transferred to a syringe connected with a syringe plunger, followed by the connection of the syringe with the contact angle measuring machine (KRUSS G10 contact-angle measuring instrument, Hamburg, Germany). After that, a pendant drop below the needle was photographed by a camera for analysis through drop shape analysis software (KRUSS G10 for Windows 9x/NT4/2000). The surface tensions of DI water and PBS were set in the range of 71-73 mN m^{-1} at 25°C, and the data are presented as the mean ± standard deviation (SD) (n=3).

2.2.3 Preparation of micelle systems by direct dissolution

Micelles were prepared as outlined in the work of Pepic *et al*, with slight modifications.[212] Stock solutions of PF127 (31 %(w/v)) were prepared by dissolving PF127 in DI water (pH 6-7) or PBS solution (pH 7.4) for 24 h at 4°C. Solutions of PF127 were then prepared by diluting the stock solution in the concentration range of 5.21×10^{-5} %(w/v) to 31 %(w/v) at 25°C. One set of solutions was prepared in DI water only, and another set was prepared with PBS.

2.2.4 Size and zeta potential measurement of Pluronic F127 micelles

The particle size (percentage by volume), polydispersity index (PDI), and zeta potential (ZP) of the micelles were measured by DLS using a Microtrac Nanotrac Wave II instrument. The temperature was maintained at 25°C with an angle of detection of 180° with the heterodyne-backscatter arrangement. This measurement was performed directly after preparing the PF127 blank micelles in different concentrations. Specifically, 1 mL

of the PF127 micelles was placed in a sample cell. Then, the analysis of both electrophoretic mobility for ZP and the volume size distribution was performed using FLEX software. All results presented as the mean ± SD (n=3).

2.2.5 Stability assay of micellar solutions

PF127 micelles (23.04 %(w/v)) in solution, as prepared in Section 2.2.3, were immersed in liquid nitrogen (-196°C) for 20 min. The samples were then placed in a laboratory freeze dryer (Labconco, UK). Freeze-dried samples were reconstituted by adding the original volume of DI water to a final PF127 concentration of 140 mg/mL while stirring at 25°C for 20 min. Reconstituted micelles were diluted with DI water in different concentration ranges (0.15-14 %(w/v)), with continued stirring for a further 24 h, before measuring the micelle size and size distribution by DLS (Microtrac Nanotrac Wave II, US), as per Section 2.2.4. Then, each of the reconstituted micelles at different concentrations was sonicated (Sonics vibra-cell ultrasonic processors, US) for 5 min with an amplitude of sonication of 60% at 25°C and analysed by DLS. The mean value was recorded as an average of three measurements.

2.2.6 Differential scanning calorimetry measurement

Differential scanning calorimetry (DSC) measurements were performed on a TA instrument Q2000 (TA instruments, UK). 10-20 mg of sample was accurately weighed out and placed in a standard Tzero pan with a lid. A pinhole to prevent the pan from bursting and to allow the escape of water vapour was then created in the crimped pan before inserting it in the DSC sample holder and heating it from 0 to 140°C at 1°C/min, followed by holding the temperature at 140°C for 10 min. After that, the sample was cooled from 140°C to 20°C at 10°C/min.[205]: An empty aluminum pan was used as a reference.

2.2.7 Transmission electron microscopy analysis of Pluronic F127 micelles

The morphologies of PF127 blank formulations in solution were examined by transmission electron microscopy (TEM) (Thermo-Fisher Scientific FEI double-aberration-corrected monochromatic Titan Themis Z) at the Bernal Institute, University

of Limerick, Ireland. The PF127 micelles were diluted with distilled water and stained with 0.1% uranyl acetate, followed by placement on nickel grids for TEM observation. TEM imaging was carried out using a Gatan OneView camera.

2.2.8 Statistical analysis

Statistical significance was determined using independent samples t-test analysis of variance on the mean ± SD from three different experiments for comparing the hydrodynamic measurement of the Pluronic F127 micelles experiment with the literature studies. A comparison between the groups of the stability test of the Pluronic F127 micelle dispersion study was performed using One-way ANOVA followed by Dunnett's multiple comparison test. GraphPad Prism software (Prism 10.1.1) was employed for the statistical analysis, and results were considered significant if $p \leq 0.05$.

2.3 Results and discussion

The goal of this chapter was to optimise and prepare micelles using PF127 copolymers. To that end, parameters including the PF127 concentration and the particle size, will be discussed in detail.

2.3.1 Surface tension determination of the critical micelle concentration

Our primary focus lies on utilizing micelles as a DDS. In such an application, the critical micelle concentration (CMC) plays a fundamental role in determining the stability and efficacy of the system. Here, surface tension studies were performed to determine the CMC value of the PF127 copolymers. Micelles are formed when the surfactant concentration is higher than the CMC (Figure 2.1), which is the minimum surfactant concentration required to form the micelles, and this value determines the thermodynamic stability of the micelles against possible dilution of the DDS.

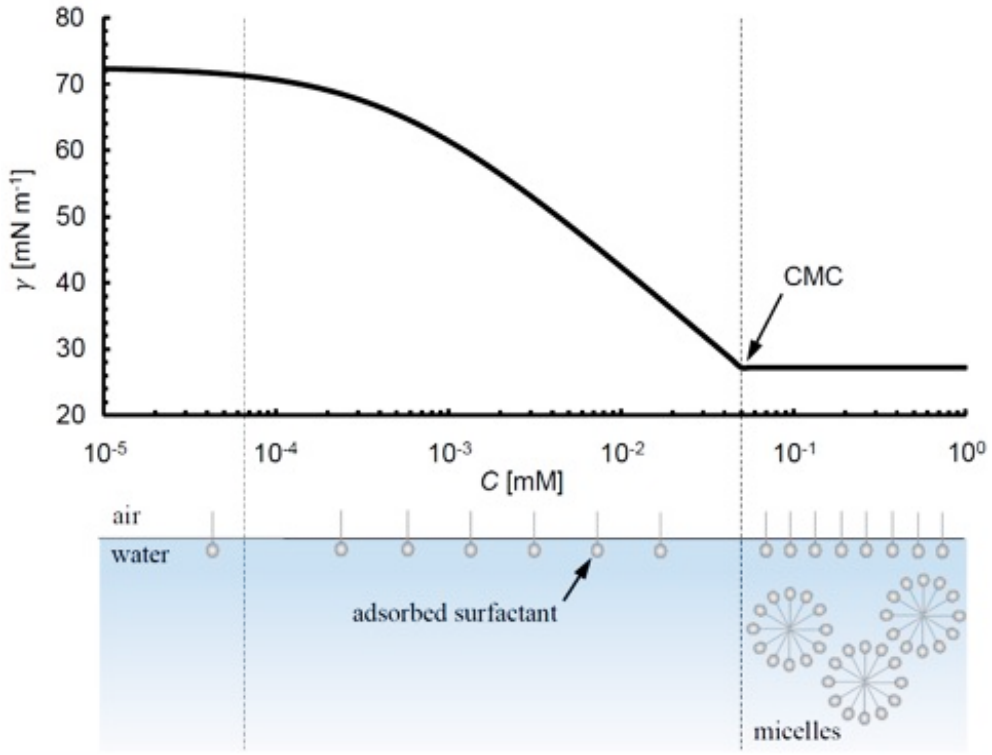

Figure 2.1: A schematic plot of surface tension as a function of the surfactant concentration and the transition of the formation of micelles.[206]

As illustrated in Figure 2.1, at low concentrations of surfactants, polymers tend to arrange themselves at the air/water interface, which has only a slight effect on surface tension. When more surfactant molecules are added to the solution, the surface tension value rapidly decreases until the interface of the solution is fully loaded with surfactant molecules. At this, the CMC point, surface tension reaches equilibrium, and the interface of the solute becomes too crowded, resulting in an arrangement of the surfactant molecules into micelles (Figure 2.1). Consequently, the surface tension of the solution is independent of concentration, and the addition of surfactants will no longer affect the surface tension at concentrations above this value. Therefore, surface tension measurements can be utilized to determine the CMC, a pivotal parameter in understanding the behavior of surfactants. In addition, the CMC is crucial for designing efficient DDS as it governs the formation and stability of micelles, which play a crucial role in drug encapsulation and targeted delivery. For instance, the concentration of the surfactant

needs to be higher than the CMC to ensure the formation of micelles and maintain the drug encapsulated within the micelles.

Furthermore, the PF127 concentration at which gelation takes place must be considered since it can significantly impact the properties and behavior of the solutions. Also, temperature is an essential factor that can significantly affect the ability of PF127 to form a gel, particularly at high temperatures (Figure 2.2(I)).[207]

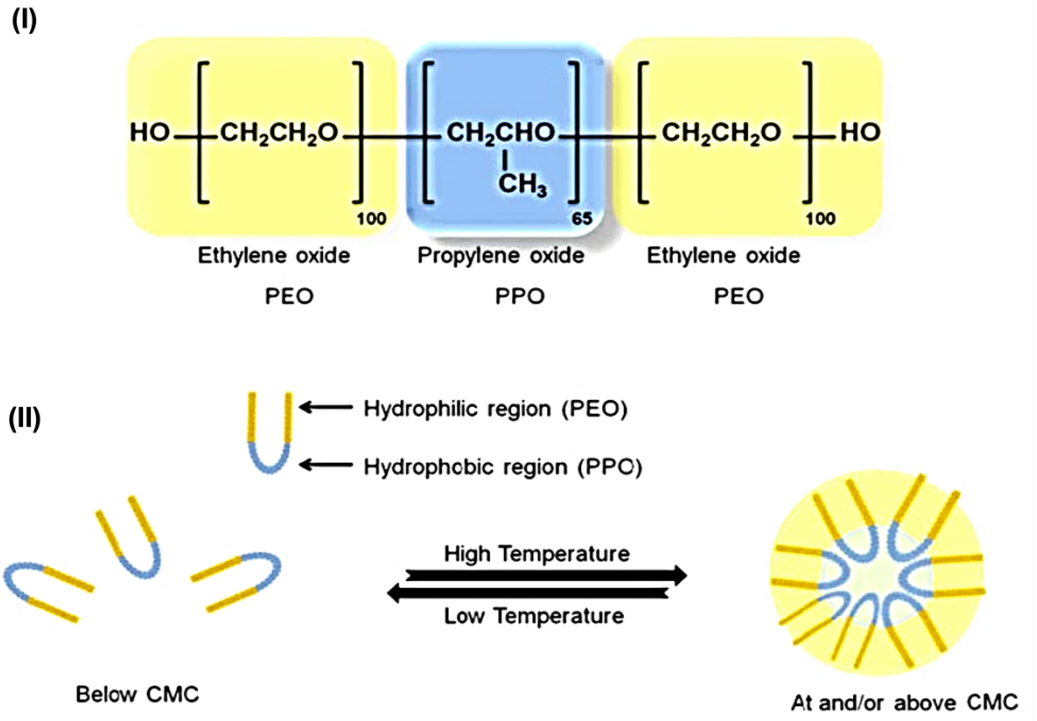

Figure 2.2: (I) the structural formula of PF127 block copolymer and (II) a schematic representation of the formation of micelles in PF127. CMC:critical micelle concentration; PPO:poly(propylene oxide); PEO:poly(ethylene oxide).[208,209]

As illustrated in Figure 2.2, the structure of PF127 is composed of triblock copolymers with repeated units of hydrophobic PPO as a central core surrounded by hydrophilic segments of PEO (Figure 2.2(I)). Based on this arrangement, temperature changes in the structure of the water surrounding the PPO blocks of PF127 influence the aggregation behavior and gelation process of PF127.[210,211] More precisely, at low concentrations or below the CMC, PF127 exists in solutions as individual coils or unimers, and these

unimers arrange themselves to form micelles when increasing in the concentration of the copolymer above the CMC (Figure 2.2(II)).[208] Similarly, the equilibrium shifts the unimers to form micelles with increasing temperature since the numbers of unassociated unimers are reduced owing to the gelation of the micelles. This phenomenon is attributed to an increase in the dehydration of the PEO block, which leads to aggregation of the micelles as the temperature increases, resulting in increased intermolecular hydrophobic interaction between PF127 chains. Thus, the gelation process and CMC of PF127 depend on both temperatures and the PF127 concentration used.[212]

Taking this point to our studies, it was demonstrated that when preparing different concentrations of PF127, gelation was observed with a PF127 concentration of 23 %(w/v) at 25°C (Figure 2.3).

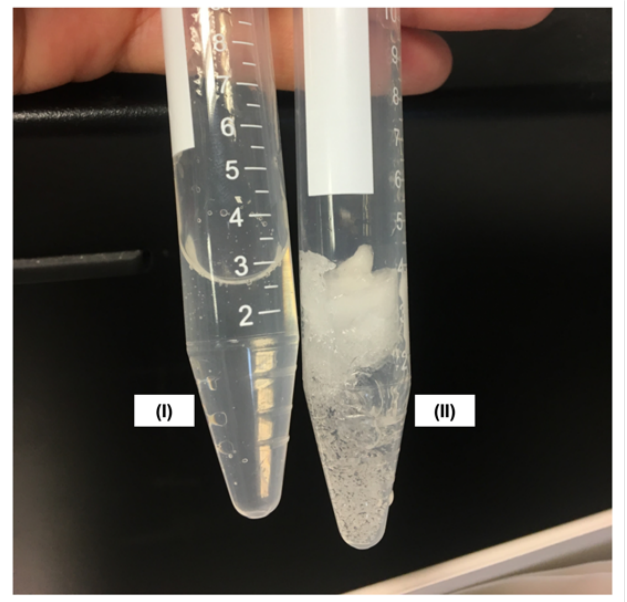

Figure 2.3: An image for the PF127 blank micelles with concentration (I) 14 %(w/v) and (II) 23 %(w/v) at 25°C.

Based on the present study, it was found that below 14 %(w/v), PF127 did not form gels at 25°C (Figure 2.3(I)), but above 14 %(w/v) of the PF127 solution at 25°C, gels were formed (Figure 2.3(II)), which was in accordance with the results of other studies reported previously.[207,213] Consequently, the study focused on preparing PF127 micelles in the

form of a micelle solution for OcDD, choosing concentrations below 14 %(w/v) for further study since the gelation of PF127 can cause potential disadvantages, such as limited drug release, administration difficulties, and patient discomfort during administration.

2.3.1.1 Critical micelle concentration for Pluronic F127 solutions

As previously mentioned, PF127 concentrations ranging from 5.21 x 10^{-5} %(w/v) to 14 %(w/v) were selected for surface tension measurement. The surface tension studies of PF127 were carried out in DI water and PBS solutions. Figure 2.4 shows a graph plotted between the surface tension (σ) and logarithm concentration (ln C, mol/L) of PF127 solutions.

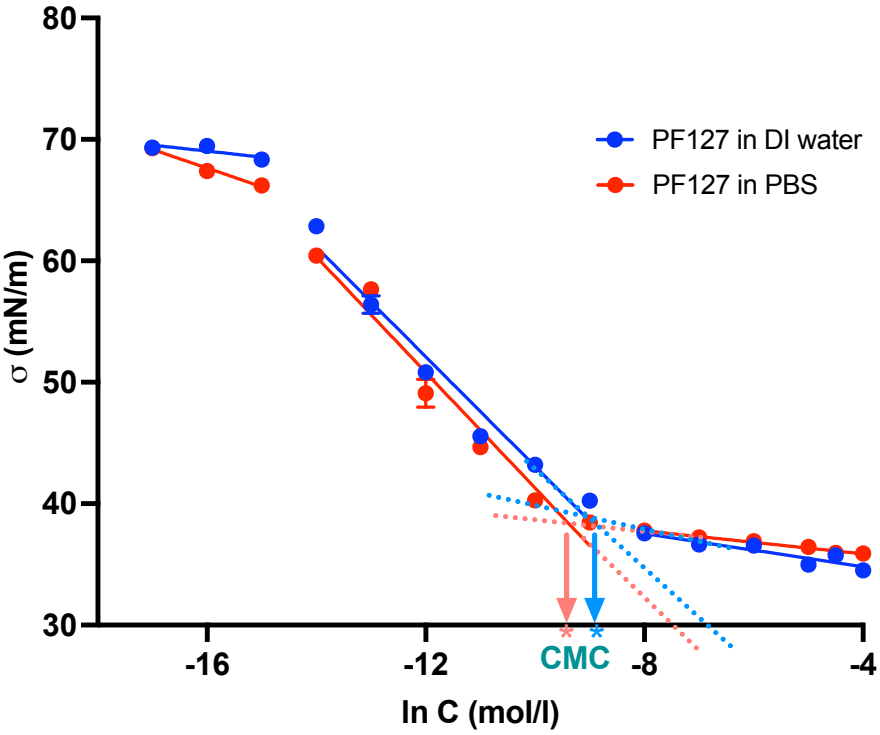

Figure 2.4: The isotherm of surface tension in aqueous solutions of PF127 copolymer at 25°C of PF127 solutions in DI water (pH6-7) and PF127 in PBS solution (pH 7.4); CMC=critical micelle concentration. All measurements were repeated three times, and the bars indicate the standard deviation (SD) of the mean.

As shown in Figure 2.4, the CMC is identified at the intersection point of two straight lines between the surface tension and PF127 concentration. Based on this study, the CMC for PF127 in DI water and PBS solution were 0.21 ± 0.04 %(w/v) and 0.16 ± 0.05 %(w/v), respectively. The result was in the same order of magnitude as the results of other investigators, e.g. Pepic *et al.* have found the CMC value of 0.50 ± 0.2 %(w/v) and 0.51 ± 0.3 %(w/v) in DI water and PBS solution, respectively, at 25 ºC (p>0.05 in DI water and PBS).[214] Similarly, Gyulai *et al.* also reported that the CMC value of PF127 in DI water was equal to 0.33 ± 0.1 %(w/v) at 25 ºC (p>0.05 in DI water).[215] Hence, the data provides preliminary evidence and theoretical support for the formation of micelles based on PF127 copolymers.

When applying eye drops, it is crucial to consider the tear volume and the interaction between the drop and the natural tear film. On average, the capacity of the tear volume in a healthy human eye (~7-10 μL) is smaller than the volume of commercial drop dispensers (25-50 μL), causing the volume of the commercial eye drops to exceed the tear film's capacity when applied onto the ocular surface. Liquid drops mostly drain out of the eye via blinking, tear turnover, and nasolacrimal drainage, with a small amount reaching the anterior ocular tissue for further absorption.[216] For this reason, the concentration selection to prepare the micelles is essential as it relates to the micelle stability upon dilution into physiological conditions before reaching the target site. On the one hand, micelles below the CMC concentration may disassemble, leading to instability of the formulation and poor drug release. On the other hand, micelles above the CMC are more stable and can efficiently encapsulate drugs, protecting them from degradation or dilution when administered, which results in delivering a proper therapeutic drug dose to reach the target site. Consequently, to improve ocular topical drug delivery, previous research studies have developed several strategies of nanoformulations to minimize precorneal drug loss and maximize corneal drug absorption. Alambiaga-Caravaca *et al*. designed progesterone (PG)-loaded Pluronic F68/Soluplus® micelles to increase the drug dose of PG by increasing its solubility.[217] Their study found that around 4 nm-sized Pluronic F68 (23.95 mM) and 59 nm-sized Soluplus® (1.74 mM) increased the PG solubility up to 250 and 25 μg/mL, respectively.

Furthermore, their results indicated the advantage of Soluplus®, with the extremely low CMC value ($6.6x10^{-5}$ mM), to be more stable against dilution when applying the formulation to the ocular surface than Pluronic F68 ($4.0x10^{-2}$ mM), enhancing PG drug penetration into porcine eyes' corneas. 1 mL of both Soluplus® and Pluronic F68 micelle solution added into the donor chamber showed greater PG accumulations in the cornea of the porcine eyes in the receptor compartments at 4 h in diffusion tests with 2.44 μg/cm^2 and 0.77 μg/cm^2, respectively, supporting the enhancement of the micelles at the concentration above CMC point in helping permeation of the PG drug into the corneal tissue. Similarly, Uchegbu *et al.* developed micelles for cyclosporine A (CsA) enhancement into ocular tissues using molecular envelope technology (MET) polymer (N-palmitoyl-N-monomethyl-N,N-dimethyl-N,N,N-trimethyl-6-O-glycolchitosan) that had the CMC value in the low micromolar region (1-2.4 μM)).[218] Their study demonstrated that their new CsA eye drop at the concentration above CMC (0.75 %(w/v)) with a topical drug dose of 12.5 μg showed a 5- to 6-fold increase in drug absorption into the rabbit's cornea compared to the Restasis commercial formulations at the same drug dose, supporting the efficient delivery of the CsA-loaded MET micelles at a concentration above CMC on the ocular surface.

Therefore, understanding the CMC of micelles in OcDD is important for designing efficient and stable drug delivery vehicles that can improve the efficacy of ocular therapies.

2.3.2 Thermal analysis of the micellization process

Differential scanning calorimetry (DSC) is a thermal analysis technique used for measuring the CMC of surfactants by detecting changes in the heat flow associated with micelle formation or dissolution. Micellization is an endothermic process that can be measured by DSC (Figure 2.5).[219,220]

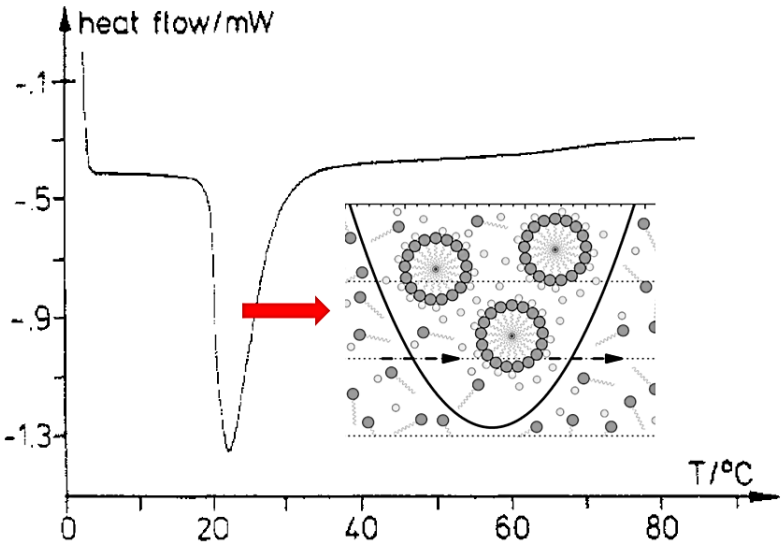

Figure 2.5: Representative transient DSC signal for the micelle formation and scheme of the micellization process observed in DSC experiments.[221]

As depicted in Figure 2.5, no spontaneous formation of micelles occurs at temperatures below the micellization temperature. In contrast, when the temperature increases, the solution undergoes a monomer-micelle transition for constant concentration. Indeed, water molecules surrounding the hydrophilic part of the surfactant will evaporate at a higher temperature. It affects the solubility of the surfactant by decreasing the polarity of both the hydrophobic and hydrophilic parts of the surfactant. Consequently, it permits the chains of the surfactant to come together, resulting in micellization at a specific temperature. Additionally, this heat is due to the dehydration of the hydrophobic PPO groups from the block copolymers of PF127, known as the heat of micellization (ΔH_m), during the heating process of DSC, in which the large change of the critical micelle temperature (CMT) value can be quantitatively measured by the large ΔH_m values.[230] Thus, DSC can obtain temperature-dependent thermodynamic parameters for micellization.[229]

In this study, the PF127 solutions above the CMC, determined by surface tension (Figure 2.4), in which micelles are formed, were selected for DSC characterization. Figure 2.6 shows the DSC thermogram of PF127 solution in DI water and PBS (Figure 2.6 (I)-(II)),

respectively, including the graph of CMT from DSC at different concentrations of PF127 copolymer solution in DI water and PBS (Figure 2.6(III)).

(I)

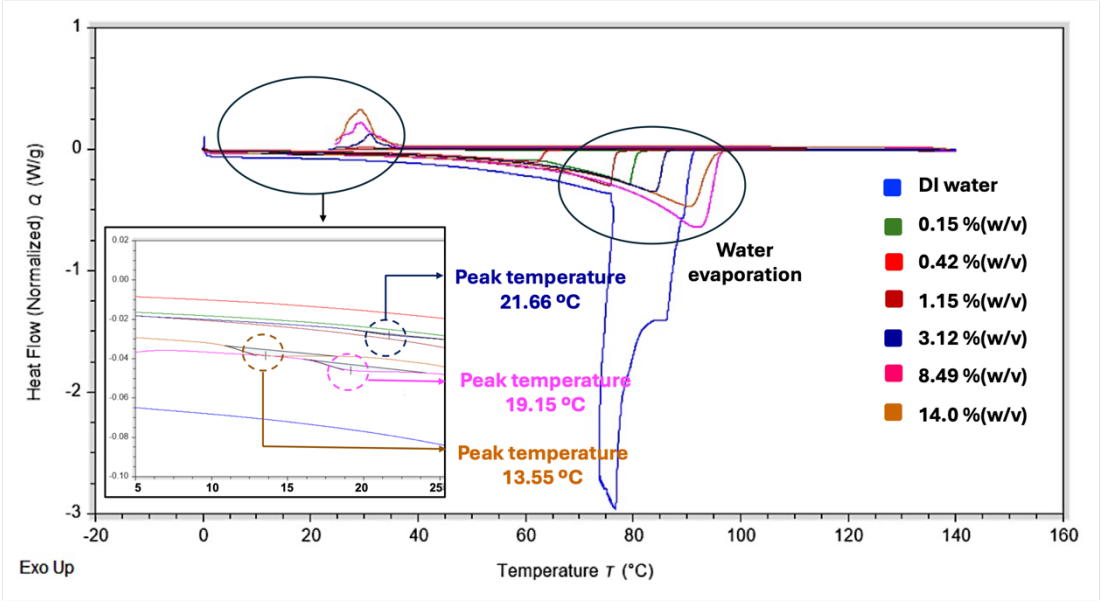

(II)

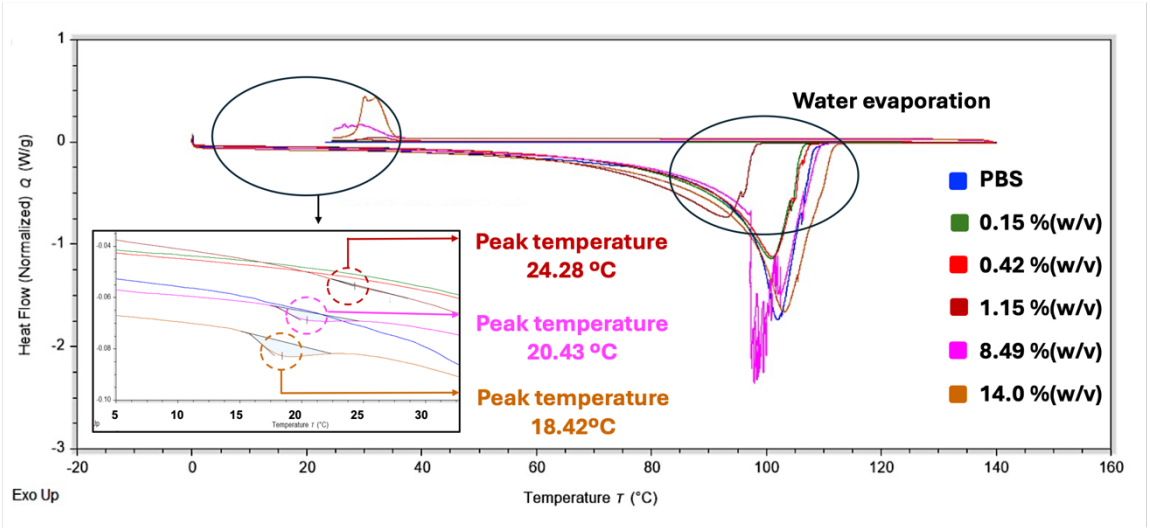

(III)

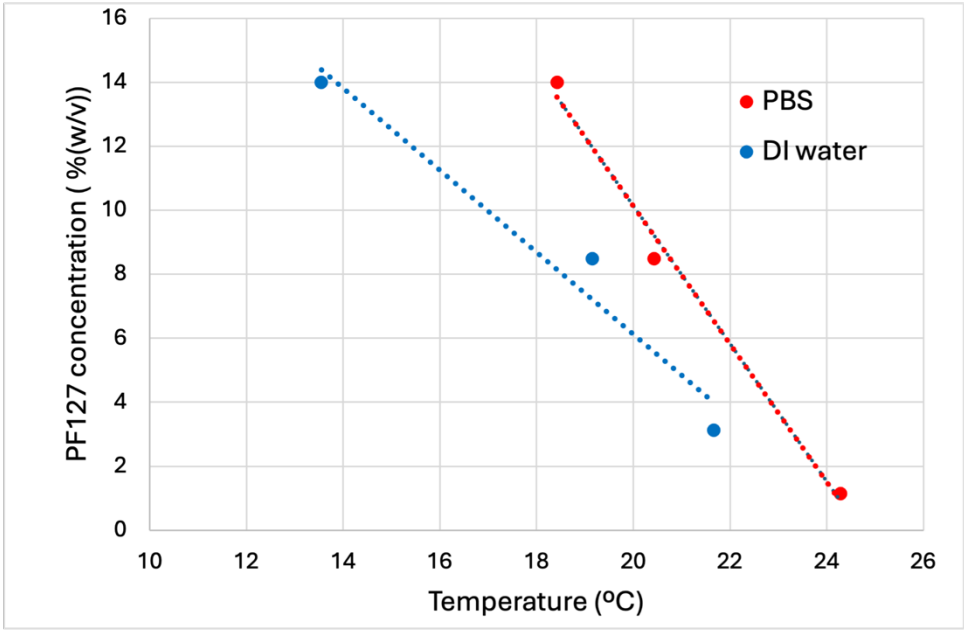

Figure 2.6: DSC signal recorded during the heating/ cooling of freeze-dried PF127 micelles (0.15 %, 0.42 %, 1.15 %, 3.12 %, 8.49 % and 14 %(w/v)) in (I) DI water and (II) PBS. The continuous line represents the DSC signal. Insert is the zone where micellization occurs and (III) values for the temperature at the maximum of the DSC peak at different concentrations of PF127 copolymer solution in DI water and PBS.

As shown in Figure 2.6, during PF127 sample heating, the first phenomenon that takes place was identified as micellization, which is an endothermic phenomenon. In terms of PF127 solution in DI water, it indicated that the micellization phenomenon of PF127 micelles with concentrations between 3.12 and 14 %(w/v) took place around 14-22°C (Figure 2.6(I)). In comparison, micellization temperatures ranging from 18 to 25°C were obtained from PF127 solution (1.15-14 %(w/v)) in PBS (Figure 2.6(II)).

Moreover, the data provided convincing evidence that the CMT values for PF127 solution in both DI water and PBS decrease linearly with increasing PF127 concentrations (Figure 2.6(III)), which was similar to other previous studies.[201,222] This refers to the fact that increasing concentrations can lead to more frequent interactions between the hydrophobic portions of the surfactant molecules, promoting micelle formation at lower temperatures. In other words, a higher concentration of surfactant molecules would change the position

of the equilibrium towards micellization such that the surfactant molecules will 'find' each other and assemble into micelles, which can occur at lower temperatures compared to a more diluted solution. This is because the formation of micelles is a way to minimize the unfavorable interaction between the hydrophobic parts of the surfactant molecules and water. As concentration increases, the system can reach this minimized energy state at a lower temperature. Hence, a lower CMT achieved through increasing polymer concentration in a DDS could offer advantages such as improved stability, increased drug loading capacity, and controlled drug release.[223]

In addition, another large endothermic peak observed during the heating process at around 100 °C was the water evaporation process, which requires a significant amount of energy (Figure 2.6 (I)-(II)). Additionally, during the cooling process, the exothermic peak of PF127 from solidification appeared around 30°C in both DI water and PBS solution (Figure 2.6 (I)-(II)), a result that also corresponded with other investigators.[205,224] For example, Barba *et al.* have found that the solidification with a related exothermic peak was around 35°C for a PF127 solution in DI water (20 %(w/w)).[205] In the same way, the study carried out by Mata *et al.* revealed that a small peak observed in the DSC curve of Pluronic L64 ($EO_{13}PO_{30}EO_{13}$) at a high temperature (~85°C) was the precipitation temperature peak of the Pluronic L64 copolymers.[207] Thus, DSC results in the present study also confirmed the formation of micelles in PF127 solutions in conjunction with the surface tension measurement.

2.3.3 Hydrodynamic diameter measurements of Pluronic F127 micelles

The direct dissolution method, as per Section 2.2.3, was employed for the preparation of PF127 micelles. Here, micelle size was studied using DLS at PF127 concentrations ranging from 0.15-14 %(w/v), with the lowest concentration chosen (0.15 %(w/v)) due to its concentration at the CMC. Table 2.1 presents the particle size measurement of these micelle systems.

Table 2.1: The hydrodynamic diameter (D_h, percentage by volume) and polydispersity index (PDI) results of PF127 solution in different concentrations in DI water and PBS solution. All measurements were repeated 3 times. The data are presented as the mean ± SD (n=3).

Formulation code	Solution	PF127 %(w/v)	DLS	
			D_h (nm, vol%)	PDI
BK5-1	DI water	0.15	4.47 ± 1.76	1.35 ± 0.98
BK5-2		0.42	4.56 ± 0.28	0.96 ± 1.52
BK5-3		1.15	4.66 ± 0.44	1.07 ± 0.78
BK5-4		3.12	4.01 ± 0.09	0.81 ± 0.13
BK5-5		8.49	3.48 ± 0.09	0.49 ± 0.59
BK5-6		14.00	3.22 ± 0.11	0.35 ± 0.22
BK5-7	PBS	0.15	7.91 ± 8.91	1.55 ± 1.27
BK5-8		0.42	3.65 ± 0.65	1.18 ± 1.23
BK5-9		1.15	4.08 ± 0.46	0.62 ± 0.74
BK5-10		3.12	3.68 ± 0.14	0.16 ± 0.07
BK5-11		8.49	3.52 ± 0.01	0.93 ± 0.66
BK5-12		14.00	3.53 ± 0.19	0.57 ± 0.63

The PF127 solution in both DI water and PBS was seen to self-assemble into micelles (Table 2.1). The ZP value is not shown in Table 2.1, as the particle size was below the limit of measurement for ZP on this particular instrument. Based on the study, it revealed that there was no statistical difference between the mean particle sizes and PDI values of all concentrations of PF127 solutions in DI water and PBS (p>0.05, independent samples t-test) (Table 2.1). The average size (hydrodynamic diameter) of PF127 micelles in both DI water and PBS were in the range of 3-5 nm, with PDI ranging from 0.19 to 1.55. Additionally, the particle size distribution of PF127 solution in DI water and PBS solution was further evaluated (Figure 2.7).

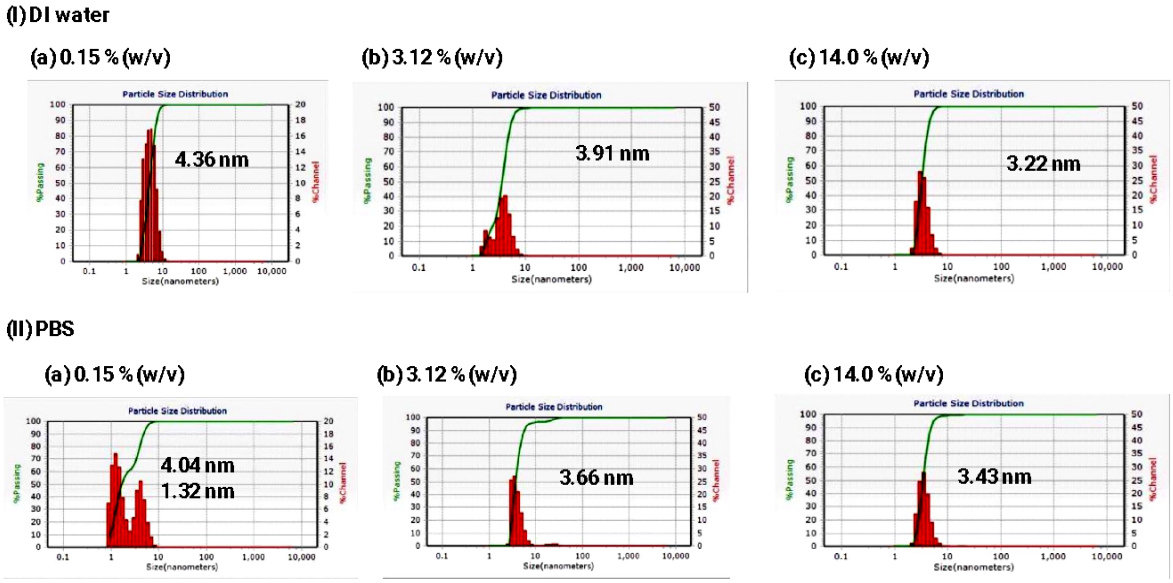

Figure 2.7: A representative example of particle size distribution curves comparing PF127 nanomicelles in different concentrations in (I) DI water and (II) PBS solutions; (a) 0.15 %(w/v), (b) 3.12 %(w/v) and (c) 14 %(w/v).

As shown in Figure 2.7, the particle size distribution graphs illustrated that PF127 micelles in different concentrations over the CMC point in both DI water and PBS displayed a monodisperse distribution of particle sizes, results that were consistent with previous studies.[225,226] For instance, Song *et al.* prepared ultra-small micelles based on rebaudioside A (RA) to prolong the therapeutic effects of pterostilbene (Pt).[225] Nanomicelles sized less than 4 nm with a PDI of 0.3 were observed in the RA-Pt ophthalmic solution (RA:Pt=14:1). Also, results produced by Pepic *et al*. showed the nanosized micelles (29 nm) prepared from dexamethasone-loaded PF127/chitosan (CH) micelles with a PDI value of 0.52.[146]

In addition, our study was further examined the morphology of the PF127 micelles by TEM (Figure 2.8). In this study, micelles with a PF127 concentration of 3.12 %(w/v) were selected for this investigation since this concentration was over the CMC point and did not become gel at 25°C.

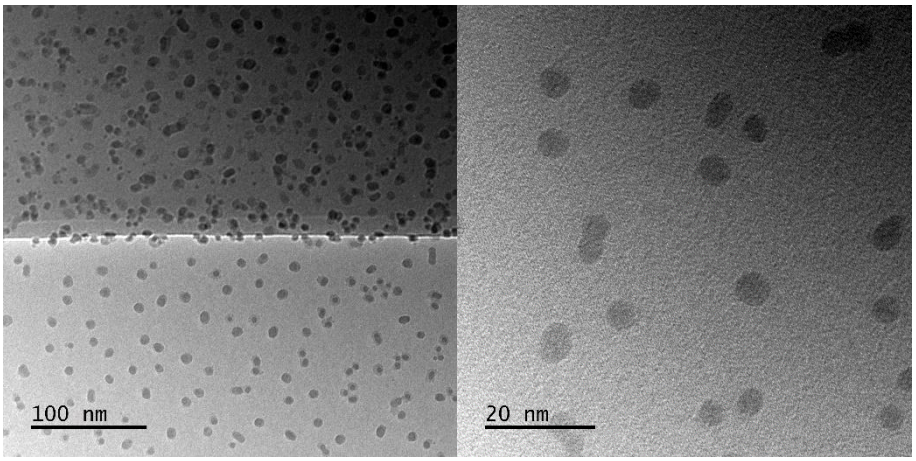

Figure 2.8: Transmission electron microscopy morphology of PF127 micelles (3.12 %(w/v)) (bar=100 nm and 20 nm).

Based on the DLS result, PF127 had an ultra-small micelle size (4.01 ± 0.09 nm) and a uniform size distribution (PDI value~0.81) under such conditions (BK5-4, Table 2.1). Moreover, TEM observation showed that the micelles were spherical in shape (<20 nm) and lacked obvious aggregation (Figure 2.8). Hence, our findings provide strong evidence that PF127 could form the micelles, as per reference to the work carried out by Wu and colleagues using TEM to confirm their micelle formations with a particle size of around 4 nm.[225,227]

Therefore, in the context of OcDD, PF127 micelles with a size range of 3-4 nm can efficiently solubilize hydrophobic drugs, increasing their bioavailability and therapeutic efficacy in ocular tissues. Furthermore, this small size of micelles may enhance their permeability across ocular barriers, allowing for better drug penetration into the target tissues, such as the cornea and sclera, with reduced irritation compared to the larger micelles.[196,217,228] However, rapid clearance due to the small sizes of the micelles could be one of the major problems. In other words, the small-size micelles may have more rapid drug release than large micelles, reducing the duration of drug action and requiring more frequent dosing. For example, Lin *et al*. exhibited a high *in vivo* drug release rate of exenatide-microspheres (MSs) from small MSs (3.8 μm) (C_{max}=270 ng/mL) compared to large MSs (18.2 μm) (C_{max}=200 ng/mL) during the first 8 h.[229] This high initial drug release of the small MSs could lead to a high surface area to volume ratio compared to

larger MS. Indeed, this increased surface area provides more sites for plasma molecules to be exposed to the surrounding medium, resulting in faster initial drug release.[229]

Overall, while small particles can offer advantages including improved bioavailability and tissue penetration, they are more prone to burst drug release owing to their physicochemical properties. Therefore, these literature studies, combined with our results, indicated that the micelle size and PDI value depend on both the concentration of surfactant used and the amount of surfactant added. Also, the particle sizes affect the drug release profiles of the drug. Optimization of these parameters, along with conducting the stability study, is crucial to ensure the long-term viability and efficacy of the nanoformulations as effective OcDD systems based on PF127 micelles. As a consequence, the following section is focused on studying the effect of freeze-drying and sonication on the particle sizes and PDI of the PF127 micelles.

2.3.4 The stability of the Pluronic F127 micelle dispersions after resuspension of the freeze-dried samples in DI water and additional sonication

This section will further investigate the stability of the PF127 micelle system in different concentrations to evaluate their stability after processing using two techniques: freeze-drying and sonication.[230,231] The former is a useful process for obtaining a micelle powdered form that preserves the original properties of the pharmaceutical product over an extended period of time. While the latter method is used to de-agglomerate and disperse micelles in the solution. Hence, both techniques may be necessary to improve the homogeneity and stability of the suspension.

To evaluate the effect of freeze-drying and sonication processes on the micelle size and PDI of the PF127 micelles, the hydrodynamic diameter and the size distribution were measured by DLS (Table 2.2).

Table 2.2: The particle size (nm, percentage by volume) and size distribution of PF127 blank micelles in different concentrations of PF127 in DI water before and after freeze-drying and sonication processes. Data are presented as the mean ± SD (n=3).

Solution, PF127% (w/v)	DLS measurement					
	After preparing		After freeze-drying		After sonication	
	D_h (nm, vol%)	PDI	D_h (nm, vol%)	PDI	D_h (nm, vol%)	PDI
0.15	4.47 ± 1.76	1.35 ± 0.98	4.13 ± 1.75	0.91 ± 0.64	3.82 ± 0.81	0.98 ± 0.63
0.42	4.56 ± 0.28	0.96 ± 1.52	4.36 ± 0.53	0.77 ± 0.38	4.65 ± 1.00	0.56 ± 0.27
1.15	4.66 ± 0.44	1.07 ± 0.78	4.46 ± 0.15	0.41 ± 0.33	4.61 ± 0.04	1.14 ± 0.75
3.12	4.01 ± 0.09	0.81 ± 0.13	3.94 ± 0.06	0.66 ± 0.25	4.33 ± 0.42	0.57 ± 0.20
8.49	3.48 ± 0.09	0.49 ± 0.59	3.80 ± 0.36	1.07 ± 1.27	3.58 ± 0.09	0.79 ± 0.86
14.00	3.22 ± 0.11	0.35 ± 0.22	3.92 ± 1.13	1.00 ± 0.72	3.56 ± 0.09	1.00 ± 0.68

DLS results showed that all the particle sizes of PF127 micelles were small (3-4 nm, PDI=0.35-1.35) (Table 2.2). In addition, there was no significant change in the mean values across the particle sizes and PDI of all concentrations of PF127 triblock copolymer (p>0.05, One-way ANOVA followed by Dunnett's multiple comparison test), although there was a noticeable variation in the PDI value of the PF127 micelles after freeze-drying and sonication (Table 2.2), results that were again similar to previous studies.[226,232,233] Furthermore, the appearance of prepared PF127 micelles after freeze-drying and sonication was photographed, as the results are shown in Figure 2.9.

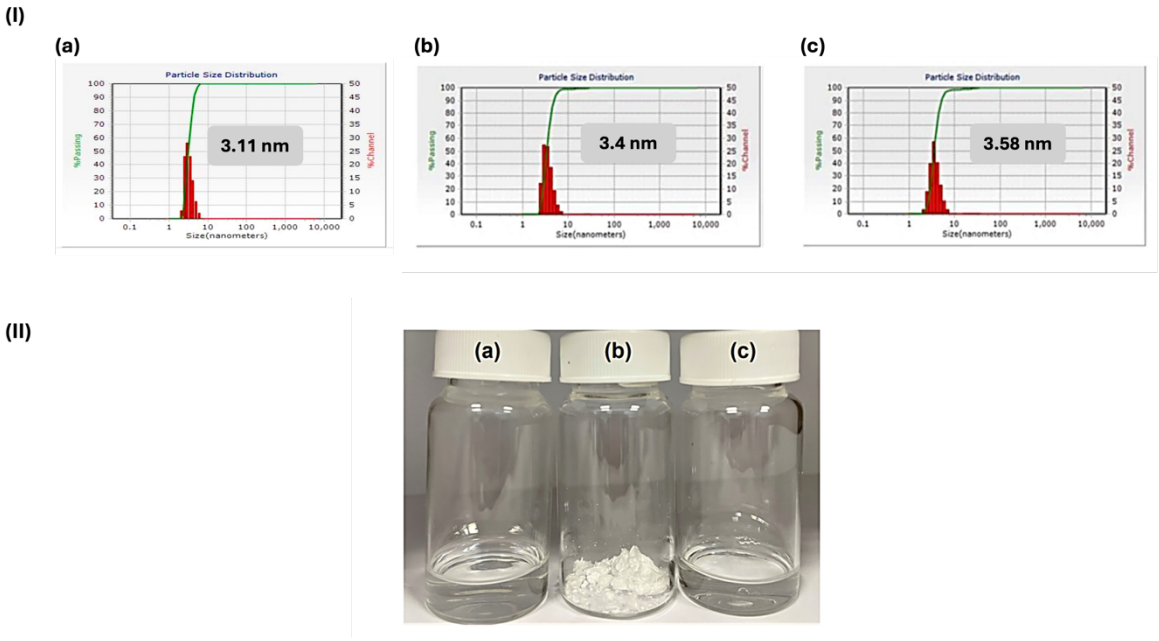

Figure 2.9: A photograph representation of (I) an example of particle size distribution curve comparing PF127 nanomicelles (13.19 %(w/v)) in DI water in different stages; (a) after preparation, (b) resuspended in DI water after freeze-drying, and continued with (c) sonication, and (II) the appearances of (a) PF127 blank micelles after preparation (b) freeze-dried PF127 blank micelles and (c) reconstituted PF127 blank micelles at 13.19 %(w/v) in DI water.

Figure 2.9(I) showed that the particle size distribution displayed a monodisperse sample of the micelles. Additionally, in terms of the appearance of the freeze-dried micelles and reconstituted micellar solution, it was clear that the freeze-dried PF127 micelles were completely dispersed in DI water by gently stirring at room temperature without heating, which also suggests that the PF127 micelles were relatively stable during freeze-drying (Figure 2.9(II)). Thus, this study shows that freeze-drying and sonication processes had negligible effects on both the particle sizes and PDI of the studied PF127 micelles within the concentration range of 0.15-14 %(w/v), indicating the stability of all reconstituted PF127 micelles after freeze-drying and sonication. A similar investigation has also been made by Varshosaz *et al.*[234] They examined the stability of the folic acid-targeted PF127/cholesteryl hemisuccinate micelles upon dilution with PBS pH 7.4 after freeze-drying and found that the particle sizes and PDI of the nanomicelles remained approximately constant with no significant change after dilution for 24 h (size=156.9 ±

6.15 nm, PDI~0.385). In addition, most of the research on studying the effect of sonication on the micelle size demonstrates that the sonication process of freeze-dried samples helps to disperse or break up agglomerated particles of the micelle in the aqueous suspensions, leading to a decrease in PDI values and a more unimodal distribution of the PF127 micelle size after sonication.[235] For example, the study carried out by Zhao *et al.* demonstrated that the energy provided by sonication could break the large polymeric aggregates formed by PEO-based amphiphilic block copolymers in the aqueous solution, which leads to monodisperse micelles.[230,235,236] As the sonication time increased from 1 to 7 min, the hydrodynamic radius distribution of PEO-*b*-polyisoprene (PEO=82 %(w/w)) decreased substantially from 100 nm to 50 nm, respectively. Similarly, Kataoka and co-workers pointed out the efficacy of sonication in breaking large copolymer PEO-*b*-poly(amino acid) based polymeric micelles into well-dispersed micelles after dialysis.[236] The large particle sizes (approximately 200-800 nm) were broken down into 71 nm sized copolymer PEO-*b*-poly(amino acid) based polymeric micelles after 60 min of sonication. Therefore, these studies provide support for the validity of using freeze-drying and sonication processes to prepare micelles that are readily dispersed in aqueous solutions.

Taken together, this study demonstrated a monodisperse sample distribution of PF127 nanomicelles, which means that the nanomicelles are all of similar size or have a narrow size distribution. This uniformity can lead to more consistent behavior without aggregation and sedimentation compared to polydisperse samples in drug delivery applications where precise control over particle size can be crucial for effective targeting and release.[237,238] Also, the results showed the stability of the PF127 micelles in the concentrations ranging from 0.15-14 %(w/v) after freeze-drying and sonication processes, which supported the advantages in storage stability of the nanomicelles in freeze-dried powder for clinical use.

2.4 Conclusion

Micelle systems composed of the polyoxyethylated nonionic surfactant Pluronic F127 (PF127) were successfully prepared by direct dissolution. Solutions of surface active PF127 in the vicinity of the CMC were produced in DI water and PBS. The CMC of

PF127 solution in DI water and PBS solution were 0.21 ± 0.04 and 0.16 ± 0.05 %(w/v), respectively. Furthermore, the micellization phenomenon of the PF127 micelles was confirmed by DSC analysis, which took place around 25°C and 21°C in DI water and PBS solution, respectively. The PF127 micelles were then characterized by their hydrodynamic diameter, which ranged between 3 and 5 nm, with PDIs ranging from 0.015 to 0.16. TEM also confirmed that the particle sizes of PF127 micelles were less than 20 nm. This supported that PF127 could be self-assembled into small micelles in a homogeneous distribution state when dissolved in DI water and PBS. As such, the system provides strong evidence that PF127 can form nanomicelles at specific concentrations and temperature ranges. Moreover, the PF127 micelles showed good stability during the freeze-drying and sonication processes, which could improve their shelf life in pharmaceutical applications. Therefore, these PF127 micelles may prove to be effective nanocarriers for targeted OcDD. Additionally, careful consideration is needed when designing DDS since small changes in the system can produce a different outcome.

Chapter 3

Curcumin-loaded PF127 micelles

3.1 Introduction

Curcumin (CUR) is a water-insoluble pigment extracted from the Curcuma longa (turmeric) plant, which displays a wide range of physiological and pharmaceutical properties including anti-antioxidant, and anti-vascular endothelial growth factor (anti-VEGF) properties, as previously described in Chapter 1.[239] For that reason, CUR has been investigated for the treatment of age-related macular degeneration (AMD).[240–242] However, several challenges, namely the poor bioavailability resulting from low aqueous solubility (0.6 μg/mL, log P=3.4) and photodegradation of CUR, as well as the low oral bioavailability (1%) present restrictions in medical applications, including limitations on the efficacy of the drug in ocular tissues.[152,158,243,244] Consequently, the pharmaceutical application of CUR has been limited.

Developing CUR-loaded nanocarriers to overcome these problems is of significant usefulness as they have small sizes and can protect drugs from degradation, leading to higher drug concentrations in the target tissue and providing solubility and stability improvements of the drug.[58,245] Moreover, as discussed extensively in Chapters 1 and 2, considerable research attention has been paid to polymeric micelles (PMs) for ocular drug delivery (OcDD) owing to several advantages, such as improved drug solubility and enhanced tissue penetration.[122,158,246] In particular, PMs made from Pluronic block copolymers have proved to be effective carriers for hydrophobic drugs. Among other commercially available triblock copolymers, Pluronic F127 (PF127), which has FDA approval for pharmaceutical and medical applications, is an interesting copolymer due to its aggregation behaviour, as previously described in Chapter 2.[201] Recent studies have explored the use of the PF127 micelle as a potential carrier in the drug delivery system (DDS) of CUR. For example, Anirudhan *et al.* found that 22 nm-sized PF127/Pluronic P123 mixed micelles coated with hyaluronic acid (polydispersity index (PDI)~0.94)

could sustain a slow release of CUR (encapsulation efficiency (EE)~89%) and paclitaxel (PTX) (EE~85%) up to 4 days in pH 7.4 buffer solution.[247] Similarly, results obtained by Vaidya and co-workers revealed that the encapsulation of CUR into PF127 micelles (~26 nm) increased its chemical stability in water and slowed its metabolism, which supported an increase in cellular uptake with the slow and sustained release of CUR in human breast cancer cells.[248] However, some research on Pluronic block copolymers for micellar drug delivery revealed poor stability and a non-homogenous solution of micelles in the particle size due to different concentrations of PF127 used in the preparation of the micellar system.[201,249]

Although a variety of compounds can be encapsulated and solubilised in PF127 micelles, the potential of these block copolymers for the delivery of CUR, including the effects of different techniques used to prepare the CUR-encapsulated PF127 micelles, has not been studied. Herein, this research aims to investigate the hypothesis of using PMs from PF127 to encapsulate a small molecule therapeutic drug to potentially treat diseases in the back of the eye via topical administration. CUR-loaded PF127 micelles were prepared using different techniques for comparison. Furthermore, the influence of freeze-drying and sonication processes on the particle size of the micelles was examined. The physicochemical characterisation of the CUR/PF127 micelles, as well as the stability and drug release profiles, were also evaluated.

3.2 Materials and methods

3.2.1 Materials

As per Section 2.2.1 with the following additions: acetone (purity≥99.9%, HPLC grade), Tween-80, vanillic acid, coumarin 6 (Cou6), ortho-phosphoric acid (purity≥85%, MSDS), and fluorescein isothiocyanate (FITC) were all purchased from Sigma Aldrich (Arklow, Ireland). CUR (purity≥95%, HPLC grade) was purchased from Carbosynth Ltd. (Berkshire, UK) and was used as received without further purification. Vanillin was purchased from Honeywell Fluka (Ireland). Acetonitrile (ACN, HPLC grade), glacial acetic acid (HPLC grade), Methanol (MeOH, HPLC grade), and dimethyl sulfoxide (DMSO, HPLC grade) were provided by Fisher Scientific (Dublin, Ireland). Sodium

dodecyl sulfate (SDS) was purchased from Prolabo® (VWR, Ireland). Immortalized human corneal epithelial (IM-HCEpi) cells (P10871-IM) were obtained from Innoprot (Bizkaia, Spain). Reagents and solutions for medium preparation of human corneal epithelial (HCE-T) cells including dulbecco's modified eagle medium/nutrient mixture F-12 (DMEM/F-12, Gibco 31330-038), FBS (Gibco 10270-106), penicillin/streptomycin (Gibco 15140-122), insulin (Gibco 12585-014), human epidermal growth factor (hEGF, Gibco PHG0311), trypsin-EDTA (Gibco 25200-056), and PBS pH 7.4 (Gibco 14190-094) were purchased from Life Technologies (Finland). Whilst DMSO (D2650), iodonitrotetrazolium chloride (INT), beta-nicotinotinamide adenine dinucleotide sodium salt (NAD), triton X-100, lithium L-lactate and tris Base (2-Amino-2-(hydroxymethyl)-1,3-propanediol) were provided from Sigma-Aldrich (Finland).

3.2.2 Preparation of curcumin-loaded Pluronic F127 micelles

CUR-loaded PF127 micelles were prepared using three different techniques (Figure 3.1).

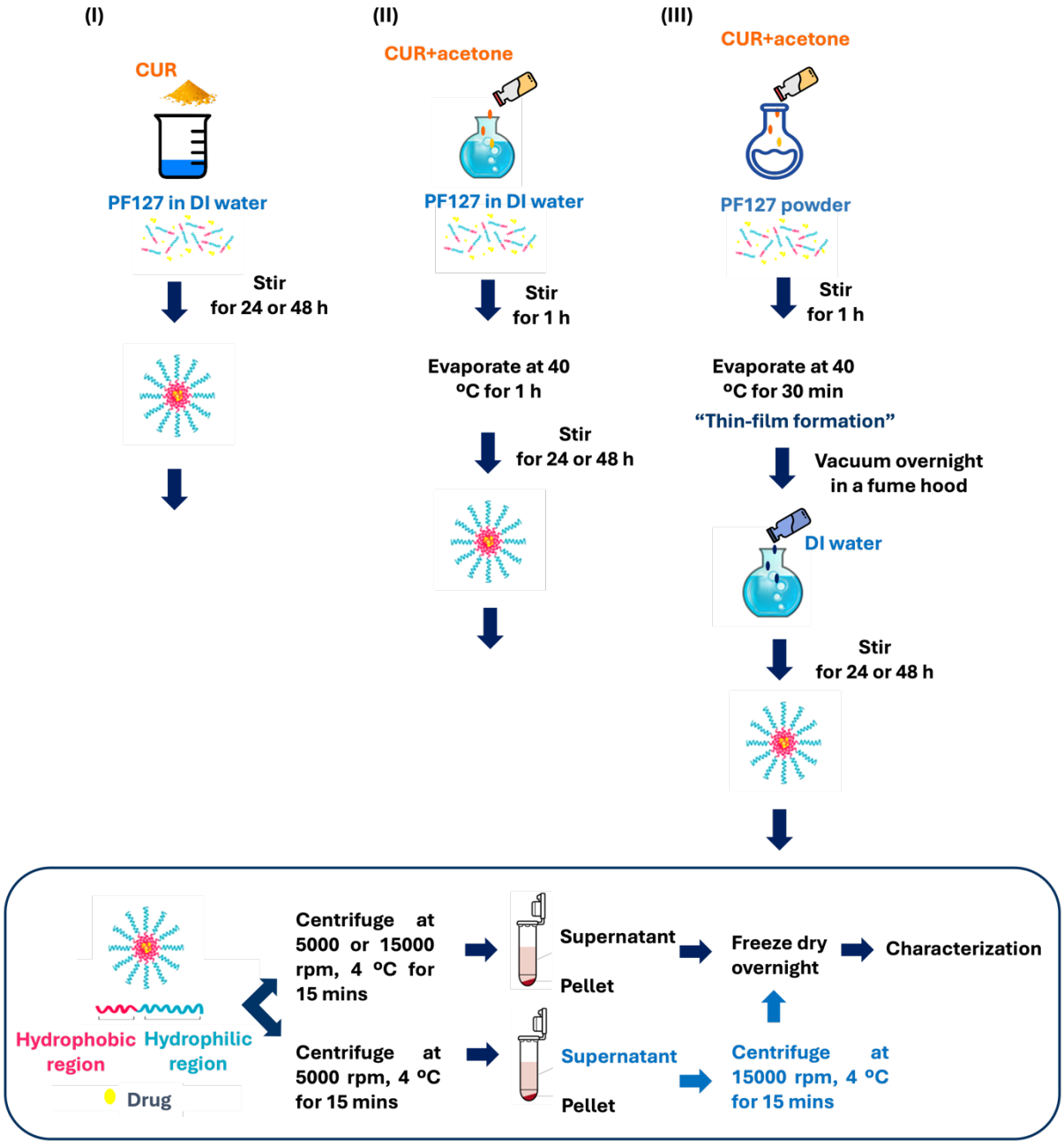

Figure 3.1: A schematic illustration of the preparation of CUR-loaded PF127 micelles using (I) direct dissolution, (II) co-solvent evaporation and (III) thin-film hydration method.

In terms of the direct dissolution method, CUR (10 mg) was added to 10 mL of 3.12 %(w/v) PF127 solution in deionized (DI) water (Figure 3.1(I)). This mixture was then gently stirred for either 24 h or 48 h at 25°C on a magnetic hotplate stirrer before the centrifugation step. CUR-loaded PF127 micelles were also prepared using the co-solvent

evaporation method outlined by Gerardos *et al.* with a slight modification (Figure 3.1(II)).[250] A solution of CUR (10 mg) and acetone (5 mL) was added dropwise to 10 mL of the PF127 solutions (3.12 %(w/v)) while stirring constantly (Figure 3.1(II)). Then, the CUR-loaded PF127 suspension was evaporated in a rotary evaporator at 40°C for 1 h to remove acetone. After that, the mixture was continually stirred for either 24 or 48 h at 25°C on a magnetic hotplate stirrer before centrifugation to remove the unencapsulated CUR. For the thin-film hydration method, CUR (10 mg) and PF127 (31.2 mg) were dissolved in 5 mL of acetone. After 1 h of mixing, the organic solvent was evaporated by rotary evaporation at 40°C for about 30 min to obtain drug-containing polymer films. The residual organic solvent remaining in the films was removed by keeping them in a fume hood with airflow overnight at room temperature. After that, the films were rehydrated in MilliQ water (pH 6-7, 10 mL) by vigorous stirring for either 24 h or 48 h at 25°C to prepare drug-encapsulated micelles.

In all three preparation methods for CUR-loaded PF127 micelles, the centrifugation step to obtain the micelles was carried out in the same manner as follows: For one centrifugation step study, the sample solution was placed in the centrifuge tube, which was operated at either low (5000 rpm) or high (15000 rpm) rotor speed for 15 min at 4°C to remove unencapsulated materials. The resultant pellet was separated from the supernatant. At this stage, the supernatant was freeze-dried and stored at 4°C for further characterization.[251,252] In the case of the two-step centrifugation study, the supernatant, after centrifuging at 5000 rpm was transferred to a new centrifuge tube, with further centrifugation at 15000 rpm for 15 min at 4°C. After that, the supernatant was separated from the pellet before freeze-drying for further characterization.

3.2.3 Characterization of curcumin-loaded Pluronic F127 micelles

3.2.3.1 Differential scanning calorimetry measurement

As per Section 2.2.6 with the following additions; the crimped pan was heated from 0°C to 200°C at a 1°C/min rate. An empty aluminium pan was used as a reference.

3.2.3.2 Size and zeta potential measurement

The particle size, PDI, and zeta potential (ZP) of the CUR-loaded PF127 micelles presented from Table 3.1 to Table 3.3 were measured by DLS using a Microtrac Nanotrac Wave II instrument, as per Section 2.2.4. All results presented as the mean ± standard deviation (SD) (n=3).

The distributions of the CUR micelle sizes and average ZP in Table 3.11 were conducted using a Malvern Zetasizer Ultra-Red analyzer (Malvern Panalytical, UK). The particle size distribution test was performed without dilution of the CUR micelles. 1 mL sample volume of each CUR micelle solution was transferred to a 10 mm square polystyrene disposable cuvette (DTS0012), and the temperature was maintained at 25°C with the light scattered by the sample at a backscattering angle of 173°. For measurement of ZP, the same sample at a volume of 1 mL was injected into the polycarbonate disposable folded capillary cell with a gold-plated beryllium-copper electrode (DTS1070), which was rinsed with DI water and sample dispersion before filling. The refractive index of the micelles and water were 1.46 and 1.33, respectively. The samples were equilibrated in the instrument chamber for 120 s at 25°C. The measurement for each sample was repeated in triplicate to ensure reproducibility.

3.2.3.3 Viscosity study

The viscosity of the CUR-loaded PF127 micelle solutions was measured using the AR-G2 magnetic bearing rheometer (TA Instrument Ltd, US) equipped with cone and plate geometry (Peltier plate steel). Before the measurement, the viscometer was calibrated using DI water, a standard viscosity reference fluid, with the inertia set to maintain between 18.7 and 18.8 $\mu N.m.s^2$. The following parameters were selected for the geometry setting: diameter (40 mm), gap (1000 μm), loading gap (30000 μm), and trim gap offset (500 μm). Then, 1 mL sample volume of the CUR micelle solution was loaded onto the lower plate of the rheometer, and the upper plate was lowered to the desired gap distance. The temperature of the sample was controlled using the Peltier system to maintain a constant temperature throughout the measurement at 25°C. The viscosity data obtained from the slope between stress and strain rate were recorded and analyzed using TRIOS software. Each measurement was performed in triplicate.

3.2.4 Stability study of curcumin-loaded Pluronic F127 micelles in deionized water

As per Section 2.2.5 with the following additions; CUR-loaded PF127 micelles in DI water, as prepared in Section 3.2.2, were immersed in liquid nitrogen (-196°C) for 10 min. The freeze-dried samples were reconstituted with DI water (final PF127 concentration: 31.2 mg/mL), measured by DLS, and sonicated for 5 min before being analyzed using DLS.

3.2.5 Encapsulation efficiency and drug loading of curcumin-loaded Pluronic F127 micelles

3.2.5.1 High-performance liquid chromatography method development for curcumin

CUR was assayed by an isocratic reversed-phase high-performance liquid chromatography (RP-HPLC) methodology using a Waters Nova-Pack® C18 column (150x4.6 mm column, 4 μm particle size). Method conditions were adapted from the study carried out by Alshanrani *et al.* with an increase in flow rate from 0.5 to 1 mL/min, an injection volume of 20 μL, and a 420 nm detection wavelength.[253] The column temperature was held constant at 25°C. The mobile phase composed of 40 %(v/v) ACN, 20 %(v/v) MeOH, and 40 %(v/v) 3 %(v/v) of glacial acetic in water and the mobile phase was degassed in an ultrasonic bath before use for at least 45 min. Each injection was carried out in triplicate, and the run cycle time for each injection was set at 10 min. All CUR standards were dissolved in MeOH. A standard calibration curve ranging from 0.01-0.1 μg/mL was constructed for the optimal mobile phase conditions.

3.2.5.2 Encapsulation efficiency and drug loading measurements of curcumin in micelles

Drug content experiments were based on the methodology of Gou *et al.* with slight modifications.[254] To determine the percentage drug encapsulation efficiency (%EE) and percentage drug loading (%DL) of CUR-loaded micelles, the aqueous samples were either diluted by ACN (10 %(v/v)) or dried and redissolved in MeOH, followed by measurement using either UV spectrophotometry at 422 nm or using the HPLC system

as described in Section 3.2.5.1. Each measurement was repeated three times, and the %EE and %DL were calculated using the following methods:

3.2.5.2.1 Direct method

The %EE and %DL of CUR in the PF127 micellar formulations were determined by centrifugation of the colloidal samples at either 5000 or 15000 rpm at 4°C for 15 min. The entrapped CUR amounts in the aqueous phase of the supernatant obtained after centrifugation of the micellar formulation were determined by either UV spectrophotometry or HPLC listed in Section 3.2.5.1.

The %EE of CUR entrapped within micelles was calculated from the mass of CUR detected in the supernatant layer by the weight of the initial mass of CUR added following Equation 3.1, and the %DL was calculated from the mass of CUR detected in the supernatant by the total initial mass of PF127 and CUR added according to the Equation 3.2.

$$\%\mathrm{EE} = \frac{\text{Mass of CUR detected in the supernatant}}{\text{The initial mass of CUR added (mg)}} \mathrm{x}100 \qquad \text{Equation 3.1}$$

$$\%\mathrm{DL} = \frac{\text{Mass of CUR detected in the supernatant}}{\text{The initial mass of PF127 and CUR added}} \mathrm{x}100 \qquad \text{Equation 3.2}$$

3.2.5.2.2 Indirect method

The %EE and %DL of CUR in PF127 micellar formulations were analyzed by centrifugation of the colloidal samples. In terms of indirect method calculation, the free amount of unencapsulated CUR in the pellet after centrifugation was analyzed by HPLC. The %EE of CUR entrapped within micelles was calculated by dividing the difference between the initial amount of CUR added and the amount of free CUR present in the pellet part as solid (Mass of CUR detected) by the total initial amount of CUR used according to the Equation 3.3. Whereas the %DL was obtained by dividing that difference by the total initial mass of PF127 and CUR added according to Equation 3.4.

$$\%\mathrm{EE} = \frac{\text{The initial mass of CUR added} - \text{Mass of CUR detected in the pellet}}{\text{The initial mass of CUR added}} \mathrm{x}100 \qquad \text{Equation 3.3}$$

$$\%DL = \frac{\text{The initial mass of CUR added} - \text{Mass of CUR detected in the pellet}}{\text{The initial mass of PF127 and CUR added}} x100 \quad \text{Equation 3.4}$$

3.2.6 Forced degradation study

The influence of temperature on the degradation of CUR was studied by diluting the stock solution of CUR/MeOH (100 μg/mL) to the final concentration of 33 μg/mL. After that, the samples were heated at 80°C on the magnetic stirrer hotplate with a thermometer for different interval times (1, 2, 6, 18, and 24 h). Samples of 100 μL were withdrawn at different time points, added to 900 μL of methanol, followed by filtration through 0.22 μm filter and analyzed using HPLC, as per Section 3.2.5.1. The photodegradation of CUR was assessed by analyzing the CUR dissolved in MeOH (10 μg/mL). The samples were exposed to visible light at different times (1, 2, 6, 18, and 24 h) before filtering (0.22 μm filter) and being subjected to HPLC analysis without any further dilution. The experiment was repeated in triplicate (n=3).

3.2.7 Cytotoxicity study and reactive oxygen species (ROS) formation study

3.2.7.1 Cytotoxicity study of immortalized human corneal epithelial cells by acid phosphatase colorimetric assay

Immortalized human corneal epithelial (IM-HCEpi) cells were cultured in ocular epithelia cell medium supplemented with 5 %(v/v) FBS, 1 %(v/v) epithelial cell growth supplement (EpiCGS) solution, and 1 %(v/v) penicillin/streptomycin solution at 37°C in a humidified atmosphere with 5% CO_2. The cytotoxicity of CUR (1-18 μg/mL) and the CUR-loaded PF127 micelles, as well as the blank PF127 as a control, was determined on IM-HCEpi cells. After passaging of IM-HCEpi cells, the cells were seeded in 96-well plates at a density of 5000 cells/well for 24 h. Then, the cell medium was removed and treated with a free drug, blank PF127 micelles, and a formulation drug concentration of 1, 2, 4, 7, 11 and 18 μg/mL for 24 h in an incubator (37°C). Blank PF127 micelles were prepared with the same concentration of PF127 copolymer at their drug-loaded micelles. Cell viability was then assessed using an acid phosphatase colorimetric (APA) assay. After the 24 h treatment with the listed test formulations, the wells were washed three times with 0.01 PBS (pH 7.4), followed by the addition of the para-nitrophenyl phosphate

substrate (100 µL) and incubated for 2 h (37°C, 5% CO_2). Then, 20 µL of 1M NaOH, a stop solution, was added to each well, and the analysis was performed by fluorescence intensity measurement at an absorbance wavelength of 405 nm using a BioTek Epoch®microplate reader (Agilent Technologies, Dublin, Ireland). The measurement for each sample was repeated in triplicate (n=3).

3.2.7.2 Cytotoxicity study of human corneal epithelial cells by lactate dehydrogenase (LDH) release, resazurin and reactive oxygen species (ROS) assay

Human corneal epithelial (HCE-T, RIKEN BRC Cell Engineering Division, cell bank Tsukuba, Japan) cells were cultured in the growth medium (500 mL) supplemented with DMEM/F-12 (467 mL), fetal bovine serum (FBS, 25 mL), penicillin/streptomycin (5 mL), insulin (625 µL), hEGF (5 µL), and DMSO (2.5 mL) at 37°C in an incubator with 5% CO_2. HCE-T cells were seeded in 96-well plates (16000 cells/200 µL medium/well) for 3 days. Subsequently, the culture medium was removed, and the cells were treated with 100 µL of various concentration ranges of the CUR micelles (1-75 µg/mL), along with the blank PF127 micelles and MilliQ-water as controls, in three technical replicates for 24 h. As the formulations were suspended in MilliQ-water, MilliQ-water was used as the control to assess its impact on LDH release, resazurin and ROS formation studies in the absence of micelles or drug components. The cytotoxicity effects of CUR micelles were assessed using LDH cytotoxicity detection. Following the 24-hour treatment, 50 µL of the cell culture supernatants in each well were transferred to the new 96-well plate and stored at -20°C for 24 h. Then, the samples were thawed and equilibrated to room temperature, followed by the addition of 50 µL assay reagent to each well, which contained 1 mM iodonitrotetrazolium chloride, 1.6 mM nicotinamide adenine dinucleotide, 80 mM lithium lactate, 7.5 µM 1-methoxy-5-methlyphenazinium methyl sulfate in 0.2 M Tris-HCl, pH 8.2. The wells were mixed briefly on the orbital shaker at 300-500 rpm for 15 s. After that, the plates were covered with aluminum foil and incubated in a dark environment for 1 h at room temperature. Following 1 h of incubation, 50 µL acetic acid was added to each well to stop the reaction and stabilize the cells and mixed on the orbital shaker at 300-500 rpm for 15 s. LDH release was quantified by

measuring the absorbance at 490 nm using a microplate reader. Data was normalized to the untreated control conditions. Regarding the cell viability study using resazurin assay, after collecting the LDH release samples, the remaining cell culture supernatants in each well were removed by suction. Then, the cells were washed by 100 µL of warm HBSS three times. After removing the last washing solution, 100 µL of the mixture of resazurin and chloromethyl derivative of 2',7'-dichlorodihydrofluorescein diacetate (CM-H_2DCFDA), containing resazurin (0.01 mg/mL) and CM-H_2DCFDA (5 µM) in HBSS, was added to each well and incubated at 37°C in the oven for 1 h. After 1 h of incubation, the resazurin measurement was conducted using Cytation 3 multi-mode reader, Gen 5 program, BioTek Instruments (Winooski, VT, USA) at Ex 560 nm/Em 590 nm). Furthermore, after measurement of resazurin by the plate reader, the resazurin/CM-H_2DCFDA mixture was removed in each well and replaced with 100 µL HBSS, followed by incubation for 30 min at 37°C. The fluorescent intensity of highly fluorescent 2',7'-dichlorofluorescein (DCF) was thereafter measured by the plate reader at an excitation wavelength of 492 nm and an emission wavelength of 522 nm. The experiment was repeated two to three times as reported in the results section.

3.2.8 In vitro drug release study

3.2.8.1 Curcumin solubility profiles in release media

The solubility of CUR was studied in 0.01 M PBS (pH 7.4), 0.01 M PBS (pH 7.4) containing 1 %(w/v) SDS and 1.06 %(w/v) Tween-80. Specifically, an excess amount of CUR was first dissolved in the three media to obtain solutions with a CUR concentration of around 2 mg/mL. Afterwards, the Eppendorf® tubes containing CUR solutions were kept away from light and placed in a shaking incubator at 37°C with a shaking speed of 120 rpm for 24 h. Finally, the mixtures were centrifuged at 15000 rpm for 15 min in the benchtop centrifuge (Hettich® EBA 21 centrifuge, Tuttlingen, Germany), and the supernatant part was filtered through a 0.22 µm filter. Samples of 100 µL were taken from the supernatant solution and diluted with MeOH for HPLC analysis. The experiment was repeated three times, and the results are presented as the mean ± SD.

3.2.8.2 The stability of free curcumin in different release media

The stability of CUR was studied in 0.01 M PBS (pH 7.4), 0.01 M PBS (pH 7.4) containing 1 %(w/v) SDS and 1.06 %(w/v) Tween-80. An excess amount of CUR was dissolved in the three media to obtain solutions with CUR concentrations of around 2 mg/mL before putting in the shaking incubator for 24 h (37°C, 120 rpm). A mixture solution in each Eppendorf® was then centrifuged at 15000 rpm for 15 min (Hettich® EBA 21 centrifuge, Tuttlingen, Germany), and the supernatant solution was collected for studying at various time intervals. After that, the Eppendorf® tubes were kept away from light and placed in a shaking incubator at 37°C with a shaking speed of 120 rpm at different time intervals. Finally, samples of 100 µL were taken at specified time intervals and diluted with MeOH before filtering through a 0.22 µm filter for HPLC determination.[267] The experiment was repeated three times, and the results presented as the mean ± SD.

3.2.8.3 Curcumin release from micelles

The *in vitro* release of CUR from the CUR-loaded PF127 micelles was evaluated using a dialysis method. 0.01 M PBS (pH7.4) containing 1 %(w/v) SDS was used as the release medium to maintain sink conditions. 1 mL of CUR-loaded micellar solution (CUR loading content 0.2-0.3%) was added into a dialysis membrane (with a molecular weight cut-off of 14 kDa). Subsequently, the dialysis tube was suspended in 10 mL of release medium to maintain sink conditions. The release experiments were then conducted in an incubator at 37°C with a shaking speed of 120 rpm. At various time intervals, the medium solution outside the dialysis bag was collected and replaced with fresh medium. After this, the medium solution was diluted with MeOH for quantitative CUR content by HPLC.[252,255] The experiment was repeated three times, and the results presented as the mean ± SD. The cumulative percentage of drug release of CUR in the PF127 micelle was calculated using the following Equation 3.5:

$$\text{Cumulative percentage release (\%)} = \left(\frac{\text{Volume of sample withdrawn (mL)}}{\text{Bath volume (mL)}} \text{x} P_{t-1}\right) + P_t \qquad \text{Equation 3.5}$$

Where P_t = Percentage release at time t

P_{t-1} = Percentage release previous to 't'

3.2.9 Ex vivo corneal and scleral permeation study

An *ex vivo* permeation study was carried out on porcine cornea and sclera, according to the method previously described by Pescina *et al*.[237,256] Fresh porcine eyes obtained from a local abattoir (Dawn Meats, Grannagh Business Park, Waterford, Ireland) were used for the *ex vivo* permeation within 24 h. After being transported to the laboratory, the eyeballs were rinsed with 0.9% NaCl solution to remove blood and other contaminants before immersing in PBS at 4 °C. The corneal and the scleral tissues were used within 6 h after extraction from the eyeballs in the laboratory. The permeation studies were conducted using a Franz-type diffusion cell. The cornea and sclera were excised and mounted on the top of the receptor compartment of the diffusion cell, with the endothelium side (the corneal experiment) and the stromal side (the sclera experiment) facing the receptor chamber. After that, the donor compartment of the Franz-diffusion cell was applied and clamped. The receptor solution was filled with PBS solution containing 1.06 %(w/v) Tween-80 (4 mL), and the donor chamber was filled with 200 µL of PBS. The Franz cell was thereafter incubated for 30 min at 37°C in the incubator before replacing the PBS solution in the donor compartment with the CUR micelle formulations at the same volume (200 µL), followed by covering the donor part with parafilm and aluminium foil. The experiment was performed in the incubator (120 rpm, 37°C). At predetermined time points, 200 µL of the medium in the receptor chamber was removed by a 1 mL syringe. The withdrawn samples were replaced with fresh receptor solutions to maintain sink conditions throughout the experiment. After 6 h, the CUR formulation was removed, and the corneal and scleral tissues were washed with 2 mL DI water, dried with filter paper, and cut into small pieces to immerse into 2 mL MeOH in the 20 mL vials. The drug retained in the tissue was extracted by sonication for 5 min. The extracted drug solutions were filtered with 0.22 µm cellulose filters before HPLC analysis. Similarly, the concentration of CUR in the withdrawn samples was analyzed using HPLC by diluting with 800 µL of MeOH.[237] Experiments were repeated at least three times.

3.2.10 Ex vivo uptake study of the coumarin-6 micelles in the cornea of the porcine eyes

Coumarin-6 (Cou6)-loaded PF127 micelles were prepared using the thin-film hydration method at 15000 rpm, as per Section 3.2.2 with the drug being replaced by 10 mg of Cou6. After that, an *ex vivo* corneal permeation study, as per Section 3.2.9, was performed by adding Cou6 micelles into the donor compartment instead of the CUR micelles. After finishing the experiment, the corneal tissue was washed with 2 mL DI water and fixed with 4% formaldehyde solution for 5 min at room temperature. After fixation, the corneal tissue was rewashed with PBS and counterstained with 4',6-diamidino-2-phenylindole (DAPI) (PBS:DAPI=1:1000) for 5 min and covered with the aluminium foil to visualize the cell nuclei. The cellular uptake of the Cou6-loaded PF127 micelles was examined using an Olympus BX51 fluorescent microscope (Waltham, MA, USA) equipped with appropriate filter sets for Cou6 and DAPI.

3.2.11 Statistical analysis

As per Section 2.2.8 with the following additions: the difference in %EE and %DL of the test formulations comparing between direct and indirect methods, %EE between UV and HPLC techniques, and the difference in drug retention between the control and the test formulation after an *ex vivo* permeation study was performed by independent samples t-test. The paired samples t-test was used to compare the difference in the particle sizes after freeze-drying and after the sonication process. Statistical analysis comparing between the control and experimental groups of cell viability, LDH release, and ROS production percentage was performed using One-way ANOVA, followed by Dunnett's multiple comparisons tests. GraphPad Prism software (Prism 10.1.1) was employed for the statistical analysis, and results were considered significant if $p \leq 0.05$.

3.3 Results and discussion

3.3.1 Preparation of drug-loaded Pluronic F127 micelles

Many methods, as pointed out in the review paper of Mandal *et al.*, have been used for preparing drug-encapsulated micelles in which drug loading in micelles could be

achieved by physical entrapment or chemical conjugation.[115] Due to the complication and challenge of the series of chemical reactions regarding the chemical method, physical methods (e.g., direct dissolution, dialysis, oil-in-water emulsion, solvent evaporation, and freeze-drying methods) are much simpler and more practical to produce drug-encapsulated carriers.[115] For example, in the present study, micellar solutions of PF127 were successfully produced from either direct dissolution or solvent evaporation methods, as discussed in Chapters 1 and 2.[247,257] Therefore, in this section, several physical strategies were investigated for encapsulating a small molecule, potentially therapeutic drug, using PF127 at a concentration of 3.12 %(w/v). This concentration was chosen for further experimentation as the results from Chapter 2 demonstrate that it was suitable for the preparation of PF127 micelles (Section 2.3.3).

3.3.1.1 Investigation of micelle preparation method

Three different approaches: direct dissolution, co-solvent evaporation, and thin-film hydration, were selected for the study to enhance the loading efficiency of drug-encapsulated PMs. While there has been a great deal of research on drug-encapsulated PMs, very few studies have looked into the effects of centrifugation speeds on the particle sizes of the nanoparticles, including the micelles.[258,259] Consequently, screening experiments were initially performed to study the impact of centrifugation speeds on the particle size of the micellar formulation. The findings of the CUR-loaded PF127 micelles prepared by different methods are presented in Table 3.1.

Table 3.1: Particle size (D_h, percentage by volume), zeta potential (ZP), PDI, and %yield of the CUR encapsulated PF127 after centrifugation at 24 h. Particle size represents the diameter of the particle (nm). The mean ± SD is obtained from replication of the experiment 3 times.

Ctf (rpm)	Method	Code	DLS measurement			%Yield
			D_h (nm, vol%)	PDI	ZP (mV)	
5000	Direct	BK22-1	451 ± 8 (84%)	0.14 ± 0.04	-11 ± 20	91 ± 0.42
	Co-solvent	BK36-1	2071 ± 493 (65%) 353 ± 87 (15%) 3482 ± 2685 (20)	0 .58 ± 0.39	-2 ± 12	84 ± 2.13
	Thin-film	BK24-1	4024 ± 1696 (99%)	0.11 ± 0.08	+12 ± 26	86 ± 4.0
5000 and 15000	Direct	BK32-3	1 ± 0.02 (52%) 1671 ± 338 (29%) 546 ± 216 (20%)	0.55 ± 0.28	+29 ± 8	88 ± 0.84
	Co-solvent	BK36-3	3044 ± 1992 (72%) 128 ± 143 (19%)	0.29 ± 0.05	-7.87 ± 1.68	77 ± 6.24

	Thin-film	BK24-3	1.02 ± 0.01 (52%) 2249 ± 545 (46%) 21 ± 3 (26%)	0.46 ± 0.09	+11 ± 16	77 ± 5.8
15000	Direct	BK32-2	4 ± 0.1 (66%) 313 ± 60 (29%)	0.97 ± 0.72	-58 ± 114	85 ± 6.40
	Co-solvent	BK36-2	19 ± 8 (62%) 3 ± 2 (35%) 5770 ± 162 (3%)	1.44 ± 0.91	-139 ± 106	69 ± 15.9
	Thin-film	BK24-2	15 ± 3 (60%) 3 ± 3 (39%)	0.19 ± 0.13	-16 ± 8	82 ± 3.4

*Direct:Direct dissolution method; Co-solvent:co-solvent evaporation method; Thin-film:thin-film hydration method; Ctf:centrifugation speed

The result demonstrated that the particle sizes of the micellar solution obtained from one-step centrifugation at 5000 rpm and two-step centrifugation (5000 and 15000 rpm) were large (450-4025 nm) compared to one-step centrifugation at 15000 rpm of the samples (4-19 nm, Table 3.1). Moreover, in all preparation methods, the particle sizes after centrifugation at 5000 and continuing with 15000 (1-3044 nm) were smaller than the sizes produced by a speed of 5000 rpm (451-4024 nm, Table 3.1), although there were multimodal particle size variations. Additionally, the ZP was slightly negative in all cases for the micelles centrifuged at 15000 rpm, which could be attributed to the ionization of hydrophilic groups in water molecules located at the periphery when the PF127 micelles were dispersed in DI water.[260] Therefore, these findings suggest a benefit of higher centrifugation in breaking the large particle size as DLS results show that the CUR/PF127 micelles prepared by one centrifugation step at 15000 rpm presented good properties in terms of size stability as compared to centrifugation of the sample at either 5000 rpm or 5000 followed by 15000 rpm. The reason behind this can be explained according to Stokes' Law for settling velocity (Equation 3.6):

$$V_T = \frac{2}{9}\frac{(\rho_s - \rho_f)gr^2}{\eta} \qquad \text{Equation 3.6}$$

Where V_T = terminal velocity

r = radius of the particle

ρ_s = density of the particle

ρ_f = density of the fluid

η = viscosity of the fluid

g = acceleration due to gravity

Stokes' Law is a mathematical description of the force required to move a sphere through a viscous fluid at a specific velocity.[261,262] In addition, settling or terminal velocity (V_T) is directly proportional to the square of the particle radius (r^2), which refers that larger particles will settle faster than smaller particles (Equation 3.6). In other words, the larger particles will experience a greater centrifugal force (Equation 3.7) when centrifuging a mixture of particles at high speeds compared to smaller particles.

$$F = m\omega^2 r \qquad \text{Equation 3.7}$$

Where F = centrifugal force

m = mass of the moving body

ω^2 = angular velocity

r = distance of the moving body from the center

The centrifugation force (F) acting on the particle is proportional to its mass (m) and the radial distance from the center of rotation (r) (Equation 7).[263] More precisely, this equation explains that larger particles will experience a greater centrifugal force at higher centrifugation speeds owing to their larger mass. Thus, combining Stokes' law with centrifugal force theory, it can be concluded that a high-speed centrifuge (15000 rpm) is more effective in removing large particles compared to a low-speed centrifuge (5000 rpm) because of the increased centrifugation force acting on the large particles. This results in better separation and removal of large particles from the mixture at high centrifugation speed.[235,262]

Our experimental results revealed that centrifugation at lower speeds results in larger particle sizes of CUR-loaded PF127 micelles compared to centrifugation at higher speeds. This observation was consistent with the findings from the previous study by Mahajan *et al.* who demonstrated that both the tocopherol polyethylene glycol succinate (TPGS):drug ratio and rotary evaporator's rotational speeds played a noticeable influence on the particle size and EE of their lopinavir-loaded vitamin E-TPGS micelles.[264] Indeed, the smaller particle size with higher EE was obtained when centrifuging at a higher rotational

speed at 125 rpm (~91 nm, 99% EE) compared to a lower speed at 89 rpm (~298 nm, 96% EE), which suggested that smaller particles had less mass and more surface area to encapsulate drug, allowing them to sediment faster and separate more efficiently from larger particles and aggregates at high rotational force. In addition, their study also found that increased TPGS to drug ratio from 150:30 to 214:30 leads to smaller particle sizes from 298 nm to 127 nm, possibly due to compact micelle formation and colloidal steric stabilization as a result of several hydrophilic polar heads of TPGS, which limited Brownian movement and made their formulation stable.

The variability in particle sizes observed in our study could be related to the variations in the interactions between the CUR drug molecules and the PF127 components that form the CUR micelles under varying centrifugation conditions. During centrifugation at lower speeds (5000 rpm), the relatively weaker centrifugal forces may not be sufficiently strong to fully compact the micelles, resulting in the formation of larger particle sizes. On the other hand, increasing the speed of centrifugation might apply greater tension to the micellar system, leading to more compact structures and smaller particle sizes.

Moreover, our results suggest that the particle size of CUR-loaded PF127 micelles was not only influenced by the centrifugation speeds but also by the specific technique used in the preparation process. Studies performed by Kumari *et al.* using the thin-film hydration method (MeOH and chloroform) and centrifuged their CUR-poly(ethylene glycol) monomethyl ether (mPEG)-poly(lactic acid) (PLA) micelle formulations at 13500 rpm showed that the average size of their CUR micelles was 110 ± 5 nm (PDI~0.15).[265] A similar result was found in the work of El-Banna *et al.* which revealed the average diameter of CUR-loaded PLA/PF127 nanomicelles prepared by another technique, which was the solvent evaporation method (dichloromethane, DCM) after centrifugation at 14000 rpm were 130-160 nm, respectively.[266] Conversely, the research study carried out by Vaidya *et al*. using the same preparation method (co-solvent evaporation, MeOH) at low centrifugation speed (5000 rpm) produced a smaller size of the CUR-loaded PF127 micelle (26 nm, PDI~0.195).[248] Recently, it has been reported that filtration (e.g., 0.22-µm and 0.45-µm membrane filters) was another technique to remove unencapsulated materials or unincorporated drug aggregates after preparation of drug-loaded polymeric

materials, including CUR, and obtained a small particle size (4-20 nm).[75,227,267] Thus, our research studies presented here provide evidence that large particles (80-100 nm) were obtained when operating at a high-speed centrifuge, which contradicted the present study results (Table 3.1). In addition, the previous particle size results showed that an increase in the particle size of the micellar formulations was observed compared to the PF127 blank micelle size at the same concentration (3.12 %(w/v), D_h=4.01 ± 0.09, Table 2.1), suggesting an expansion of the core of the PF127 that was occupied by CUR as a hydrophobic drug (Table 3.1).[268]

Taken altogether, this finding indicated that not only centrifugation speeds but also other parameters, such as types of polymers, volatile solvents and techniques used to prepare the micelles, affected the formation of aggregated PMs under the experimental condition, resulting in different outcomes of the micellar sizes. Additionally, this study confirmed that the CUR/PF127 micelles were successfully prepared by three different methods: direct dissolution, co-solvent evaporation, and thin-film hydration. Furthermore, our findings highlight the importance of the effect of centrifugation speed on the resulting particle sizes of CUR-loaded PF127 micelles. In other words, these CUR micelles had a unimodal or bimodal distribution of the particle sizes when prepared using a single centrifugation step at either 5000 or 15000 rpm. However, the multimodal particle size distribution of the CUR micelles was obtained for the two centrifugation steps of preparation. For this reason, the CUR micelles prepared at one centrifugation step were chosen for the subsequent investigation since unimodal or bimodal particle size distributions consist of particles that are predominantly one size or two sizes, which can help to achieve uniform behaviour in DDS. For example, a narrow unimodal distribution can be advantageous for controlled release formulations as it provides more precise control over the release rate of the drug compared to formulations with multimodal particle size distributions, referring to a wide range of particle sizes.

3.3.1.2 Impact of preparation time on micelle properties

As previously described, understanding how centrifugation speed affects the particle size of micelles is crucial, much like the impact of preparation time on micelle characteristics. In this part, the effect of two times on the preparation of CUR-loaded PF127 micelles

centrifuged at either 5000 or 15000 rpm was studied, and DLS measurement was performed to characterize the micelles (Table 3.2).

Table 3.2: Particle size (D_h, percentage by volume) of the CUR encapsulated PF127 micelles after centrifugation at 48 h. Particle size is the representation of the diameter of the particle (nm) (n=3).

Ctf (rpm)	Method	Code	Stirring time (h)	
			24 h	48 h
			D_h (nm, vol%)	D_h (nm, vol%)
5000	Direct	BK27	451 ± 8 (84%)	449 ± 105 (52%) 3418 ± 3383 (39%) 2598 ± 104 (8%)
	Co-solvent	BK28	2071 ± 493 (65%) 353 ± 87 (15%) 3482 ± 2685 (20%)	1574 ± 5530 (26%) 436 (30%) 31 ± 19 (24%)
	Thin-film	BK29	4024 ± 1696 (99%)	687 (53%) 21 (25%) 4090 (22%)
15000	Direct	BK27	4 ± 0.1 (66%) 313 ± 60 (29%)	2901 ± 2219 (65%) 11 ± 9 (32%) 552 ± 430 (3%)
	Co-solvent	BK28	19 ± 8 (62%) 3 ± 2 (35%) 5770 ± 162 (3%)	2653 (41%) 3 (29%) 13 (27%)
	Thin-film	BK29	15 ± 3 (60%) 3 ± 3 (39%)	4 (62%) 11 (38%)

After increasing the reaction time up to 48 h, all CUR-loaded PF127 micelles appeared as a non-homogenous solution of micelles and aggregates, as reported in the review paper by Lu *et al*. (Table 3.2).[269] Stirring for more extended periods of time could destabilize the particles and break up the particles into different sizes in the aqueous suspensions, resulting in various particle sizes and broadening PDI values.

As an example of CUR-loaded mPEG(5kDa)-PCL(2kDa) copolymers with particle size around 29 nm (PDI~0.05), consider the study of Gupta *et al.*, which investigated the stability of CUR-loaded mPEG-PCL micelles in a liquid state at 4°C.[281] Their studies revealed that CUR apparently precipitated from the micelles after 10 days owing to destabilization, resulting in an increase in the particle size of the CUR formulations in liquid state from 25 nm (PDI~0.1) to 75 nm (PDI~0.4).[270] Therefore, this study would suggest that stirring time at 24 h, as already reported in the previous Section 3.3.1.1, was the most suitable time to prepare CUR-loaded micelles.

3.3.1.3 Impact of freeze-drying and sonication on micelle properties

The experiments focused on examining the effects of freeze-drying and sonication processes on the structural properties of the CUR micelles to determine their stability and potential for targeted drug delivery applications. Subsequently, as per micelles prepared by three different methods (section 3.3.1.1), the impact of freeze-drying following micelle resuspension in DI water and then sonication on the micelle sizes was investigated (Table 3.3).

Table 3.3: Particle size (D_h, percentage by volume), and PDI of the CUR encapsulated PF127 micelles after preparation and freeze-drying, including after sonication. Particle size represents the diameter of the particle (nm). The readings from the DLS analysis were taken three times.

Ctf (rpm)	Method	Code	DLS measurement					
			After preparation		After freeze-drying		After sonication	
			D_h (nm, vol%)	PDI	D_h (nm, vol%)	PDI	D_h (nm, vol%)	PDI
5000	Direct	BK22-1	451 ± 8 (84%)	0.14 ± 0.04	398 ± 280 (64%) 4 ± 0.1 (36%)	0.11 ± 0.003	4 ± 2 (67%) 14 ± 5 (33%)	1.19 ± 0.74
	Co-solvent	BK36-1	2071 ± 493 (65%) 353 ± 87 (15%) 3482 ± 2685 (20%)	0.58 ± 0.39	13 ± 0.09 (50%) 3 ± 2 (32%) 1090 ± 1538 (18%)	0.33 ± 0.54	3 ± 1 (50%) 1 ± 0.27 (25%) 11 ± 8 (25%)	0.71 ± 0.25
	Thin-film	BK24-1	4024 ± 1696 (99%)	0.11 ± 0.08	1946 ± 29 (83%) 4940 ± 2 (36%)	0.24 ± 0.06	5460 ±14 (45%) 4 ± 2 (36%) 440 ± 54 (19%)	0.66 ± 0.07
15000	Direct	BK32-2	4 ± 0.1 (66%) 313 ± 60 (29%)	0.56 ± 0.18	4 ± 0.7 (86%) 10.71 (14%)	0.40 ± 0.07	5 ± 1 (100%)	2.26 ± 0.52
	Co-solvent	BK36-2	19 ± 8 (62%) 3 ± 2 (35%) 5770 ± 162 (3%)	1.44 ± 0.91	4 ± 0.65 (83%) 19 ± 3 (17%)	0.25 ± 0.29	17 ± 3 (97%) 4.85 (3%)	0.05 ± 0.06
	Thin-film	BK24-2	15 ± 3 (60%) 3 ± 3 (39%)	0.19 ± 0.13	22 ± 5 (90%) 3 ± 2 (10%)	0.45 ±0.30	17 ± 3 (67%) 2 ± 2 (33%)	0.84 ± 0.45

The study revealed that the particle sizes of CUR/PF127 micelles prepared by the one-centrifugation speed at 15000 rpm of three preparation methods retained their initial sizes (>60%vol) after freeze-drying and sonication processes without the use of cryoprotective

agents compared to the CUR micelles after preparation (p>0.05, One-way ANOVA followed by Dunnet's multiple comparisons), indicating stability in the particle sizes (Table 3.3). On the other hand, the study illustrated that CUR micelles were unstable after freeze-drying and sonication processes in the samples centrifuged at 5000 rpm in three preparation methods, with multimodal particle size distribution and higher PDI values (p<0.05, One-way ANOVA followed by Dunnet's multiple comparisons) (Table 3.3).

In previous studies, Rasoulianboroujeni *et al.* reported that no significant difference (p>0.05) in paclitaxel (PTX) encapsulation (50-65%) and the average particle sizes (20-50 nm) obtained from PTX-loaded PEG-*b*-PLA micelles prepared at 25°C after the freeze-drying process with no other cytoprotectant added.[271] Similarly, the work of Luo *et al*. also found that the freeze-drying process did not affect the particle size and PDI of the poly (lactic-co-glycolic acid) PLGA/polyvinyl alcohol (PVA) polymeric nanoparticles (size~240 nm, PDI~0.1) without additional cryoprotectants, possibly due to the presence of PVA on the surface of the nanoparticles that served as a steric barrier.[272] However, some studies, as has been reported in the literature by Mandal *et al.,* revealed that cytoprotective agents were required to protect the structure of the micelles and preserve the integrity of the micelles during the freeze-drying process.[115] For example, Ojha *et al.,* also reported that the docetaxel-entrapped crosslinked PM size was largely dependent on the freeze-drying process in which the non-cryoprotected clinical-stage docetaxel-entrapped core-crosslinked PMs (CPC634) samples was turbid with visible precipitation after reconstitution of the freeze-dried sample in NaCl solution.[231] Their studies found that the mean size of the CPC634 micelles increased from 65 nm (PDI~0.10) before freeze-drying to 85 nm (PDI~0.18) at the freezing condition at -45°C for 3 h under atmospheric pressure, indicating aggregates of the particle after freeze-drying.

Therefore, different types of nanocarriers face different challenges in freeze-drying differently. Our findings in investigating the stability of CUR-loaded PF127 micelles after the freeze-drying process without the use of cryoprotective agents were consistent with the previous studies in the works of literature that have demonstrated the ability of PMs to maintain their initial sizes following freeze-drying without the use of cryoprotective

agents. This phenomenon could be attributed to the amphiphilic structure of the PF127 micelles, namely their core-shell structures and stabilizing interactions between the polymer chains. In our study, the poly (propylene oxide) PPO unit in the hydrophobic core of the PF127 micelles serves to encapsulate CUR using hydrophobic interactions and can shield the encapsulated CUR from external stresses during the freeze-drying process. While the poly (ethylene oxide) (PEO) hydrophilic shell of PF127 micelles helps maintain the structural integrity of the micelles by forming a protective layer around the hydrophobic core of the CUR-loaded PF127 micelles, preventing them from coming into close contact and aggregating when freeze-drying. Thus, these factors, including the core-shell structures, intermolecular interactions and structural integrity, collectively contribute to preventing aggregation and maintaining the stability of the CUR-loaded PF127 micelles and their ability to retain their initial sizes even under harsh processing conditions, as observed in our study.

Moreover, after sonication of this reconstitution process, the size and PDI of all the reconstituted CUR-loaded PF127 micelles at 15000 rpm of three techniques were similar to those of the micelles after freeze-drying ($p>0.05$, paired sample t-test) (BK32-2, BK36-2 and BK24-2, Table 3.3), which supports that the CUR-loaded micelles at 15000 rpm were relatively stable during the sonication process. Conversely, all of the CUR-loaded PF127 micelles centrifuged at 5000 rpm produced different particle size ranges ($p<0.05$, paired sample t-test) (BK36-1 and BK24-1, Table 3.3), indicating a heterogonous population of particles with a high PDI in the CUR micelle samples. Subsequently, these lead to the instability of the particle size in the system after the sonication process.[288] This study was similar to that reported by Vorobiova *et al*.[273] They examined the effect of sonication on polymeric aggregates formed by SDS micelles and found that the particle size of the polymeric aggregates decreased from 6 nm to 4.6 nm after sonication at 130 Watts for 2 min. Similarly, the work of Schulnies *et al.*, focusing on micellar casein concentrate micelle preparation, illustrated that particle diameter decreased from 230 nm to 200 nm when the sonication power increased from 20 J/g to 250 J/g, respectively, indicating particle disruption due to ultrasonic treatment.[274]

Based on the stability study of the CUR micelles shown in Table 3.3, the CUR micelles centrifuged at 15000 rpm and prepared by the thin-film hydration method were selected for the following study due to the small sizes with consistent particle size distributions and good stability after freeze-drying and sonication process (BK24-2, Table 3.3). DLS was used to measure the diameters of the CUR micelle supernatant across multiple stages (Figure 3.2).

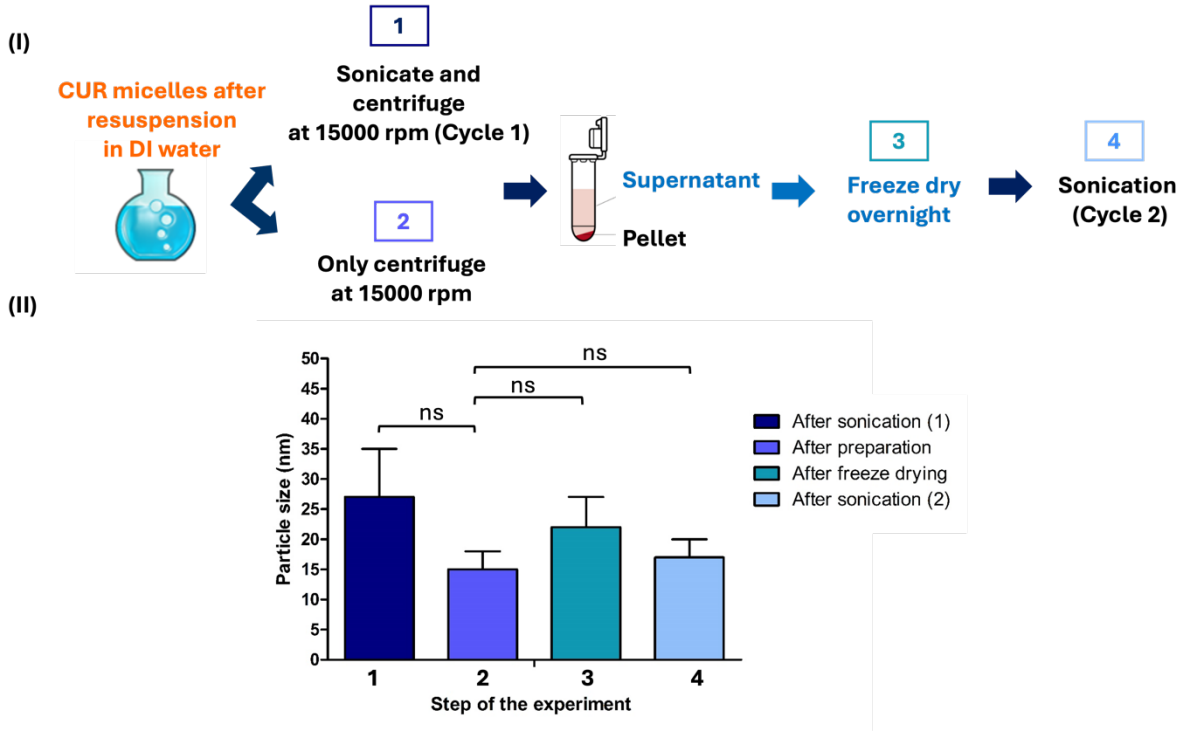

Figure 3.2: A schematic representation of (I) approaches to evaluating the stability of the CUR micelles according to the thin-film hydration technique, and (II) the particle sizes of the CUR micelles in different steps of the experiment for stability test (n=3). Statistical significance was analyzed by the One-way ANOVA followed by Dunnett's multiple comparisons (p>0.05 compared to the mean values of the mean particle size values obtained after preparation step 2). Data are presented as the mean ± SD of three experiments (n=3).

Based on the stability study, the results showed that there was no statistical difference in the mean particle sizes of the CUR micelles in DI water at four different steps compared to the mean particle size values obtained after preparation step 2 (p>0.05) (Figure 3.2 (I)-(II)). The average size of the CUR micelles in DI water was in the range of 15-27 nm,

with a PDI of 0.19-0.85. Consequently, it indicated that the CUR micelles prepared by the thin-film hydration method at one centrifugation speed of 15000 rpm were stable during freeze-drying and sonication processes. An example of the appearance of the freeze-dried micelles and reconstituted micellar solution of CUR-loaded PF127 prepared by the thin-film hydration method is presented in Figure 3.3.

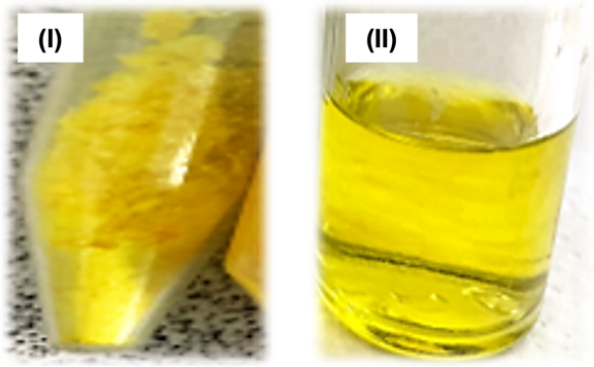

Figure 3.3: The appearances of (I) the freeze-dried CUR-loaded PF127 micelles (BK24-2 from Table 3.3), and (II) reconstituted micelles prepared by thin-film hydration method at 15000 rpm.

As shown in Figure 3.3, these prepared CUR-loaded PF127 micelles were freeze-dried without any cryoprotective agents and can reconstitute in DI water without heating after freeze-drying. Furthermore, it was clear that the freeze-dried CUR-loaded micelles were completely dispersed in DI water. Results obtained by Mohamet *et al.* are consistent with our findings that a mean particle size of approximately 97 nm of vorinostat-loaded PF127 micelles (PDI~0.33, 96% EE) prepared by the thin-film hydration method using MeOH presented a good solubility after the freeze-drying process, which was more convenient for clinical use and suitable for scale-up.[275] A similar investigation was also carried out by Patil *et al.* They examined the re-dispersal of nelfinavir mesylate loaded mixed micelles of PF127 and D-α-tocopherol PEG 1000 succinate (particle size~105 nm) after freeze-drying and found that the freeze-dried micelles were completely redispersed in the water and remained stable over 3 months.[276]

Taken altogether, the CUR-loaded PF127 micelles centrifuged at 15000 rpm had obvious advantages in the freeze-drying and dispersion as well as sonication processes compared

to another centrifugation step at 5000 rpm. As a consequence, the CUR-loaded PF127 micelles after centrifugation at 15000 rpm were more convenient for clinical use in terms of storage stability that can preserve the functionality of the micelles and ensure their ability to encapsulate and deliver the drug.

3.3.1.4. Differential scanning calorimetry characterization of the drug-loaded micelles

Differential scanning calorimetry (DSC) analysis was performed to analyze the variance in the solid state of the drug in different samples. Indeed, the transition of the drug from crystalline to an amorphous state when encapsulated in the PMs can be determined by DSC, as previously investigated by numerous researchers.[203,248,277] Therefore, in this work, a DSC thermogram was used to determine the thermal properties of CUR when encapsulated in PF127 micelles. An example of the freeze-dried CUR-loaded PF127 micelles prepared by thin-film hydration method at 15000 rpm of centrifugation speed was selected to study (BK24-2, Table 3.3), and the results are shown in Figure 3.4.

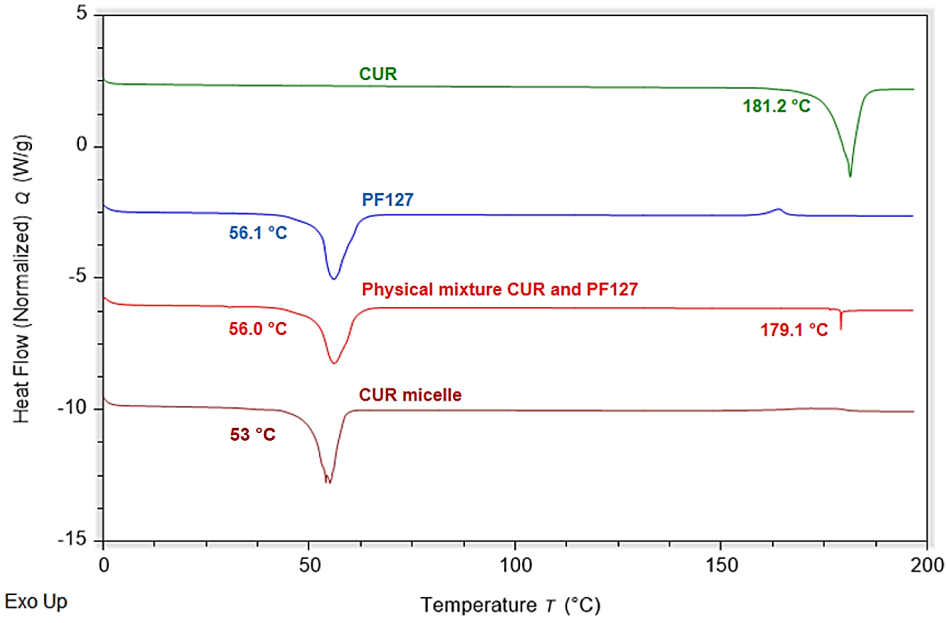

Figure 3.4: DSC profiles showing the peak temperature of CUR, PF127, physical mixture of PF127/CUR (PF127:CUR ratio=31.2:1), and freeze-dried 3.12 %(w/v) CUR/PF127 micelles after centrifugation at 15000 rpm from thin film hydration method (BK24-2 from Table 3.3).

CUR showed a sharp endothermic peak at 181.2°C, corresponding to the melting point of CUR (Figure 3.4).[251] Similarly, PF127 had a sharp peak at 56.1°C, which was associated with the endothermic melting of PF127.[203] Additionally, the CUR and PF127 melting points remained at approximately the same temperatures for a physical mixture of PF127 and CUR. Furthermore, after forming CUR-loaded PF127 micelles, the endothermic peak displayed a shift in peak position to lower temperature (from 56°C to 53°C), indicating that the carrier formed a new phase rather than a simple physical mixture or this could be due to a melting point depression effect caused by CUR mixed in with PF127 compound (Figure 3.4). At the same time, the melting peak of CUR at 181.2°C disappeared completely, suggesting that CUR was changed to an amorphous phase and encapsulated in CUR-loaded PF127 micelles. This study was similar to that reported by Vaidya and coworkers.[248] They examined PF127 micelles encapsulated CUR by using the DSC technique and found that the DSC curve of the CUR-loaded micelles was similar to PF127, which displayed a peak at 59°C. Additionally, no distinct peak of melting temperature near 176°C, which was the melting point of CUR, was observed in the DSC curve of both PF127 and the CUR-loaded PF127 micelles, indicating that the microencapsulation process of CUR in their prepared micelles did not affect the PF127 structure. A similar observation has also been reported by Bao *et al.* studying the celecoxib micelles.[203] The result showed that the specific peak for PF127 (57.3°C) shifted to a lower temperature (54.3°C) in the thermogram of the celecoxib micelles, whereas the specific peak for only celecoxib (164.8°C) was not observed.

These results might be attributed to the drug being amorphously dispersed in the micelles and likely having a relatively strong hydrogen bond interaction with the PF127 matrix. Therefore, the results yielded some interesting findings that the CUR/PF127 micelle was successfully prepared by the thin-film hydration method, which can be confirmed by DLS and DSC.

3.3.2 Method development for the quantitation of curcumin

3.3.2.1 UV spectroscopy for the curcumin detection

This study used UV spectrophotometry to analyze the percentages of EE and DL of CUR micelles. To calculate both EE and DL, the first study investigated the impact of PF127 on the degree of CUR absorbance (Figure 3.5).

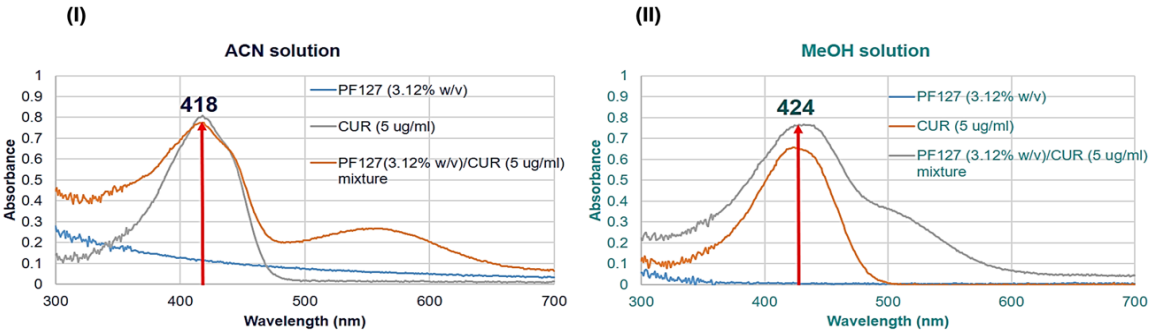

Samples	Absorbance at wavelength 418 nm
PF127	0.117
CUR	0.808
PF127/CUR	0.776

Samples	Absorbance at wavelength 424 nm
PF127	0.008
CUR	0.657
PF127/CUR	0.762

Figure 3.5: UV-Vis spectra of PF127 (3.12 %(w/v)), CUR (5 µg/mL), and a mixture of CUR/PF127 in (I) ACN and (II) MeOH.

Differences in PF127 absorbance values in acetonitrile (ACN) and methanol (MeOH) solvents were evaluated (Figure 3.5). The results showed that PF127 in ACN (absorbance value at 418 nm=0.117) had more impact on the degree of absorbance on CUR than PF127 in MeOH (absorbance value at 424 nm=0.008). Consequently, MeOH was chosen as the solvent for preparing an external standard calibration curve by UV-vis spectrophotometry at 424 nm (Figure 3.6).

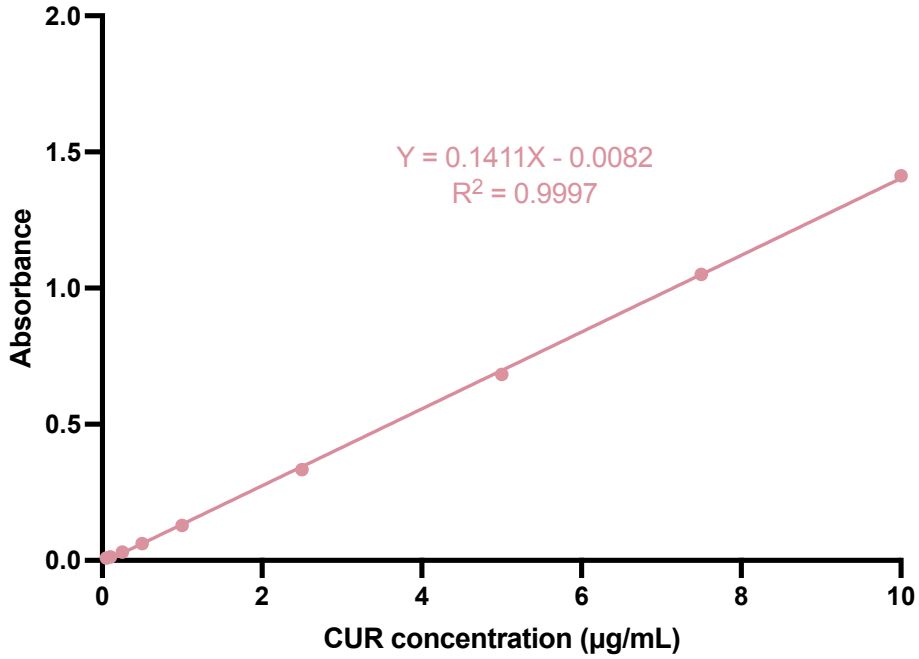

Figure 3.6: Standard curve of CUR in MeOH using UV-Vis spectrophotometry.

The standard curve for drug encapsulation efficiency was set up from 0.05 to 10 µg/mL (Figure 3.6), and the standard regression equation obtained was y=0.1411x-0.0082, R^2=0.9997.

3.3.2.1.1 Analytical method validation by matrix-matched calibration

As previously stated, MeOH had little impact on the degree of absorption of CUR (Figure 3.5). In this study, matrix matching was used to evaluate the matrix interference on the analysis results to suppress a major problem in accurate quantitative analysis of the CUR from the CUR-loaded PF127 micelles.

Matrix-match calibration is based on measuring the absorption of the CUR from the matrix micelles. The data are shown in Figure 3.7.

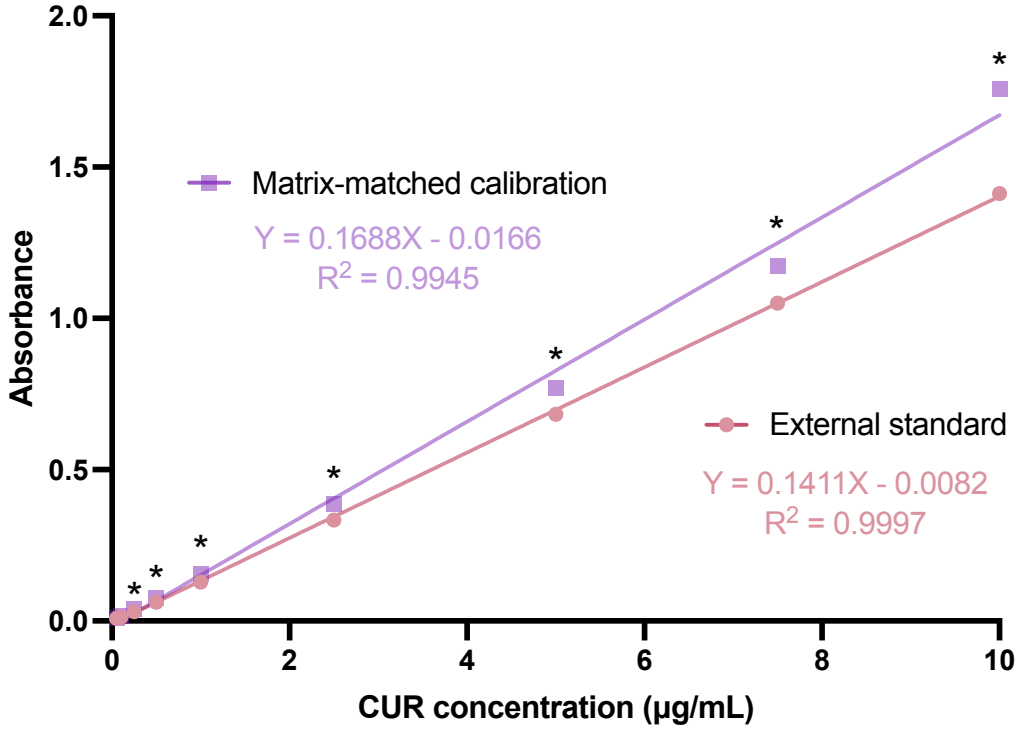

Figure 3.7: Comparison of matrix-matched calibration curve of CUR with external calibration curve (n=3). The diluent for the external standard was MeOH, whereas the diluent for matrix-matched calibration was freeze-dried PF127 micelles (3.12 %(w/v)) in MeOH. Statistical analysis was performed using an independent samples t-test (*p<0.05 compared to the external standard as a control). Data are presented as the mean ± SD of three experiments (n=3).

A comparison of the slopes obtained from the linear regression curves of the spiked blank matrix and the analyte in solution showed that the relative response between external calibration and matrix-matched calibration curves was significantly (p<0.05) different (Figure 3.7). This implied that an operative matrix within the sample significantly increased the detection of CUR in the samples. Specifically, when the CUR is added to the PF127 matrix, the CUR/PF127 complex will give a slightly higher absorbance reading than the absorbance generated with the same concentrations of CUR in the MeOH matrix. However, the matrix-matched calibration techniques present some drawbacks. Owing to the lack of an internal standard, no losses during sample preparation are compensated, leading to the lack of a sample that does not contain the analyte of interest.[203]

For that reason, the next section will deal with the standard addition method as it was investigated to counter issues with the matrix-matched method.

3.3.2.1.2 Standard addition method

To overcome the issues of matrix-matched analysis, the method of standard additions or spiked method is a quantitative analysis technique used to minimize matrix effects that interfere with analyte measurement signals. A representative example of this in an actual sample is presented in Figure 3.8.

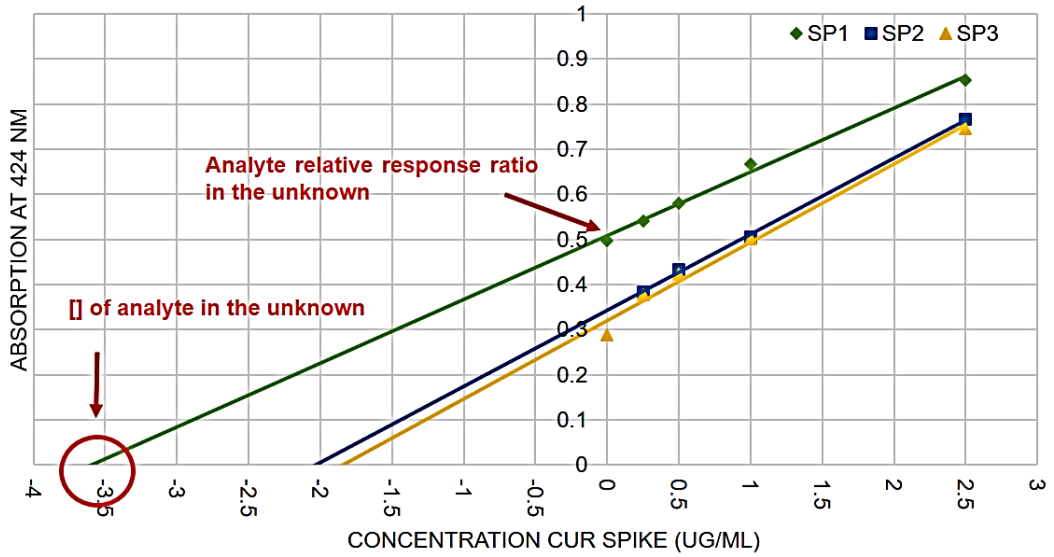

Figure 3.8: An example of a standard addition plot of sample BK37 (repeated from BK24-2, Table 3.3) used to determine the concentration of CUR in an unknown sample by UV-Vis spectrophotometry (n=3).

The intercept of the regression line with the x-axis corresponds to the amount of analyte in the sample (Figure 3.8). For that reason, the standard addition is a more reliable method to accurately quantify the analyte concentration than a matrix-matched calibration in case the amount of a specific analyte is close to particular threshold values. Table 3.4 presents the percentage of EE calculated by comparing between external calibration and standard addition calibration.

Table 3.4: The calculation of %EE of CUR-loaded PF127 micelles (BK37, repeated from BK24-2, Table 3.3) using external standard and standard addition calibration methods (n=3).

Formulation	%EE (Direct method)	
	External standard calibration	Standard addition calibration
BK37-S1	9.76	10.64
BK37-S2	6.33	5.78
BK37-S3	6.26	5.24
Average ± SD	7.45 ± 2.00	7.22 ± 2.97

No significant (p>0.05, independent samples t-test) difference in the percentage of EE of BK37 samples following external standard and standard addition calibrations (Table 3.4). Therefore, the external standard calibration was used to measure the EE of CUR in this study (Figure 3.8).

3.3.2.2 High-performance liquid chromatography for the determination of curcumin

3.3.2.2.1 High-performance liquid chromatography method optimization

The separation and identification of CUR was carried out using HPLC. Several mobile phase conditions and mobile phase compositions were tested to obtain a sharp peak of CUR with an appropriate retention time. An example of a chromatogram of CUR detected by HPLC in different mobile phase conditions is displayed in Figure 3.9.

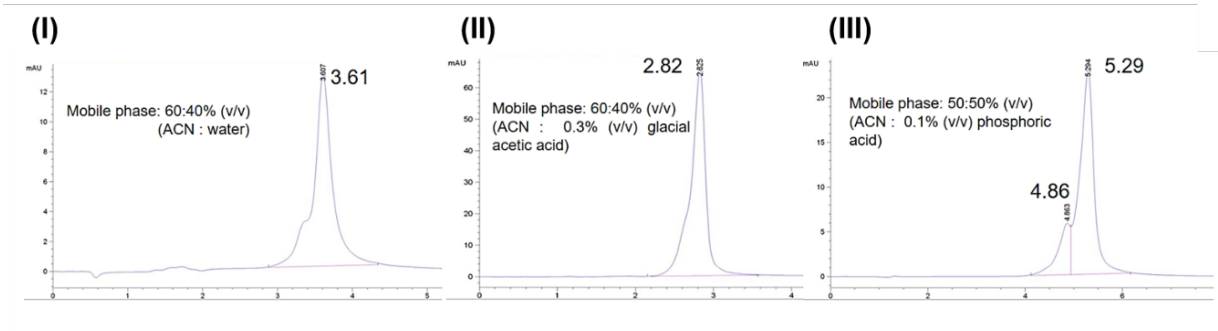

Figure 3.9: HPCL chromatograms of CUR/ACN (5 µg/mL). Conditions are as follows: stationary phase:Waters Nova-Pack® C18 column (150x4.6 mm column, 4 µm) with flow rate 1 mL/min. The mobile phase employed consisted of (I) ACN:water, (II) ACN:3 %(v/v) glacial acetic acid, and (III) ACN:0.1 %(v/v) phosphoric acid. UV detection was performed at λ=425 nm. Injection volume and column temperature were set at 20 µL and 25°C, respectively.

The retention time of the CUR/ACN sample was evaluated using different mobile phase compositions and ratios (Figure 3.9). However, the poor peak shape of the CUR peak was observed in all mobile phase conditions. This could be due to weak bonding among CUR molecules and column stationary phase caused by ACN.[278,279] For example, the study by Yang *et al.* found that increasing the proportion of ACN in the mobile phase leads to earlier elution and better separation of CUR.[278] Conversely, decreasing the ACN ratio results in inadequate separation.[278] Their study suggested that ACN suppresses π-π interactions between analytes and the phenyl stationary phase, leading to successful separation. Therefore, the HPLC mobile phase optimization method was then examined (Figure 3.10).

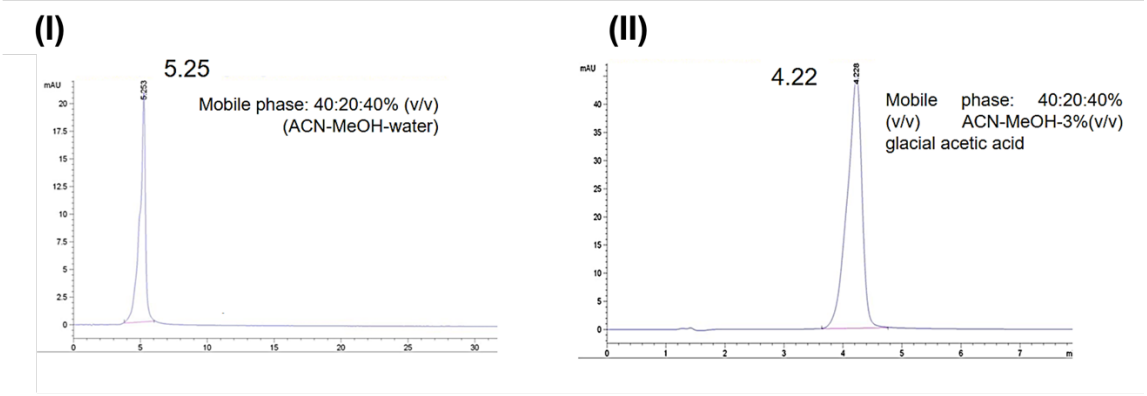

Figure 3.10: HPCL chromatograms of CUR/ACN (5 µg/mL). The mobile phase employed consisted of (I) ACN-MeOH-water and (II) ACN-MeOH-3 %(v/v) glacial acetic acid.

The mobile phases composed of ACN-MeOH-water (40:20:40 %(v/v)) were first selected to study at the wavelength of 420 nm (Figure 3.10(I)).[280] However, the chromatogram showed inadequate separation at 420 nm. Consequently, when the mobile phase composition was changed to ACN-MeOH-3 %(v/v) glacial acetic acid (40:20:40 %(v/v)), a single peak of CUR was detected at a retention time of 4.22 min (Figure 3.10(II)). Hence, drug loading and release studies of CUR-loaded PF127 micelles have been quantified following this mobile phase condition.

3.3.2.2.2 Quantification of curcumin by high-performance liquid chromatography

An external standard calibration curve was prepared to calculate both %EE and %DL using HPLC (Figure 3.11).

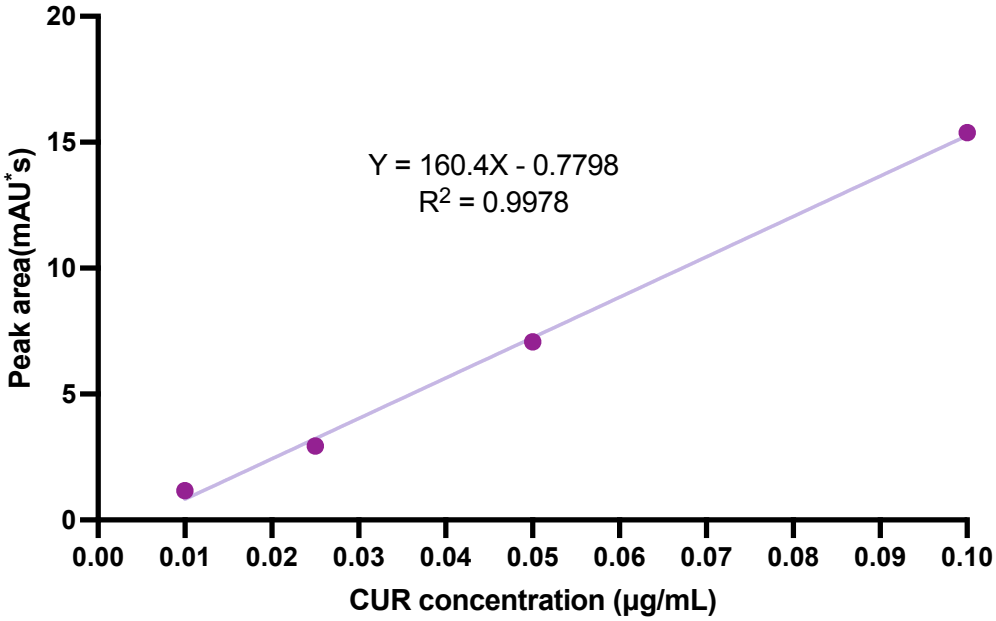

Figure 3.11: An external calibration curve for HPLC of CUR in MeOH.

CUR was quantified using a calibration curve with demonstrated linearity in the range of 0.01-0.1 µg/mL, and the linear regression equation obtained was y=160.4x-0.7798, R^2=0.9978 (Figure 3.11). Based on the SD and slope of the calibration curve, the limit of detection (LOD) and limit of quantification (LOQ) of CUR were 0.0002 µg/mL and 0.0007 µg/mL, respectively. Therefore, the standard calibration curve of CUR in MEOH obtained from both UV (concentration range between 0.05 and 10 µg/mL) (Figure 3.6) and HPLC (concentration range between 0.01 and 0.1 µg/mL) (Figure 3.11) was utilized to evaluate the percentage of EE and DL of the CUR/PF127 micelles in the following study.

3.3.3 Curcumin quantitation in Pluronic F127 micelles

Encapsulation assays were carried out with systems containing total copolymer concentration far above the CMC previously established (Chapter 2). This ensures the presence of micelles. The percentage of EE and DL of CUR was studied by UV-vis spectrophotometry following the external standard calibration curve (Figure 3.6), and extensive research over the last half century has revealed several techniques for quantifying CUR encapsulated in micelles. Encapsulation efficiency studies were carried out using either a micellar solution or a freeze-dried sample dissolved in different organic solvents, such as MeOH, ethanol, ACN, and DMSO-d6.[152,265,281,282] The study carried out by Wang *et al.* using ACN to dissolve the micellar solution of CUR-loaded Soluplus® and Solutol®HS15 micelles with particle size ranging from 71 to 300 nm.[152] Moreover, Patil *et al.* demonstrated the efficacy of using MeOH to determine the EE by diluting the CUR-loaded PF127/Gelucire micelles (182-415 nm) with 10-fold MeOH.[282] Similarly, the research work carried out by Wu *et al.* used MeOH to disrupt the small sizes of CUR-loaded PF123/PF127 micelles (~23 nm) for the EE study.[281] Besides, the work of Gou *et al.* revealed that drug encapsulation studies were also analyzed by using freeze-dried samples. In their study, 10 mg of freeze-dried CUR/mPEG-polycaprolactone (PCL) micelles (~24 nm) were dissolved in 0.1 mL of DCM before diluting with MeOH for drug quantification.[254] A similar study by Chen *et al.* demonstrated the determination of CUR in freeze-dried CUR-loaded cochleate with size 540 nm was accomplished by mixing 0.5 mL CUR micellar solution with 200 μL DCM, followed by sonication of the mixed solution for 5 min to disrupt the micellar structure.[283] Then, the demulsified solution was adjusted to 5 mL by EtOH before CUR quantification by HPLC. Taken altogether, in this study, several strategies were performed to evaluate the optimization of EE and DL of CUR-loaded PF127 micelles (Table 3.5).

Table 3.5: Comparison of EE and DL percentages obtained from several conditions. A sample selected to study was BK22-1 from Table 3.1.

Parameters	Sample preparation before UV analysis	Mixing time (min)	Sonication time (min)	Direct method	
				DL (%)	EE (%)
Solution sample	1:10 %(v/v) of supernatant solution in MeOH	2	-	5.60	0.17
Freeze-dried sample	10 mg freeze-dried sample in 2.5 mL MeOH			10.67	0.32
	185 mg freeze-dried sample in 2.5 mL MeOH			2.48	0.08
	10 mg freeze-dried sample in 2.5 mL MeOH	1440		10.10	0.34
	10 mg freeze-dried sample in 2.5 mL DMSO	2		7.07	0.21
	10 mg freeze-dried sample in 2.5 mL MeOH		5	11.00	0.33
	10 mg freeze-dried sample in 2.5 mL MeOH		15	10.89	0.33

Firstly, the effect of types of samples, either freeze-dried sample or solution, was studied (Table 3.5). The freeze-dried sample demonstrated a two-fold increase in both %EE and %DL compared to the solution form (0.17% EE, 5.6% DL). Nevertheless, increasing the amount of freeze-dried samples reduced the EE from 0.32 to 0.08%. Additionally, mixing time did not affect the EE and DL, standing at around 0.34% for EE and 10.10% for DL. In the context of solvent, MeOH was presented as more efficient in CUR quantification than DMSO (0.21% EE). Also, the percentage of EE of CUR maintained the same value at around 0.33% after the sonication process at different time intervals (Table 3.5).

In summary, these studies would suggest a strong association between CUR/PF127 micelles and MeOH solvent in CUR quantification. Mixing freeze-dried samples with MeOH for 2 min was the optimal condition to obtain the highest EE and DL according to direct method calculation. Furthermore, to ensure complete dissolution of the CUR-loaded micelles for drug quantification by UV following the optimal condition as shown in Table 3.5, a solubility study of PF127 copolymers in MeOH was conducted and found that the solubility of PF127 copolymers in MEOH were more than 255 ± 7 mg/mL (n=3). This confirmed the PF127 copolymers dissolved completely in MeOH, allowing the micelles to break down for CUR quantification by UV measurement. Table 3.6 presents the mean particle size, PDI, percentage of EE and DL by UV spectrophotometry according to the direct and indirect method calculations for the CUR-loaded PF127 micelles prepared by one-centrifugation step of each preparation technique following the optimal condition in the particle size, as aforementioned in section 3.3.1.1.

Table 3.6: The main characteristics of the CUR-loaded PF127 micelle systems. The limitation of particle size range for zeta potential (ZP) analysis is 10 nm-20 µm. The readings were taken 3 times from DLS analysis. The mean ± SD are obtained from the replication of the experiment 3 times.

Method	Ctf (rpm)	Direct method		Indirect method		DLS measurement	
		DL (%)	EE (%)	DL (%)	EE (%)	D_h (nm, vol%)	PDI
Direct	5000	0.31 ± 0.07	9.44 ± 2.57	0.75 ± 0.37	23.50 ± 11.16	451 ± 8 (84%)	0.14 ± 0.04
	15000	0.08 ± 0.03	2.47 ± 0.83	1.22 ± 0.28	37.80 ± 8.75	4 ± 0.1 (66%) 313 ± 60 (29%)	0.97 ± 0.72
Co-solvent	5000	0.98 ± 0.31	31.42 ± 10.4	1.41 ± 0.45	45.35 ± 14.11	2071 ± 493 (65%) 353 ± 87 (15%) 3482 ± 2685(20%)	0 .58 ± 0.39
	15000	0.34 ± 0.04	10.98 ± 1.40	2.84 ± 0.03	92.12 ± 1.00	19 ± 8 (18%) 3 ± 2 (35%) 5770 ± 162 (3%)	1.44 ± 0.91
Thin-film	5000	0.32 ± 0.15	10.20 ± 4.39	1.53 ± 0.27	48.72 ± 7.12	4024 ± 1696 (99%)	0.11 ± 0.08
	15000	0.23 ± 0.12	8.44 ± 1.88	0.90 ± 0.06	27.33 ± 0.38	15 ± 3 (60%) 3 ± 3 (16%)	0.19 ± 0.13

According to the results in Table 3.6, the EE and DL of the nanocarriers can be calculated by using the direct or indirect method, as explained earlier in Section 3.2.5. In relation to the direct method, the results showed that the percentage of EE of the formulations prepared from the co-solvent evaporation and thin-film hydration was higher than in the direct dissolution method, at around 10-31% and 7-10%, respectively (p<0.05, One-way ANOVA followed by Tukey's multiple comparisons test). Furthermore, it was remarkable that the formulations centrifuged at low speed (5000 rpm) displayed both high EE and DL, which might be caused by the greater internal volume of the larger particles of the CUR micelles prepared at 5000 rpm compared to 15000 rpm (Table 3.6). These results are consistent with observations made by Cheng and colleagues.[284] In their work, a 73 nm sized micelle with EE of 33% based on mPEG-PLA micelles combined with docetaxel nanocrystals (drug:polymer=4:150 mg/mg) was produced by a thin-film hydration method at 13000 rpm. Similarly, Kumari *et al.* demonstrated the efficiency of 100 nm-sized copolymer mPEG-PLA loaded CUR micelles (CUR:Polymer=1:5 mg/mg with 92% EE) prepared by thin-film hydration at 13500 rpm of centrifugation.[265] Their study found that micelles with higher hydrophobic groups in the core of the mPEG-PLA micelles facilitated efficient loading of CUR in the hydrophobic PLA compartment of the mPEG-PLA PMs, indicating the hydrophobic group effect on micelle EE.[265]

Thus, the results in the present study, as shown in Table 3.6, yielded some interesting findings that the addition of acetone, as a co-solvent, promoted efficient loading of CUR in the hydrophobic part of the PF127 PMs by the interaction between CUR and hydrophobic PPO unit of PF127 micelles. This led to a more uniform distribution and solubility enhancement of CUR in the hydrophobic part during the lipid film preparation, resulting in a higher %EE of the CUR prepared from co-solvent evaporation and thin-film hydration.[285–287]

Referring to the indirect method of calculation, our findings revealed a higher percentage of EE and DL as compared to direct method calculation (p<0.05, independent samples t-test, Table 3.6). A related idea that might explain the higher amount of drug content detected from the indirect method is that the whole un-entrapped drug may not get into the pellet owing to the low solubility of CUR (0.6 μg/mL).[152,244] On the contrary, the un-entrapped drug might precipitate out with the micelles in the supernatant part (direct method calculation), and the results were similar to the previous studies.[288] For example, Khoshneviszadeh *et al.* compared methods for studying the EE of hydroquinone in a liposomal system after centrifugation. Their study utilized the direct method to calculate EE from the bottom pellet, while the indirect method measured hydroquinone concentration in the supernatant. They found that indirect methods (SD=2.1-2.8) had better repeatability and higher dispersion than direct methods (SD=8.7), and their study suggested that the pellet part may be associated with the supernatant, leading to a false increase in EE.[288]

The next study was to clarify the role of the mismatch result of EE and DL between direct and indirect methods detected by UV spectrophotometry. A comparison of the experimental techniques of EE of CUR-loaded PF127 micelles was conducted. The study was achieved by applying several conditions and parameters to increase the EE and DL of the direct method to equal the indirect method. Firstly, the CUR-loaded PF127 micelles prepared at one-centrifugation step by thin-film hydration method were selected to optimize the following two parameters, which were an increased drug-to-polymer ratio and the addition of sonication before the centrifugation step, as previously shown in Figure 3.2. Table 3.7 displays the result of this study.

Table 3.7: The %yield and EE of the CUR-loaded PF127 micelle systems according to the thin-film hydration method. The mean ± SD are obtained from experiment replication 3 times.

Code	Drug:PF 127 ratio (w/w)	Condition	Ctf (rpm)	Yield (%)	Direct method		Indirect method	
					DL (%)	EE (%)	DL (%)	EE (%)
BK24-1	1:31.2	Ctf before SN	5000	86 ± 2.0	0.32 ± 0.15	10.20 ± 4.39	1.53 ± 0.27	48.72 ± 7.12
BK24-2			15000	82 ± 3.4	0.23 ± 0.12	8.44 ± 1.88	0.90 ± 0.06	27.33 ± 0.38
BK39	1:31.2	SN before Ctf	5000	91 ± 1.5	0.72 ± 0.08	23.43 ± 3.01	1.75 ± 0.27	56.43 ± 8.19
BK37	1: 31.2		15000	91 ± 0.9	0.26 ± 0.06	7.45 ± 2.00	1.17 ± 0.11	33.87 ± 2.70
BK40	1:140		15000	95 ± 1.5	0.70 ± 0.06	93.00 ± 6.62	-	-

*SN:sonication, Ctf:centrifugation

To begin with, the effect of centrifugation and sonication steps on the EE was studied. Sonication for 5 min before centrifugation could enhance the percentage yield, producing more solids in the supernatants (BK37, BK39, and BK40 Table 3.7). However, the EE and DL results did not change significantly, remaining at the same amount as the preparation without sonication (p<0.05, independent samples t-test, Table 3.7). Moreover, the percentage yield increased with increasing PF127 concentrations, obtaining the highest EE of 93% at the drug-to-polymer ratio equal to 1:140 w/w. At this condition, no pellet was observed after the centrifugation step, resulting in no drug quantification following the indirect method. This indicated that around 7% of the drug was lost from detection, although there was no pellet according to direct method calculation. Still, the EE and DL calculated by the direct method were lower than the indirect method. Secondly, the next parameter applied to enhance the EE and DL was using a heating process to improve the solubility of CUR (Table 3.8).

Table 3.8: Comparison of EE and DL obtained from the optimized condition of CUR encapsulated PF127 copolymers (BK37 and BK39 from Table 3.7). The mean ± SD are obtained from the replication of the experiment 3 times.

Formulation code	Ctf (rpm)	Preparation before UV	Direct method		Indirect method	
			DL (%)	EE (%)	DL (%)	EE (%)
BK39	5000	Mix with MeOH and stir for 2 min at rt	0.72 ± 0.08	23.43 ± 3.01	1.75 ± 0.27	56.43 ± 8.19
BK37	15000		0.26 ± 0.06	7.45 ± 2.00	1.17 ± 0.11	33.87 ± 2.70
BK39	5000	Mix with MeOH and stir for 1 h at 56°C	0.82 ± 0.06	26.51 ± 1.41	1.75 ± 0.27	56.43 ± 8.19
BK37	15000		0.23 ± 0.04	6.68 ± 1.20	1.17 ± 0.11	33.87 ± 2.70

After heating for 1 h, the results showed that the EE and DL of the CUR micelles insignificantly increased under both low and high-speed centrifuge conditions in comparison to the EE and DL of the CUR micelles before the heating process (p>0.05, independent samples t-test, Table 3.8). Thus, this study illustrated that heating of the CUR-loaded PF127 micelles could not enhance the solubility of the drug or break up the micelles to quantify more of the drug. In turn, it disturbed the stability of the drug-loaded micelles, resulting in a negligible increase or decrease in EE and DL quantification following the direct method calculation. Lastly, the study was performed by calculating the CUR recovery in each strategy (Table 3.9).

Table 3.9: An example of calculation for CUR recovery following the CUR-loaded PF127 micelles prepared by thin-film hydration method from Table 3.7.

Formulation code	CUR detected by UV (mg)		Theoretical CUR in the supernatant (mg)	Recovery of CUR in total (%)
	CUR in supernatant	CUR in Pellet		
BK24-1	1.18 ± 0.58	5.26 ± 0.70	4.79 ± 1.20	64 ± 4
BK24-2	0.75 ± 0.37	6.71 ± 1.78	3.75 ± 1.49	71 ± 11
BK39	2.33 ± 0.26	4.34 ± 0.84	5.62 ± 0.85	67 ± 6
BK37	0.83 ± 0.20	7.38 ± 0.20	3.78 ± 0.36	74 ± 4
BK40	9.83 ± 0.89	-	-	97 ± 4

*Calculations: Theoretical CUR in the supernatant (mg)=Mass of theoretical CUR put in-Mass of CUR detected by UV (pellet part), Recovery of CUR in total (%)=(Mass of total CUR detected by UV/Mass theoretical CUR put in)x100%

The results showed that more than half of CUR in all formulations were in the pellet part based on the calculation of theoretical CUR in the supernatant (Table 3.9). Additionally, nearly 100% of the drug was detected by UV spectrophotometry of the CUR micelles prepared at the highest drug-to-polymer ratio at 1:140 w/w (BK40, Table 3.9), whilst other CUR micelles lost around 30% of the drug (BK24, BK39 and BK37, Table 3.9). This supported that the direct method might be a reliable method for drug quantification since the CUR micelles prepared at 1:140 of the drug-to-polymer ratio had no pellet, suggesting that all of the CUR drugs in the supernatant were included in calculating the overall CUR recovery percentage, which achieved nearly 100%. As a result, the following study was to clarify the role of using a direct method for quantifying %EE and %DL of

CUR from the micelles between the two techniques. Table 3.10 shows a comparison between HPLC and UV spectrophotometry methods to determine the percentage of EE and DL of CUR from the formulation.

Table 3.10: A comparison between HPLC and UV methods to determine %EE and %DL of CUR encapsulated PF127 copolymers prepared by using thin-film hydration technique (BK37, BK39, and BK40 from Table 3.7). The mean ± SD are obtained from the replication of the experiment 3 times.

PF127 (% w/v)	Ctf rpm (code)	Method	Type of calibration curve	Direct method		Indirect method	
				DL (%)	EE (%)	DL (%)	EE (%)
3.12	15000 (BK37)	HPLC	External calibration	0.23 ± 0.05	6.76 ± 1.72	0.18 ± 0.10	5.11 ± 2.70
		UV	External calibration	0.26 ± 0.06	7.45 ± 2.00	1.17 ± 0.11	33.87 ± 2.70
			Standard addition	0.25 ± 0.10	7.22 ± 2.97		
14	15000 (BK40)	HPLC	External calibration	0.75 ± 0.20	101.01 ± 28.95	No Pellet	
		UV		0.70 ± 0.06	92.96 ± 6.62		
3.12	5000 (BK39)	HPLC	External calibration	0.81 ± 0.10	26.21 ± 4.53	2.70 ± 0.53	13.06 ± 14.05
		UV		0.72 ± 0.08	23.43 ± 3.01	1.75 ± 0.27	56.43 ± 8.19

As illustrated in Table 3.10, the study employed a quantitative approach combining HPLC and UV techniques for studying both the EE and the DL of CUR from the CUR-loaded PF127 micelles. The results demonstrated that there was no difference in the %EE and %DL of all CUR micelles calculated following the direct method from both UV and HPLC techniques (p>0.05, independent samples t-test, Table 3.10). Conversely, the EE and DL of all CUR-loaded PF127 micelles calculated by the indirect method were notable changes between UV and HPLC techniques (p<0.05, independent samples t-test, Table 3.10). Moreover, there was a slight difference in the %EE of BK40 across both methods in which the EE of BK40 without pellet detected by HPLC was around 100%, suggesting more sensitivity of HPLC than UV spectrophotometry in the detection of CUR quantification. In addition, the EE results obtained from direct method calculation by HPLC of the CUR micelles prepared at the lower drug-to-polymer ratio (BK37 and BK39, Table 3.10) were similar to the results obtained by the indirect method (HPLC) (p>0.05, independent samples t-test). As a consequence, these findings could be compared to the

results of earlier studies of CUR determination by UV spectrophotometry (Table 3.7) that the direct method can be used to measure the %EE and %DL of CUR by HPLC.

In the literature studies, researchers commonly employ both direct and indirect methods to calculate the EE and DL of drug-loaded nanocarriers, including micelles. In the direct method, the amount of drug encapsulated within the nanocarriers was measured directly after the separation of the drug-loaded nanocarriers from the free drug by several techniques, such as centrifugation and filtration. On the contrary, the EE in the indirect method was calculated by subtracting the total amount of drug feeding and the amount of free drug that was not entrapped in the nanocarriers.[289] Thus, each technique had its advantages and limitations, so researchers chose the most appropriate method based on their specific experimental setup and requirements. For example, Ardhi *et al.* applied a direct method to calculate the EE of the thymoquinone (TQ)-loaded black seed oil emulsions using a centrifugation technique (12000 rpm, 30 min).[290] Their study found that the common centrifugation (62% EE) obtained a noticeably higher %EE of TQ compared to ethanol-centrifugation (5% EE), indicating extraction solvent type of the disperse phase affected EE of TQ. Similarly, Bhuptani *et al.* obtained the %EE of lornoxicam drug up to 70% from Soluplus® micelles when using a direct method to calculate the %EE.[291] Furthermore, some research studies compared the %EE calculation between direct and indirect methods to select the most suitable method for their nanocarriers.[288,292] For instance, Garms *et al.* compared the direct and indirect methods to calculate the %EE of CUR-loaded PLGA/PVA nanoparticles and found that the %EE obtained between both direct and indirect methods were significantly different.[292] Indeed, the indirect method (57% EE) estimated a higher %EE compared to the direct method (32% EE) of CUR. Their study suggested that this result could be ascribed to CUR loss by degradation during the fabrication process of 4 h at 24°C. For these results, their study concluded to use the indirect method to calculate the %EE of CUR. Therefore, different studies may prefer one method over the other methods based on several factors such as the sensitivity of the analytical technique, the nature of the drug and carrier system, and the research objectives.

Overall, the choice between indirect and direct methods for calculating EE and DL in drug-loaded micelles should be carefully considered according to the specific research subjects and objectives. Researchers must have an understanding of the potential limitations related to each methodology and their impacts on the reliability and precision of their research findings. By integrating both approaches and evaluating findings using supplementary methodologies, it allowed researchers to improve the precision and reliability of the data interpretation, ultimately improving their understanding of DDS.

In our study, given the importance of accurately determining the %EE and %DL of CUR-loaded PF127 micelles, the direct method might be more accurate and suitable for %EE and %DL calculation of CUR-loaded PF127 micelles since the direct method directly quantified the amount of CUR content entrapped within the PF127 micelles from the supernatant part by mixing the suspension with the organic solvent. Whereas, using the indirect method may lead to overestimation of %EE and %DL owing to factors such as incomplete separation of free CUR drug from the CUR-loaded PF127 micelles to the pellet part after the centrifugation step, as previously described in the work of Khoshneviszadeh *et al*.[288] Altogether, these CUR quantitation studies would suggest that the direct method by HPLC was more suitable for the EE and DL measurements of CUR compared to the indirect method.

3.3.3.1 Optimization strategy for encapsulation efficiency

To enhance drug encapsulation and loading of CUR-loaded PF127 micelles, previous results focusing on CUR quantitation in PF127 micelles have demonstrated an efficacy of using either co-solvent evaporation or thin-film hydration method to prepare CUR/PF127 micelles, leading to high EE and DL (Table 3.6). As a consequence, in this study, the thin film hydration method was selected for optimization since the particle sizes obtained from this method were about 20 nm, which was a small size and could be an effective OcDD system by enhancing corneal absorption, improving ocular bioavailability, and prolonging the ocular retention time.[228,293] In this study, the drug-to-polymer ratios were investigated. Table 3.11 reports the respective drug quantitation and size distributions at different drug-to-polymer ratios, which were optimized to obtain the CUR micelle particles with different EE and DL values.

Table 3.11: The particle sizes (D_h, percentage by intensity), polydispersity index (PDI) and zeta potential (ZP), drug encapsulation, and loading efficiency at different polymers to drug ratios of CUR-loaded PF127 polymers prepared using the thin-film hydration method at 15000 rpm of centrifugation speed. The mean ± SD are obtained from the replication of the experiment 3 times.

Code	Drug : PF127 (w/w)	Drug quantitation (Supernatant)		DLS measurement			Viscosity (mPa.s)
		EE (%)	DL (%)	D_h (nm, Int%)	PDI	ZP (mV)	
BK66-1	1:10	4 ± 1	0.4 ± 0.1	78 ± 32 (80%) 7 ± 1 (20%)	0.50 ± 0.05	-8.84 ± 4.67	1.1 ± 0.1
BK66-4	1:30	6 ± 2	0.2 ±0.05	55 ± 3 (61%) 7 ± 1 (39%)	0.57 ± 0.11	-2.93 ± 0.92	1.4 ± 0.06
BK66-7	1:50	10 ± 1	0.2 ±0.03	46 ± 5 (76%) 6 ± 1 (23%)	0.53 ± 0.01	-1.8 ± 0.81	1.9 ± 0.1
BK66-10	1:70	14 ± 4	0.2 ±0.05	52 ± 2 (87%) 5 ± 1 (12%)	0.44 ± 0.07	-0.23 ± 0.71	2.9 ± 0.1
BK66-13	1:100	26 ± 2	0.3 ±0.02	65 ± 15 (88%) 6 ± 1 (12%)	0.46 ± 0.09	-0.57 ± 0.45	5.7 ± 0.1
BK66-16	1:120	72 ± 2	0.6 ±0.02	51 ± 3 (83%) 5 ± 0.1 (17%)	0.61 ± 0.12	-0.47 ± 0.18	21.8 ± 8.3
BK40	1:140	100 ± 35	0.8 ± 0.2	50 ± 7 (65%) 5 ± 0.03(35%)	0.58 ± 0.35	-0.74 ± 0.86	55.1 ± 15.7

For the optimization of the prepared CUR micelles, the influence of the drug-polymer ratio on the particle size, ZPs, DL, and EE of the CUR-loaded PF127 micelles was investigated. As shown in Table 3.11, the particle sizes of the CUR micelles in different drug-to-polymer ratios ranged from 50 to 78 nm. A slight increase in particle size was also observed under certain conditions, which may have resulted from a higher drug encapsulation at a high drug-polymer feed ratio. Furthermore, the ZPs of all the produced CUR micelles were slightly negative (-0.23 to -8.84 mV). This could be related to the hydration layer formation of water molecules around the CUR-loaded PF127 micelles in an aqueous environment in which this layer can contain ions and polar molecules to interact with the CUR micelles outer surface, leading to a net negative charge on the micelles. In addition, at an applied drug-to-polymer weight ratio from 1:10 to 1:140, the EE increased from 4% up to 100%, with the DL increase in the range between 0.4% and 0.8%. This demonstrated that when the drug-to-polymer ratio was increased in the CUR-loaded PF127 micelles, there was a greater availability of polymer chains to encapsulate the drug molecules. The higher polymer concentration could lead to enhanced EE since more CUR drug molecules were effectively entrapped within the

micellar core, rather than being present in the external aqueous phase. This result was similar to the work of Arukkunakorn *et al*. In their studies, they developed dimethyl CUR-loaded PF127 micelles, which could self-assemble into a small micelles size (20-50 nm) using a thin-film hydration method, followed by vortex and sonication for 10 min. Additionally, their result showed that the %EE of the drug of PF127 copolymers increased from 74% to 82% when increasing the drug-to-polymer ratio from 0.4:200 to 2:200 (w/w).[294] Similarly, the study of Wang *et al.* also found that di-block polymers based on Soluplus® and Solutol®HS15 at a high ratio (160:40) enhanced the EE of CUR into the PMs (~82 nm) up to 91% by using the solvent evaporation method at 3000 rpm of centrifugation speed.[152]

However, our present study also indicated that as the drug-to-polymer ratio was increased, the overall concentration of the PF127 polymers in the formulations increased accordingly, leading to a more viscous solution of CUR-loaded PF127 micelles (Table 3.11). The final viscosity of the CUR micelle suspension increased up to nearly 52 mPa.s. An increase in viscosity could also be attributed to the greater number of polymer chains of PF127 presented in the solution to interact and entangle with each other, resulting in hindrance to the flow of the system and challenge in the separation of the unentrapped drug molecules from the micellar dispersion in the supernatant part through centrifugation and filtration methods. In other words, an increase in the amount of PF127 enhanced the EE of CUR to the micelles because it increased the hydrophobic PPO segments of PF127 to interact with CUR and to form the micelles, resulting in a high level of CUR encapsulation in PF127 micelles.[295]

Applying this to the OcDD applications, the viscosity of the administered drops is a vital factor that may impact the rate of drainage.[296] A low viscosity, measured in the range of 1-12 mPa.s, was often preferred for eye drops in OcDD to ensure that they were well-tolerated and could quickly disperse across the eye without causing discomfort or blurring of vision. In accordance with the review by Singh *et al.*, the viscosity between 2 and 3 mPa.s. was appropriate for ocular preparation.[297] Similar to the work of Arif *et al.* in evaluating the viscosity of 18 artificial tears, they demonstrated that the mean viscosity for all 18 artificial tears was 12 ± 10 mPa.s.[298] In addition, Kassem *et al*. developed

dorzolamide HCl-loaded cationic nanoemulsion consisting of isopropyl myristate, Tween-80, and cetyl trimethyl ammonium bromide and found that their formulations (1.31 mPa.s) with control the viscosity below 20 mPa.S showed an enhanced and extended lowering effect of intraocular pressure in male albino New Zealand rabbits compared to plain DRZ and marketed DRZ eye drops (100 mPa.S).[299] In turn, this indicated that the formulations with higher viscosity levels may accelerate reflex tearing and, hence, accelerate the drug removal from the surface. Moreover, many patients, as emphasized in the review article by Grassiri *et al.*, found high viscosity eye drops uncomfortable caused by ocular surface irritation, and they could also result in reflex blinking after administration with inconsistent drug dosing.[300]

Therefore, our experimental results aligned with these literature studies in terms of the viscosity of the micelles for OcDD. The optimized CUR micelles with a viscosity under 20 mPa.s were suitable and selected for further study.

3.3.3.2 Storage stability study of curcumin-loaded Pluronic F127 micelles

Our study investigated the storage stability of the prepared CUR micelles (Figure 3.12).

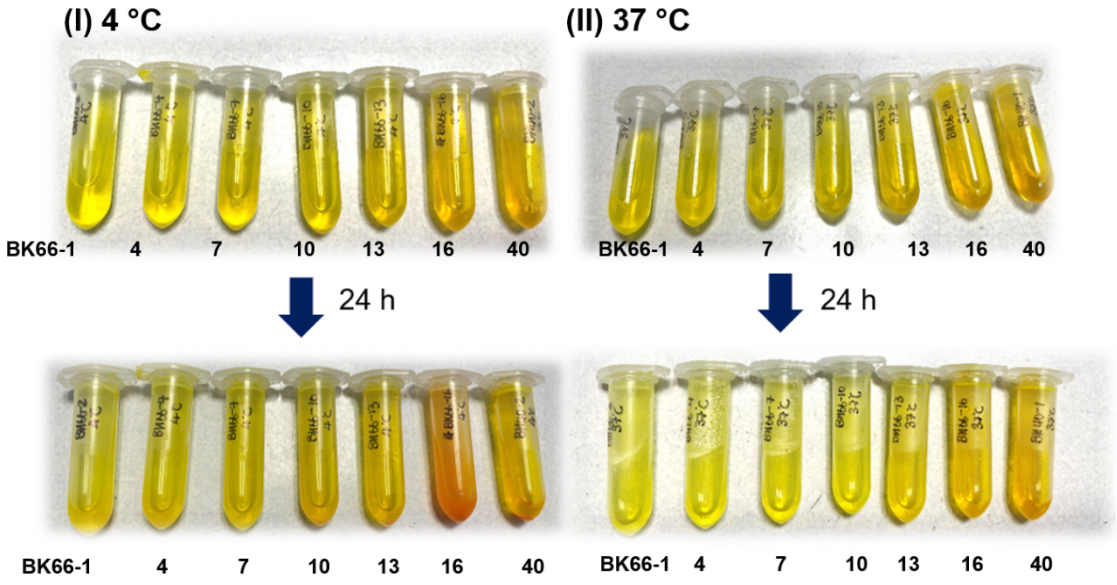

Figure 3.12: Comparison of the appearance of the CUR micelles prepared by thin-film hydration method (the samples from Table 3.11) at (I) 4°C and (II) 37°C after 24 h.

As displayed in Figure 3.12, a clear yellow-coloured solution of the CUR micelles in all conditions occurred at 37°C. However, drug precipitation was observed at 4°C for the CUR micelles at a higher drug-to-polymer ratio (1:120 and 1:140), indicating the instability of the CUR micelles under these conditions. The possible reason might be the drug was suspended in the viscous solution without encapsulation into the micelles at the high viscous condition due to the hindered diffusion of the drug molecules within the viscous matrix of the micelles during storage time for 24 h, leading to increased possibility of drug aggregation and subsequent precipitation.

3.4 Cytotoxicity study of the curcumin micelles on immortalized human corneal epithelial (IM-HCEpi) cells and human corneal epithelial (HCE-T) cells

The study compared the cytotoxicity and biocompatibility of free CUR drug, blank PF127 micelles, and CUR-loaded PF127 micelles on cells, providing insights for potential therapeutic applications and assessing their impact on IM-HCEpi cells and HCE-T cells. Therefore, cell viability analysis was first performed to determine the toxic effects of the free CUR, blank, and CUR-loaded PF127 micelles on IM-HCEpi cells using APA assay, as described in Section 3.2.7.1. Figure 3.13 is a graphic summary of the cell viability studies according to IM-HCEpi cells.

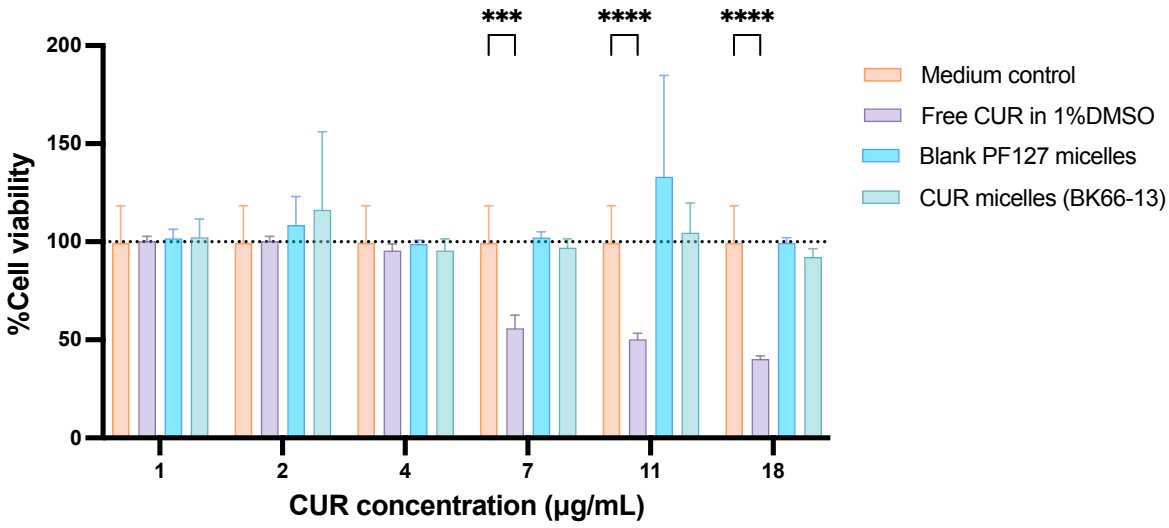

Figure 3.13: Assessment of cell viability of IM-HCEpi cells treated with Free CUR in 1% DMSO, Blank PF127 micelles, and CUR-loaded PF127 micelles at CUR concentration of 0-18 µg/mL for 24 h. Statistical significance was analyzed by the One-way ANOVA followed by Dunnett's multiple comparisons (*p<0.05, **p<0.01, ***p<0.001 and ****p<0.0001 compared to the mean values of the medium control condition). Data are presented as the mean ± SD of three experiments (n=3, each experiment by the mean of its three technical replicates).

The results of the APA assay showed that both blank PF127 micelles and the CUR micelles showed more than 80% cell viability for all treatment concentrations, indicating no toxicity at all concentration ranges of the study after 24 h (Figure 3.13). However, toxicity was observed in the secondary corneal cell line cytotoxicity study for the free CUR at a concentration equal to or above 7 µg/mL (p<0.0001), which was in agreement with previous studies.[319,320] For example, Bagheri *et al.* conducted an *in vitro* cytotoxicity study on mPEG(5kDa)-*b*-PEG-*b*-poly(N-2-benzoyloxypropyl methacrylamide)-based PMs loaded with CUR. They found a significant decrease in cell viability at 24 hours of free CUR concentration, while CUR micelles and empty micelles showed over 80% cell viability at lower concentrations.[301]

Furthermore, the following cell viability assay study was performed to confirm the cell viability of the CUR formulations compared to the blank PF127 micelles and DI water as controls. In this study, the effects of listed formulations on HCE-T cells were carried out following three strategies: the resazurin assay, the cellular LDH release, and ROS

formation (Figure 3.14). The assays were performed to confirm the effects of the CUR formulations compared to the blank PF127 micelles and DI water as controls.

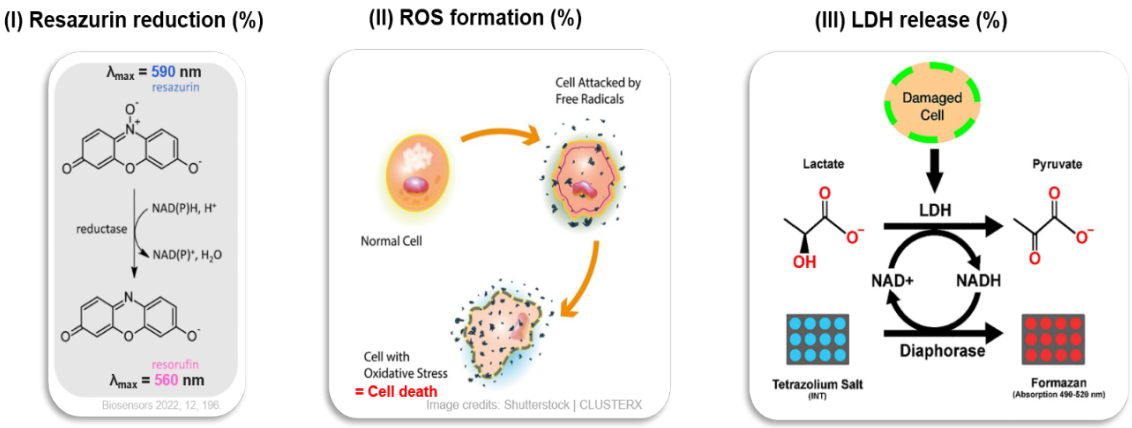

Figure 3.14: Schematic representation of (I) the resazurin to resorufin conversion, (II) ROS, and (III) LDH release assay.

In the resazurin assay, a blue non-fluorescent dye called resazurin is added to the cell culture (Figure 3.14(I)). Metabolically active cells will reduce resazurin to resorufin, a pink, highly fluorescent compound. The extent of fluorescence produced is proportional to the metabolic activity of the cells, providing a quantitative measure of cell viability. Additionally, ROS formation is the assay used to detect and measure free radicals in biological systems. The build-up of the ROS to a high level within the cells will happen when the system is out of control, leading to cell death (Figure 3.14(II)). Moreover, LDH release is the study of the presence of a cytosolic enzyme in the cells, which refers to cell membrane damage (Figure 3.14(III)). Consequently, the cell viability study was conducted, and the summary of the results is illustrated in Figure 3.15.

(I) Resazurin reduction

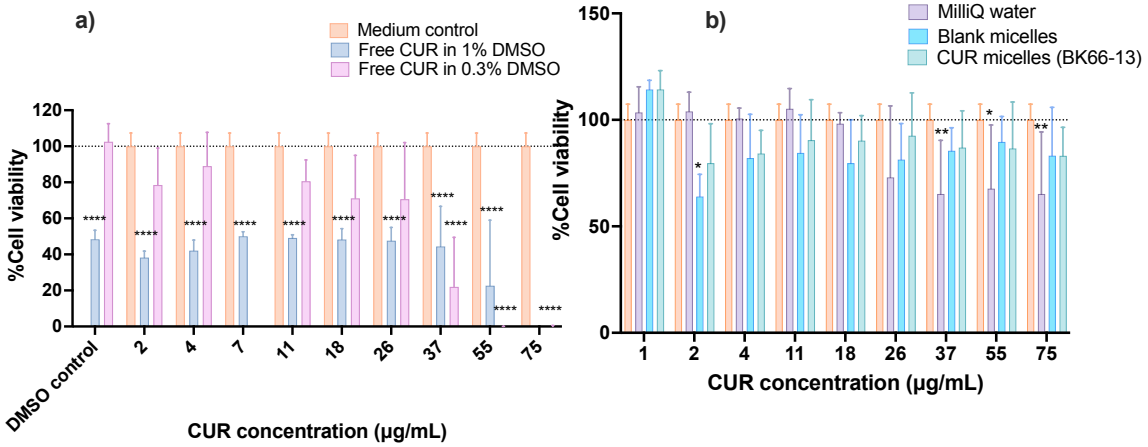

(II) LDH release

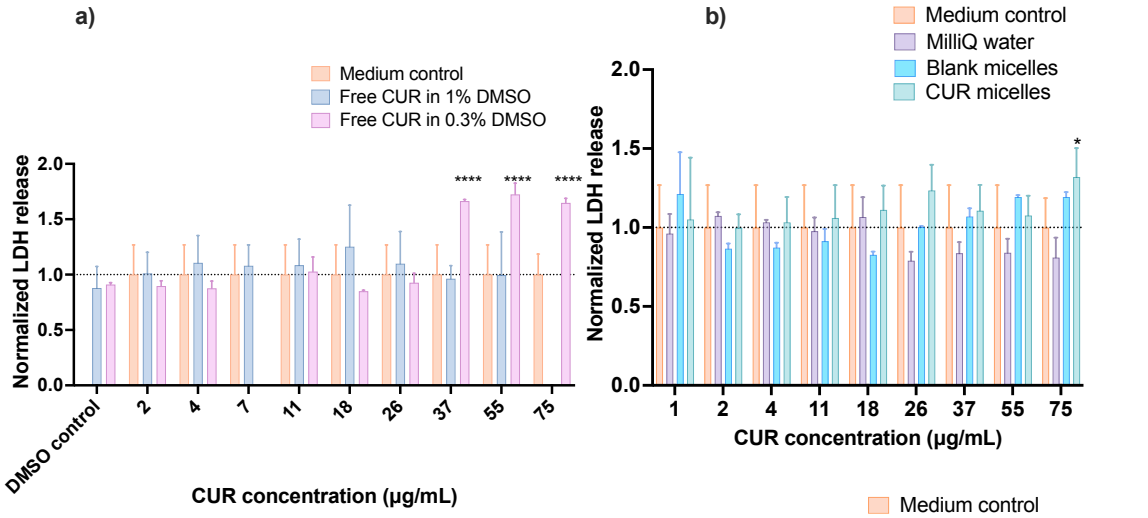

(III) ROS formation

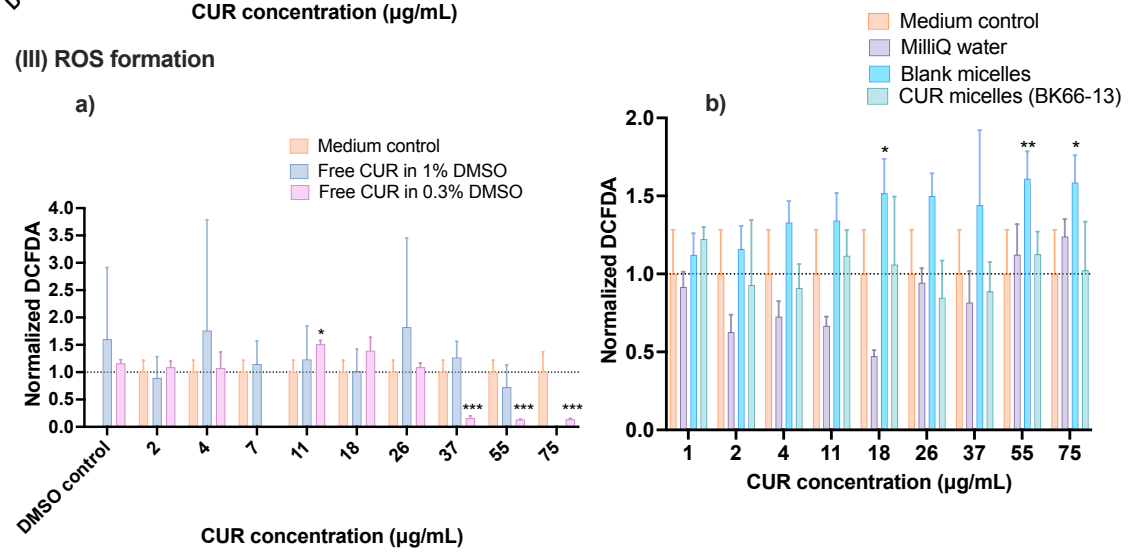

Figure 3.15: Assessment of (I) cell viability (II) LDH release and (III) ROS formation of HCE-T cells treated with (a) Free CUR at 1% and 3% DMSO and (b) MilliQ water, blank PF127 micelles, and CUR-loaded PF127 micelles (BK66-13, Table 3.11) at CUR concentration of 1-75 µg/mL for 24 h. Statistical significance was analyzed by the One-way ANOVA followed by Dunnett's multiple comparisons (*p<0.05, **p<0.01, ***p<0.001 and ****p<0.0001 compared to the mean values of the medium control condition). Data are normalized to the untreated control conditions. Data are presented as the mean ± SD of three experiments (n=3, each experiment by the mean of its three technical replicates) or the mean of two experiments (n=2, experiment contained three technical replicates, LDH release and ROS formation).

As illustrated in Figure 3.15, the results showed that the cell viability outcomes derived from the resazurin assay of all formulations were found to be congruent with those obtained using the APA assay, as previously displayed in Figure 3.13. More precisely, the CUR at a high DMSO concentration (1%) exhibited a significant decrease in cell viability throughout the concentration range tested compared to the free drug at a lower DMSO concentration (3%) (Figure 3.15(I-a)). CUR showed a clear dose response towards decreased cell viability at higher concentrations (>37 µg/mL), leading to higher LDH release and ROS formation on the HCE-T cells (Figure 3.15(II-a) and (III-a)). It demonstrated that CUR at high concentrations killed the HCE-T cells completely, resulting in cellular damage and stress. In addition, the blank micelles and CUR micelles did not affect the cell viability at all concentration ranges, whereas MilliQ water affected the cell viability at a concentration above 37 µg/mL (Figure 3.15(I-b)). This indicated that the PF127 encapsulating CUR could enhance the cell viability at higher drug concentrations without inducing toxicity to the cell, in contrast to CUR administered on its own, which exhibited toxicity to the cells at lower concentrations. Moreover, taking into account LDH release, even though the CUR micelles showed minimal impact in LDH release at the highest CUR concentration (75 µg/mL), there was no significant difference in the mean value of the cell viability in each concentration compared to the media control (p>0.05, Figure 3.15(I-b) and (II-b)), suggesting their biocompatible nature without an indicator of cell membrane damage or cell death at all concentrations tested of these formulations. Besides, the blank PF127 micelles exhibited a slight increase in the normalized DCFDA in ROS formation compared to the CUR micelles and DI water

(Figure 3.15(III-b)). A possible explanation is that the cells might be experiencing oxidative stress at a lower level than the cell damage stage, as highlighted in the review paper by Nikzamir *et al*.[302] Therefore, this observation suggests that encapsulating the CUR within the micelles might mitigate its cytotoxic effects to some degree, possibly through controlled release or enhanced targeting of the CUR to the cells. Besides, the cell viability study comparing the CUR with the empty micelles and the CUR-loaded micelles provides important insights into their cytotoxicity and biocompatibility profiles, leading to the groundwork for their potential applications in DDS and therapeutic interventions.

3.5 *In vitro* release of curcumin from micelles

Due to the hydrophobicity and instability of CUR at pH 7.4, as highlighted in previous work by Gupta *et al*. this experiment examined both CUR solubility (Figure 3.16) and stability (Figure 3.19) in different media to identify the most suitable medium for a CUR release study.[303]

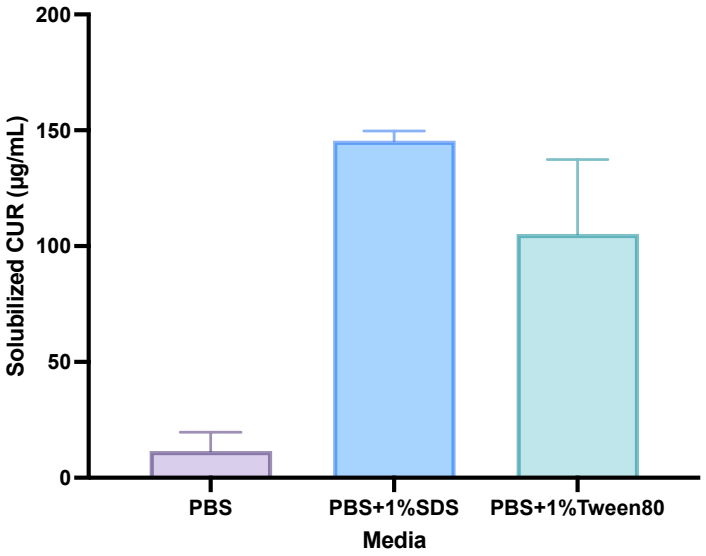

Figure 3.16: Solubilization of free CUR in different release media (PBS (0.01 M, pH 7.4, 37°C), PBS containing 1 %(w/v) SDS or 1.06 %(w/v) Tween-80 at 24 h. Data are presented as the mean ± SD (n=3).

The result illustrated that all three media, namely PBS (0.01 M, pH 7.4) and PBS (0.01 M, pH 7.4) containing 1 %(w/v) SDS and 1.06 %(w/v) Tween-80, dissolved CUR. Adding a surfactant increases the CUR solubility, which was around a 13-fold increase for PBS containing 1 %(w/v) SDS and a 9-fold increase for PBS containing 1.06 %(w/v) Tween-80. Accordingly, to investigate the stabilities of CUR in three media, CUR content was monitored over 8 days (Figure 3.17).

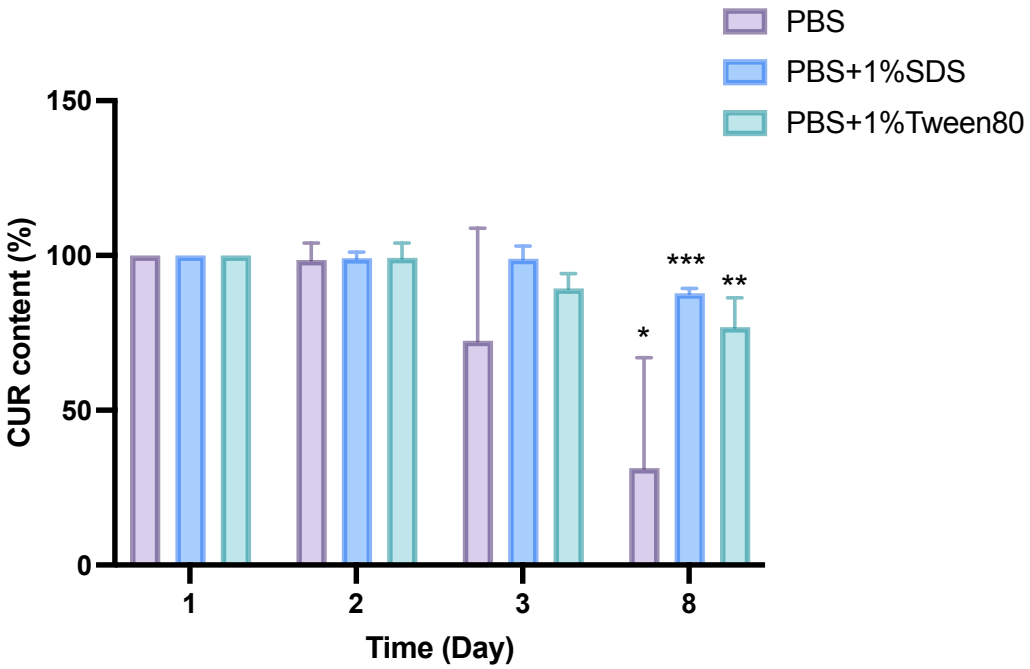

Figure 3.17: Free CUR stability in different release media (PBS (0.01 M, pH 7.4, 37°C), PBS (0.01 M, pH 7.4, 37°C) containing 1 %(w/v) SDS or 1.06 %(w/v) Tween-80. Data are presented as the mean ± SD (n=3). Statistical significance was analyzed by the One-way ANOVA followed by Dunnett's multiple comparisons (*p<0.05, **p<0.01, ***p<0.001 and ****p<0.0001 compared to the mean values of the control group of CUR content in each medium at the start). Data are presented as mean ± SD of three experiments (n=3, each experiment by the mean of its three technical replicates).

As illustrated in Figure 3.17, for PBS with 1 %(w/v) SDS, approximately 99% of the CUR content remained at 72 h and 88% at 192 h, whereas for the PBS with 1.06 %(w/v) Tween-80, the CUR content slightly dropped to 89% at 72 h, and even to 77% at 192 h. Similarly, the CUR content went down to nearly 30% at 192 h for only the PBS medium,

suggesting degradation of CUR.[304] Hence, it was obvious that CUR showed good stability in both PBS and PBS containing surfactants for 8 days, but the CUR solubility was very low in the medium with only PBS. Consequently, PBS (0.01 M, pH 7.4) containing 1% SDS was finally selected as the release medium for CUR-loaded micelles. For the drug release study, as earlier described (Table 3.11), two CUR/PF127 micelles prepared by the thin-film hydration method, which had different EE and DL, were chosen for developing the drug release method (BK66-4 and BK66-13). The drug release profile comparing the CUR micelles at different EE and DL is depicted in Figure 3.18.

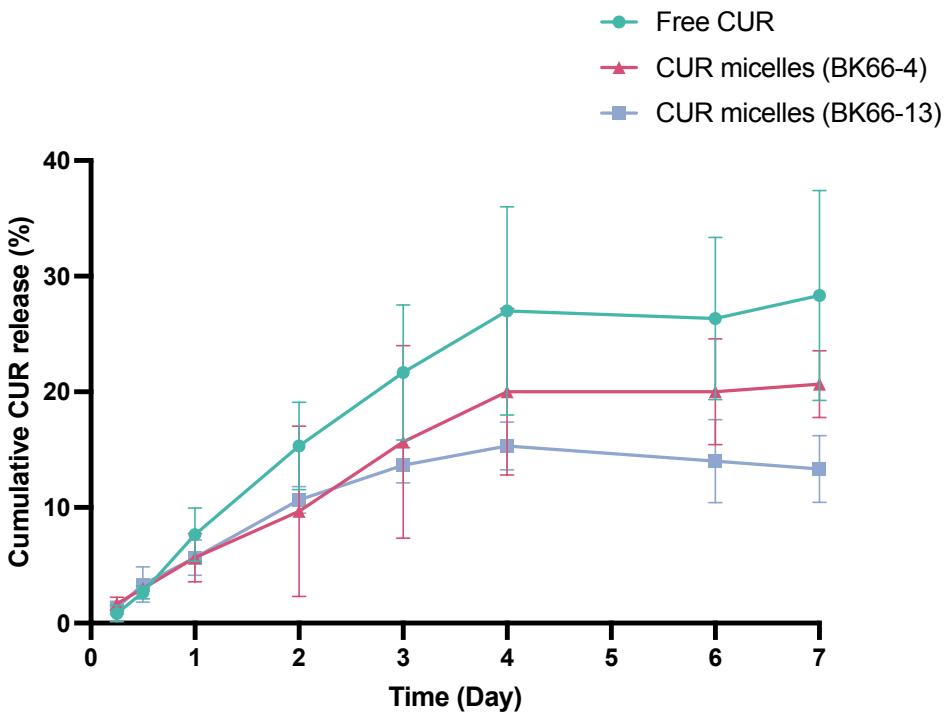

Figure 3.18: Cumulative drug release profiles of 200 µg/mL CUR from DI water and CUR-loaded micelles (BK66-4 and BK66-13 from Table 3.11) in pH 7.4 phosphate buffer containing 1 %(w/v) SDS. Data are presented as the mean ± SD (n=3).

Figure 3.18 shows the drug release profile of CUR as the free drug suspension (Free CUR) and in CUR-loaded PF127 micelles over 7 days in PBS containing 1 %(w/v) SDS. The CUR release profile demonstrated a gradual, sustained release of CUR from both BK66-4 and BK66-13 micelles of up to 24% and 14% at 7 days, respectively. However, the

control release profile showed a limitation in the release of the free drug suspension as a control group across the dialysis membrane, with only 28% release at 7 days. Additionally, the smaller sizes of CUR-loaded PF127 micelles (BK66-4, Table 3.11) provided a higher drug release rate than those larger micelles (BK66-13, Table 3.11). The possible explanation might be a higher surface area-to-volume ratio of the small-sized micelles than the larger micelles, which facilitated faster diffusion of the encapsulated drug out of the micelles, resulting in higher drug release rates, as stated in the review paper by Bose *et al*.[305] Therefore, this study exhibited that the PF127 micelles showed a sustained-release property for the incorporated CUR due to the intermolecular force between CUR and carriers, which made CUR stable in the simulated physiological environment.[270] In addition, Kumari *et al.* examined the CUR release from CUR-mPEG-PLA micelles (100 nm, 92% EE) in 5% SDS solution and the free CUR in propylene glycol solution using dialysis method (2kDa MWCO dialysis cassettes).[265] In their study, nearly 55% of CUR was slowly released from the CUR micelles, while more than 90% of free CUR was released from the propylene glycol solution within 24 h at 37 °C, indicating rapid release in the control group. This result was similar to the reported studies carried out by Xu *et al.* showing a rapid transfer of free DEX (99%) across the dialysis cassette (3500 MWCO) in water at 37°C within 6 h of incubation, whereas the release of DEX from 65-nm sized chitosan oligosaccharide-valylvaline-stearic acid/DEX micelles (62% EE) presented a gradual release at 40% during the same time.[306]

Contrary to these research investigations, the present study on *in vitro* drug release of CUR from CUR-loaded PF127 micelles demonstrated a potential issue with experimental procedures for quantifying CUR content using the dialysis method since the free CUR suspension showed limited release across the dialysis membrane. More details are presented in Table 3.12.

Table 3.12: Quantification of CUR from free CUR and PF127 micelles (BK66-4 and BK66-13 from Table 3.11) in pH 7.4 phosphate buffer containing 1 %SDS. Data are presented as the mean ± SD (n=3).

Code	Experiment			Theory
	Total amount of CUR in the dialysis bag at start (A)	Amount of CUR detected after 7 days (µg)		Total CUR remaining inside the dialysis bag (µg) (D)=(A)-(B)
		Outside the dialysis bag (B)	Inside the dialysis bag (C)	
BK66-4	81 ± 28	15 ± 4	4 ± 3	66 ± 24
BK66-13	247 ± 18	32 ± 8	5 ± 1	215 ± 11
Free CUR	267 ± 58	72 ± 35	57 ± 89	194 ± 32

As illustrated in Table 3.12, the CUR release study of CUR-loaded PF127 micelles demonstrated that less than half of the total amount of CUR was released from the dialysis bag (MW cutoff 14 kDa) in both a control group (free CUR) and CUR-loaded micelles (D and A, Table 3.12). Besides, the mass of CUR detected inside the dialysis bag following the experiment was lower than the amount of CUR calculated from the theory (C and D, Table 3.12). A possible reason might be ascribed to the fact that the amount of CUR remaining or CUR-loaded PF127 micelle suspension was stuck in the dialysis bag knots. Consequently, CUR content could not pass through the dialysis bag membrane, as shown in Figure 3.19.

Figure 3.19: The appearance of BK66-13 micelles during drug release study (n=3).

CUR was encapsulated within the core of the PF127 copolymers. These micelles were very small in size and tended to adhere to the surface of the dialysis bag due to their

amphiphilic nature. When conducting drug release studies using a dialysis bag, the micelles may stick to the knot or mesh of the dialysis bag so that the dialysis bag turns yellow during the drug release experiment, leading to a loss of drug rather than being released into the release medium (Figure 3.19). This study was similar to the research study by Weng *et al.* found extra damage to the Vitamin D3-loaded PEG nanoparticles (42 ± 4 nm) during drug release by dialysis membrane method because of an interaction between cellulose and the surface of PEG nanoparticles, resulting in particle aggregation and destabilization of their prepared formulations with low drug release (3% over 400 min).[259]

To address this issue, the following experiment in quantification of the mass of CUR attached to the dialysis bag was studied (Table 3.13).

Table 3.13: Mass balance after drug release study, including CUR mass attached to the dialysis bag. The samples were free of CUR and the CUR micelles (BK66-4 and BK66-13 from Table 3.11) in pH 7.4 phosphate buffer containing 1% SDS. Data are presented as the mean ± SD (n=3).

Code	Experiment			Theory
	Total amount of CUR in the dialysis bag at start (A)	Amount of CUR detected at day 7 (µg)		Total CUR remaining inside the dialysis bag (µg) (D)=(A)-(B)
		Outside the dialysis bag (B)	Inside+attach the dialysis bag (C)	
BK66-4	81 ± 28	15 ± 4	4 ± 0.5	66 ± 24
BK66-13	247 ± 18	32 ± 8	18 ± 7	215 ± 11
Free CUR	267 ± 58	72 ± 35	2 ± 1	194 ± 32

As shown in Table 3.13, still, the amount of CUR detected in the dialysis bag following the experiment and the theory were far different (p<0.05, paired samples t-test) even though the mass of CUR attached to the dialysis bag was included in the calculation (C and D, Table 3.13). Therefore, this result, along with the previous study result in Table 3.12, supported the loss of CUR mass, which might have been caused by the degradation of CUR itself during the drug release study. Furthermore, our study explored alternative drug release quantification methods using ultracentrifugation (CU) techniques that minimize micelle adhesion.[259] The summary of the steps for studying the drug release using the CU technique and the results are presented in Figure 3.20.

(I)

Free CUR/DI water + 6 %(v/v)MeOH + 5ml of medium (PBS+1%SDS) (CUR content = 26.33±0.06 µg/ml)

Incubate shaker at 37 ± 3 °C, 120 rpm

Transfer the samples to an ultrafiltration tube (MWCO 3kDa) and centrifuge at 10000 rpm for 5 min

HPLC to quantify the amount of CUR in the bottom part

(II)

$$\text{Drug recovery (\%)} = \frac{\text{conc. of filtrate}}{\text{conc. of solution}} x\ 100\%$$

Time (hr)	Amount of CUR detected (µg/ml)		Drug recovery (%) obtained from ultracentrifugation (CU) technique	
	The solution inside the filter	The filtrate	The solution inside the filter	The filtrate
0	Start = 26.33 ± 0.06 ug/ml		-	-
6	25.99 ± 0.08	0.33 ± 0.05	98.73 ± 0.50	0.01 ± 0.002
48	14.04 ± 0.16	Couldn't detect	53.34 ± 0.51	-

(III)

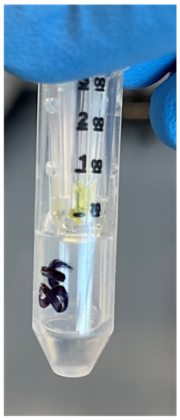

Figure 3.20: A schematic diagram of (I) the experimental study of drug release following the CU technique, (II) CUR quantification after 24 and 48 h of the drug release study by the CU method, and (III) the appearance of the ultra-centrifugal tube after 48 h of study. Data are presented as the mean ± SD (n=3).

The drug release experiment using the CU technique (MWCO 3kDa) was performed with slight method modification by Weng *et al*.[259] The experiment was performed by studying the behavior of the free drug in the CU technique to establish a baseline for how the drug behaves in the absence of any delivery system or formulation, which serves as a reference point for evaluating the performance of DDS (Figure 3.20(I)). The results illustrated that there was a significant decrease in CUR content after 48 h of study (p<0.05, One-way ANOVA followed by Dunnett's multiple comparisons test) compared to the CUR content of the time at the start, supporting a degradation of CUR over time (Figure 3.20(II)). Moreover, free CUR content remained in the holder tube after 48 hours of studying and could not pass through the ultracentrifugal filters to the collection tube (Figure 3.20(III)). Taken altogether, these findings would suggest that CUR showed a limited release across the dialysis membrane. The possible reason could be that some of the CUR was lost during the CU process and that CUR might stick to the walls of the tubes or filter membranes, leading to lower recovery rates. In addition, CUR is known to be sensitive

to light and heat, and CU may degrade during the CU process, resulting in lower detected concentrations. Consequently, a degradation was carried out to clarify this issue

3.5.1 Forced degradation study of curcumin by high-performance liquid chromatography

In this study, the investigation of the forced degradation of CUR under conditions of thermal and photodegradation was examined to assess its chemical stability, degradation pathways, and the formation of degradation products. Thus, the results provided valuable insights into the potential impact of environmental factors on the stability of CUR, as well as its degradation product (Figure 3.21).

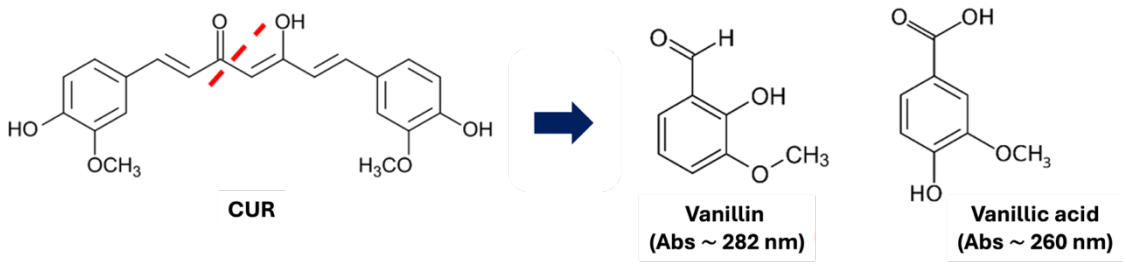

Figure 3.21: Possible structures of curcumin degradation products.[326]

CUR is known to undergo degradation under various conditions, resulting in the formation of several potential degradation products. Some of the possible degradation products include vanillin by demethylation or vanillic acid, which is derived from ferulic acid (Figure 3.21).[307,308] As earlier described in Section 3.2.6, the observed impact of thermal and photo-degradations on CUR analyzed by HPLC is shown in Table 3.14.

Table 3.14: Forced degradation study by HPLC. Data are presented as the mean ± SD (n=3). Data was analysed using two-way ANOVA followed by Dunnett's multiple comparisons test, ******p*<0.001 and *******p*<0.0001.

Time (h)	% Degradation		% Decrease in peak area	
	By thermal	By photo	By thermal	By photo
Start	0	0	0	0
6	31 ± 12***	3 ± 4	22 ± 18	3 ± 4
18	51 ± 3****	7 ± 2	54 ± 29	6 ± 2
24	60 ± 16****	5 ± 2	51 ± 28	5 ± 2

Our findings revealed that thermal energy would lead to a notable decrease in the CUR stability resulting in the degradation of CUR, as evidenced by the significant loss of CUR content up to 60% after 24 h detected by HPLC (p<0.05) (Table 3.14). Whilst the exposure of CUR under photodegradation after 24 h did not affect the degradation of CUR compared to the start time (Table 3.14). Additionally, the HPLC chromatogram from the thermal degradation experiment of the CUR peak after 24 h did not show the peak that belonged to vanillin and vanillic acid as the degradation products (appendices Figure S1). The study carried out by Peram *et al.* also reported similar results that the absence of degradation peaks or no change in the peak area accounting for CUR was observed by thermal degradation heating at 80°C.[309] Therefore, the CUR samples after both thermal and photodegradation studies were further studied by running UV spectrophotometry (appendices Table S1). The results showed a decrease in absorbance at 420 nm for thermal degradation, while there was no change in the absorbance value at 420 nm for photodegradation samples. Additionally, thermal degradation led to a significant increase in absorbance values at 260 and 280 nm, indicating the formation of new chemical compounds due to the degradation of CUR. Furthermore, based on the forced degradation study of CUR by HPLC, the HPLC condition used might not be suitable, leading to no separation of the degradation products. As a result, the next section was focused on the optimization process of the HPLC to study the degradation products of CUR.

3.5.2 High-performance liquid chromatography development to confirm degradation products of curcumin

To isolate a single peak corresponding to vanillin and vanillic acid, the experimental design for HPLC analysis was carefully tailored to optimize chromatographic conditions, including mobile phase composition. In this study, the HPLC conditions were optimized in two conditions, which were high organic phase (ACN:MeOH:3 %(v/v)acetic acid=60:20:20 %(v/v) and high aqueous phase ACN:MeOH:3 %(v/v)acetic acid=15:5:80 %(v/v), as detailed in Figure 3.22.

(I) High organic phase condition

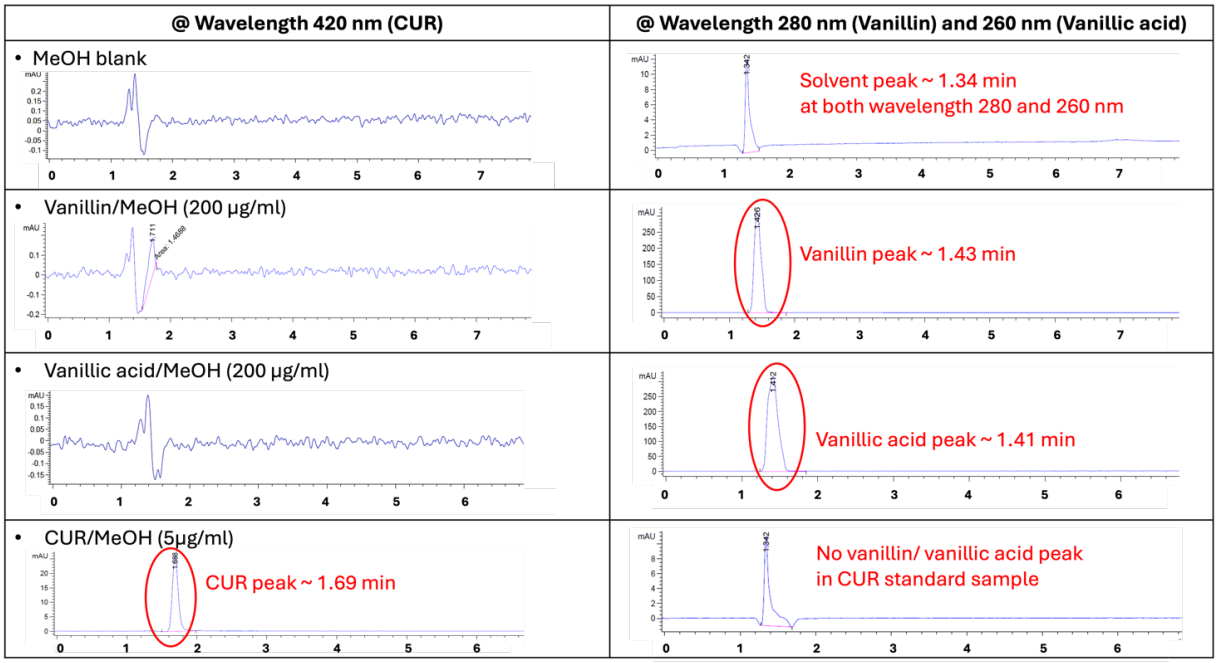

(II) High aqueous phase condition

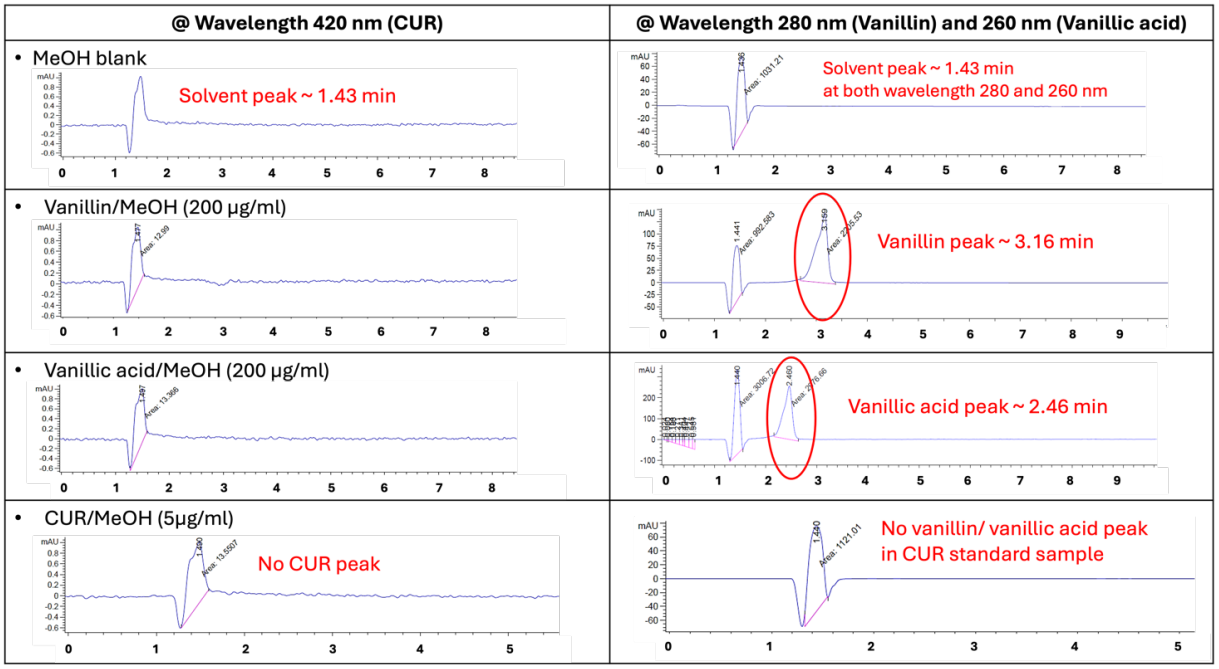

Figure 3.22: A schematic diagram of HPLC chromatogram of vanillin, vanillic acid, and CUR in MeOH after the HPLC run following (I) high organic phase and (II) high aqueous phase conditions of the mobile phase.

The chromatogram obtained using the high organic mobile phase showed distinct peaks corresponding to the vanillin, vanillic acid, and CUR at different retention times and wavelengths (Figure 3.22(I)). However, the CUR/MeOH sample did not show a peak at 260 and 280 nm wavelengths. Similarly, the chromatogram obtained using the high aqueous mobile phase exhibited the specific chromatogram relating to each compound with longer retention times (Figure 3.22(II)). For this reason, the study was further continued to apply the HPLC condition following the high organic mobile phase with the samples. Indeed, in the following study, the samples selected to run for each condition were the pure compound in MeOH and, the CUR sample from the last day of the *in vitro* drug release study, and the free CUR sample from the forced degradation study by thermal after 24 h. The summary of the results is displayed in Figure 3.23.

Sample	Retention time (min)		
	Wavelength 420	Wavelength 280	Wavelength 260
MEOH blank	-	1.34	1.34
Vanillin/ MeOH (200 µg/ml)	-	1.43	1.33
Vanillic acid/ MeOH (200 µg/ml)	-	1.35 1.40	1.41
CUR/MEOH (5µg/ml)	1.69	1.34	1.34
A sample from thermal degradation study after 24 h	1.69 (A decrease in the peak area)	1.34	1.69 1.49 1.34
A sample from drug release study at day 10	1.69 (A decrease in the peak area)	1.34	1.34

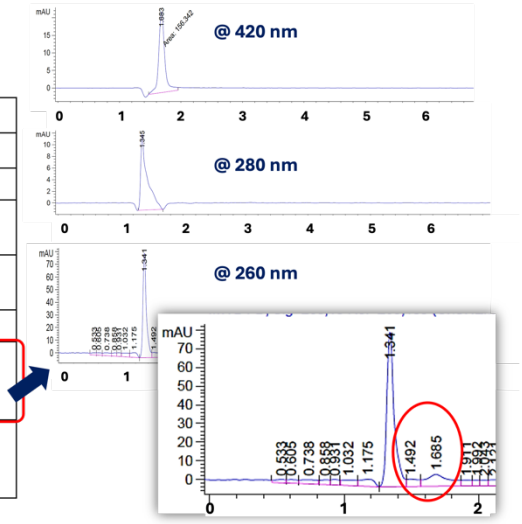

Figure 3.23: Summarization of the retention time of pure compounds (CUR, vanillin, and vanillic acid in MeOH) and the samples from the experiment (the *in vitro* drug release at day 10 and forced degradation study by thermal after 24 h) from HPLC condition using high organic phase condition, as previously stated in Figure 3.22. Insert the examples of HPLC chromatogram of the 24 h thermal degradation sample running at different wavelengths.

The results yielded some interesting findings in that there was a decrease in the peak area of the CUR peak observed from both thermal degradation and drug release samples at wavelength 420 nm (Figure 3.23). Additionally, the sample from the thermal degradation

study after 24 h displayed a HPLC chromatogram corresponding to the vanillic acid at the retention time of 1.49 min, confirming CUR degradation during the study. Hence, these findings emphasized the necessity of method development and optimization to select an appropriate mobile phase that can effectively resolve the separation of each compound in complex mixtures.

To sum up, the degradation study of CUR used UV spectrophotometry and HPLC analysis to confirm its degradation and identify specific degradation products, vanillin and vanillic acid. The results confirmed the degradation of CUR, with changes in the UV absorption spectrum and the appearance of vanillin and vanillic acid peaks in HPLC chromatograms. Therefore, the thermal degradation study led to the temperature thresholds at which CUR started to degrade and created degradation products. Considering this result with the drug release profile of CUR-loaded PF127 micelles, CUR might start undergoing degradation at 37°C during the drug release process to create the degradant products (vanillin and vanillic acid), which could then impact the amount of CUR available for release, resulting in a variation in drug release kinetics.

3.6 *Ex vivo* permeation assay

The *ex vivo* permeation study was performed to assess the potential of the prepared CUR micelles for enhanced trans-corneal and trans-scleral drug delivery. As previously discussed in Section 3.3.3.1, the optimized CUR micelles with a %EE of 26 and viscosity of 5.7 mPa.s were selected for this since this CUR showed a sustained release over a period of time following the *in vitro* drug release study.

Pig cornea and sclera were isolated from fresh eyes and mounted in vertical Franz-diffusion cells at 37°C with 1.06 %(w/v) Tween-80 as the receptor medium, as stated in Section 3.2.9. CUR permeated across the corneal and the scleral tissues to the receptor chamber and was monitored for 6 h, and the results of the study are shown in Figure 3.24.

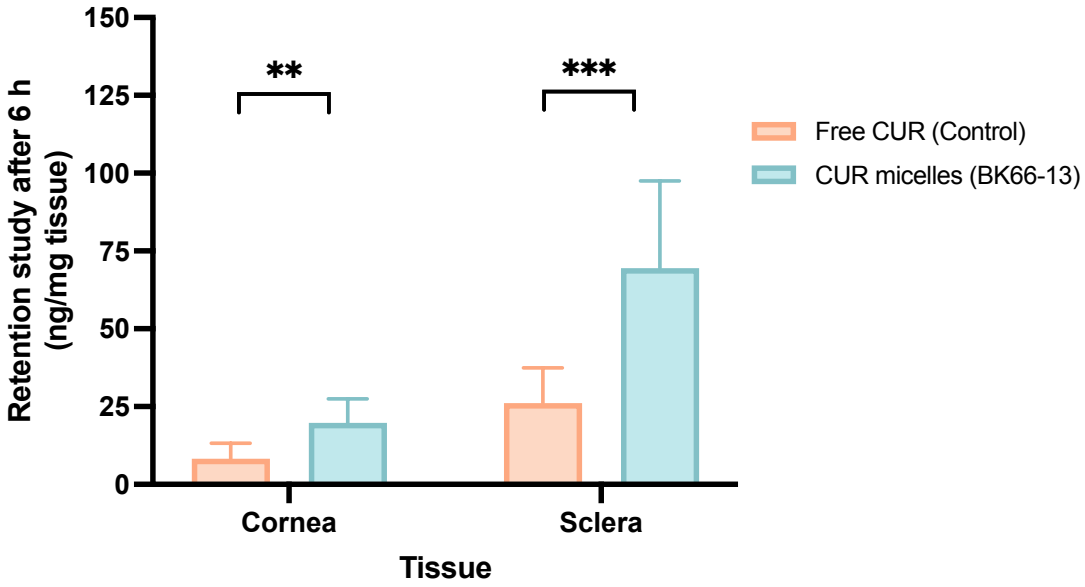

Figure 3.24: Drug retention in the cornea and sclera of the porcine eyes after 6 h of contact with the CUR-loaded PF127 micelles (BK66-13 from Table 3.11) and the free CUR control. The medium in the receptor chamber was PBS+1.06 %(w/v) Tween-80. The concentration at the start of the free CUR in the MilliQ water as a control group was 32 ± 2 µg/mL. Statistical significance was analyzed by the independent samples t-test (*p<0.05, **p<0.01, ***p<0.001 and ****p<0.0001 compared to the mean values of the free CUR control group in each tissue). Data are presented as the mean ± SD of three experiments (n=3, each experiment by the mean of its three technical replicates).

The *ex vivo* study revealed that there was no CUR detected in the receptor chamber after 6 h of study, possibly due to a lower level of drug in the receptor phase than the quantification limit of HPLC detection, which was similar to other previous studies.[158,193] However, despite the limited ability of the CUR micelles to penetrate the cornea and sclera, it was shown that CUR had accumulated in both tissues at levels over the quantitation limit (Figure 3.24). Importantly, the CUR micelles provided higher amounts of drug accumulated than the free CUR as a control group in both cornea (p<0.01) and sclera (p<0.001) (Figure 3.24), indicating that the PF127 micelles helped CUR uptake into the ocular tissues compared to the control group. In addition, the level of the CUR detected inside the sclera tissue was 3-fold higher than the amount of CUR found in the cornea tissue, which suggested a better tissue penetration of the CUR micelles to the

sclera. Therefore, this finding indicated that the CUR-loaded micelles effectively interacted with the cornea and the sclera, which might be useful for drug delivery for both anterior and posterior segment eye diseases. Besides, these findings underlined the importance of further exploring in the following section whether the CUR micelles absorbed into the deeper layers of the ocular tissue.

3.7 *Ex vivo* tissue uptake study of coumarin-6 micelles across the cornea of the porcine eye

In this study, the cell uptake study of the CUR-loaded PF127 micelles across the cornea tissue was performed by using coumarin-6 dye, as explained in Section 3.2.10. The Cou6-loaded PF127 micelles were dropped onto the corneal tissue, which was crimped with the Franz-diffusion cells, and the experiment was conducted for 6 h at 37°C. Then, the corneal tissue was tested under a fluorescence microscope, as displayed in Figure 3.25.

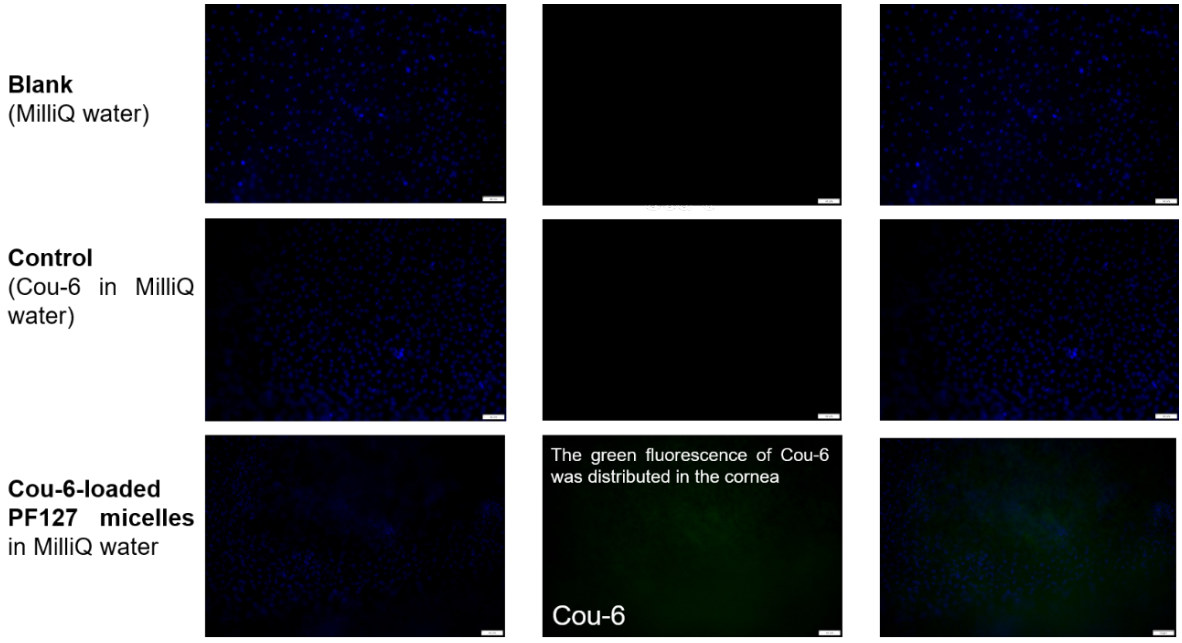

Figure 3.25: Fluorescence microscope of the cornea of porcine tissues after Cou6-loaded PF127 solution eye drops administration (20x magnification) (n=3).

The cellular uptake study of the Cou6-loaded PF127 micelles across the corneal tissue, assessed using fluorescence imaging, revealed the green fluorescence of Cou6 dye was detected and distributed in the cornea. Whereas the green fluorescence did not show in the blank and the free drug samples as a control. This demonstrated the efficient internalization of the micellar formation of the PF127 micelles by corneal cells, highlighting its potential for deeper penetration of the micelles into the deeper layer of the cornea tissue.

Therefore, these CUR-loaded PF127 micelles proved to be potentially efficient nanocarriers for treating anterior segment eye disease, where efficient drug delivery to the cornea is essential. Additionally, the accumulation of CUR inside the sclera supported an improvement in the bioavailability of CUR in the ocular tissues in the form of micelles.

3.8 Conclusion

In summary, in this chapter, we described the development of nanomicelles based on PF127 copolymers for increasing the solubility and stability of CUR. CUR encapsulated PF127 formulations were prepared through three strategies, which were direct dissolution, co-solvent evaporation, and thin-film hydration methods, and obtained a particle size in the nanometer size range, which was confirmed by DLS. Comparing centrifugation at high and low centrifugal speeds, the study found that the particle sizes of CUR-loaded PF127 micelles obtained from one-step centrifugation at 5000 rpm and two-step centrifugation (5000 and 15000 rpm) were larger than those produced by the CUR micelles centrifugated at 15000 rpm. Additionally, particle sizes after centrifugation at 5000 and continuing with 15000 were smaller, with multimodal particle size variations. The ZP was slightly negative for micelles centrifuged at 15000 rpm. This study suggested the benefit of centrifugation at high speed at 1500 rpm to remove large particles from the mixture according to Stokes' law. The optimal condition (15000 rpm) showed that PF127 triblock copolymer readily formed and self-assembled into small micelles (~20 nm) in aqueous solutions. Also, DSC studies provide preliminary evidence of the successful forming of CUR/PF127 nanosized micelles. Furthermore, several parameters were performed to produce the CUR-loaded PF127 micelles with higher EE and DL, as well

as an acceptable viscosity value for the OcDD application. The stability study revealed that the optimized CUR-loaded PF127 micelles were easy to reconstitute without heating and using a cryoprotective agent after the freeze-drying and sonication process, which highlighted the stability of the CUR-loaded PF127 micelles under these harsh processing conditions. Moreover, the encapsulation of the drug in micelles was highly dependent on the drug-to-copolymer ratio and the direct method was selected to calculate %EE and %DL in this study since it could directly quantify the amount of CUR entrapped within the PF127 micelles, minimizing the false calculation obtained from the indirect methods such as drug leakage or incomplete drug precipitation. In addition, at an applied drug-to-polymer weight ratio from 1:10 to 1:140, the EE increased from 4% to 100%, with the DL increased between 0.4% and 0.8%. Moving forward, further investigations, the *in vitro* cytotoxicity study using IM-HCEpi and HCE-T cell lines revealed that the CUR-loaded micelles were safe at a higher CUR concentration range of study (1-75 μg/mL) compared to the free CUR drug (1-4 μg/mL), supporting the reduction in toxicity of CUR when encapsulating into the PF127 micelles. In addition, the *in vitro* drug release study using the dialysis method revealed that the optimized CUR-loaded PF127 micelles (26% EE) could slow the release of the drug compared to the CUR-loaded PF127 micelles at a %EE around 6. However, the *in vitro* drug release could not reach 100% during the time of the study. The experiment was further studied to assess the extent to which parameters affect the CUR release study using the dialysis method. The mass balance results after the drug release study demonstrated that more than half of the amount of CUR was lost from the study. After that, the forced degradation study of the CUR under thermal and photodegradation was performed to clarify the degradation of CUR during the drug release study. The forced degradation study by thermal analysis of the CUR yielded an interesting finding that there was a significant decrease in the CUR content after 24 h. However, no peak corresponded to the degradation product of CUR presented in the HPLC chromatogram. As a result, the optimization process of the HPLC method was conducted to evaluate the degradation products, including vanillin and vanillic acid. Adjustment of the mobile phase composition between the high organic mobile phase and the high aqueous mobile phase resulted in good separation of the compounds between

CUR and its degradation products. The samples from both the *in vitro* drug release study and thermal degradation study were thereafter run according to the high organic mobile phase condition, observing the peak of the vanillic acid at wavelength 260 nm. Therefore, the chromatogram comparison serves as a valuable tool for evaluating the impact of mobile phase composition on the HPLC separation of CUR and degradation products of CUR, as well as for informing the selection of suitable chromatographic conditions for accurate and reliable analysis. Furthermore, the study continued to use the CU technique for the *in vitro* drug release study of CUR from CUR-loaded PF127 micelles instead of the dialysis technique. Unfortunately, the free CUR could not pass through the filter following the CU technique after 48 h. Consequently, further investigation of *ex vivo* permeation study across the corneal and scleral tissues was launched. The study found that the CUR micelles could permeate into both tissues. Moreover, the cell update study also supported the deeper permeation of the Cou6 drug with the help of the PF127 micelles. Hence, these findings provided compelling evidence for the potential of the CUR-loaded micelles as an innovative and effective strategy for OcDD in both anterior and posterior segment eye diseases.

Chapter 4

The formation of host-guest complexes between surfactants and cyclodextrins for ocular drug delivery of fenofibrate

4.1 Introduction

As briefly mentioned in Chapter 1, fenofibrate (FEB) is a prodrug of fenofibric acid, which is a ligand-activated transcription regulator expressed in multiple organs, including the retina, as previously stated in Chapter 1.[59] In clinical trials, FEB displayed a therapeutic effect on the treatment of diabetic retinopathy (DR) and neovascular age-related macular degeneration (AMD).[50,59,310,311] For example, the study of Hsu *et al.* assessed the protective effects of FEB on retinal/choroidal vascular endothelial cells under oxidative stress, using RF/6A cells as a model and paraquat (PQ) to induce oxidative stress.[311] Their study found that FEB significantly reduced reactive oxygen species (ROS) and decreased cellular apoptosis after cell exposure to PQ but increased mRNA levels of proinflammatory cytokines in retinal/choroidal vascular endothelial cells under oxidative stress, suggesting that FEB could be a promising treatment for ocular oxidative stress-related disorders like DR.[311]

However, FEB presents some drawbacks that limit its therapeutic use. For instance, the solubility of FEB in water is very low (<0.5 μg/mL in water, log P=5.24), and small molecular weight drugs were very difficult to get into the vitreous, which prevented the topical drug from reaching the target sites in the posterior eye segments, as highlighted in the review by Kumar *et al*.[312] Also, a short half-life with elimination time (~20 h) in the blood after oral administration by the choroidal blood flow results in low bioavailability via the oral route.[313]

Therefore, various strategies have been explored to increase FEB solubility and stability, precorneal residence time, and corneal permeability, including penetration through the sclera.[314–317] To date, multiple technologies and materials have been investigated to

deliver FEB in a highly dispersed form to improve its bioavailability for ocular drug delivery (OcDD), including nanoparticles, hydrogels, and drug/cyclodextrin (CD) complexes.[318–321] Among these formulations, an increased interest in CDs has emerged in recent years. CDs are cylindrical oligosaccharides with a hydrophilic outer surface and a lipophilic inner surface that are capable of forming inclusion complexes with hydrophobic drugs. As a result, CDs can enhance drug permeation across biological barriers and deliver the drug to the targeted site.[317,322,323]

CDs are known for their ability to form inclusion complexes with guest molecules. In addition, CD molecules are employed as the host molecules to form a poly(pseudo)rotaxanes (PPRs) structure, a type of molecular architecture that is mechanically interlocked and consists of polymer backbones connected through cyclic molecules. As a result, CDs could form inclusion complexes with guest molecules by encapsulating them within the cyclodextrin cavities.

In terms of OcDD, CDs are added to increase the solubility of the drug in polymeric micelles (PMs) and thus have been shown to efficiently enhance permeation and reduce cytotoxicity when in contact with the cornea of the eye.[192] Lorenzo-Veiga *et al.* focused on the encapsulation of natamycin, a model drug for fungal treatment, in single or mixed micelles and PPRs.[324] In their work, Soluplus® and Pluronic P103 dispersions were prepared in NaCl and pH 6.4 buffer with α-cyclodextrin (α-CD). Micelles sized 90-103 nm and 150-100 nm were prepared from Soluplus® and Soluplus® combined with Pluronic P103, respectively. Moreover, a combination of Soluplus®, Pluronic P103, and their mixed micelles increased drug solubility up to 6-fold, 3.27-fold, and 2.77-fold, respectively, and ocular tolerance studies demonstrated that all the formulations were non-irritant. Additionally, *ex vivo* corneal and scleral permeability studies revealed PPRs from mixed micelles of α-CD had a 2-fold increase in natamycin accumulation into both the cornea and sclera in comparison to mixed Soluplus®/Pluronic P103 micelles without CD (1 μg/cm^2) after 6 h. Similarly, Sayed and coworkers developed β-cyclodextrin (β-CD) consolidated micellar dispersions (CMD) composed of β-CD, poloxamer synperonic F108, Poloxamer synperonic P84, and poly (ethylene oxide) (PEO), which could self-assemble into CMD to solubilize the hydrophobic drug itraconazole by a melt dispersion

technique.[194] The results illustrated that a 204 nm-sized CMD with zeta potential (ZP) of -17.4 mV and 4.1% of solubilization efficiency (the total surfactant to drug ratio) was obtained from the optimized formulation, which was composed of 17:1 w/w surfactant:drug, 30:1 w/w CD:drug ratios, and 0.02% PEO. In addition, an *ex vivo* permeation study in rabbit corneas indicated a 2-fold higher permeation for the optimized CMD compared to the drug suspension (0.30 mg/cm^2) over 26 h. Therefore, these demonstrated the advantages of using triblock copolymers composed of PEO-poly (propylene oxide) (PPO)-PEO in combination with CDs to form soluble PPRs complexes, resulting in encapsulation efficiency (EE) enhancement, aqueous solubility, and therapeutic activity of the drug. Furthermore, a recent line of research has also established that nanomicelles prepared with Soluplus®, consisting of polyvinyl caprolactam, polyvinyl acetate, and polyethylene glycol (PEG) graft copolymer with amphiphilic properties, presents good stability against dilution owing to a low critical micelle concentration (CMC) value.[325–327] For example, Alvarez-Rivera *et al.* illustrated the improvement of solubility, stability, and corneal permeability of α-lipoic acid by using Soluplus® micelles.[327]

Taken altogether, as previous studies in Chapter 3 revealed several strategies using PF127 triblock copolymers to prepare curcumin (CUR)-loaded PF127 micelles, this study aimed to evaluate the effectiveness of CD-micelle combined systems of CDs/PF127, CDs/Soluplus®, and CDs/mixed PF127/Soluplus® to enhance FEB solubility and stability for OcDD. To investigate these hypotheses, a set of dispersions was prepared combining Soluplus® and PF127 with CDs. After that, physicochemical characterizations, including drug solubility particle size, ZP, and polydispersity index (PDI), were evaluated. Finally, the cytotoxicity study and the *in vitro*/*ex vivo* permeation studies were performed on the prepared FEB formulation.

4.2 Material and methods

4.2.1 Materials

As per Section 2.2.1 with the following additions: acetonitrile (ACN); ortho-phosphoric acid (85%), and deuterium oxide (D_2O, 99.9 atom % D) were all purchased from Sigma Aldrich (Missouri, USA). Soluplus® (mw:118000 g/mol) from BASF (Ludwigshafen, German) and fenofibrate (FEB, >98.0%, GC grade, mw:360.83 g/mol) from TCI EUROPE N.V. (Zwijndrecht, Belgium) were used as received without further purification. α-cyclodextrin (α-CD) and γ-cyclodextrin (γ-CD) were provided by Wacker Chemie AG (Asse, Belgium). 2-hydroxypropyl-β-cyclodextrin (2-HPβCD, DS 4.2; mw:1380 g/mol) was provided from Janssen Pharmaceutica (Geel, Belgium). Milli-Q water (Millipore, Billerica, MA resistivity=18.2 MΩ.cm) was used to prepare all solutions.

4.2.2 Solubility studies of fenofibrate in copolymer and cyclodextrin solutions

An accurately weighed excess amount of FEB (~8-9 mg) was added to 2 ml of the aqueous solutions of copolymers (PF127, Soluplus®) or CD (α-CD, γ-CD, and 2-HPβCD) at various concentrations in phosphate buffered saline (PBS) solution pH 7.4. The mixtures were stirred for 7 days at 25 ± 3°C to reach equilibrium. After that, the samples were filtered using a 0.2 μm polytetrafluoroethylene (PTFE) membrane filter. The filtered samples were analyzed by high-performance liquid chromatography (HPLC) with a detection wavelength of 285 nm. The experiment in each copolymer and CD type was repeated three times, and the results presented as the mean ± standard deviation (SD).

4.2.2.1 Calculation of the association constant, the complexation efficiency, and the drug-to-cyclodextrin molar ratio

- One drug (D) molecule associates with one CD molecule; the association constant ($K_{1:1}$) is described by the following equation

$$K_{1:1} = \frac{[D:CD]}{[D]x[CD]} = \frac{Slope}{S_0(1-Slope)} \qquad \text{Equation 4.1}$$

Where slope = the slope of the phase solubility profile of drug/CD

- The complexation efficiency (CE) of the different systems is calculated from the slope of the phase solubility profiles

$$CE = \frac{[D:CD]}{[CD]} = S_o x\, K_{1:1} = \frac{Slope}{(1-Slope)} \qquad \text{Equation 4.2}$$

- The drug-cyclodextrin molar ratio was calculated from the CE according to the following equation

$$D:CD\ molar\ ratio = 1:\ \frac{(CE+1)}{CE} \qquad \text{Equation 4.3}$$

4.2.3 Preparation of fenofibrate-loaded micelles

PF127 and/or Soluplus® (5 %(w/v)) were dissolved in a PBS solution (pH 7.4) with stirring at 370 rpm for 24 h at room temperature. 10 mg of FEB was thereafter added to the polymer solutions and stirred for a further 2 days before filtering with 0.22 μm cellulose filters to remove any unincorporated FEB. The filtrate solution was collected for dynamic light scattering (DLS) and HPLC analysis. The experiment was repeated three times, and the results presented as the mean ± SD.

4.2.4 Preparation of poly(pseudo)rotaxanes

PPRs were prepared by mixing Solution A (copolymers) and Solution B (2-HPβCD) in PBS (pH 7.4). Solution A (PF127 or Soluplus®) at 5 %(w/v) was dissolved in 10 mL of PBS pH 7.4 with stirring until a clear solution was obtained. Then, Solution B at a concentration of either 7.5 or 15 %(w/v) was added to Solution A and stirred at 370 rpm for 24 h at room temperature to form the PPRs. After that, 10 mg of FEB was added to the solution by stirring at room temperature at 370 rpm for 2 days to allow for the loading of FEB into the PPRs. The final concentration in each medium was set at 5 %(w/v) of copolymers and 7.5 or 15 %(w/v) of 2-HPβCD. Dispersions containing only the copolymers and drug at the same final concentration were also prepared for comparison. The solution was filtered through 0.22 μm cellulose filters before DLS and HPLC

analysis. The experiment was repeated three times, and the results presented as the mean ± SD.

4.2.5 Phase solubility studies of fenofibrate-loaded cyclodextrins by high-performance liquid chromatography

Samples after filtration of each solution from the drug solubility study (100 µL) were diluted with 50 %(v/v) ACN (900 µL) and the concentration of FEB in the solution was assayed by using a HPLC system at a wavelength of 285 nm, equipped with a Kinetex® 5µm C18 150x4.6 mm column. ACN-0.1 %(v/v) phosphoric acid (75:25 %(v/v)) was used as the mobile phase with a flow rate of 1.5 mL/min. The FEB content was calculated using the calibration curve equation (FEB in ACN), and the concentration in µg/mL was determined. The experiment was repeated three times, and the results were presented as the mean ± SD.

4.2.6 Characterization of fenofibrate-loaded poly(pseudo)rotaxanes

4.2.6.1 X-ray powder diffraction characterization

The x-ray powder diffraction (XRD) patterns were obtained using a Bruker D8 Advance x-ray diffractometer in Bragg-Brentano set up. Samples were irradiated with monochromatized CuKα radiation (λ=1.5406 Å) at a scanning rate of 1° per minute over the 2θ range of 5° to 40°. The XRD measurements were performed at room temperature.

4.2.6.2 Proton nuclear magnetic resonance spectroscopy

The sample was characterized using spectroscopy (Joel ECX) to elucidate the molecular structure of the samples. The ^{1}H-NMR spectra were acquired on a high-field NMR spectrometer operating at a proton frequency of 399.79 MHz. Before analysis, the freeze-dried sample was dissolved in D_2O to provide a suitable NMR medium. The NMR measurements were performed at a controlled temperature of 25°C to ensure reproducibility and stability of the samples. A standard 90° pulse sequence was employed to acquire the free induction decay (FID) signal, which was subsequently processed using Fourier transformation to obtain the ^{1}H-NMR spectrum. The spectral acquisition parameters included a relaxation delay of 16 seconds and a number of scan of 64.

4.2.6.3 Particle size distribution

As per Section 3.2.3.2. using a Malvern Zetazier Ultra-Red analyzer (Malvern Panalytical, UK).

4.2.7 Forced degradation study of fenofibrate

As per Section 3.2.6 with the following additions: The FEB/ACN samples for both thermal and photodegradation were prepared at 1 mg/mL. The thermal degradation temperature was set at 50 ± 3°C, where the FEB/ACN sample was exposed directly to visible light in the fume hood. The samples of 100 µL were withdrawn at different time points, added to 900 µL of ACN, filtered through the 0.45 µm filter, and analyzed using HPLC, as per Section 4.2.5. The measurement for each sample was repeated in triplicate (n=3).

4.2.8 Cytotoxicity study

As per Section 3.2.7 with the following additions: Immortalized human corneal epithelial (IM-HCEpi) cells were cultured and exposed to free FEB, FEB-loaded single and mixed micelles, FEB-loaded PPRs, and the blank PPRs formulation (a control) at the highest ratio of polymer components without drug at various concentration ranging from 1 to 70 µg/mL for 24 h. Cytotoxicity was assessed using an acid phosphatase colorimetric (APA) assay. Similar to the cytotoxicity study of the free FEB and FEB formulations in human corneal epithelial (HCE-T) cell line, the cells were treated with various concentration ranges of the free FEB and the prepared FEB formulations (single and mixed micelles as well as PPRs) at a concentration range between 1 and 90 µg/mL, along with the blank PPRs at the highest ratio of polymer components and PBS buffer as controls.

4.2.9 Ex vivo corneal and scleral permeability study

As per Section 3.2.9 with the following additions: after equilibration for 30 min, the PBS solution in the donor chamber was replaced by the FEB formulation samples (200 µL) and the control groups, i.e. free FEB and PBS solution (200 µL).

4.2.10 Liquid chromatography-mass spectrometry of the formulations

Samples were prepared by mixing the samples (200 µL) collected from either the donor chamber at the start or the receiving chamber after the *ex vivo* permeation study, as per

Section 4.2.9, with 50 %(v/v) ACN aqueous solution (800 µL). The mixture was then filtered through a 0.45 µm filter for analysis. A liquid chromatography equipped with a EclipsePlus C18 RRHD column (50x2.1 mm, 1.8 µm) was used for the separation of the analytes at wavelengths of 200, 285 and 254 nm. The mobile phase consisted of a gradient of solvent A (water) and solvent B (ACN) at a flow rate of 0.5 mL/min. A gradient method started with running the mobile phase with A:B ratios of 50:50 %(v/v) for 15 min before adjusting the mobile phase ratios between A and B to 25:75 %(v/v) for 5 min. Additionally, the liquid chromatography was coupled to a mass spectrometer equipped with a dual AJS electrospray ionization (ESI) source (Agilent Cross lab 6545 Q-TOF, Ireland), and the mass spectrometer operated in positive ion polarity mode with a scan range of m/z 50-1700. Data analysis for each analyte, including peak integration, retention time, and peak area, was performed using the MassHunter qualitative analysis 10.0 software, and the quantification of the analytes in the collected samples was calculated based on the calibration curves of the drug and cyclodextrin on its owns.

4.2.11 In vitro permeability assay of the fenofibrate formulations across human corneal epithelial cells

As per Section 3.2.7.2 with the following additions, the HCE-T cells were seeded in a Transwell-12 cell culture supports (Corning, Corning, NY) (100000 cells/0.5 mL medium/insert). The fresh cell medium (0.5 mL/insert and 1.5 mL/well) was replaced three times a week until the cells were confluent, and thereafter, cells were grown in the air-liquid interface for three weeks. After 3 weeks, the cell culture medium was removed, and the bottom wells were washed with 35°C BSS plus (Alcon, Geneva, Switzerland) (1.5 mL). Then, the cells inserted (0.5 mL) and the bottom wells (1.5 mL) were washed with 35°C BSS plus three times. In the last cycle, the cells inserted and the bottom containing BSS plus were kept in a mixing platform to equilibrate at 35 °C for 15 min without shaking. After the equilibration process, the equilibrate buffer in the insert part was replaced by 0.5 mL of the test formulations, and the reference molecule solutions (a mixture between 50 µM 6-carboxyfluorescein (6-CF) and 50 µM Rhodamine B (Rho-B) in BSS plus) at 35°C, whereas the bottom part was replaced by fresh 35°C BSS plus (1.5 mL). The multiwell plate was then placed on the mixing platform at 35°C and 150 rpm.

The samples were taken from the receiver (100 µL) to 96-well plates at a specific time point (10, 20, 30, 45, 60, 75, 90, 120 min). Similar to the donor or insert part, the samples (7.5 µL or 10 µL) were collected at 0, 60, 90, and 120 min. At the end of the experiment, cells were inactivated with 10% sodium hypochlorite. The samples were analyzed for FEB concentration using HPLC, whereas the fluorescent reference molecules were analyzed, 6-CF 490 nm (ex) 520 nm (em) Rho-B 554 nm (ex) 627 nm (em), using Cytation 3, multi-mode reader (BioTek Instruments, Winooski, VT, USA). All experiments were performed in triplicate and repeated three times, a total of n=9 cell inserts per test formulation were performed.

4.2.12 Tube formation assay

The tube formation assay using a µ-Slide 15 well 3D with endothelial cells (human umbilical vein cells, HUVECs) on Matrigel® was performed with a slight modification of the previous research study of Arnaoutova *et al.*[328] All the following protocol steps were performed under sterile conditions. Firstly, to prepare the 3D Gel, the Matrigel (Corning, Corning, NY, USA), was thawed by placing it on ice in the fridge at 4°C overnight before starting the experiment. On the day of the experiment, the µ-Slide 15 well 3D (Ibidi, Gräfelfing, Grrmany) was unpacked from the sterile packing and 10 µL of Matrigel was pipetted to each inner well of the µ-Slide 15 well before closing the µ-Slide with the lid. It should be noted that the pipet tips needed to be used in the precooled condition (4°C) for pipetting the gel. After that, the µ-Slide with gel loading was then placed in the petri dish containing water-soaked paper towels as an extra humidity chamber. After closing the lid, the petri dish containing the µ-Slide with gel loading was incubated for polymerization at 37°C in 5% CO_2/95% humidity for 30-60 min. HUVECs were prepared by culturing medium supplemented with growth factors and serum (EGM) for cell suspension preparation. On the day of the experiment, the HUVECs were detached using trypsin-EDTA and resuspended in a fresh culture medium without VEGF. HUVECs were calculated and centrifuged at 200 × g for 5 minutes to pellet the cells. HUVECs cell pellets were resuspended in respective test formulations of different compounds with the samples that were taken from the receiver chamber after the *in vitro* permeability experiment across HCE-T cells, as per Section 4.2.10, and diluted in the

EGM (1 %(v/v)) of the original receiver, negative control (EGM) and positive control (sulforaphane 50 µM). Known amount of angiogenic factor (15 ng/ml VEGF) was supplemented and cells were seeded 7500 cells per well on polymerized Matrigel and incubation at 37°C in 5% CO_2/95% humidity for 4 h to allow the formation of tube-like structures by endothelial cells. After that, the cells were stained with calecin-AM to visualize the tubes. The tube-like structures were imaged using Thunder imager (Leica, Wetzlar, Germany). Images were analysed to quantify tube formation parameters such as total tube length, number of junctions and tube areas using WimTube: Tube Formation Assay Image Analysis Solution, Release 4.0. (Wimasis, 2016, Available from: https://www.wimasis.com/en/products/13/WimTube). The study was carried out by the team members at Experimentica Ltd., Finland, as a part of the secondment program. One experiment (n=1) was performed in triplicate (three technical replicates). Data analysis was performed using GraphPad Prism software.

4.2.13 Calcein retention assay

Calcein-AM stock solution (1 mM) was prepared by mixing 50 µg of calcein-AM with 50 µL DMSO, and cyclosporine (CsA) stock solution (10 mM) was prepared by dissolving 2.7 mg CsA in 224.5 µL DMSO. In terms of preparation of test solutions, vehicle (0.5% DMSO) was prepared by mixing 13 µL DMSO with 2587 µL BSS plus solution, and CsA (15 µM) was prepared by mixing 9.1 µL DMSO, 3.9 µL CsA and 2587 µL BSS plus. For the preparation of the test formulation, the concentration of FEB formulations was selected based on the cell viability study, which was set at 20 µg/mL for each FEB formulation in 0.3% DMSO. In a calcein retention study, the HCE-T cells were seeded onto 96-well plates (16000 cells/200 µL medium/well) and cultured for three days in an incubator (37°C, 5% CO_2). After incubation, the cell culture medium in each well was removed, and 50 µL of the test solutions were added into each well before keeping the plate in the incubator at 37°C for 20 min. Then, 150 µL of 2.7 µM calcein-AM (a mixture between 5.3 µL calcein-AM stock/2 mL of the control solutions and 2.7 µL calcein-AM stock/1 mL of the test formulations) were added into the test formulation and placed the plate in 37°C for 20 min, allowing the calcein-AM to enter the cells and became fluorescent calcein by intracellular esterases. At the time point at 40 min, the test

solutions were removed from the wells, and 200 µL cold BSS plus was added into each well before placing the plate on cold beads and covered with foil. The retained calcein fluorescence within the cells was measured and quantified using Cytation 3 at 490 nm (ex) and 520 nm (em). One experiment (n=1) was performed. The experiment contained of 12 technical replicates for vehicle and positive control CsA and 6 technical replicates for test formulations.

4.2.14 Statistical analysis

As per Section 3.2.11 with the following additions: statistical significance was assessed using One-way ANOVA followed by Dunnett's multiple comparisons tests (solubility of FEB formulations in different PF127:Soluplus®:2-HPβCD ratios, flux and permeability coefficient, tube formation assay and calcein retention assay) by using GraphPad Prism version 10.1.1 GraphPad Software (Boston, MA, USA). Statistical significance was set at $p \leq 0.05$.

4.3 Results and discussion

In line with the hypothesis that the encapsulation of FEB within the copolymers and PPRs may enhance its solubility and improve its bioavailability, overall, this study aimed to investigate the preparation of FEB-loaded micelles, mixed micelles, and PPRs, which could act as a potential drug delivery system (DDS).

4.3.1 Fenofibrate solubility in different copolymers and cyclodextrins

To evaluate the maximum solubility of FEB in copolymers and CDs before PPR formation, an external standard calibration curve was prepared (Figure 4.1).

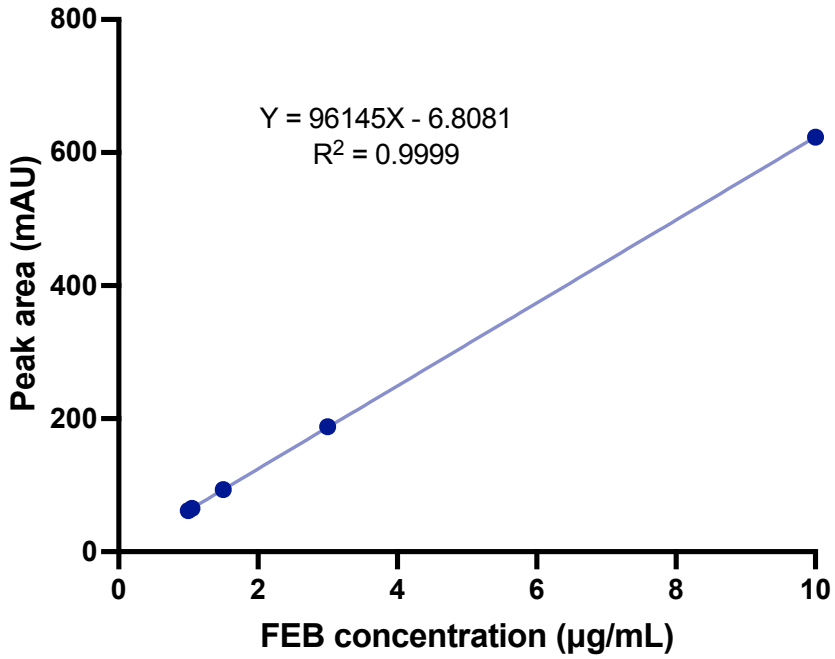

Figure 4.1: An external standard curve for HPLC of FEB in ACN. The HPLC condition is as follows: stationary phase: Waters Nova-Pack® C18 column (150x4.6 mm column, 4 µm) with flow rate 1 mL/min. The mobile phase employed consisted of ACN: 0.1 %(v/v) phosphoric acid in a ratio of 75:25. UV detection was performed at λ=285 nm. The injection volume and column temperature were set at 20 µL and 25°C, respectively.

The calibration curve for the solubility study of FEB was set up from 1 to 10 µg/mL, and the standard regression equation obtained was y=96145x-6.8081, R^2=0.9999 (Figure 4.1). Based on the standard deviation and slope of the calibration curve, the limit of detection and the limit of quantification of FEB were 0.18 µg/mL and 0.56 µg/mL, respectively.

Regarding the method for preparation of PPRs, the solubility of copolymers and the capability of CDs to form an inclusion complex with FEB were verified as this study sought to shed light on the influence of copolymers (PF127 and Soluplus®) and CDs including γ-CD, α-CD, and 2-HPβCD, on the solubility of FEB. PBS at pH 7.4 was selected for the aqueous solution in this study since the pH of 7.4 closely mimics the physiological pH of the human eye, making it well-tolerated and less likely to cause irritation or adverse reactions when used for OcDD.[329–331] For this purpose, the apparent

solubility of FEB in PBS pH 7.4 with different copolymers was first examined (Figure 4.2).

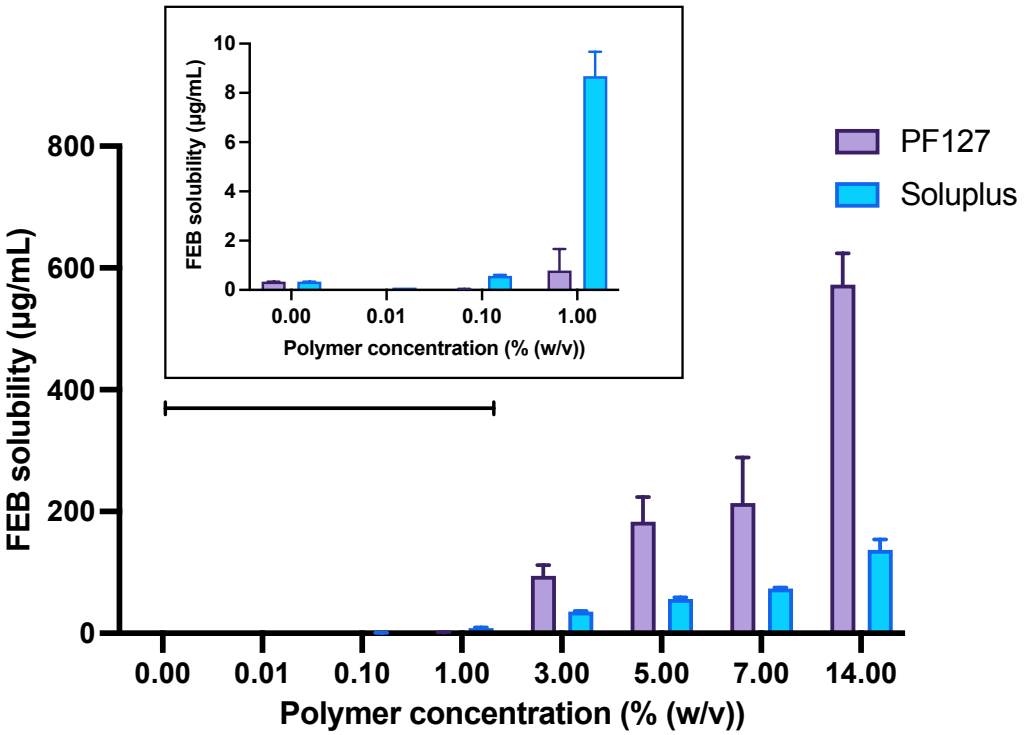

Figure 4.2: Solubility of FEB in PF127 and Soluplus® dispersions (0-14 %(w/v)) prepared in PBS pH 7.4 at 25°C. Data are presented as the mean ± SD (n=3).

The solubility of FEB in PBS (0% block copolymer) was 0.34 ± 0.0011 µg/mL, corresponding to previous studies.[332,333] The results demonstrated that increasing the concentration of both copolymers in the PBS medium resulted in increased FEB solubility (Figure 4.2). Indeed, the solubility of FEB in the presence of PF127 was higher than in Soluplus® copolymers. The reason may be attributed to the fact that PF127 molecules (hydrophilic-lipophilic balance (HLB=22) have more hydrophilic parts as compared to Soluplus® (HLB=16), resulting in well-distributed FEB in PF127.[334] Similar investigations were carried out by the aforementioned group of Lorenzo-Veiga *et al.*[324] They observed an increase in the solubility of natamycin for both copolymers at concentrations equal to or above 1 %(w/v). In contrast, the increase was significantly

greater for Soluplus® dispersions (~140 µg/mL at Soluplus® concentration 5 %(w/v) in 0.9% NaCl solution) due to less hydrophobic of Soluplus® (HLB=16) than Pluronic P103 (HLB=9).[334] Therefore, in the present study, it was found that the higher solubility of FEB in PF127 was due to its higher HLB value, indicating greater hydrophilicity, which enhanced its ability to form micelles and solubilize hydrophobic drugs like FEB more effectively than Soluplus®, which had lower HLB values.

To further investigate the FEB solubility, three types of CDs were used (Figure 4.3).

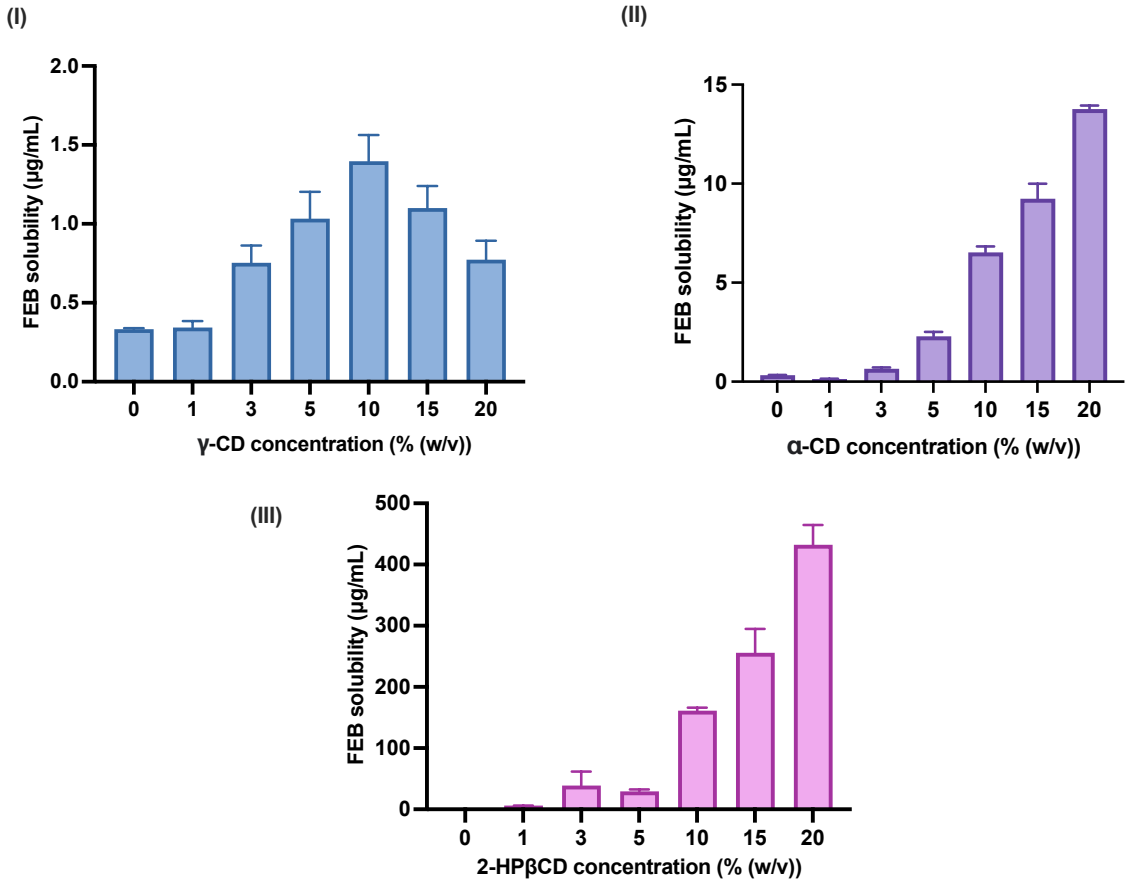

Figure 4.3: Apparent solubility of FEB without CDs and containing (I) γ-CD (II) α-CD and (III) 2-HPβCD in the concentration ranging from 1 % to 20 %(w/v) in PBS pH 7.4 at 25°C. Data are presented as the mean ± SD (n=3).

As illustrated in Figure 4.3, the maximum apparent solubility of FEB in aqueous 5 % and 10 %(w/v) γ-CD was in the range between 1.0-1.5 µg/mL in PBS solution (Figure 4.3(I)).

However, with more than 10 %(w/v) of γ-CD concentration, the solubility of the drug/CD complex was limited. A possible explanation for this finding might be related to β-type diagrams of phase-solubility profiles, according to Higuchi and Connors, as highlighted in the review paper by Saokham *et al*.[335] This type of diagram is observed when the complex between drug and CDs has limited solubility in the media due to the nature of the CDs. Another possible reason could be that only some part of the FEB molecule (mw=360.83 g/mol, size~294 nm) was situated within the γ-CD cavity (mw=1297.1 g/mol and inner cavity diameter=0.95 nm, size~538 nm), leading to less stability of complexation between FEB and γ-CD.[317]

Consequently, the stoichiometry of the drug:CD inclusion complex gradually changed from a ratio of 1:1 to higher-order drug:CD complexes and precipitated drug:γ-CD obtained, resulting in decreased CD solubility in the aqueous complexation media. The study of Schonbeck *et al.* concentrating on the phase-solubility diagram of hydrocortisone and γ-CD also revealed that the formation of water-soluble 1:1 complexes was observed for the initial increase in hydrocortisone solubility from 10 to 50 mM, while the precipitation of complexes with a 3:2 ratio of γ-CD:hydrocortisone was presented after 50 mM of the γ-CD concentration in Milli-Q water, leading to a strong decrease in the solubility of hydrocortisone.[336] This indicated that an excess amount of γ-CD above the optimum concentration may result in a significant reduction in drug solubility. Therefore, the experimental study was further explored to clarify the role that γ-CD precipitated after 10 %(w/v) by measuring the particle sizes of only γ-CD solution at a concentration above 5 %(w/v). The results revealed that the particle sizes of self-aggregation γ-CD presented at approximately 293 nm (PDI~0.98, ZP=-3.06) (data is not shown). This study supported that when γ-CD molecules aggregate, the hydrophobic cavities of γ-CD may become less accessible to FEB molecules to occupy, reducing the ability of the CD to encapsulate and solubilize FEB effectively. As a result, the aggregation of γ-CD can lead to a decrease in the effective concentration of CD molecules available for forming inclusion complexes with FEB.

In terms of α-CD, significantly (p<0.05) higher FEB solubility values were obtained for the FEB/α-CD system (~2.3-6.5 μg/mL at 5-10 %(w/v) α-CD) in comparison to γ-CD in

PBS solution (Figure 4.3(II)). The results of this analysis suggested that hydrophobic interaction inside the CD cavity between the drug and α-CD was improved due to a smaller α-CD cavity (mw=972.84 g/mol and inner cavity diameter=0.57 nm) than γ-CD.[337] This result and proposed mechanisms were consistent with the explanation made by Wong and coworkers focusing on the investigation of the inclusion complexation of artemisinin with natural CDs, namely α-, β- and γ- CDs.[338] The result showed an almost 17-fold increase in the stability constant value of artemisinin in β-CD compared to α-CD and γ-CD, suggesting the strongest complex-forming ability between β-CD and the drug. Specifically, the high stability constant values of β-CD reflected favorable positioning or fit of the drug inside the cavity of the CD molecules, implying a better spatial relationship between artemisinin and β-CD, whereas, in the case of γ-CD, its cavity may be too large, enabling the drug molecule to move more freely in and out of the cavity, resulting in a weaker complex being formed.

Besides, the FEB solubility in aqueous 5 and 10 %(w/v) 2-HPβCD showed an at least 20-fold increase in FEB solubility compared to γ-CD (~1.0-1.5 μg/mL) and α-CD (~2.3-6.5 μg/mL), indicating a better improvement of FEB solubility as a result of complexation with 2-HPβCD (Figure 4.3(III)). Additionally, a further increase in 2-HPβCD concentration leads to an increase in FEB solubility, which agrees well with the values previously reported.[339,340] For example, the study carried out by Jagdale and co-workers working on the enhancement of the dissolution rate of FEB by complexation with HPβCD revealed an increase in solubility of FEB from 2 mM to 10 mM when the amount of HPβCD increased from 0.007 mM to 0.058 mM, respectively.[27] This can be attributed to the synergistic enhancement of FEB solubility caused by HPβCD. Moreover, the improvement in solubilisation presented in this study is possibly caused by the strong hydrophilic character of 2-HPβCD (solubility in water>600 mg/mL), which improves the water penetration and wettability of the hydrophobic FEB.[341] Also, the intermolecular hydrogen bonds and the molecular dispersion of FEB on 2-HPβCD lead to partial miscibility, enhancing the hydrophilic characteristics of the drug substance via interactions with 2-HPβCD.

Overall, from the observations of solubility studies, the data provided preliminary evidence that 2-HPβCD could be useful in the preparation of PPRs due to the strongest complex-forming ability with FEB.

4.3.2 Preparation of poly(pseudo)rotaxane formulations

The capacity of CDs to form an inclusion complex with FEB, which was more soluble than free FEB, was confirmed before the preparation of the PPRs, as previously described in Section 4.3.1. Since 2-HPβCD formed a strong inclusion complex with FEB, leading to a high FEB solubility, it was selected to prepare PPRs. 2-HPβCD was used for this investigation at two different concentrations: 7.5 and 15 %(w/v), as safety concerns prevented testing of a higher concentration of 2-HPβCD above 15 %(w/v).[342] Furthermore, the experiment was carried out to determine the maximum concentration of copolymers and 2-HPβCD for preparing PPRs based on Soluplus® polymer gelation (Figure 4.4).

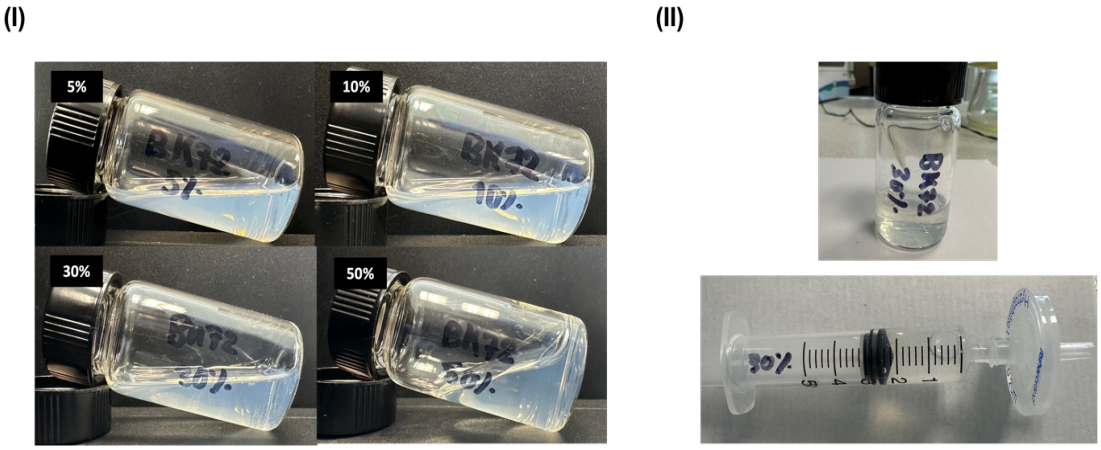

Figure 4.4: An image of (I) Soluplus® solution in PBS pH 7.4 at different concentrations (5, 10, 30, and 50 %(w/v)) and (II) the appearance of Soluplus® in PBS pH 7.4 at 30 %(w/v)) stuck inside the syringe filter, unable to pass through a 0.22 µm cellulose filter.

As illustrated in Figure 4.4, the Soluplus® solution completely underwent gelation and could not be stirred at a concentration exceeding 50 %(w/v) (Figure 4.4(I)). Similarly, the Soluplus® solution at a concentration of 30 %(w/v) was a very viscous solution and could not be passed through a 0.22 µm cellulose filter (Figure 4.4 (II)). Conversely, at lower

concentrations (5 and 10 %(w/v)), the Soluplus® solution did not show gelation and could be stirred and passed through the 0.22 μm cellulose filter. As a result, the concentration of Soluplus® was set at 5 %(w/v). Moreover, the study of finding a suitable ratio between Soluplus® and PF127 to form PPRs was after that conducted to determine the optimal polymer composition for achieving a stable and well-defined inclusion complex, with the results shown in Figure 4.5.

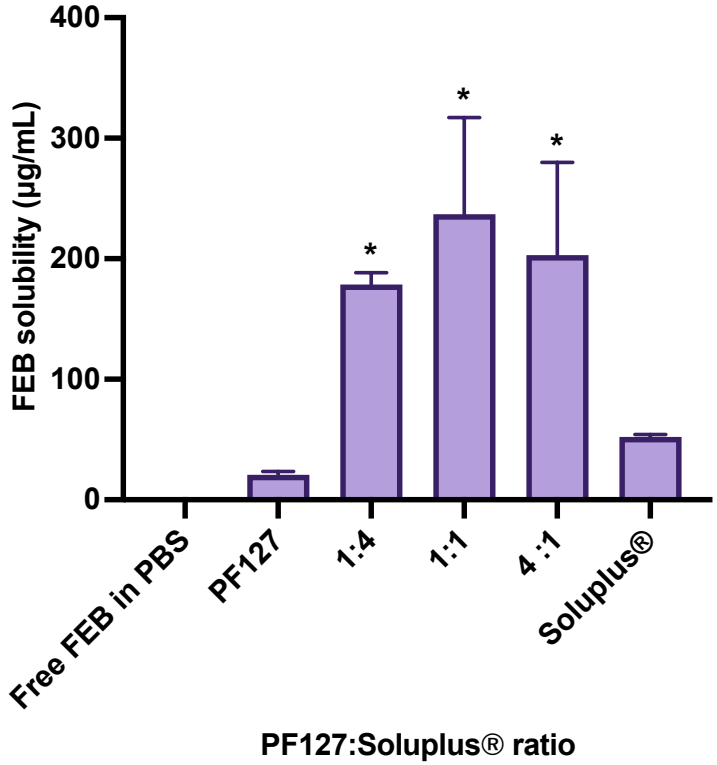

Figure 4.5: Apparent solubility of FEB in micelle dispersions of 5 %(w/v) of Soluplus® and 5 %(w/v) of PF127 and their mixtures (PF127/Soluplus®) prepared at various volume ratios in PBS pH 7.4 (n=3). The total copolymer concentration was 5 %(w/v) in all cases. Statistical analysis was analyzed by the One-way ANOVA followed by Dunnett's multiple comparisons (*p<0.05 compared to the mean values of the average FEB solubility in Soluplus®) (n=3).

The findings demonstrated that the apparent solubility of FEB increased when mixing PF127 and Soluplus® polymers (Figure 4.5). In addition, decreasing the Soluplus® ratio significantly (p<0.05) increased the FEB solubility, and the FEB solubility increase was

more pronounced at a ratio of 1 to 1 for PF127 to Soluplus®, reaching around 230 µg/mL, which was in agreement with previous findings showing that the mixed micelles could enhance the drug loading compared to the single micelles.[324,343]

Therefore, a combination of the findings between the initial investigation in Section 4.3.1 and the present study as shown in Figure 4.5 led to the selection of 5 %(w/v) PF127, 5 %(w/v) Soluplus®, and the binary systems containing 5 %(w/v) PF127 and 5 %(w/v) Soluplus® (1:1 v/v) in an aqueous PBS buffer solution (pH 7.4) for the formation of PPRs. The total copolymer concentrations were set at 25 %(w/v). The polymer component, the solubility of FEB in each prepared formulation, and the particle size distribution are illustrated in Table 4.1.

Table 4.1: Mean size and size distribution of formulations from CD-micelle combined systems prepared in pH 7.4 buffer. Numbers represent as the mean ± SD (n=3).

Code	Components (% (w/v))			FEB solubility (mg/mL)	DLS measurement		
	2-HPβCD	PF127	Soluplus®		D_h (nm, Int%)	PDI	ZP (mV)
BK53-1	-	5	5	0.20 ± 0.03	67 ± 3.4 (100%)	0.14 ± 0.07	-0.64 ± 1.89
BK53-2	7.5	5	5	0.28 ± 0.05	66 ± 0.9 (100%)	0.02 ± 0.007	+1.06 ± 1.55
BK53-3	15	5	5	0.31 ± 0.03	65 ± 1.6 (100%)	0.02 ± 0.003	-1.16 ± 1.68
BK53-4	15	5	-	0.22 ± 0.01	8 ± 0.3 (57%) 243 ± 19 (23%) 2 ± 0.2 (20%)	0.45 ± 0.09	-0.91 ± 2.02
BK53-5	15	-	5	0.24 ± 0.02	58 ± 0.2 (100%)	0.01 ± 0.01	-1.79 ± 0.52
BK53-C1	-	5	-	0.02 ± 0.003	5 ± 1 (80%) 28 ± 4 (20%)	0.49 ± 0.12	-2.09 ± -0.68
BK53-C2	-	-	5	0.05 ± 0.002	61 ± 0.3 (100%)	0.03 ± 0.02	-1.95 ± -0.46
BK53-C3	7.5	-	-	0.05 ± 0.002	2 ± 0.3 (74%) 375 ± 54 (26%)	0.25 ± 0.07	-2.08 ± -2.38
BK53-C4	15	-	-	0.16 ± 0.02	2 ± 1 (86%) 618 ± 44 (14%)	0.24 ± 0.05	-0.31 ± -2.68

*Total copolymer concentration in all cases was 5 %(w/v) copolymers and either 7.5 % or 15 %(w/v) 2-HPβCD in the presence of an excess amount of FEB (~8-9 mg).

The results demonstrated the successful formation of micelles, mixed micelles, and PPRs of FEB with PF127, Soluplus®, and 2-HPβCD, which obtained small particle sizes (<100 nm) in all prepared formulations. Additionally, the particle sizes of the single PF127 micelles (5 ± 1 nm) and Soluplus® micelles (61 ± 0.3 nm) were quite small compared to the mixed micelles (PF127/Soluplus® micelles) (67 ± 3.4 nm) and the PPR formulations (~58-66 nm) (p<0.05, One-way ANOVA followed by Dunnett's multiple comparison

tests). This can be attributed to the complexation and assembly behavior of the polymers and 2-HPβCD. In other words, when PF127 or Soluplus® polymers were used alone, they formed smaller micelles owing to self-assembly driven by their amphiphilic nature. However, when mixed with CDs to form PPRs, the inclusion of complexation and host-guest interactions between the polymers and CDs could lead to the formation of larger structures, namely mixed micelles and PPRs, due to the increased complexity of the assembly resulting from the multivalent host-guest interaction between the polymers and the CDs.[344,345]

Moreover, the increase in apparent solubility of FEB was evident for the PF127/Soluplus® mixed micelles at concentrations equal to 5% (0.13 mg/mL, BK53-1, Table 4.1). Whilst, the addition of 2-HPβCD (either 7.5% or 15 %(w/v)) resulted in a noticeable increase in FEB solubility up to 0.31 mg/mL compared to the drug-loaded mixed micelles (p<0.05, One-way ANOVA followed by Dunnett's multiple comparison tests) (BK53-2 and BK53-3, Table 4.1), supporting the synergistic effect of 2-HPβCD for enhancing drug solubility. Thus, the study found that the solubility of FEB improved in single and mixed micelles as well as PPRs compared to the free drug, possibly due to its encapsulation within these structures through hydrophilic polymer complexation and inclusion complex with CDs.

Overall, the studies on particle size and FEB solubility supported the idea that Soluplus® and PF127 could solubilize FEB in their micelles and interact with 2-HPβCD to form small particle size PPRs, which could act as potential OcDD nanocarriers by enhancing ocular penetration of FEB, a poorly water-soluble drug, as highlighted in the review by Jansook *et al*.[346] Also, this study provided valuable insights into the behavior of the drug within the polymer systems, laying the groundwork for the subsequent confirmation of PPR formation in the next section.

4.3.3 Confirmation of poly(pseudo)rotaxane formation

To gain an insight into the structure of the complexes of 2-HPβCD with amphiphilic block copolymers, the appearance of the solution-prepared samples was first analyzed to check the transformation of the dispersion (Figure 4.6).

Figure 4.6: Appearance of a control dispersion (BK56-C1) (left) and poly(pseudo)rotaxane formulation (BK56-3) (right) (repeated from BK53-C1 and BK53-3, Table 4.1, respectively) in different conditions in PBS pH 7.4 buffer after storage for 6 h at room temperature.

Figure 4.6 showed the transformation of the initial transparent dispersion of PF127 polymer into opalescent dispersions in the presence of PPRs, supporting the formation of inclusion complexes and changes in the microstructure of the dispersion system. Moreover, the formation of inclusion complexes between copolymers and CDs can lead to a change in the solubility and aggregation behavior of the copolymers, leading to turbidity in the dispersion. Results obtained by Simões *et al*. were also consistent with our findings.[347] In their study, three PEO-based polymers, including PEG, PF127, and Tetronic® 908, were tested for their interaction with poly-αCD. When the copolymers mixed with α-CD, the systems formed turbid dispersions, with phase separation observed after 1 hour, indicating PPR-like structures. Therefore, the visualization study of PPR formation provided valuable insights, which were further explored in the study of inclusion complexes to understand the host-guest interactions between the drug and the copolymer as well as CDs.

The drug-CD molar ratio calculation is an essential aspect of formulating drug-CD complexes, as it determines the stoichiometry of the complexation and the efficiency of the drug encapsulation, as stated in the review paper by Saokham *et al*.[335] In the case of FEB and 2-HPβCD, the molar ratio calculation is crucial for optimizing the complexation

process and understanding the behavior of the resulting inclusion complex. Therefore, to calculate the molar ratio, the phase-solubility diagram was constructed to determine the stoichiometry of the inclusion complex and the stability constant ($K_{1:1}$) of the complexation (Figure 4.7).

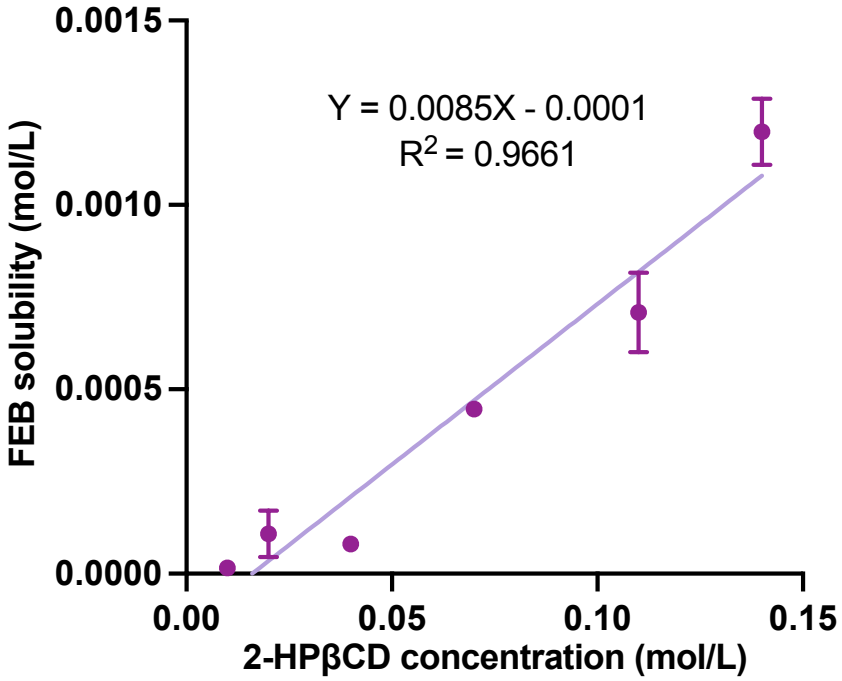

Figure 4.7: Phase solubility profile of FEB in 2-HPβCD.

Phase solubility tests confirmed that the CD derivatives effectively solubilized FEB in water, with linear, A_L-type phase solubility curves in the function of CD concentration, according to Higuchi and Connors (Figure 4.7).[317] The slope of the intersection obtained from the phase solubility profile of FEB in 2-HPβCD was used to calculate the stability constant ($K_{1:1}$), the complexation efficiency (CE), and the drug to CD (D:CD) molar ratio, as previously described in Section 4.2.2.1 (Figure 4.7). By analyzing the resulting data, the calculation showed that although the $K_{1:1}$ was high (9098), the CE (0.0085) and D:CD (1:118) molar ratios were quite low, which were in agreement with the previous research studies.[339,348] Low ratios in CE and D:CD values could be explained by the fact that CDs formed both inclusion and non-inclusion complexes with FEB in aqueous solutions, but

the majority was occupied by the non-inclusion complexes that the CD molecules were free in the FEB/CD solution without forming the inclusion complex with the drug, resulting in only a small fraction of the molecules being available to create a complex with the CDs.[349] Therefore, the results showed that there was an inclusion complex formation between FEB and 2-HPβCD even though the D:CD value was low.

Additionally, the following study was focused on using NMR spectroscopy and X-ray diffraction techniques to further characterize the drug-CD inclusion complex and confirm the complexation. The BK53-3 sample, containing all three components of PF127, Soluplus®, and 2-HPβCD, was selected to test (Table 4.1). The NMR result is shown in Figure 4.8.

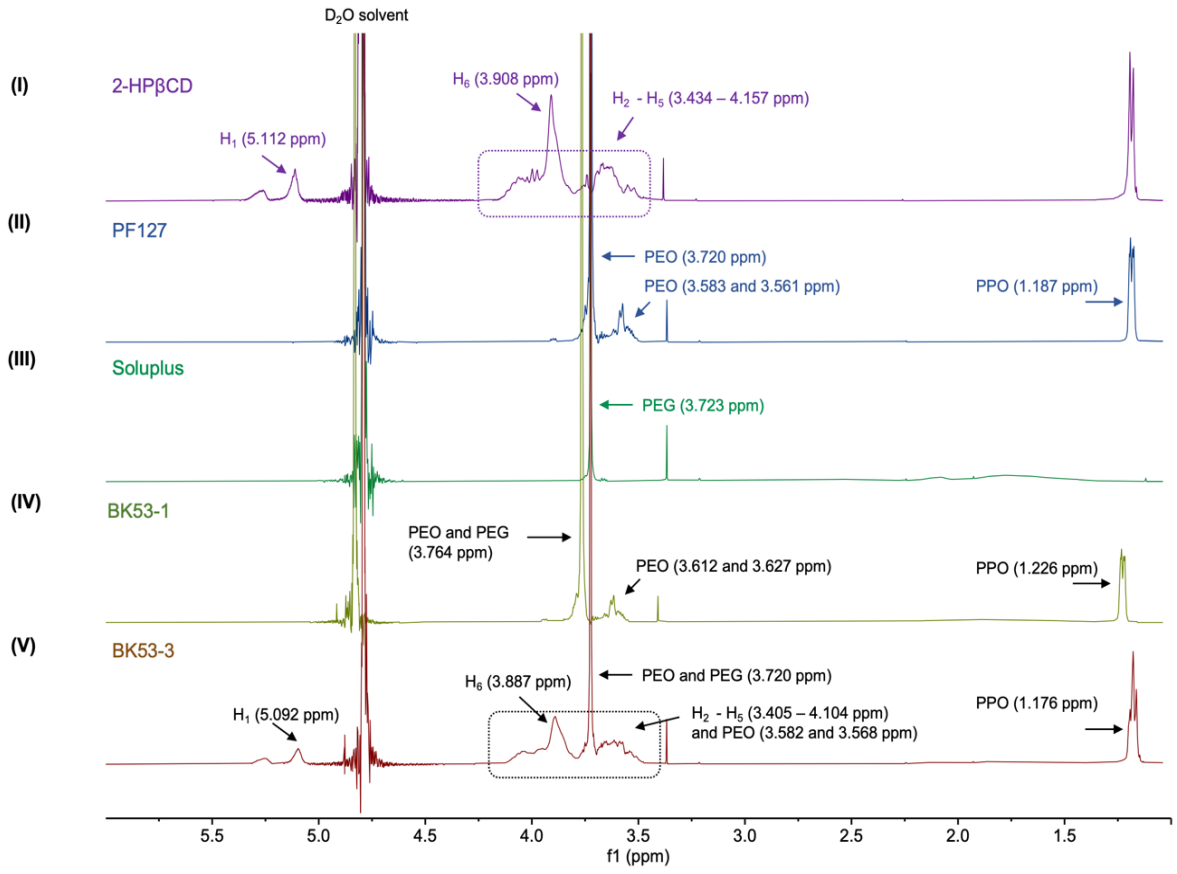

Figure 4.8: (I) The ^{1}H NMR spectrum of the raw materials of (I) 2-HPβCD, (II) PF127, (III) Soluplus® and the FEB formulations of (IV) the mixed PF127/Soluplus® micelles (BK53-3 from Table 4.1) and (V) the PPRs (BK53-3 from Table 4.1) in D_2O.

^{1}H NMR spectra of unmodified 2-HPβCD, PF127 and Soluplus® compared with the mixed micelles (BK53-1) and PPRs (BK53-3) formulations are shown in Figure 4.8. The spectra of 2-HPβCD showed one peak ca. 5 ppm and the peaks at the ranges 4.2-3.4 ppm which were assigned to the hydroxyl groups of the glucose unit (Figure 4.8(I)).[350] Furthermore, the PF127 polymers showed peaks belonging to PEO and PPO units at around 3.7 ppm and 1.2 ppm, respectively (Figure 4.8 (II)).[351] Also, the peak of the PEG unit from Soluplus® was displayed at 3.7 pm (Figure 4.8 (III)). In addition, the interaction between copolymers regarding the mixed micelle sample caused a shift in the peaks of PEO and PPO units from PF127, including the merging peaks (ca. 3.7 ppm) between the PEO unit from PF127 and PEG unit from Soluplus® (Figure 4.8 (IV)). A similar result was found in the ^{1}H NMR spectrum result of BK53-3 polyrotaxane samples, showing a chemical shift in protons from C-OH of the hydrophilic PEO part of PF127 and a shift in proton positions from 2-HPβCD when compared to the proton NMR spectrum of the pure 2-HPβCD and PF127 compounds in D_2O (Figure 4.8 (V)). Moreover, the interactions across three different compounds, including PF127, Soluplus® and 2-HPβCD, caused a broadening of the proton peaks between 4.1 and 3.4. ppm, corresponding to protons from hydroxyl groups of the 2-HPβCD, PEO of PF127 and PEG from Soluplus®.

Therefore, this study supported the specific interaction between the PEO block of PF127 and the PEG unit of Soluplus® to the 2-HPβCD cavity. Indeed, when a polymer interacts with a CD to form a complex, the local electronic environment of the protons in both the polymer and the CD can be affected. This interaction-induced change in the electronic environment leads to a shift in the resonance frequencies of the protons, which is observed as changes in the chemical shifts in the NMR spectrum of the BK53-3 sample. Thus, the ^{1}H NMR study supports evidence of an inclusion complex between the copolymers and the CD.

Furthermore, X-ray analysis was carried out to gain more insight into the structure of the FEB-loaded PPRs with copolymers (Figure 4.9).

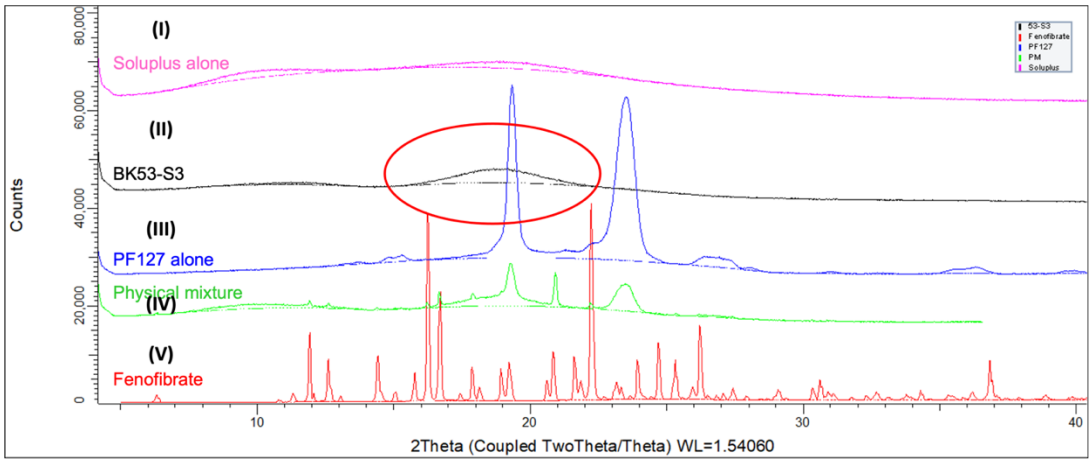

Figure 4.9: XRD patterns of (I) Soluplus® copolymer, (II) the BK53-3 sample from Table 4.1, (III) PF127 copolymer, (IV) physical mixture of FEB/PF127 and (V) free FEB drug.

The XRD pattern of the free FEB compound exhibited distinct diffraction peaks at different 2θ values, indicative of its crystalline nature (Figure 4.9(V)). Additionally, powdered Soluplus® was amorphous, and the XRD pattern of the PF127 polymer showed distinct diffraction peaks at 2θ values of 19.5° and 23.5°, indicating its crystalline structure based on the known crystal structure of the PF127 compound (Figure 4.9(I) and 4.9 (III)).[312] Also, the physical mixture—a combination of PF127 and free FEB—had reflection angles for each component that matched to those of the PF127 and free FEB separately (Figure 4.9(IV)). However, the XRD pattern of the BK53-3 sample was amorphous (Figure 4.9(II)). It showed a single broad band without a sharp diffraction peak in the 2θ values of 19.0°, suggesting the absence of long-range order or crystalline structure within the BK53-3 sample. In conclusion, the XRD analysis demonstrated an amorphous phase of the FEB-loaded micellar or PPRs.

Taken altogether, the comprehensive use of multiple analytical analyses, including NMR, XRD, DLS, and visual observation in the transformation of the dispersion, provided strong evidence confirming the successful formation of FEB-loaded PPRs. Briefly, NMR spectroscopy revealed distinct chemical shift changes of PF127, Soluplus® and 2-HPβCD, indicative of the treading of polymer chains through the cyclodextrin rings. XRD analysis demonstrated the amorphous phase of the FEB-loaded PPRs formulations, supporting the encapsulation of the drug within the CD and copolymers. Also, DLS

measurement, as stated in Section 4.3.2, illustrated changes in the hydrodynamic size and distribution of the FEB-loaded PPRs, suggesting the encapsulation of the drug within the micelles or CD cavity. Furthermore, the observed change in the turbid solution provided a visual indication of the formation of the PPRs complex. Collectively, these findings not only confirm the successful formulation of drug-loaded PPRs but also highlight the effectiveness of employing a multi-technique approach for supramolecular assemblies.

4.3.4 Cytotoxicity studies of the fenofibrate-loaded micelles and poly(pseudo)rotaxanes

This investigation was performed to study the cytotoxicity of prepared FEB formulations, as previously mentioned in Section 4.3.1, on IM-HCEpi cells (Figure 4.10).

(I)

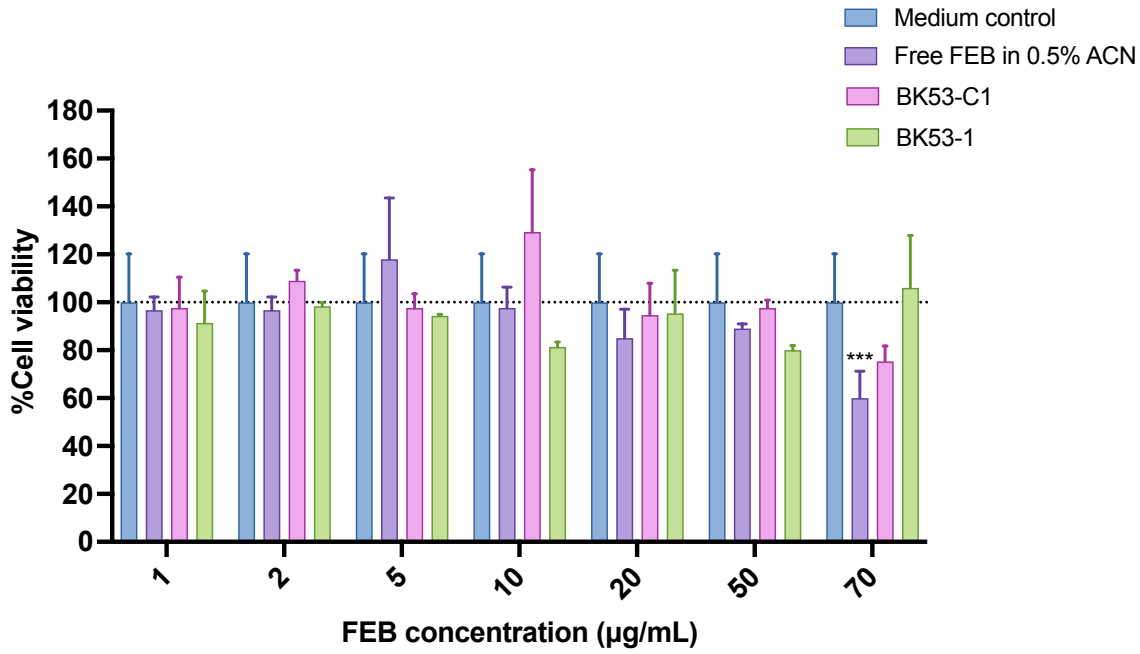
Medium control
Free FEB in 0.5% ACN
BK53-C1
BK53-1
%Cell viability
180
160
140
120
100
80
60
40
20
0
***
1
2
5
10
20
50
70
FEB concentration (μg/mL)

(II)

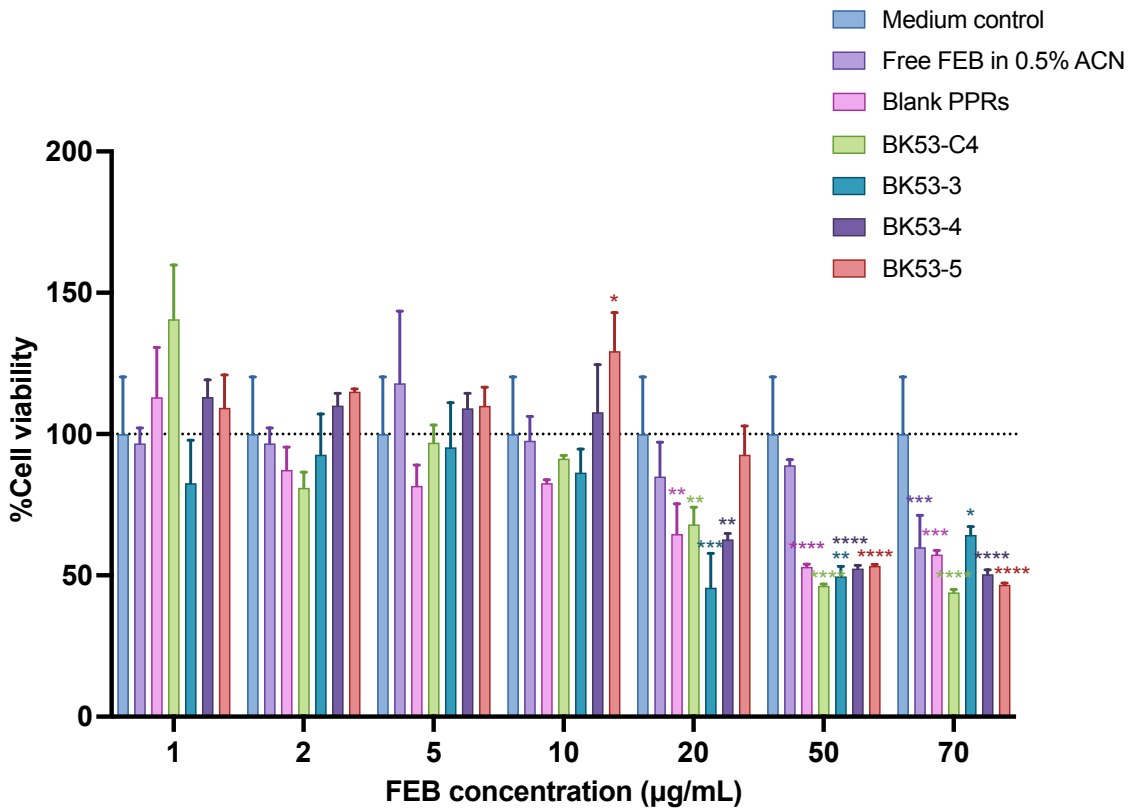
Medium control
Free FEB in 0.5% ACN
Blank PPRs
BK53-C4
BK53-3
BK53-4
BK53-5
%Cell viability
200
150
100
50
0
1
2
5
10
20
50
70
FEB concentration (μg/mL)

Figure 4.10: Assessment of cell viability of IM-HCEpi cells treated with (I) Free FEB in 0.5% ACN and FEB-loaded micelles and mixed micelles (BK53-C1 and BK53-1 from Table 4.1), and (II) Free FEB in 0.5% ACN, FEB-loaded PPRs (BK53-C4, BK53-3, BK53-4 and BK53-5 from Table 4.1) and blank PPRs at FEB concentration of 1–70 µg/mL for 24 h. Statistical significance was analyzed by the One-way ANOVA followed by Dunnett's multiple comparisons (*p<0.05, **p<0.01, ***p<0.001 and ****p<0.0001 compared to the mean values of the medium control condition). Data are presented as the mean ± SD of three experiments (n=3, each experiment by the mean of its three technical replicates).

The cytotoxicity study revealed that FEB-loaded micelles (BK53-C1) and mixed micelles (BK53-1) did not show statistically significant cytotoxic effects on IM-HCEpi cells while free FEB demonstrated significant (p<0.001) decreased cell viability at 70 µg/mL, suggesting potential cytotoxic effects of the free FEB drug (Figure 4.10 (I)). Moreover, at FEB concentrations above 20 µg/mL, the cell viability was higher in the FEB-loaded micelles and mixed micelles (Figure 4.10 (I)) compared to blank PPRs formulation, which indicated significantly reduced cytotoxicity (Figure 4.10 (II)). Additionally, cells treated with FEB-loaded Soluplus®/2-HPβCD PPRs (BK53-5) displayed a significant (p<0.05) decrease in viability at a concentration above 50 µg/mL compared to the medium control. On the other hand, the cells treated with other FEB-loaded PPRs (BK53-C4, BK53-3 and BK53-4) and the control groups of blank PPRs demonstrated a cell viability of over 80% at a concentration below 20 µg/mL (Figure 4.10 (II)).

In a similar manner to the previous cell viability assay in IM-HCEpi cells, the following cell viability assays were performed in HCE-T cells, including resazurin assay, lactate dehydrogenase (LDH) release and reactive oxygen species (ROS) formation, to assess the cytotoxicity of FEB-encapsulated micelles and PPRs, aiming to further confirm their cytotoxic effects and biocompatibility (Figure 4.11).

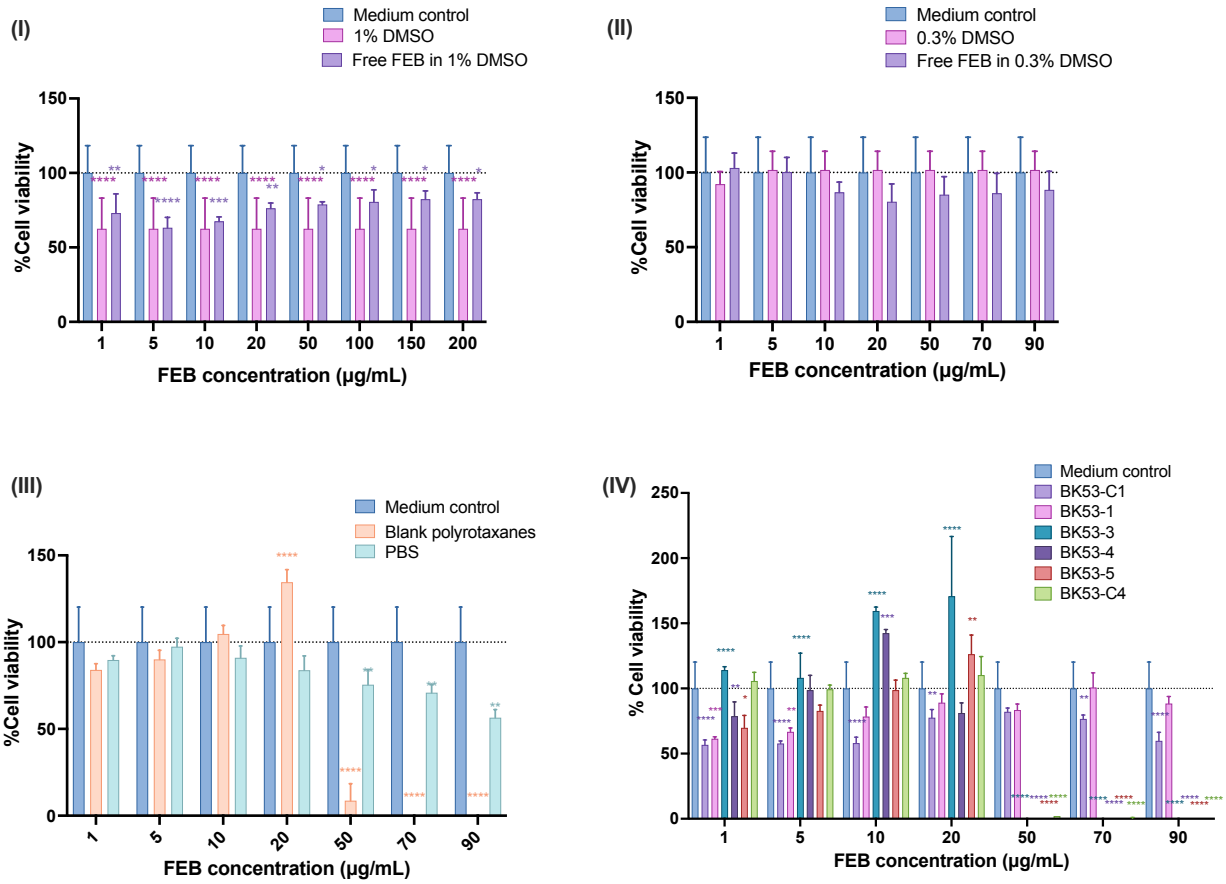

Figure 4.11: Assessment of cell viability of HCE-T cells treated with free FEB at (I) 1% DMSO (FEB concentration of 1-200 µg/mL) and (II) 0.3% DMSO (FEB concentration of 1-90 µg/mL), (III) blank PPRs and PBS, and (IV) FEB-loaded PPR formulations from Table 4.1 at FEB concentration of 1-90 µg/mL for 24 h. Data are normalized to the medium control condition. Statistical analysis was analyzed by the One-way ANOVA followed by Dunnett's multiple comparisons (*p<0.05, **p<0.01, ***p<0.001 and ****p<0.0001 compared to the mean values of the medium control condition). Data are presented as the mean ± SD of three biological replications (n=3) for (I)-(II) and two biological replications (n=2) for (III)-(IV).

The cell viability assay of the FEB formulation across HCE-T cells was conducted, as per Section 3.2.7.2. Our results illustrated that free FEB in 1% DMSO and 1% DMSO solvent as a control statistically significantly (p<0.05) decreased cell viability compared to the medium control condition (Figure 4.11(I)), indicating a significant vehicle (DMSO) effect. Therefore, the concentration of DMSO was decreased (0.3%), affecting the

solubility of FEB, and the highest tested FEB concentration in 0.3% DMSO was 90 μg/mL. FEB in 0.3% DMSO did not show significant cytotoxicity up to 90 μg/mL (Figure 4.11(II)). Moreover, HCE-T cells treated with FEB-loaded PPRs (BK53-3) and the control of blank PPRs at the same copolymer concentrations displayed a cell viability of over 80% ranging between 1-20 μg/mL of FEB (Figure 4.11 (III)-(IV)) which may indicate pre-cytotoxic effect and metabolic activation of the cells before cytotoxic threshold. Notably, the PBS solution as a control also showed a statistically significant (p<0.05) impact on the cell viability at 50 μg/mL and higher concentrations, which might be related either to the dilution of nutrients in the cell culture medium (Figure 4.11 (III)). Furthermore, the study found no cytotoxicity effects in HCE-T cells at higher FEB concentrations for mixed micelles (BK53-1, 10-90 μg/mL) and FEB-loaded PF127 micelles (BK53-C1) at 50 μg/mL compared to PPRs formulations at other copolymer concentrations (1-20 μg/mL) (Figure 4.11(IV)), which was similar to the cytotoxic effect of the encapsulated formulations obtained from the APA assay in the previous study (Figure 4.10(I)). Our study observed a similar trend in cell viability of FEB formulation to that reported by Khin *et al.*, which revealed that PVA-stabilized FEB/RMβCD-loaded Eudragit® nanoparticles significantly improved cell viability (>80%) in rabbit cornea cell lines at FEB concentration below 50 μg/mL.[317]

In addition, the present study showed that free FEB in 0.3% DMSO did not increase LDH release but significantly (p<0.05) decreased the LDH release, suggesting a synergistic protective effect of DMSO and low concentrations (0-20 μg/mL) of FEB (appendices Figure S2(I)). However, ROS formation was significantly increased in both FEB in 0.3% DMSO (1-90 μg/mL) compared to the medium control condition (appendices Figure S2(I)). Blank PRRs demonstrated a pre-cytotoxic effect (apparently higher cell viability) at 20 μg/mL (Figure 4.11(III)) just before the cells lost their viability completely. However, blank PPRs did not reach statistically significant LDH release from the cells, although they tend significantly to increase intracellular ROS formation at low (1 μg/mL) and medium (20 μg/mL) concentrations (appendices Figure S2(II)). FEB-loaded mixed micelles (BK53-1) and FEB-loaded PF127/ 2-HPβCD PPRs (BK53-4) did not show statistically significant LDH release up to 90 μg/mL. Still, other FEB-loaded PPRs and

the PF127 micelles (BK53-C1) had a trend to increase LDH release at 20 μg/mL (BK53-3) and higher concentrations (50-90 μg/mL for BK53-5, 20-50 μg/mL for BK53-C4 and 90 μg/mL for BK53-C1) (appendices Figure S2(II)). This suggested cell membrane damage at those concentrations of the test formulations.

Furthermore, regarding ROS formation, FEB encapsulation with micelles and PPRs could decrease cellular ROS formation compared to the free FEB drug, supporting their improved safety profiles at concentrations under 20 μg/mL (appendices Figure S2). In addition, FEB-loaded mixed micelles (BK53-C1) increased ROS formation at three concentrations (10,20 and 90 μg/mL), although it did not show an LDH release effect on the cells (appendices Figure S2(III)). This result was similar to the FEB-loaded PPRs (BK53-3) that showed ROS formation at 10-20 μg/mL even though there was no statistical significance in the cell viability at these two concentrations, indicating intracellular pre-cytotoxic effects in the cells (appendices Figure S2(III)).

In conclusion, the results of this cytotoxicity study conducted on both IM-HCEpi cells and HCE-T cells indicated that the FEB-loaded micelles and mixed micelles were safe at concentrations below 50 μg/mL, and FEB-loaded PPRs were safe at concentrations under 20 μg/mL. This supported the inclusion of CDs in the formulation, which has been found to slightly significantly impact the cell viability in our study. Upon evaluating the effects of the formulation with CDs compared to the formulations without CDs on cell cultures, it was observed that the presence of CDs led to a notable decrease in cell viability. A decline in cell viability can be ascribed to the interactions between CD molecules and the cells, which may impact the integrity of the cell membrane and cellular processes, as evidenced by the study on LDH release and ROS formation. In addition, the cytotoxicity study in HCE-T cells showed that the PBS solution affected the cell viability. In turn, FEB-loaded micelles and PPRs exhibited reduced cytotoxic effects compared to free FEB. These findings highlighted the potential of FEB-loaded micelles/mixed micelles and PPRs as safe and effective delivery systems for the ocular administration of FEB since micelles and PPRs were offered to be biocompatible and could reduce the direct interaction of the FEB drug with the HCE-T cells, confirmed by the lower cytotoxicity values compared to the free drug at the same concentration in the cell viability study.

Consequently, further *ex vivo* permeation studies were warranted to validate the efficacy of these delivery systems in ocular applications.

4.3.5 Ex vivo corneal and scleral permeability study

To investigate the permeability properties of the FEB formulations and provide insight into potential OcDD applications, an *ex vivo* permeation experiment was carried out on porcine cornea and sclera. In this investigation, porcine cornea and sclera were extracted from fresh eyes and mounted in vertical Franz-diffusion cells with PBS containing 1.06 %(w/v) Tween-80 as the receptor medium (37°C). The amount of FEB that permeated through ocular tissues to the receptor chamber was monitored for 6 h, and the results are shown in Figure 4.12.

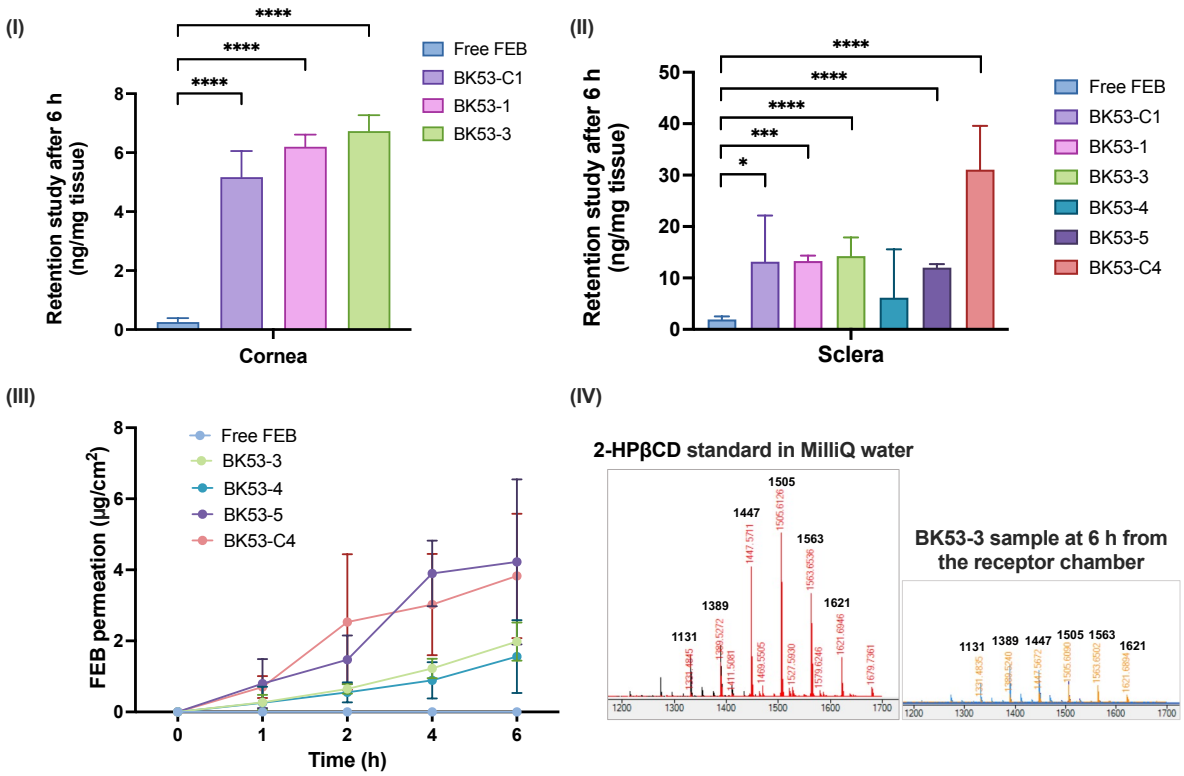

Figure 4.12: A graphical representation of drug retention in (I) the cornea and (II) the sclera of the porcine eyes after 6 h of contact with different types of FEB formulations and the free FEB control (n=3). The medium in the receptor chamber was PBS+1.06 %(w/v)Tween-80. The concentration at the start of the free FEB in the MilliQ water as a control group were 20 ± 9 and 19 ± 1 µg/mL in the cornea and sclera, respectively, (III) permeation profiles of the FEB-loaded PPRs formulations

across the scleral tissue of the porcine eyes, and (IV) characterization of the component comparing between the standard 2-HPβCD and in the receiving chamber after *ex vivo* permeation study) distribution by mass spectrometry. Statistical analysis was analyzed by the One-way ANOVA followed by Dunnett's multiple comparisons (*p<0.05, **p<0.01, ***p<0.001 and ****p<0.0001 compared to the mean values of the free FEB control group). Data are presented as the mean ± SD of three biological replications (n=3) (n=3 eyes for each group).

Our investigation revealed distinct permeation profiles for FEB from micelles, mixed micelles, and PPRs prepared in PBS buffer solution (pH 7.4), with FEB-loaded single and mixed micelles exhibiting no drug permeation into both the cornea and scleral tissues of the porcine eyes (Figure 4.12 (I)-(II)). However, the FEB-loaded PPRs demonstrated measurable permeation through the scleral tissue barriers (Figure 4.12 (II)-(III)). The amount of FEB concentration of FEB-loaded PPRs that penetrated across the sclera varied from 0.27 to 4.65 μg/cm^2 (Figure 4.12 (III)). Besides, the mass spectrometry study confirmed the presence of 2-HPβCD in the receptor chamber of FEB-loaded PPRs across porcine sclera, indicating potential interactions affecting formulation transport (Figure 4.12 (IV)). In the case of cornea permeation tests, despite their poor corneal penetrations of the FEB micelles and PPRs, they demonstrated detectable FEB levels at 6 hours in the cornea tissue (Figure 4.12(I)). This indicated that the drug levels that permeated from the FEB micelles for the first five hours were below the quantification limit (0.03 μg/mL, FEB standard calibration ranging from 0.1-1 μg/mL) (Figure 4.12 (I)).

Additionally, higher drug retention was observed in the sclera compared to the accumulation of drug in the cornea of the porcine eyes in all prepared formulations (Figure 4.12 (I)-(II)). The possible reason could be the lower density of tight junctions with relatively large interstitial spaces of the sclera, which could facilitate the retention and distribution of drugs within the sclera due to its permeable nature, as highlighted in the review by del Amo *et al.*[352] In contrast, the compact structure of the cornea composed of multiple layers presented a challenging barrier for drug diffusion compared to the more porous scleral tissue. Other investigators have observed similar types of results in the *ex vivo* permeation study of the hydrophobic drug-loaded nanocarriers, which demonstrated low transcorneal flux of their formulations.[158,324,353] Similar results were found in the

work by Christensen *et al.* They found that the P_{app} of their cyclic guanosine monophosphate analogue-loaded lipid nanocapsules across the conjunctiva-sclera-chloroid-retina was three times higher than that of the full-thickness cornea (666 μm).[354] Thus, these factors collectively contributed to the differential retention of drugs within the cornea and sclera tissues of the porcine eyes, highlighting the importance of understanding tissue-specific drug distribution and retention for developing effective OcDD systems.

As previously described, the permeability study of FEB-loaded PPRs revealed distinct permeability profiles across scleral tissue, prompting the calculation of permeability coefficients for each formulation to quantitatively assess their transport characteristics. The ratio of flux (J) and the concentration of FEB in the donor phase obtained was used to calculate the permeability coefficient (P_{app}) of FEB over porcine sclera (Table 4.2).

Table 4.2: The retention concentration (C_s), transscleral steady-state flux (J), and permeability coefficients (P_{app}) recorded for FEB formulated in PPRs results obtained from Figure 4.12(III) after 6 h of the *ex vivo* transscleral permeation (n=3). Statistical analysis was analyzed by the One-way ANOVA followed by Dunnett's multiple comparisons (*p<0.05, **p<0.01, ***p<0.001 and ****p<0.0001 compared to the mean values of BK53-5). Data are presented as the mean ± SD of three biological replications (n=3 eyes for each group).

Code	Components, %(w/v)			C_s (μg/mL)	J (μg/cm²h)	P_{app} x 10^3 (cm/h)
	2-HPβCD	PF127	Soluplus®			
BK53-5	15	-	5	3.83 ± 0.26	0.82 ± 0.19	23.4 ± 5.52
BK53-4	15	5	-	2.21 ± 3.37	0.26 ± 0.20**	9.61 ± 7.40*
BK53-3	15	5	5	3.62 ± 0.68	0.31 ± 0.07*	7.88 ± 1.69*
BK53-C4	15	-	-	10.1 ± 2.15	0.62 ± 0.16	18.2 ± 4.75

The calculation analysis showed that the highest P_{app} was for FEB-loaded PPRs with Soluplus® and 2-HPβCD, whereas the lowest P_{app} corresponded to FEB-loaded PPRs with PF127, Soluplus® and 2-HPβCD (BK53-3) (7.88×10^{-3} cm/h) (p<0.05, Table 4.2). In addition, the apparent P_{app} of FEB-loaded PPRs with Soluplus® and 2-HPβCD (BK53-5) was significantly (p<0.05) higher than the P_{app} of FEB-loaded PF127/ 2-HPβCD and PF127/ Soluplus®/ 2-HPβCD PPRs (BK53-4 and BK53-3) (9.61×10^{-3} and 7.8×10^{-3} cm/h,

respectively, Table 4.2). The possible reason may be attributed to the fact that the FEB-loaded PPRs with Soluplus® and 2-HPβCD had high drug solubility (0.24 ± 0.02 mg/mL, Table 4.1), referring to its ability to enhance the solubility FEB through the inclusion of complex formations. Additionally, the higher P_{app} of FEB-loaded Soluplus®/2-HPβCD PPRs may be linked to the efficient solubilization, and improved dissolution of FEB facilitated by 2-HPβCD and Soluplus® copolymers, which could, in turn, enhance its permeation across the scleral tissues. Conversely, the presence of a combination of either PF127/2-HPβCD or mixed PF127/Soluplus® micelles with 2-HPβCD in the PPRs formulations could influence the permeation of FEB by altering the microstructure of the formulation or introducing additional complexities in the interaction between the components, thereby impacting the P_{app} of FEB. A similar investigation has also been made by Ghezzi *et al.,* revealing that the presence of Solutol® HS15 in cyclosporine-loaded D-α-tocopheryl polyethylene glycol succinate (TPGS)-Solutol® HS15 mixed micelles reduced TPGS metabolism, leading to degradation in contact with ocular tissue in both the porcine cornea and sclera.[158]

Therefore, the *ex vivo* permeation study of the FEB-loaded micelles and PPRs across corneal and scleral tissue of porcine eyes provided valuable insights into the potential of drug-loaded micelles and PPRs to permeate the ocular barriers, including cornea and sclera, which were critical for effective drug delivery to the eye. Furthermore, this also prompted the initiation of an *in vitro* permeability assay of the FEB formulations across HCE-T cells to further elucidate its transport behavior at the cellular level, which was addressed in the following section.

4.3.6 In vitro permeability assay of the fenofibrate-loaded poly(pseudo)rotaxanes across human corneal epithelial cells

As per Section 4.2.11, the *in vitro* permeability assay of the FEB-loaded micelles and PPRs across HCE-T cells was conducted on a 12-well Transwell cell culture plate. The receptor phase was filled with BSS plus buffer (35°C), and the FEB concentration that permeated through the cell membranes to the receptor chamber was studied for 2 h. The

concentration of FEB in the insert part was divided by the ratio of flux (J) to get the permeability coefficient (P_{app}) of FEB across the HCE-T cells (Table 4.3).

Table 4.3: The steady state flux (J) and permeability coefficients (P_{app}) recorded for 6-carboxyfluorescein (6-CF) and Rhodamine-B (Rho-B) across HCE-T cells in BSS plus buffer. Statistical analysis was analyzed by the One-way ANOVA followed by Dunnett's multiple comparisons (*p<0.05, **p<0.01, ***p<0.001 and ****p<0.0001 compared to the mean values of the MilliQ water group). Data are presented as the mean ± SD of three biological replications (n=6).

Formulation	6-CF (low permeability ref)		Rho-B (high permeability ref)	
	J (μg/cm² h)	P_{app} x 10^3 (cm/h)	J (μg/cm² h)	P_{app} x 10^3 (cm/h)
MilliQ water	0.132 ± 0.006	8.79 ± 0.57	0.48 ± 0.10	50.8 ± 8.7
Blank PF127	0.099 ± 0.030*	8.23 ± 1.48	0.84 ± 0.08****	43.1 ± 4.01
Blank PPRs (BK53-3 without FEB)	0.058 ± 0.073****	6.61 ± 0.75**	0.17 ± 0.03****	11.9 ± 1.12****

The results illustrated that there was no drug permeation across HCE-T cells of all FEB-loaded micelles and PPRs, which were correlated with the results obtained from the *ex vivo* transcorneal permeation study, as previously mentioned in Section 4.3.5. In contrast, two reference molecules, 6-CF and Rho-B, could be detected in the receptor phase to analyze the data following this *in vitro* permeation study (Table 4.3). Comparing the transport behavior of the low (6-CF) and high (Rho-B) permeability reference molecules across the HCE-T cells revealed that the speed of the drug track (P_{app}) across HEC-T cells from both blank PPRs or PF127 and MilliQ water as controls was faster for Rho-B compared to 6-CF (Table 4.3). Furthermore, there was a significant (p<0.05) difference in mean values across the J and P_{app} between the blank formulations and MilliQ water in both 6-CF and Rho-B reference molecules. The lower P_{app} of blank PPRs than the blank PF127 and MilliQ water could be due to the complexation of the blank PPRs composed of PF127, Soluplus®, and 2-HPβCD that affected the permeability of the reference molecules across the cell layer. In other words, the polymer micelles, such as PF127 and Soluplus® in the blank PPRs, may interact with the cell membranes or reference molecules, resulting in a slower permeation from both micelles and PPRs to come across the cell layer compared to the free reference molecules in the blank PF127 or MilliQ water.

Taken altogether, the observed lack of permeation of FEB micelles in the cornea and scleral tissues indicated a significant barrier against this particular formation, while FEB-loaded PPRs showed enhanced penetration across the scleral tissue of the porcine eye. Therefore, the study in the next section was focused on determining the retention of FEB drug in the donor phase through a mass balance study to clarify the point that no drug permeation across the corneal tissue or cells to the receptor phase of the micelles owing to the drug accumulation within the tissues.

4.3.7 Mass balance study of fenofibrate drug following permeability studies

By addressing these points in the discussion, although HPLC could not detect the FEB in the receptor phase for both *ex vivo* and *in vitro* permeation assays, as per Section 4.3.5 and 4.3.6, there was a decrease in the mass of FEB in the donor chamber after 2 h of the *in vitro* permeability experiment with around 0.02-2% compared to the mass of drug at the start. Similar results were observed for the *ex vivo* permeation study across the porcine cornea (8-44%) and sclera (7-14%) tissues after 6 h (Figure 4.13).

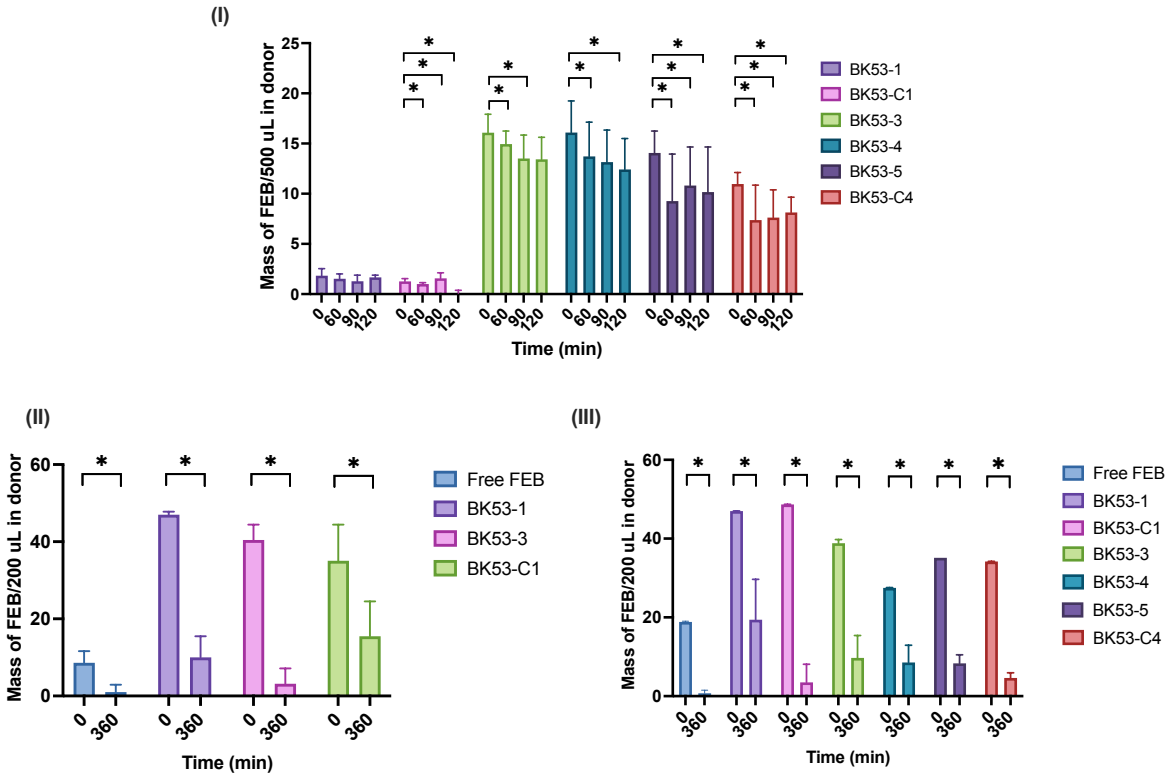

Figure 4.13: Mass balance study to quantify the amount of FEB before and after the experiment of (I) the *in vitro* permeability assay across HCE-T cell, and the *ex vivo* permeation study across (II) cornea and (III) sclera of the porcine eyes (n=3). Statistical analysis was analyzed by the paired sample t-test (*p< 0.05 compared to the FEB concentration at time 0).

As illustrated in Figure 4.13, the *in vitro* and *ex vivo* permeation studies showed a statistically significant (p<0.05) decrease of FEB mass quantification in the donor chamber from the FEB formulations after 2 and 6 hours of the experiment, respectively (Figure 4.13 (I)-(III)), suggesting a mass loss of FEB from the donor chamber due to drug permeation into the biological barrier and accumulation within the tissues or cells. To address this point, the subsequent study aimed to investigate the impact of FEB degradation on the quantification of mass loss during the experimental research following the forced degradation study, as the results are shown in Figure 4.14.

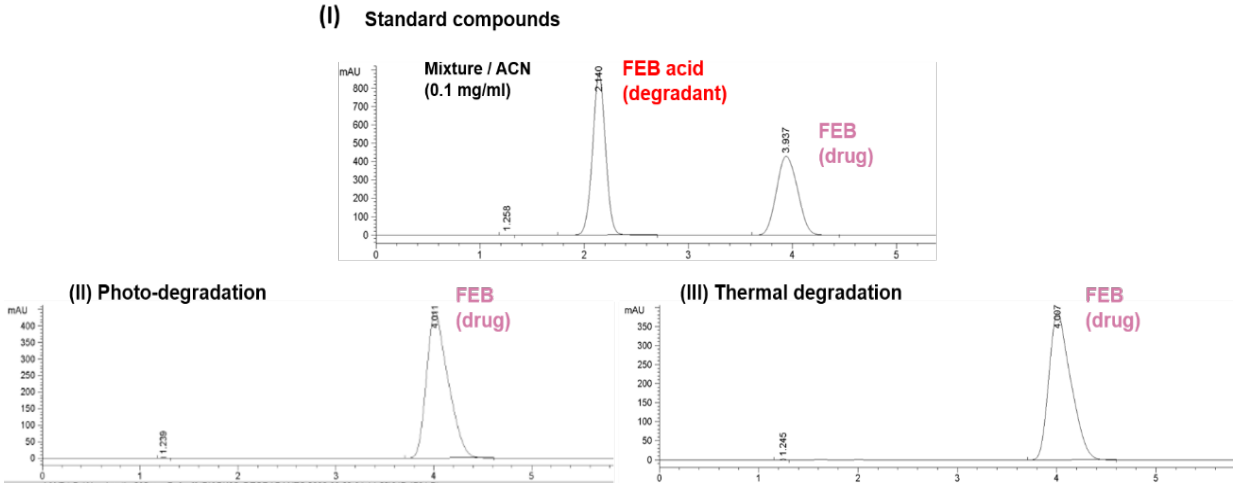

Figure 4.14: A graphic representation of HPLC chromatogram of FEB and FEB acid from (I) the mixture of the standard FEB/FEB acid at concentration 0.1 mg/mL in ACN, (II) photo-degradation and (II) thermal degradation (50°C) experiment at wavelength 285 nm at 6 h.

The primary by-product of FEB metabolism is fenofibric acid (FEB acid), which is formed when FEB is metabolized in the body, as highlighted in the review research by Gunwal *et al*. (Figure 4.14 (I)).[355] In this study, the HPLC condition, as per Section 4.2.5, was used to run the standard FEB/FEB acid compound mixture to identify the chromatogram for each compound. The results demonstrated that the retention times of FEB acid and FEB were 2.14 and 3.93 min, respectively (Figure 4.14 (I)). Moreover, the forced degradation study in both photo and thermal degradations revealed no FEB acid peak on the HPLC chromatogram at wavelength 285 nm after 6 h of the experiment (Figure 4.14 (II)-(III)), suggesting the stability of the FEB during the experiment without degradation.

Therefore, the results of the mass balance study, along with *ex vivo* permeation results of FEB retention in the cornea and sclera tissue of the porcine eye as per Section 4.3.5, indicated that drug loss from donor chambers was due to drug accumulation within the tissue or cells. Interestingly, this provided an important aspect of drug delivery, as it reflected the potential aspect for therapeutic action at the target sites of the FEB-loaded micelles and PPRs without drug degradation.

4.3.8 Tube formation assay

To evaluate the mechanism of angiogenesis and screen potential anti-angiogenic compounds, the tube formation assay was performed by using the samples that were taken from the receiver chamber after the *in vitro* permeability experiment at 2 h, as per Section 4.3.6., and were diluted (1:5) in EGM. This study was conducted as a part of the secondment program of the PhD student at Experimentica Ltd, Finland. The results are shown in Figure 4.15.

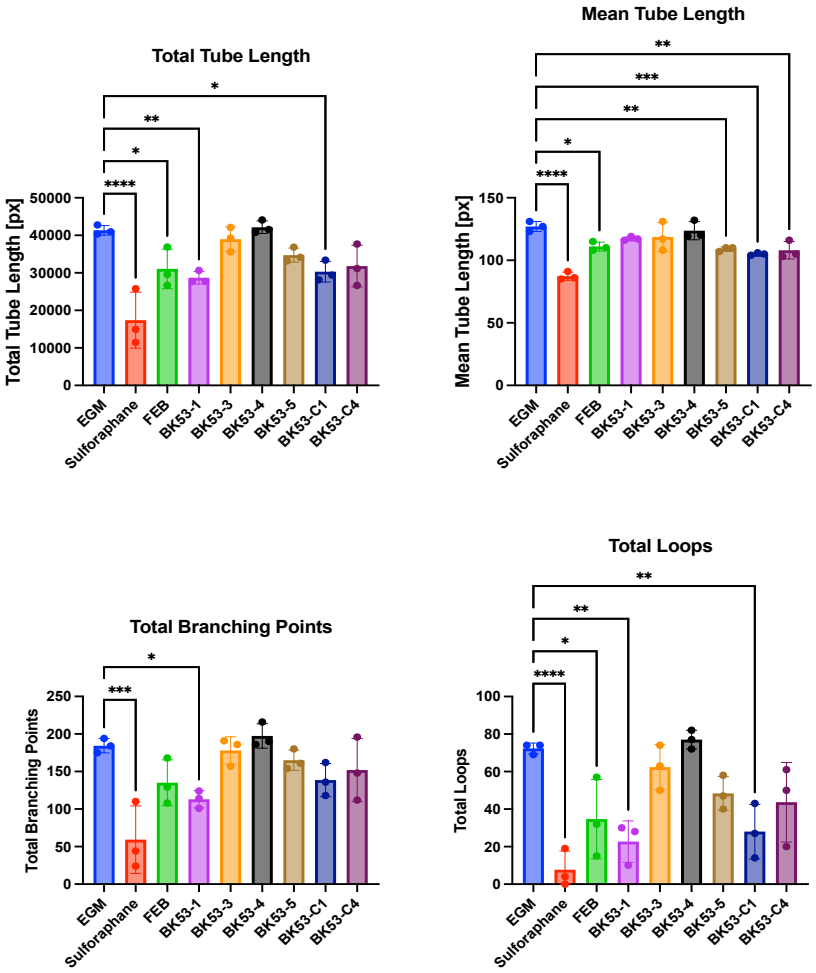

Figure 4.15: Tube formation assay of different FEB formulations collected after 2 h HCE-T permeability assay from the receptor phase. Data was analyzed using One-way ANOVA followed by Dunnett's multiple comparisons test, *p<0.05, **p<0.01, ***p<0.001 and ****p<0.0001. Data are presented as the mean ± SD of one experiment (n=1, experiment contained of three technical replicates).

In the tube formation assay, different formulations showed statistically (p<0.05) significant anti-angiogenic properties with the range order as follows: BK53-C1>BK53-1>free FEB>BK53-C4>BK53-5. Whereas, BK53-3, BK53-4 and BK53-5 did not show effects. More precisely, the study found that FEB-loaded mixed micelles (BK53-1) had lower total branching points than the EGM control, suggesting that it suppressed the formation of complex vascular structures. Whilst, other formulations had minimal impact on the branching complexity of the vascular network. Moreover, the study also found a decrease in total loops, total tube length, and mean tube length in FEB-loaded micelles (BK53-C1), FEB-loaded mixed micelles (BK53-1), and FEB-loaded PPRs (BK53-5 and BK53-C4), supporting the suppression of longer individual vascular structures. Hence, this suggested that FEB formulations have been penetrated through corneal epithelial cells (HCE-T cells) during the *in vitro* permeability experiment, although they were not detected in the HPLC.

4.3.9 Calcein retention assay

In this study, calcein retention studies were applied to evaluate the effects of drug and drug formulations on ATP-binding cassette drug efflux transporter interactions. The experiment was performed as a part of the secondment program of the PhD student at Experimentica Ltd., Finland. The study involved the use of calcein-AM, a cell-permeant dye that is converted to the fluorescent compound calcein by intracellular esterases. The inhibition of efflux transporter interaction by positive control CsA (inhibitor for P-glycoprotein and BCRP) increased calcein retention within the cells. The results of the study are shown in Figure 4.16.

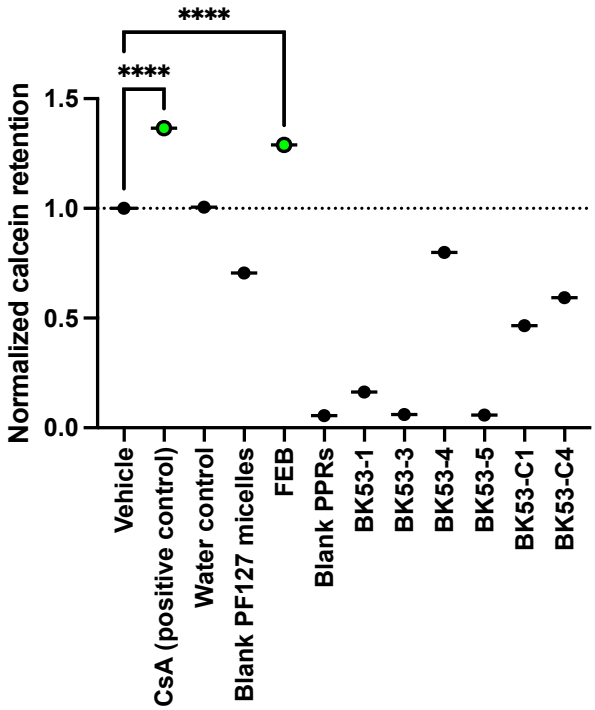

Figure 4.16: Calcein retention study of different formulations. Data are normalized to vehicle control conditions. Data was analyzed using One-way ANOVA followed by Dunnett's multiple comparisons test, ****p<0.0001. Data are presented as the mean of one experiment (n=1, experiment contained of 12 technical replicates for vehicle and positive control CsA and 6 technical replicates for test formulations).

The study demonstrated that a statistically significant increase (p<0.0001) in calcein retention was observed by FEB and positive control (CsA) only, indicating the inhibition of P-glycoprotein in cells, as FEB has been shown to be an inhibitor for P-glycoprotein.[356,357] However, the other formulations did not show the calcein retention (Figure 4.16). In micelles and PPRs treated cells indicating potential interactions with the calcein-AM dye and/or cell membranes. This might have been caused by the fact that the formulation encapsulated calcein-AM blocking the entry of calcein-AM into the cells, resulting in a low calcein retention.

Taken together, the results of our study in this chapter had significant implications for OcDD research and development. The contrasting permeation behavior of FEB micelles and FEB PPRs formulations provided valuable insights into the design and optimization

of OcDD systems, highlighting the potential of PPRs-based formulations for achieving enhanced ocular drug permeation. Hence, further investigations into underlying mechanisms governing the permeation disparities between these formulations and the impact of formulation modifications on ocular permeation may offer promising avenues for advancing OcDD technologies. Consequently, the mathematical model to understand drug delivery from both FEB micelles and FEB PPRs is presented in Chapter 5.

4.4 Conclusions

Soluplus® and PF127 copolymers, as well as CDs, namely γ-CD, α-CD, and 2-HPβCD, could encapsulate FEB. Moreover, the saturation solubility of FEB in different CDs in PBS medium was determined. The solubility of FEB increased directly with CD concentrations. Among CDs, 2-HPβCD demonstrated the greatest solubility enhancement of FEB in PBS solution achieving an almost 20-fold increase in FEB solubility compared to the solubility of FEB in either γ-CD or α-CD respectively. Furthermore, the addition of 2-HPβCD to the dispersions of micelles caused an enhancement in the water solubility of FEB in comparison to the drug-loaded micelles by using only Soluplus® and PF127 along with the drug, proving its better bioavailability of the drug when forming PPRs. Multiple analytical analyses, including NMR, XRD, and DLS, along with the visual observation, confirmed the successful formation of FEB-loaded PPRs. Specifically, NMR spectroscopy showed chemical shift changes, XRD showed an amorphous phase, DLS showed hydrodynamic changes and turbid solution indicated PPRs complex formation. These findings underscored the effectiveness of a multi-technique approach for the characterisation of supramolecular assemblies. In addition, a small size range between 58 and 67 nm was obtained from the FEB-loaded micelles and PPRs, indicating effective nanocarriers in improved drug absorption and bioavailability within the eye due to the small size particles. Moreover, FEB micelles and PPRs demonstrated no cell toxicity which FEB micelles (1-90 μg/mL) and mixed micelles (1-50 μg/mL) had higher cell viability than PPRs (1-20 μg/mL) across IM-HCEpi cells and HCE-T cell lines. The *ex vivo* permeation study across the porcine cornea and sclera demonstrated the distinct permeation profiles of FEB micelles, mixed micelles, and PPRs. FEB-loaded PPRs could

help to penetrate the FEB drug to cross the sclera tissue. Following these results, it revealed that the FEB-loaded micelles and mixed micelles merged the ocular tissue, followed by the transportation of the FEB drug across the tissue by the CDs. Therefore, the study emphasized the crucial role of formulation design in regulating ocular drug permeation and provided valuable insights for creating effective OcDD systems.

Chapter 5

Elucidation of the drug permeation across the porcine cornea and sclera by using mathematical modelling

5.1 Introduction

Chapters 3 and 4 dealt with the development of an effective ocular drug delivery (OcDD) system using micelles and poly(pseudo)rotaxanes (PPRs), which showed a great performance in enhancing drug delivery of curcumin (CUR) and fenofibrate (FEB) to ocular tissues. The development of mathematical models for eye drug delivery holds great promise for accelerating the design of the OcDD system. By combining computational modelling with experimental study, it could help researchers to advance understanding of drug transport processes in ocular tissues. Compartment models and Fick's law of diffusion could be used as theoretical frameworks to study and explain the process of drug permeation across biological membranes. Indeed, the compartment models are used to simplify complex biological systems by dividing them into different compartments, representing different physiological barriers.

Researchers can develop and consider the mass balance in each compartment according to this compartment model, which is helpful for predicting the behavior of the drugs over time across each compartment.[358–360] Worakul *et al.* outlined several models to develop the compartment model for eye drops which each compartment were interconnected by drug transfer processes such as drug diffusion and elimination.[193] Similarly, German *et al.* highlighted the benefit of using mathematical modelling to predict the pharmacokinetics and pharmacodynamics of timolol suspension in rabbits after topical administration based on their *in vitro* and *in vivo* drug release studies.[358]

Fick's law of diffusion describes the rate of diffusion of a substance across a concentration gradient.[361] More precisely, this law helps to quantify the flux (J) of the

drug across membranes based on several factors, including the thickness of the membrane, surface area and the concentration gradient of the drug. Thus, by utilizing Fick's law, researchers can mathematically model the process of drug permeation across the membrane and gain insights into factors affecting drug transport and bioavailability.

In terms of experimental study, transportation of a molecule across biological membranes such as the cornea or conjunctiva in both *in vitro* and *ex vivo* permeation studies is commonly characterized by the apparent permeability coefficient (P_{app}) where the permeability is measured by mounting the membrane in a diffusion chamber which includes the donor and the receiver chambers.[193,237,362] The drug is loaded in the donor chamber, and the drug concentration is measured in the receiver chamber at multiple time points. Thus, an increase in the concentration of drug permeation with time is then utilized to calculate the flux across the membrane, which is then utilized to calculate the permeability.[237] In addition, the calculated permeability values can be utilized as input parameters in *in vivo* models to determine tissue concentrations and bioavailability.[386,387] Pescina *et al.* measured the P_{app} values of multiple drugs loaded D-α-tocopheryl polyethylene glycol succinate (TPGS)/Poloxamer 407 micelles, including dexamethasone (DEX), cyclosporine-A (CsA), and econazole nitrate to observe the differences in their permeability profiles.[237] The study found that 12 nm-sized DEX-loaded TPGS micelles ($P_{app}=3.26x10^{-6}$ cm/s) had higher drug permeation across porcine conjunctiva compared to the CsA ($P_{app}=0.46x10^{-6}$ cm/s), whereas no econazole nitrate drug permeation occurred across the conjunctival tissue of the porcine eyes. In another study, Toffoletto *et al.* developed a mathematical model to estimate the drug concentration over time in different compartments of the eye by applying soft contact lenses (SCLs) on the cornea and studied drug permeation across different tissues to the posterior segment of the eye.[363] Their mathematical model development helped to predict the drug distribution over time in tears, sclera, retina, aqueous humor, and vitreous humor, enabling a better understanding of drug transport to posterior eye segments for clinical use estimation. Therefore, by comparing and analyzing the P_{app} values obtained from each formulation, the researchers were able to identify the most promising candidates for further development as an OcDD system.

The permeability is calculated by dividing the steady state flux by the driving force for diffusion across the membrane, which is equal to the difference in concentration across the membrane for a soluble drug. The same formula is sometimes used to calculate the permeability for hydrophobic drugs that are encapsulated in nanocarriers even though the nanocarriers are far too big to diffuse across the membrane. The permeability values are then compared across various formulations to determine the preferred formulation to achieve the highest delivery.[364,365] For example, Veiga *et al.* investigated the permeation of natamycin-loaded Pluronic P103 (PF103) micelles, PF103/Soluplus® mixed micelles and PF103/Soluplus®/α-CD PPRs (~120 nm) across the sclera of bovine eyes. Their study found that the permeability for the PPRs (P_{app}=0.91x10^{-6} cm/s) was smaller than that for the single PF103 (~20 nm) and mixed PF103/Soluplus® (~110 nm) micelles (P_{app}=1.67x10^{-6} and 1.44x10^{-6} cm/s, respectively).[364] Drawing on the work of Veiga *et al,* the dependency on the permeability of formulations is somewhat misleading because if the same drug is diffusing in both cases of PPRs and micelles, the permeability should be equal unless the components of the nanoformulations such as surfactants act as permeability enhancers.[237,366] While using the calculated permeability to choose the preferred formulation is a reasonable approach, a more fundamental understanding of the *ex vivo* transport for nanoformulations will be useful.

This chapter focuses on utilizing the drug permeation data reported in Section 4.3.5 across the excised cornea and sclera of the porcine eyes to develop an understanding of the mechanism of transport of the FEB-loaded micelles, mixed micelles, and PPRs across the epithelia based on Fick's law.

5.2 Methods

5.2.1 Formulation structure prediction

The FEB-loaded Pluronic F127 (PF127) micelles and mixed PF127/Soluplus® micelles were prepared as per Section 4.2.3, whereas the FEB-loaded PF127/Soluplus®/2-HPβCD PPRs were produced as per Section 4.2.4. To understand the mechanism of the *ex vivo* permeation across the tissue, the initial study focused on determining the structure of the

prepared FEB-loaded micelles, mixed micelles, and PPRs based on the previous results in Table 4.1 (Chapter 4) studying the particle sizes of the FEB-loaded micelles, mixed micelles and PPRs. The summary of the results was reproduced as presented in Table 5.1.

Table 5.1: Mean size and size distribution of FEB-loaded P127 micelles, PF127/Soluplus® micelles and PF127/Soluplus®/2-HPβCD PPRs prepared in pH 7.4 buffer. Numbers represent as the mean ± standard deviation (SD) (n=3).

Code	Components (%(w/v))			Particle size		
	2-HPβCD	PF127	Soluplus®	D_h (nm, Int%)	PDI	ζ (mV)
BK53-C1	-	5	-	5 ± 1 (80%) 28 ± 4 (20%)	0.49 ± 0.12	-2.09 ± -0.68
BK53-C2	-	-	5	61 ± 0.3 (100)	0.03 ± 0.02	-1.95 ± -0.46
BK53-1	-	5	5	67 ± 3.4 (100%)	0.14 ± 0.07	-0.64 ± 1.89
BK53-3	15	5	5	65 ± 1.6 (100%)	0.02 ± 0.003	-1.16 ± 1.68

The particle sizes following the DLS measurement showed that the mixed micelles (BK53-1, Table 5.1) and the PPRs (BK53-3, Table 5.1) were bigger than the single micelles of PF127 and Soluplus® micelles (BK53-C1 and C2, Figure 5.1) (p<0.05, One-way ANOVA followed by Dunnett's multiple comparison tests). Moreover, the addition of PF127 copolymer to the mixed PF127/Soluplus® micelles noticeably increased the micelle sizes from 5 nm to 67 nm, suggesting the hydrophobic poly (propylene oxide) (PPO) part of PF127 was accommodated inside the Soluplus® micelles due to smaller PF127 micelles (Table 5.1).[193] Therefore, Figure 5.1 displayed the predicted structure of FEB-loaded single and mixed micelles as well as PPRs based on these DLS results and the characterization to confirm the PPR formations including the XRD and ^{1}H-NMR, as per Section 4.3.3.

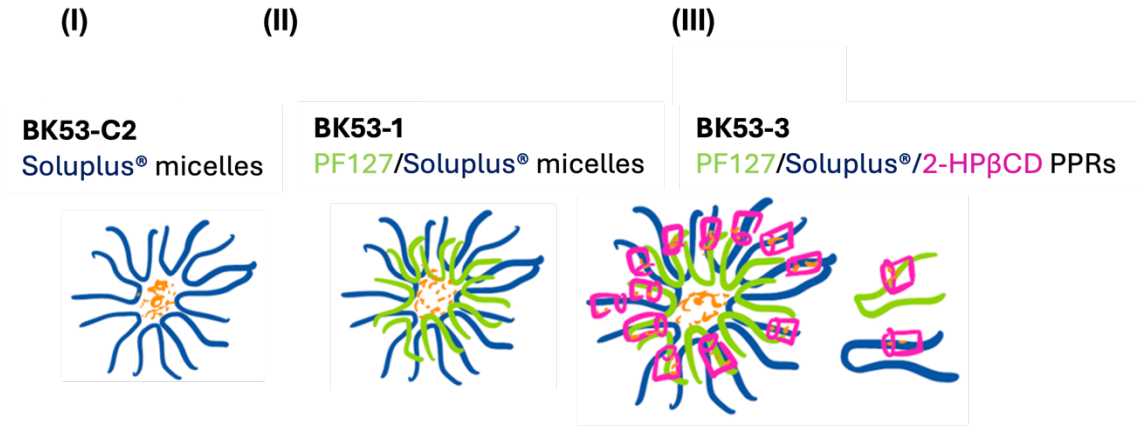

Figure 5.1: The predicted structure of (I) single and (II) mixed nanomicelles formed by self-assembly of the amphiphilic block copolymers and (III) the CD-based PPRs.

This mathematical modelling study is based on the hypothesis that PF127 and Soluplus® copolymers can encapsulate FEB in their micelles, and can also interact with 2-HPβCD to form PPRs (Figure 5.1). Thus, understanding the polymer structures could aid in comprehending how these formulations effectively deliver the drugs to the ocular surface, as discussed in Section 4.3.5.

5.2.2 Model description

The apparent permeability coefficient (P_{app}), is a parameter that provides information about the ability of the drug to penetrate the ocular tissue. As a consequence, in the context of drug permeability studies, P_{app} is calculated using the following equation:

$$P_{app} = J/C_D \qquad \text{Equation 1}$$

Where J = the transcorneal flux across full-thickness of the tissue (μg/cm^{2}min) calculated as the slope of the regression line at the steady state of the drug concentration-time profile

C_D = the initial concentration of the drug in the donor chamber at the start (μg/mL)

Permeability can be expressed as the product of the diffusivity (D) and the partition coefficient (K). While these equations are well known, it is useful to derive them from

the first principles to understand why the equation may not be directly applicable to nanoformulations and how the equation could be modified to correctly calculate transport parameters for nanoformulations.

To model the drug transport across the tissue, Figure 5.2 shows the permeation profiles and the drug retention after 6 h of *ex vivo* permeation of the FEB formulations across the sclera.

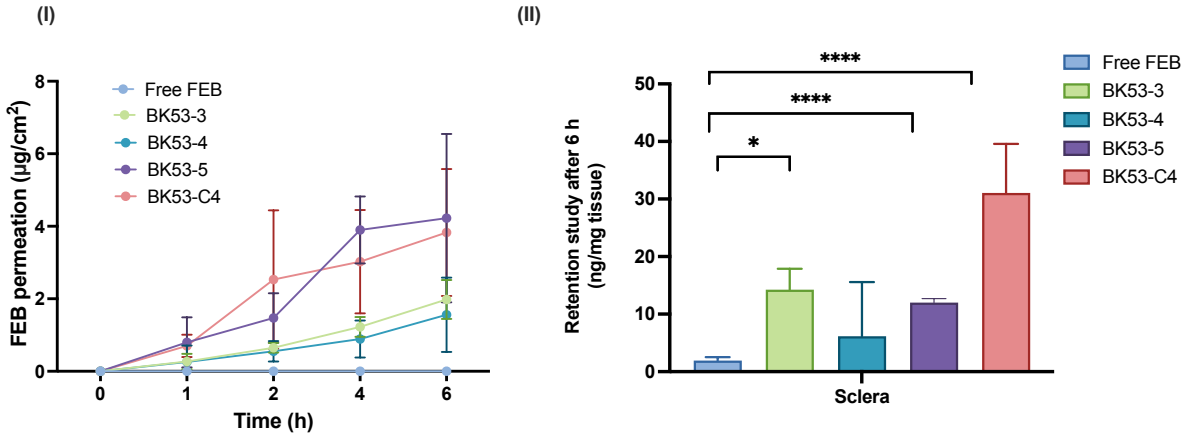

Figure 5.2: (I) Permeation profiles of FEB formulated in PPRs in PBS pH 7.4 across the scleral tissue of the porcine eyes (n=3), and (II) drug retention in the sclera of the porcine eyes after 6 h of contact with different types of FEB formulations and the free FEB control (n=3). The medium in the receptor chamber was PBS+1.06 %(w/v) Tween-80. The concentration at the start of the free FEB in the MilliQ water as a control group was 94 ± 1 µg/ml in the sclera. Statistical significance was analyzed by the One-way ANOVA followed by Dunnett's multiple comparisons (*p<0.05, **p<0.01, ***p<0.001 and ****p<0.0001 compared to the mean values of the free FEB control group). Data are presented as the mean ± SD of three experiments (n=3 eyes for each group).

Based on the *ex vivo* study, it could be assumed that the micelles delivered both drug-loaded cyclodextrins (CDs) and the free drug (Figure 5.2(I)). Furthermore, the permeation of FEB-loaded PF127/2-HPβCD (BK53-4) and FEB-loaded PF127/Soluplus®/2-HPβCD PPRs (BK53-3) was around two to three-fold lower compared to FEB-loaded 2-HPβCD PPRs (3.8 µg/cm^2, BK53-C4, Figure 5.2(I)). Whilst the drug retention of FEB-loaded Soluplus®/2-HPβCD PPRs (BK53-5) was low, the permeability profile of the drug was high in comparison to the FEB-loaded 2-HPβCD PPRs (BK53-C4, Figure 5.2(I)-(II)).

As stated previously, the hypothesis for this model is that the micelle formulations helped to merge the scleral tissue of the porcine eyes and improve the penetration of the drug-loaded CDs to come across the scleral tissue to the receiver chamber (Figure 5.3).

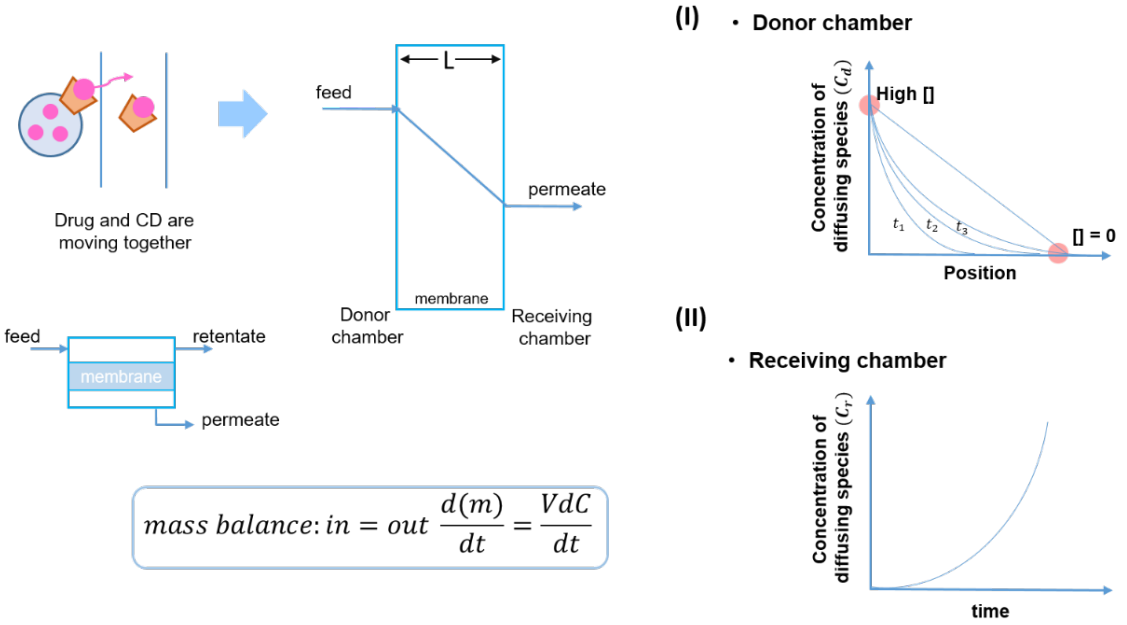

Figure 5.3: Schematic representation of the mathematical model design with transport pathway and the drug permeation profile during the *ex vivo* permeation experiment from (I) the donor chamber to (II) the receiving chamber.

The development of this mathematical model was conducted using Fick's law of diffusion to model the drug transport in the membrane[361]:

$$\frac{dC_s}{dt} = \frac{D\partial^2 C_s}{\partial x^2} \qquad \text{Equation 2}$$

Where C_s = the retention concentration of substance in the sclera,

x = the section of position being considered

t = time

According to Equation 2, Fick's law describes the rate at which a substance diffuses through a tissue or medium over time. The above differential equation needs to be solved with two boundary conditions and an initial condition (Figure 5.3). In this case, the

boundary conditions assume that the concentration at x=0, i.e., at the boundary with the donor chamber, is equal to the product of the starting concentration in the donor chamber at the partition coefficient (Figure 5.3 (I)). Moreover, Equation 2 assumes that the concentration in the donor chamber remains relatively constant throughout the experiment. Additionally, the drug concentration at the surface in contact with the receiver chamber is assumed to be zero because the concentration in the receiver chamber is usually very small compared to the drug concentration in the donor chamber. Therefore, the steady state solution to the above differential equation is a linear concentration profile, which refers to a situation where the drug concentration in a particular region remains approximately constant over time even though the drug is continuously diffusing through the medium. The linear profile also implies that the average concentration in the membrane is simply half of the concentration at the boundary with the donor (Figure 5.4).

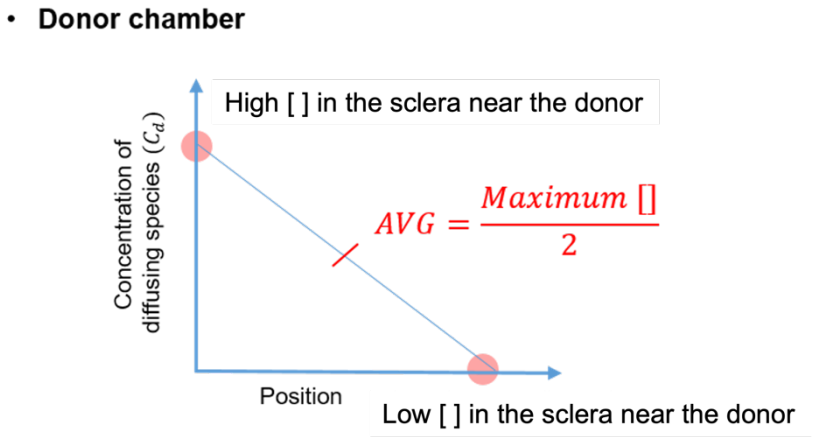

Figure 5.4: A plot of the drug permeation profile in the donor chamber at different positions across the scleral tissue of the porcine eyes based on *ex vivo* permeation.

Equivalently, the concentration at the boundary with the donor is equal to twice the average concentration in the membrane (Figure 5.4).

On the other side, the transportation of drug molecules is moved from higher to lower concentration across a concentration gradient in the receiver chamber (Figure 5.3(II)). Consequently, the concentration in the receiver chamber can be calculated by equating

the rate of accumulation to the rate of flux coming in from the membrane into the chamber (Figure 5.3(II)), i.e.,

$$\frac{VdC_r}{dt} = \frac{-D\partial C_s A}{\partial x} \qquad \text{Equation 3}$$

Where C_r = concentration of a substance in the receiver chamber
t = time
x = the section of the position being considered
A = cross-sectional area of the tissue
C_s = the retention concentration of a substance in the sclera

The drug concentration in the sclera was changed so that the drug concentration was higher near the donor chamber and lower near the receiving chamber (Figure 5.3 (II)). However, in this case, due to the straight line of the pseudo-steady state (Figure 5.4), our study assumed that the concentration of the drug in the receiver chamber was negligible compared to the concentration in the donor part. Consequently, the measured drug concentration was calculated using the average concentration in the sclera at the boundary according to Equation 4.

$$< C_s > = \frac{KC_d}{2} \qquad \text{Equation 4}$$

Where C_s = concentration of substance in the sclera
K = the partition coefficient which refers to the ratio of the concentration of a substance in one medium to the concentration in a second phase when the two concentration are at the equilibrium
C_d = drug concentration in the donor chamber.

The flux (J) calculated from the *ex vivo* permeation study was applied to calculate D (cm^2/h), which refers to the measurement of how quickly one material diffuses through another part. Moreover, the D value represents area per unit time, and it is negative

because the flow direction of the substance is considered from higher to lower concentration. Therefore, the equation is further developed from Equation 3 to Equation 5.

$$J = -D\frac{dC_d}{dX} \qquad \text{Equation 5}$$

Where J = diffusion flux, the net movement of a substance across the specified area in a specified time

D = the diffusion coefficient

C_d = concentration of a substance in the donor chamber per unit volume

Equation 5 was further developed by including the C_d parameter from Equation 4; the new equations to obtain D are as follows:

$$J = \frac{D\ x\ 2<C_s>}{L} \qquad \text{Equation 6}$$

$$\therefore D = \frac{J\ x\ L}{2<C_s>} \quad \frac{g}{cm^2\ x\ h}\ x\ cm\ x\ \frac{cm^3}{g} = \frac{cm^2}{h} \qquad \text{Equation 7}$$

Where K = partition coefficient

D = diffusivity

L = thickness of the tissue

C_s = concentration of the substance in the sclera

Therefore, in the next section, the optimized modelling according to Equation 7 of the D was applied to the previous studies by incorporating the *ex vivo* permeation results into the equation.

5.3 Results and discussion

5.3.1 Predicted permeability of the fenofibrate nanoformulations across the cornea and sclera of porcine eyes

As per Section 4.3.5, the *ex vivo* transcorneal and transscleral studies found no FEB drug penetration through the cornea, but the drug was permeated through the sclera of the porcine eye from FEB-loaded nanoformulations containing 2-HPβCD. These *ex vivo* permeation results could be utilized to enhance our understanding of how the FEB-loaded micelles and PPRs traverse biological barriers (Figure 5.5).

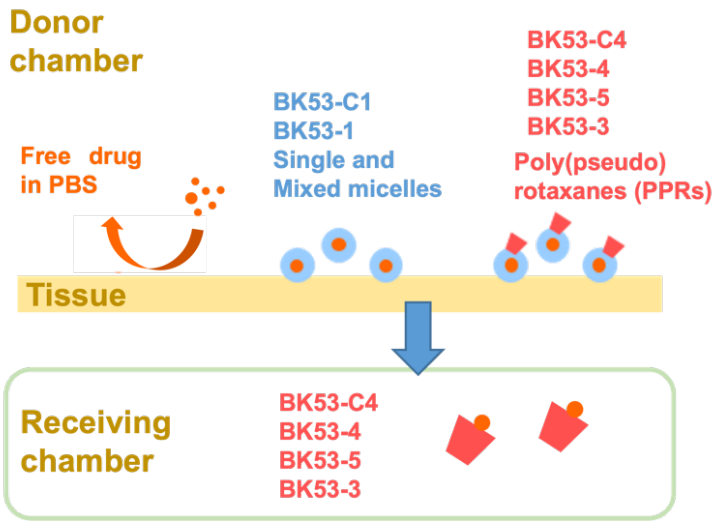

Figure 5.5: The predicted transportation of the free FEB, FEB-loaded micelles, mixed micelles, and PPRs across the porcine sclera according to the *ex vivo* permeation study from Section 4.3.5.

As illustrated in Figure 5.5, the study found that free FEB drug could not pass through the corneal and scleral tissues of the porcine eyes. Specifically, in the absence of nanocarriers, the free drug concentration in the donor chamber was very small (19 ± 1 µg/mL), and furthermore, the drug that diffused into the epithelia will likely bind to the cells due to the hydrophobicity resulting in non-detectable concentration in the receiving chamber. However, the drug was transported across the scleral tissue in the combination systems of FEB-loaded PPRs containing 2-HPβCD that had higher FEB concentration in the donor chamber compared to the free drug, leading to a detectable concentration of

FEB in the receiver chamber ranging from 0.42 to 10.65 µg/mL, as per Section 4.3.5. A possible reason could be that the FEB-loaded single and mixed micelles delivered the drug to the first layer of both corneal and scleral tissues (Figure 5.5). The micelles without the CDs would likely deliver the drug molecules, which then would bind to the cells due to hydrophobicity limiting further transport into the aqueous receiving chamber, as highlighted in the review literature by Bachu *et al.*[61] However, in the case of the FEB formulations with 2-HPβCD, the drug-loaded CDs were delivered to the cornea; possibly due to the hydrophilic characteristic of the nanoformulations, they would not exhibit significant binding to the cells. The drug-loaded CDs helped to transport the drug across the scleral tissue and thereafter released the drug into the receiving chamber of the Franz-diffusion cells (Figure 5.5). Confirmation of the FEB drug and CD detected in the receiving phase was performed by mass spectrometry, as per Section 4.3.5.

Consequently, two hypotheses were used to explain the mechanism behind this point. The first hypothesis was set as the single and mixed micelles helped bind the nanoformulations to the ocular surfaces and released the drugs (Figure 5.6).

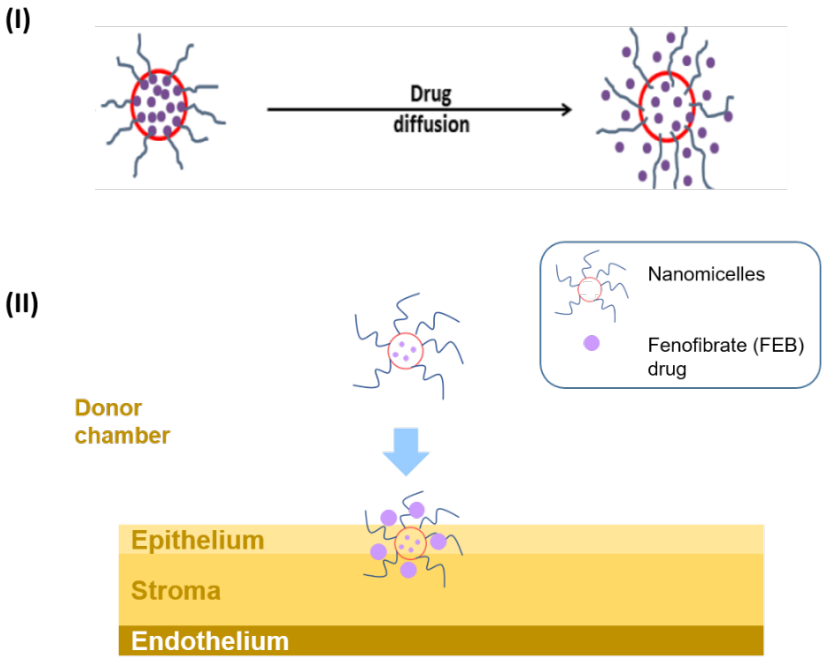

Figure 5.6: A picture represents (I) modes of drug release from the micelles by drug diffusion from the micelles and (II) the diagram showing FEB drug retention in the cornea by drug diffusion from the micelles.[115]

The mechanism of the FEB drug release from the micelles could be the drug encapsulated within the hydrophobic core was diffused to the corneal tissue (Figure 5.6(I)).[367] More precisely, the micelles came to the surface of the tissue and opened up the hydrophilic tail to merge or interact with the lipid bilayer of the corneal epithelium (Figure 5.6(II)). Then, the drug was released at the bilayer after the micelles opened up, resulting in the accumulation of the drug within the corneal tissue.[367] This result was consistent with the research of a previous study in which a lag time was observed in the first two hours of the *ex vivo* transcorneal permeation experiment of the test formulation. For example, Bao *et al.* prepared the celecoxib eye drops from PF127 micelles, and found that PF127 micelles could improve the transcorneal permeability of the celecoxib drug compared to only the celecoxib suspension (0.3 μg).[203] Additionally, the celecoxib drug started to permeate and detect in the receiver chamber after 2-3 hours of their study. Similarly, Lorenzo-Veiga *et al.* found a two hour lag time in the *ex vivo* trans-scleral permeation study of the natamycin-loaded micelles and mixed micelles in bovine eye.[193] Furthermore, their study also indicated no drug permeation across the bovine cornea of their natamycin-loaded micelles owing to the polarity of the nanoformulations. Hence, the lag time was observed when performed the permeation test in the previous research study might be related to the time required by the micelle formulations to interact with the ocular tissue and thereafter diffuse the drug into different layers.

Therefore, this study indicated that PF127 and Soluplus® polymers helped bind between the phospholipid bilayers of cellular membrane modifying their fluidity although there was no drug permeation across the cornea of the porcine eyes. Additionally, another hypothesis was CDs increased transportation of the FEB formulations across the scleral tissue. Specifically, CDs could interact with cell membranes and transiently disrupt lipid bilayers, facilitating the transport of drug molecules across biological barriers. This property could enhance drug permeation across the scleral tissues, which may not be as effectively achieved by the micelle systems alone.

The following section focused on using modelling to help explain the hypotheses about why the FEB formulations had permeation or transportation with CDs.

5.3.2 Model validation

The summary of the *ex vivo* permeation study and the D calculation are displayed in Table 5.2.

Table 5.2: The retention concentration (C_s), trans-scleral steady-state flux (J), permeability coefficients (P_{app}), diffusivity (D) and drug:CD (D:CD) ratio recorded for FEB formulated in Soluplus® and PF127 micelles, Soluplus®:PF127 1:1 w/v mixed micelles, and PPRs in PBS pH 7.4 after 6 h of the *ex vivo* trans-scleral permeation. Statistical analysis was analyzed by the One-way ANOVA followed by Dunnett's multiple comparisons (*p<0.05, **p<0.01, ***p<0.001 and ****p<0.0001 compared to the mean values of BK53-5). Data are presented as the mean ± SD of three biological replications (n=3 eyes for each group).

Code	C_s (μg/mL)	J (μg/cm²h)	P_{app} x 10^3 (cm/h)	D x 10^3 (cm²/h)	D:CD molar ratio		
					Donor	Receptor	
					Start	1h	2h
BK53-3	3.62 ± 0.68	0.31 ± 0.07*	7.88 ± 1.69*	2.16 ± 0.57	3378:1	5:12	4:1
BK53-4	2.21 ± 3.37	0.26 ± 0.20**	9.61 ± 7.40*	15.13 ± 16.15	3292:1	1:3	2:7
BK53-5	3.83 ± 0.26	0.82 ± 0.19	23.4 ± 5.52	5.31 ± 0.94	32:1	1:5	3:7
BK53-C4	10.1 ± 2.15	0.62 ± 0.16	18.2 ± 4.75	1.63 ± 0.71	59:1	1:1	1:2
BK53-1	3.80 ± 0.09	-	-	-	-	-	-
BK53-C1	2.32 ± 0.73	-	-	-	-	-	-

According to the D calculation (Equation 7), the results revealed that there was no significant (p>0.05) difference in the D values across the PPR formulations compared to the FEB-loaded Soluplus®/2-HPβCD PPRs (BK53-5, Table 5.2). In contrast, the P_{app} calculation displayed a significant (p<0.05) difference in the FEB permeation across the sclera tissues of the PF127/Soluplus®/2-HPβCD (BK53-3) and FEB-loaded PF127/2-HPβCD (BK53-4) formulations compared to the FEB-loaded Soluplus®/2-HPβCD PPRs (BK53-5) (Table 5.2). Therefore, it indicated that the D values were the same for all four formulations, suggesting that there were only CDs and drugs delivered to the receptor phases.

However, according to the mass spectrometer characterisation, the drug-to-cyclodextrin (D:CD) ratio was slightly different between the donor and receptor chambers, indicating that other factors might affect the permeation study. For example, the surfactant of PF127 and Soluplus® copolymers might have made the layer more permeable, which resulted in the difference in the D:CD ratio in each formulation. In other words, when formulating drugs using CDs, it is expected to aim for a 1:1 molar ratio of the drug to CDs to maximize complexation efficiency and enhance the solubility and stability of the drug (BK53-C4). Nevertheless, for this case, the addition of excipients like PF127 and/or Soluplus® could disturb the 1:1 molar ratio between the FEB drug and 2-HPβCD and result in a different optimal ratio for complexation. This can be due to competing interactions between the drug, CDs, and the surfactants (PF127 and Soluplus®), leading to a different equilibrium point for complex formulation.

5.4 Conclusions

Based on the *ex vivo* permeation results in Chapter 4, the hypotheses were that the single and mixed micelles merged the nanoparticles onto the ocular tissues, and CDs delivered the drug across the scleral tissue to the receiving chamber. To prove these hypotheses, Chapter 5 employed a mathematical model to address the hypothesis we posited. In this study, the modelling was developed and optimized based on Fick's law since it could provide a fundamental understanding of drug diffusion processes of the transport of small molecules that permeated through the biological barriers. Fick's law was modified to calculate the D, a true property of the membrane, and the resulting D value of the FEB-loaded PPRs was found to be in the range between 1.63×10^{-3} and 15.13×10^{-3} cm^2/h, while the calculated P_{app} value of these FEB-encapsulated PPR formulations was approximately 7.88×10^{-3}-23.4×10^{-3} cm/h. Additionally, through this approach, P_{app} and the C_s were included in the equation for a better explanation of how the drug-loaded micelles or PPRs transported across the corneal and scleral tissues of the porcine eyes. Furthermore, the diffusivity equation was applied to test the validity of the hypothesis by incorporating the *ex vivo* permeation results from Chapter 4 into the equation. The results found no difference in D value across all formulations although there was a difference in the D:CD

ratio in the donor and receptor chambers in all formulations. Therefore, this study indicated the utilization of a mathematical model of Fick's law to facilitate an exploration of the experimental data, contributing to a more comprehensive interpretation of the findings and supporting the refinement of our hypotheses.

Chapter 6

Mixed Pluronic F127/chitosan systems for fenofibrate drug and future work

6.1 Introduction

Polyoxyethylated nonionic surfactants, such as Pluronic F127 (PF127), are used for ocular drug delivery (OcDD) due to their ability to increase drug permeability, as already mentioned in Chapter 2. As a result, PF127, composed of poly (propylene oxide) (PPO) and poly (ethylene oxide) (PEO) units, can self-assemble to form the micelles, increasing the bioavailability of poorly water-soluble drugs, including curcumin (CUR) and fenofibrate (FEB), as previously outlined in Chapters 3 and 4. However, in the context of OcDD, using only PF127 micelles may not always be sufficient to overcome the ocular barriers and achieve optimal drug delivery outcomes. Recently, mucoadhesive polymers, such as chitosan (CH), are being extensively studied to enhance the performance of the delivery system because of their ability to adhere to the ocular surface through non-covalent bonding.[122,368,369] CH is a cationic polyelectrolyte that exhibits mucoadhesive properties and can act as a permeation enhancer for ocular tissue drug permeability, as highlighted in our previously published review entitled 'Posterior Segment Ophthalmic Drug Delivery:Role of Muco-Adhesion with a Special Focus on Chitosan.[370] Thus, the creation of positively charged micelles that combine the benefits of PF127 copolymers and CH molecules could improve drug loading capacity, stability, and ocular penetration. For instance, Padaga *et al.* developed moxifloxacin-loaded mixed micelles (Pluronic F68/PF127) with CH-poly (lactic-co-glycolic acid) (PLGA) conjugate for treating bacterial keratitis.[368] *In vitro* and *in vivo* experiments revealed that their mixed micelles (size~127 nm with a zeta potential (ZP) of +36 mV) with larger Pluronic proportions (1:10) exhibited higher physicochemical properties, mucoadhesion, corneal penetration, and antibacterial efficacy. In a similar study, Padaga *et al.* prepared gatifloxacin (GX)-encapsulated mono or dual chitosan oligosaccharide lactate (COL)-conjugated PF127 micelles for bacterial keratitis treatment.[371] The GX-loaded COL/PF127 micelles with a

higher COL ratio (2:1 COL:PF127) demonstrated better tissue penetration through corneal epithelial layers of the ghost eyes and a reduction in bacterial load in mice cornea, supporting that the GX-loaded COL/PF127 micelles, an eye drop formulation, has the potential for clinical translation in treating bacterial keratitis.

Therefore, all PF127/CH approaches, as mentioned previously, suggest that drug encapsulation within PF127/CH micelles may be useful and used for promising drug carriers of hydrophobic drugs for the treatment of ocular diseases. Herein, the aim of this chapter was to study if the PF127 micelles, according to Chapter 2, could be further developed to prepare PF127/CH micelles to form the positively charged micelles and encapsulate FEB, a hydrophobic drug. Moreover, another objective of this work is to provide more information on the interactions between PF127 and CH through the physicochemical property characterization of these PF127/CH micelles.

6.2 Materials and methods

6.2.1 Materials

As per Section 2.2.1 with the following additions: low-molecular weight chitosan (CH, mw:50-190 kDa with a deacetylation degree≥75%) was purchased from Sigma Aldrich (Arklow, Ireland).

6.2.2 Preparation of mixed Pluronic F127/chitosan micelles

A direct dissolution method following the previously reported procedure by Pepić *et al.* was used to prepare the FEB-loaded PF127/CH micelles.[146] In brief, a stock solution of low molecular weight CH (1 %(w/v)) or water-soluble CH (1.5 %(w/v)) was prepared in aqueous acetic acid (0.5 %(v/v)) by stirring for 24 h at room temperature. The CH solution was then filtered through a medium porosity filter in order to exclude undissolved CH. Solutions of PF127 were prepared by dilution of the stock solution in the concentration range 5.21×10^{-5} %(w/v) to 31 %(w/v) at 25°C, as per Section 2.2.3. One set of solutions was prepared in deionized (DI) water only and another set was prepared with phosphate buffered saline (PBS) solution. The mixed PF127/CH systems were prepared from PF127 and CH stock solutions as follows: stock PF127 solution was diluted in different

concentration ranges ($5.21x10^{-5}$ %(w/v) to 31 %(w/v)), then various concentrations of low molecular weight CH (0.005, 0.03, 0.06, 0.12, 0.25 and 0.75 %(w/v)) or water-soluble CH (1.5 %(w/v)) were added to the solution in DI water or PBS solution, under continuous stirring for 24 h at 25°C. The solutions of low molecular weight CH only was prepared by diluting with DI water or PBS solution in the concentration range $1.92x10^{-5}$ to $7.74x10^{-3}$ %(w/v). All systems were kept in a water circulating bath at 25 ± 0.02°C to equilibrate overnight before surface tension measurements, as per Section 2.2.2.

6.2.3 Preparation of fenofibrate-loaded mixed polymeric micelles by direct dissolution

FEB (10 mg) was mixed with the PF127 polymer solution (14 %(w/v)). After that, the stock CH solution in aqueous acetic acid, as per Section 6.2.2, was diluted to different CH concentrations (0.015-0.12 %(w/v)) and added to the FEB/PF127 micelle solution. The mixture was stirred at 120 rpm on the magnetic stirrer at 25 ± 3°C for 24 h. The solution was filtered through 0.45 μm filter, and the filtrate was collected for further characterization. The experiment was replicated 3 times, and the data are presented as mean ± standard deviation (SD).

6.2.4 Characterization of micellar solutions

6.2.4.1 Size and zeta potential measurement

As per Section 3.2.3.2 by using a Malvern Zetazier Ultra-Red analyzer (Malvern Panalytical, UK)

6.2.4.2 Infrared spectroscopy

Fourier transform infrared (FT-IR) spectra were recorded using and infrared spectroscopy (IR) spectrometer (Perkin Elmer) using the KBr disc method. A sample powder (freeze-dried formulation) (10 mg) was mixed with KBr, ground into a fine powder using an agate mortar and subsequently compressed into a disc using a hydraulic press. Each disc was scanned at a resolution of 1 cm^{-1} over a frequency region of 440-4000 cm^{-1}, with each spectrum representing an average of 64 scans.

6.2.5 Statistical analysis

As per Section 2.2.8

6.3 Results and discussion

The goal of the research study in this experimental section was to create micelles with positive charge from mixed PF127/CH systems. Below is a description of more details.

6.3.1 Surface properties of mixed Pluronic F127/chitosan systems

According to Chapter 2 about the preparation of PF127 micelles, another interesting approach for OcDD is to prepare cationic micelles by physical mixture between PF127 and low molecular weight CH solution via direct dissolution method. CH could enhance permeation by increasing transepithelial permeability in contact with the ocular mucosa, thereby enhancing and prolonging drug retention on the eye surface.

6.3.1.1 Surface tension measurements for mixed Pluronic F127/chitosan systems

As with the PF127 system, the surface tension of mixed PF127/CH was used to measure the critical micelle concentration (CMC) by the pendant drop method, as per Section 2.2.2. Mixed PF127/CH systems were analysed in DI water and PBS solutions in order to describe the aggregation behaviour of PF127 in the presence of CH (Figure 6.1).

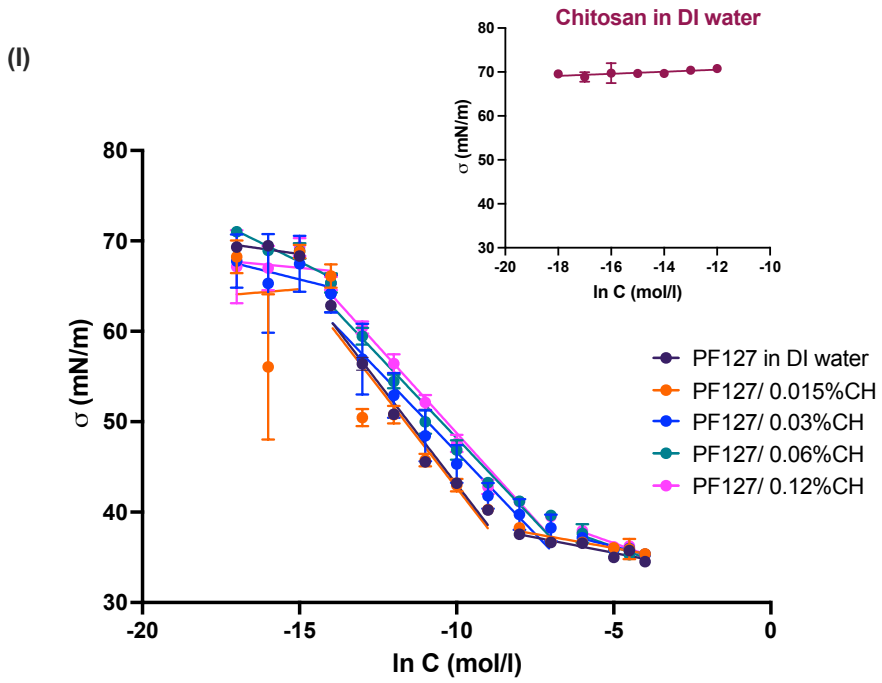

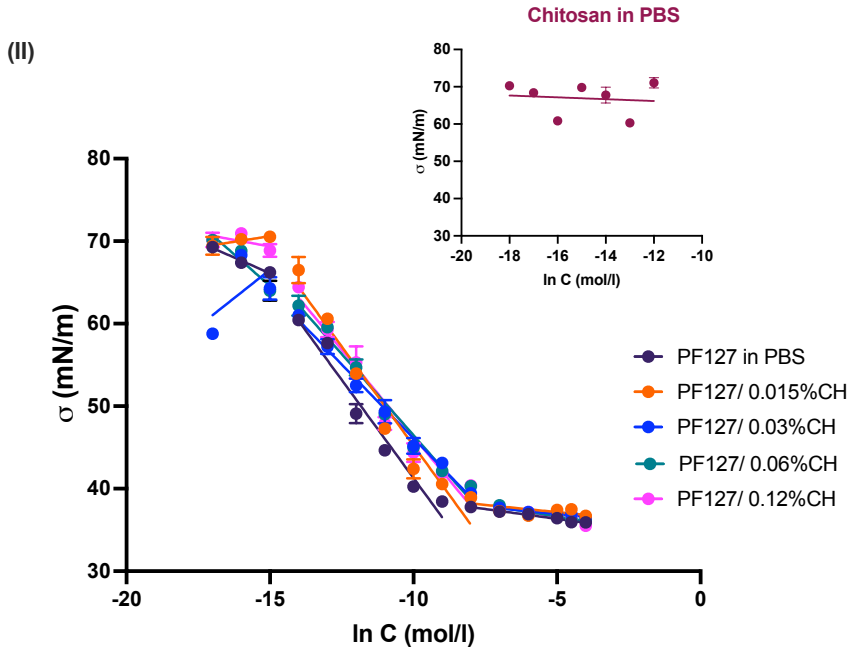

Figure 6.1: The isotherm of surface tension for PF127 and mixed PF127/CH systems in (I) DI water and (II) PBS solution containing various PF127 and constant chitosan concentrations (0.015, 0.03, 0.06 and 0.12% CH) at 25°C. Insert: chitosan solution in DI water or PBS solution without PF127 at 25°C. The readings were taken five times from each sample concentration (n=5), and the bars indicate the standard error of the mean.

Figure 6.1 displays the surface tension isotherm for PF127 and mixed PF127/CH systems in DI water and PBS solution, respectively. It can be seen that all systems had a constant surface tension value beyond the CMC. However, the addition of chitosan caused differences in slopes of the surface tension isotherm before the first break in which these differences were independent of the chitosan concentration. Specifically, the surface tension before the first break of mixed PF127/CH systems in DI water and PBS tended to be below the surface tension value of the PF127 solution by itself (Figure 6.1). In other words, the surface tension was reduced when CH was added, leading to both a lower starting value and subsequent value of the surface tension before the first break for mixed PF127/CH systems. These results might be related to pH and ionic strength in the system since CH molecules (pKa of free amino group~6.5) are less protonated at higher pH and ionic strength. Thus, the system lacks sufficient electropositive CH charges to interact

with the electronegative PEO charge of PF127, leading to weak electrostatic interaction between polymers and CH, which could disturb the interfacial PF127 layer by coadsorption.[372,373] Consequently, the surface tension of mixed PF127/CH systems shifted to lower values compared to the PF127 only system (Figure 6.1).

For all solutions, the critical aggregation concentration (CAC) (at the first break) and the CMC (at the second break) values were obtained from the intersections of two straight lines. The CAC and CMC values of PF127 and mixed PF127/CH systems in DI water and PBS are listed in Table 6.1.

Table 6.1: The critical aggregation concentration (CAC) and the critical micelle concentration (CMC) at the air/solution interface for PF127 and mixed PF127/chitosan systems in water and PBS at 25°C. Data are presented as the mean ± SD (n=3).

Formulation	Concentrations			
	CAC x 10^{-7} mol/L	CAC x 10^{-4} %(w/v)	CMC x 10^{-4} mol/L	CMC %(w/v)
DI water (pH 6-7)				
PF127	0.93 ± 0.71	1.17 ± 0.89	1.65 ± 0.34	0.21 ± 0.04
PF127/0.015 %(w/v) CH	4.72 ± 1.06	5.95 ± 1.34	1.17 ± 0.04	0.15 ± 0.005
PF127/0.03 %(w/v) CH	3.31 ± 1.43	4.18 ± 1.80	5.74 ± 1.58	0.72 ± 0.20
PF127/0.06 %(w/v) CH	2.05 ± 0.11	2.58 ± 0.14	3.98 ± 0.93	0.50 ± 0.12
PF127/0.12 %(w/v) CH	4.41 ± 1.46	5.55 ± 1.84	3.62 ± 0.41	0.46 ± 0.05
PBS (pH 7.4)				
PF127	1.70 ± 0.47	2.14 ± 0.59	1.25 ± 0.38	0.16 ± 0.05
PF127/0.015 %(w/v) CH	2.76 ±0.16	3.48 ± 0.20	1.88 ± 0.10	0.24 ± 0.01
PF127/0.03 %(w/v) CH	2.02 ± 0.56	2.55 ± 0.70	5.57 ± 0.36	0.70 ± 0.05
PF127/0.06 %(w/v) CH	12.52 ± 10.63	15.78 ± 13.39	3.58 ± 0.17	0.45 ± 0.02
PF127/0.12 %(w/v) CH	1.48 ± 0.41	1.87 ± 0.51	3.00 ± 0.12	0.38 ± 0.01

As illustrated in Table 6.1, the result provided convincing evidence that the presence of CH increased both CAC ($2.58x10^{-4}$ to $5.95x10^{-4}$ %(w/v)) and CMC (0.46 to 0.72 %(w/v)) values in DI water except for condition with 0.015 %(w/v) CH which CMC had lower value than PF127 system (0.21 ± 0.04 %(w/v)) (Table 6.1). In terms of the PBS system, the presence of CH (0.015 to 0.06 %(w/v)) significantly increased the CAC value, ranging from $2.55x10^{-4}$ to $15.78x10^{-4}$ %(w/v). Whereas the PF127/CH system with 0.12 %(w/v) CH had lower CAC than the PF127 system (Table 6.1). Also, the CMC value increased as the concentration of CH in the PBS system increased (0.24 to 0.70 %(w/v)) (Table 6.1). Evidently, the presence of CH increased both CAC and CMC values in both DI water and PBS solutions. This demonstrates the systems with higher amounts of CH form

micelles at higher PF127 concentrations. In other words, it appears that CH significantly affects the micelle formation of PF127.

These results correspond to the study of Vincekovic *et al.,* which suggested that the charge density, conformation and flexibility of the polyelectrolyte chains are pivotal factors affecting the CAC value. However, in terms of CMC, they have found that the concentration CH did not strongly affect the CMC values of PF127 in DI water since the interaction between CH and PF127 depends on the CH charge and was sensitive to both pH and ionic strength as well as temperature.[374]

6.3.1.2 Hydrodynamic diameter measurements of mixed Pluronic F127/chitosan micelles

PF127 with the highest concentration (14 %(w/v), BK5-6, Table 2.1) prior to the gelation process of PF127 was selected for this experiment. The PF127 micelles were then combined with two different concentrations of CH to generate PF127/CH micelles, as illustrated in Table 6.2.

Table 6.2: Representative particle size (percentage by intensity), zeta potential (ZP) and polydispersity index (PDI) results from PF127 and mixed PF127/CH systems in different concentrations of CH in DI water and PBS. The readings were taken three times. Data are presented as the mean ± SD (n=3).

Code	CH %(w/v)	DLS		
		D_h (nm, Int %)	PDI	ZP (mV)
DI water (pH 6-7)				
BK14-1	-	66 ± 3 (75%) 5 ± 0.1 (25%)	0.9 ± 0.04	-0.9 ± 0.4
BK11-4	0.12	48 ± 7 (68%) 5 ± 1 (32%)	0.6 ± 0.2	+7.8 ± 0.9
BK13-2	0.75	79 ± 2 (80%) 6 ± 0.2 (20%)	0.4 ± 0.02	+14 ± 2
PBS (pH 7.4)				
BK14-2	-	41 ± 3 (61%) 5 ± 0.1 (39%)	0.5 ± 0.3	-0.7 ± 0.8
BK11-8	0.12	38 ± 2 (39%) 470 ± 68 (26%) 5 ± 1 (35%)	0.6 ± 0.2	+5.2 ± 0.9
BK13-4	0.75	62 ± 5 (75%) 6 ± 1 (25%)	0.3 ± 0.05	+8.21 ± 2

The formation of PF127/CH micelles was conducted at two concentrations of low molecular weight CH (0.12 and 0.75 %(w/v)) in both DI water and PBS (Table 6.2). Additionally, the positively charged nanomicelles (<100 nm) with PDI values ranging between 0.3 and 0.6 were obtained. PF127/CH micelles prepared from DI water exhibited the size of the micelles around 48-79 nm with PDI ranging from 0.4 to 1.49. Also, approximately 38 and 62 nm-sized PF127/CH micelles (PDI~0.6 and 0.3, respectively) with positive charge were obtained when preparing micelle in PBS with the two different CH concentrations (Table 6.2). Interestingly, the positive value of ZP increased when CH was introduced into PF127 micelles at increasing concentrations in both solutions. A possible reason for this observation could be as the concentration of CH increased in the PF127 micelles, more positively charged amino groups from CH were available to interact with the negatively charged regions or polar group of PF127 molecules. This increased interaction led to a higher surface charge density on the micelles, resulting in an increase in the zeta potential value.

Therefore, this study indicated CH coated on PF127 micelles according to the switch in the charge from negative to positive charge when coating with CH. To investigate the coating of CH on PF127 micelles observed in the DLS study, FTIR analysis was performed in the next study to characterize the chemical interactions and confirm the presence of CH on the surface of PF127 micelles.

6.3.1.3 Spectroscopic characterisation of Pluronic F127/chitosan systems

FTIR analysis was employed to attempt to investigate whether the nanomicelles of PF127 and mixed PF127/CH were successfully prepared. The spectra from these investigations are presented in Figure 6.2.

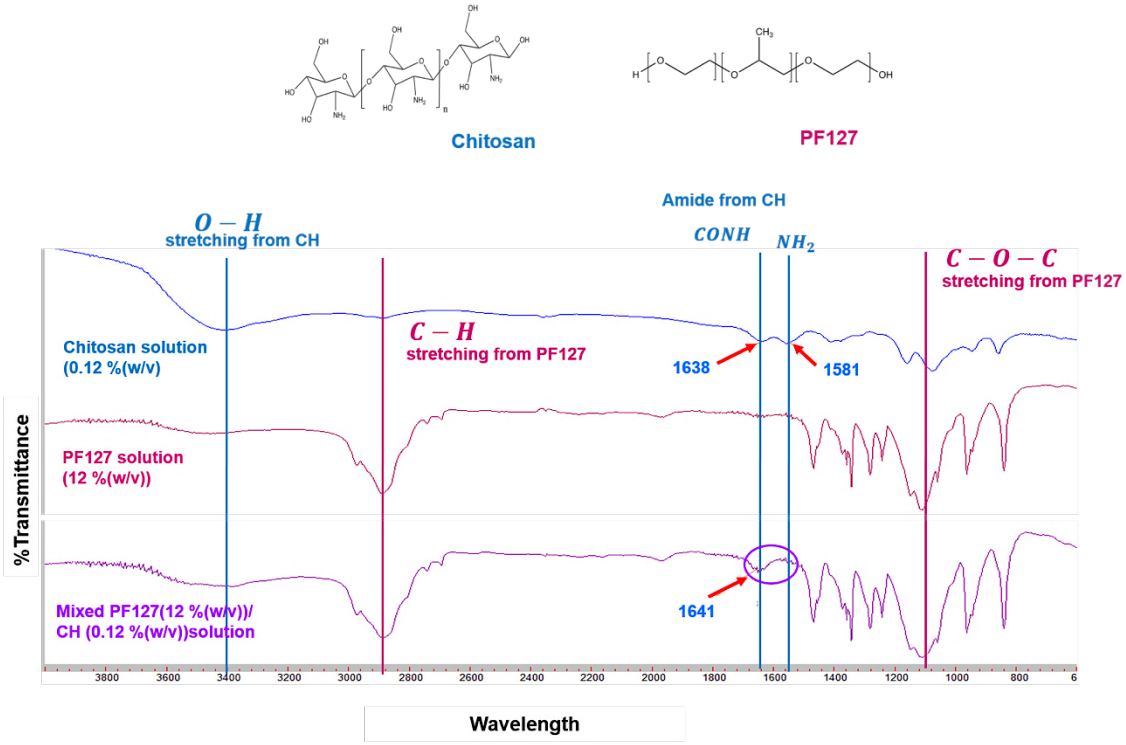

Figure 6.2: FTIR spectra analysis of freeze-dried samples of CH and PF127 solution, including mixed PF127/CH micelles (BK11-8, Table 6.2) in PBS solution.

Figure 6.2 displayed that low molecular weight CH has characteristic absorption peaks of O-H at 3460 cm^{-1}, a stretch vibration of amide I at 1638 cm^{-1} and bending of N-H at 1581 cm^{-1}. PF127 has an absorption peak caused by characteristic saturated CH_2 stretching vibration at 2880 – 3000 cm^{-1} and C-O-C stretching vibration at 1110-1300 cm^{-1}. In both PF127 and mixed PF127/CH micelles, characteristic absorption peaks at 2888 cm^{-1} and 1109 cm^{-1} were assigned to C-H stretching and C-O-C stretching from PF127, respectively (Figure 6.2). Besides, for mixed PF127/CH systems, the peak at 3437 cm^{-1} belonged to O-H stretching from chitosan. Also, the peak at 1641 cm^{-1} was attributed to the CONH from CH. In addition, there was a chemical shift of the amide peak from CH at 1638 cm^{-1} to a higher wave number at 1641 cm^{-1} of the PF127/CH solution sample, whereas the NH bending peak at 1581 cm^{-1} disappeared, which suggests surface modification by interaction between the NH group of CH and OH functional group on the PF127 (Figure 6.2).[260,375]

A similar result was also found in the study of Zhang *et al.* where the FTIR results revealed the presence of the amide I peak of CH (1637 cm^{-1}) from the PF127/CH nanocapsules, whilst the amide II peak (1560 cm^{-1}) of CH from the nanocapsules was diminished.[46] This disappearance in amide II peak might be due to the interaction between the primary amine groups (-CH_2) of CH and PEO unit of PF127.[376,377] In another research study, Lin *et al.* demonstrated characteristic absorption peak of only amide I from CH at 1657 cm^{-1} presented in the metipranolol loaded PF127/CH nanomicelles, indicating nanomicelles were prepared successfully.[260]

Taken altogether, a possible interpretation of this finding is that PF127 and PF127/CH micelles were prepared successfully.[260,375] Further information about the FTIR spectra of the micelles was provided in appendices Figure Table S2.

6.3.2 Preparation of fenofibrate-loaded Pluronic F127/chitosan micelles

This study was conducted to investigate the encapsulation of FEB drug within the prepared PF127/CH micelles to evaluate drug loading and encapsulation efficiency of the formulations. The preparation method of direct dissolution was applied to produce cationic micelles encapsulating FEB based on CH and PF127 (Table 6.3).

Table 6.3: The particle size (percentage by intensity), PDI, ZP, EE and DL of FEB-encapsulated PF127/CH micelles and PF127 micelles using direct dissolution method micelles. Data are represented as the mean ± SD (n=3).

Code	% (W/W)		% DL	% EE	DLS		
	PF127	CH			D_h (nm, Int %)	PDI	ZP (mV)
BK75-1	14	-	0.19 ± 0.03	8 ± 2	52 ± 6 (68%) 4 ± 1 (32%)	0.7 ± 0.1	-0.5 ± 0.3
BK75-4		0.015	0.15 ± 0.04	6 ± 2	35 ± 28 (43%) 602 ± 14 (40%) 4 ± 1 (17%)	0.8 ± 0.2	+3 ± 2
BK75-7		0.03	0.20 ± 0.12	9 ± 8	575 ± 131 (65%) 23 ± 2 (25%) 3 ± 1 (10%)	0.7 ± 0.3	+5 ± 4
		0.06	0.29 ± 0.10	13 ± 3	17 ± 7 (58%) 169 ± 40 (42%) 1 ± 1 (7%)	0.6 ± 0.4	+12 ± 2
BK75-13		0.12	0.31 ± 0.10	13 ± 4	661 ± 423 (83%) 2 ± 1 (12%)	0.6 ± 0.4	+14 ± 0.6

According to the DLS results, PF127 micelles presented an average hydrodynamic diameter of around 52 nm (Int%=60%), and when CH was incorporated, the polydisperse nanoparticles with two size ranges (17-52 nm and 169-661 nm) and positive ZP values were obtained from the FEB-loaded PF127/CH micelle systems (Table 6.3). Moreover, as the concentration of CH increased in PF127/CH micelles, the ZP value tended to increase, which indicated that there was a significant (p<0.05, independent samples t-test) influence of CH on the PF127 micelles since the charge of the particle switched to a positive charge compared to only FEB-loaded PF127 micelles (BK75-1, Table 6.3). Besides, the %EE of the prepared FEB-loaded PF127/CH micelles ranged between 6% and 13%. However, there was an insignificant (p>0.05, independent samples t-test) change in the %EE and %DL of the FEB encapsulated PF127/CH micelles when increasing the CH concentration to 0.12 %(w/v) in comparison to the FEB-loaded PF127 micelles and FEB-loaded PF127/CH micelles at 0.015 %(w/v) CH (BK75-1 and BK75-4, Table 6.3).

A slight increase in the %EE of the FEB drug when increasing CH concentration could be due to changes in the particle sizes, which can influence the available space within the micelles for drug encapsulations. In other words, large micelles resulting from increased CH concentration (e.g. 0.12%) may have higher internal volume, potentially allowing for more drug molecules to be encapsulated. Conversely, smaller micelles obtained from lower CH concentration (e.g. 0.015%) may have limited space for FEB drug to be accommodated, resulting in lower drug loading capacity. A similar observation has been found by a previous study of Pepic *et al.*[146] They prepared a micelles systems made of PF127 and CH (0.005, 0.01 and 0.015 %(w/v)) with dexamethasone (DEX) loading. Their studies revealed that PF127/CH micelles had hydrodynamic diameters and ZP values ranging between 25.4 and 28.9 nm and +9.3 and +17.6 mV, respectively. In addition, no significant CH influence on DEX loading was observed, with the DEX loading varied in the range between 0.5% and 0.52%.

In summary, this illustrated the successful preparation of PF127/CH micelles with a positive charge which demonstrated their potential as promising nanocarriers for efficient OcDD, benefiting from enhanced drug encapsulation.

6.4 Conclusion

Micelle systems composed of the PF127 with cationic polyelectrolyte chitosan (CH) were successfully prepared by the direct dissolution method. The investigations of mixtures of PF127 and CH revealed that the addition of CH slightly increased both CAC and CMC values in DI water and PBS solutions compared to the PF127 micelle system, possibly due to electrostatic interaction between CH and PF127. In addition, the mixed PF127/CH micelles were characterized by their hydrodynamic diameter ranging between 38 and 79 nm with PDIs ranging from 0.3 to 0.6 in DI water and PBS solutions. Moreover, no significant influence of CH on the particle size was observed. The physicochemical characterization of PF127/CH solutions was investigated by FTIR, supporting the interaction between the amino (-NH) functional group of CH and the hydroxyl (-OH) functional group of the PEO unit from PF127 on the positively charged PF127/CH nanomicelles. In addition, the successful preparation of PF127/CH micelles could encapsulate the FEB drug with an insignificant increase in the FEB DL and EE when the CH concentration increased from 0.015 to 0.12 %(w/v). As such, the system provides potential evidence that PF127 with CH combination can form the positively charged nanomicelles at specific concentrations and temperature ranges.

6.5 Future work

6.5.1 Concluding remarks

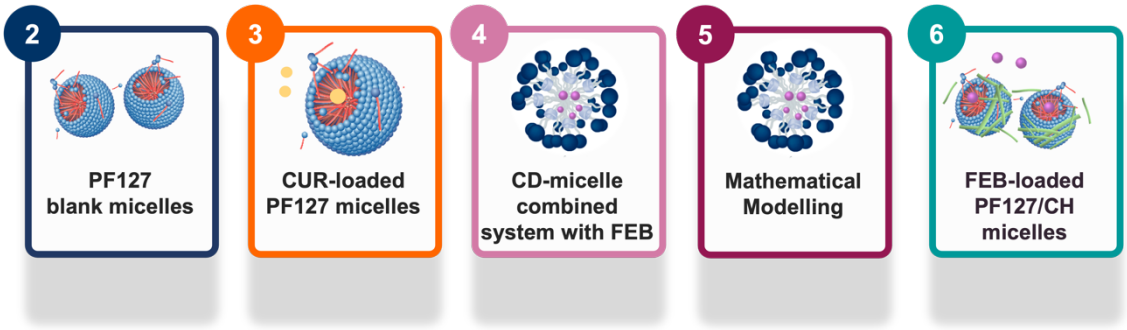

The objective of this study was to develop polymeric micelles capable of facilitating the controlled release of small therapeutic drugs, curcumin (CUR) and fenofibrate (FEB) from the micellar formulation, for the treatment of eye disease via topical administration in the form of eye drop suspension.

An initial investigation assessed the process of forming and preparing micellar solutions of polyoxyethylated nonionic surfactant Pluronic F127 (PF127) to create nanocarriers for drug loading. Micelle systems using PF127 were prepared and characterized by their hydrodynamic diameter, polydispersity index (PDIs), and particle sizes. The results showed good stability of the PF127 micelles during freeze-drying and sonication processes, improving their shelf life in pharmaceutical applications. Thus, these PF127 micelles may be effective nanocarriers for targeted ocular drug delivery (OcDD).

Subsequently, nanomicelles based on PF127 copolymers were developed to increase the solubility of CUR. PF127 micelles encapsulating CUR were produced using three different techniques:direct dissolution, co-solvent evaporation, and thin-film hydration. An optimal condition showed that PF127 triblock copolymer readily formed and self-assembled into small micelles (~20 nm). Furthermore, the encapsulation of CUR in PF127 micelles was highly dependent on the drug-to-polymer ratio. Also, cell viability following the acid phosphatase colorimetric (APA) assay revealed that the CUR-loaded micelles were safe at CUR concentrations ranging from 1 to 75 μg/mL and could slow drug release for 7 days. Regarding the forced degradation study, it revealed a significant decrease in CUR content after 24 hours, but no peak corresponded to the degradation product (vanillin or vanillic acid). The study also conducted an *ex vivo* permeation study across corneal and scleral tissues, finding that the CUR micelles could accumulate in both tissues. However, there was no drug permeation from the CUR micelles across both tissues.

Due to the degradation of CUR, the study further investigated the synergistic system, including PF127 and/or Soluplus® micelles and cyclodextrins (CDs), for delivering the FEB, another hydrophobic drug in this study. The study found that Soluplus® and PF127 copolymers, along with CDs like γ-CD, α-CD, and 2-HPβCD, could encapsulate FEB. Moreover, the solubility of FEB increased when increasing CD concentrations, with 2-

HPβCD showing the greatest solubility enhancement for the FEB drug—this improved drug bioavailability when forming poly(pseudo)rotaxanes (PPRs). Multiple analytical analyzes confirmed the successful formation of FEB-loaded PPRs, including dynamic light scattering (DLS), proton nuclear magnetic resonance (^{1}H-NMR) and X-ray powder diffraction (XRD). In addition, both FEB micelles (~5 nm) and PPRs (~65 nm) showed no cell toxicity and increased cell viability up to FEB concentrations of 50 and 20 μg/mL, respectively. Also, FEB-loaded PPRs could enhance drug permeation across the sclera tissue compared to the FEB-loaded micelles or mixed micelles.

Besides, in relation to the *ex vivo* permeation study of FEB-loaded micelles and PPRs, a mathematical model was utilized to validate the concept that single and mixed micelles help to merge the formulations onto ocular tissues, while CDs facilitated the transport of the FEB drug through the scleral tissue into the receiving chamber of the PPRs formulations. The drug transport mathematical model was constructed by applying Fick's law, which incorporates the apparent permeability coefficient and the retention concentration, to provide a more comprehensive explanation.

Additionally, a last investigation was conducted to assess the PF127 micelles and chitosan (CH) systems to create positively charged micelles with FEB drug loading. Micellar systems comprising PF127 and CH were made using the direct dissolution method. The FTIR analysis confirmed the effective formation of nanomicelles with a CH coating on the outer surface of the PF127 micelles. Moreover, the positively charged PF127/CH micelles exhibited hydrodynamic diameters ranging from 38 to 79 nm and polydispersity index (PDI) ranging from 0.3 to 0.6 with low encapsulation efficiency (EE) of around 8-13%.

In summary, as highlighted in this Thesis, three nanocarriers, PF127 micelles, micelle-CD combination systems, and PF127/CH micelles, have the potential to deliver hydrophobic drugs to the eye as nanocarriers.

6.5.2 Suggestion for future research

While this study has provided valuable insights into the use of micelles as a promising drug delivery system for ocular applications, several approaches for future research could

further advance the field, such as the preparation of drug-loaded PF127/CH micelles, as previously described earlier in Chapter 6.

The results of this study suggest that while the nanoformulations exhibited promising characteristics in terms of drug delivery efficiency, further investigation into their long-term stability under various storage conditions is warranted to ensure their potential for clinical applications. Another potential direction for future work is to investigate the safety and drug permeation of the micelles in the ocular environment through an *in vivo* experimental study. Understanding how micelles deliver drugs and interact with ocular tissues in the deeper layers over extended periods of time and assessing any potential toxicity issues are essential for the clinical translation of this technology.

Moreover, future studies could focus on optimizing the formulation of micelles to improve their drug loading capacity, release kinetics and stability. Other characterization of the properties of micelles to obtain the monodisperse particle sizes with a high drug encapsulation efficiency could lead to improved drug delivery performance and bioavailability in the eye. Additionally, investigating the potential of combining micelles with other drug delivery systems, such as nanoparticles, could open up new possibilities for treating a wide range of ocular diseases more effectively.

In addition, in the future, it would be valuable to investigate the preparation of drug-loaded micelles further using polymer-drug conjugate techniques for OcDD by exploring alternative conjugation strategies to enhance the stability of the micelles. This could improve the efficacy of delivering drugs to specific ocular tissues in specific environments. For example, the synthesis of polyethylene glycol (PEG)-*b*-poly (lactic acid) (PLA) copolymer conjugated with a model drug through an ester linkage. In this preparation, the hydrophobic drug is chemically conjugated to the hydrophobic PLA block of the copolymer via an ester bond. The amphiphilic nature of the resulting conjugate allows for self-assembly into micelles in aqueous solutions. Thus, these polymer-drug conjugated micelles can be designed to be stable in the tear fluid and cornea environment but undergo controlled drug release in response to specific stimuli present in the target sites, such as pH changes. This could allow the micelles to release the drug

at particular conditions, offering a more efficient controlled drug delivery system for ocular applications.

In term of mathematical model development, the further study to determine the validation of the model is required as it is crucial to ensure that the model's prediction results match the observed data with a high degree of accuracy in the statistical analysis test (e.g., mean squared error (MSE) or root mean squared error (RMSE)). It might also need to include the mathematical software program (e.g. MATHLAB) to help validating of this model.

In conclusion, the potential of micelles for OcDD is vast, and continued research in this area holds great promise for improving the treatment of various eye conditions. By addressing the areas as mentioned above of future work, we can further advance the field into clinical practice for the benefit of patients worldwide.

References

(1) Bourne, R. R. A.; Flaxman, S. R.; Braithwaite, T.; Cicinelli, M. V; Das, A.; Jonas, J. B.; Keeffe, J.; Kempen, J. H.; Leasher, J.; Limburg, H. Magnitude, Temporal Trends, and Projections of the Global Prevalence of Blindness and Distance and near Vision Impairment: A Systematic Review and Meta-Analysis. *Lancet Glob. Heal.* **2017**, *5* (9), e888–e897.

(2) Hajek, A.; Brettschneider, C.; Lühmann, D.; Eisele, M.; Mamone, S.; Wiese, B.; Weyerer, S.; Werle, J.; Pentzek, M.; Fuchs, A.; et al. Effect of Visual Impairment on Physical and Cognitive Function in Old Age: Findings of a Population-Based Prospective Cohort Study in Germany. *J. Am. Geriatr. Soc.* **2016**, *64* (11), 2311–2316. https://doi.org/10.1111/jgs.14458.

(3) Vaneev, A.; Tikhomirova, V.; Chesnokova, N.; Popova, E.; Beznos, O.; Kost, O.; Klyachko, N. Nanotechnology for Topical Drug Delivery to the Anterior Segment of the Eye. *International Journal of Molecular Sciences*. 2021. https://doi.org/10.3390/ijms222212368.

(4) Chen, H. Recent Developments in Ocular Drug Delivery. *J. Drug Target.* **2015**. https://doi.org/10.3109/1061186X.2015.1052073.

(5) Lens, A.; Nemeth, S. C.; Ledford, J. K. *Ocular Anatomy and Physiology*; Slack Incorporated, 2008.

(6) Gangaputra, S.; Chaigne-Delalande, B.; Gery, I.; Sen, H. N. Ocular Disease. In *The Autoimmune Diseases*; Elsevier, 2020; pp 1035–1049.

(7) Kang-Mieler, J. J.; Dosmar, E.; Liu, W.; Mieler, W. F. Extended Ocular Drug Delivery Systems for the Anterior and Posterior Segments: Biomaterial Options and Applications. *Expert Opinion on Drug Delivery*. 2017. https://doi.org/10.1080/17425247.2016.1227785.

(8) Shatz, W.; Aaronson, J.; Yohe, S.; Kelley, R. F.; Kalia, Y. N. Strategies for Modifying Drug Residence Time and Ocular Bioavailability to Decrease Treatment Frequency for Back of the Eye Diseases. *Expert Opin. Drug Deliv.* **2019**, *16* (1), 43–57. https://doi.org/10.1080/17425247.2019.1553953.

(9) Venkatraman, S.; Natarajan, J. V; Boey, Y. C. F.; Mehta, J. S.; Howden, T. T. L.;

NG, X. W.; NG, A. H. C. Nanoliposomes for Sustained Delivery of Tacrolimus for Treatment of Anterior Segment Eye Diseases. Google Patents April 25, 2019.

(10) Clayton, J. A. Dry Eye. *N. Engl. J. Med.* **2018**, *378* (23), 2212–2223. https://doi.org/10.1056/NEJMra1407936.

(11) Cursiefen, C. Dry Eye. *Ophthalmologe*. 2013, pp 498–499. https://doi.org/10.1007/s00347-013-2884-0.

(12) What Is Dry Eye? Symptoms, Treatment, Causes of Dry Eyes | Everyday Health.

(13) Messmer, E. M. The Pathophysiology, Diagnosis, and Treatment of Dry Eye Disease. *Dtsch. Arztebl. Int.* **2015**, *112* (5), 71.

(14) Lievens, C.; Berdy, G.; Douglass, D.; Montaquila, S.; Lin, H.; Simmons, P.; Carlisle-Wilcox, C.; Vehige, J.; Haque, S. Evaluation of an Enhanced Viscosity Artificial Tear for Moderate to Severe Dry Eye Disease: A Multicenter, Double-Masked, Randomized 30-Day Study. *Contact Lens Anterior Eye* **2019**, *42* (4), 443–449. https://doi.org/https://doi.org/10.1016/j.clae.2018.12.003.

(15) Zetterberg, M. Age-Related Eye Disease and Gender. *Maturitas* **2016**, *83*, 19–26.

(16) Nesterova, A. P.; Klimov, E. A.; Zharkova, M.; Sozin, S.; Sobolev, V.; Ivanikova, N. V; Shkrob, M.; Yuryev, A. Chapter 6 - Diseases of the Eye; Nesterova, A. P., Klimov, E. A., Zharkova, M., Sozin, S., Sobolev, V., Ivanikova, N. V, Shkrob, M., Yuryev, A. B. T.-D. P., Eds.; Elsevier, 2020; pp 259–296. https://doi.org/https://doi.org/10.1016/B978-0-12-817086-1.00006-3.

(17) Clinic, M. Cataracts - Symptoms and Causes - Mayo Clinic. *Mayo Clinic Website*. 2018.

(18) Tan, G. S.; Cheung, N.; Simó, R.; Cheung, G. C. M.; Wong, T. Y. Diabetic Macular Oedema. *Lancet Diabetes Endocrinol.* **2017**, *5* (2), 143–155.

(19) Duh, E. J.; Sun, J. K.; Stitt, A. W. Diabetic Retinopathy: Current Understanding, Mechanisms, and Treatment Strategies. *JCI insight* **2017**, *2* (14).

(20) Cho, N. H.; Shaw, J. E.; Karuranga, S.; Huang, Y.; da Rocha Fernandes, J. D.; Ohlrogge, A. W.; Malanda, B. IDF Diabetes Atlas: Global Estimates of Diabetes Prevalence for 2017 and Projections for 2045. *Diabetes Res. Clin. Pract.* **2018**, *138*, 271–281. https://doi.org/https://doi.org/10.1016/j.diabres.2018.02.023.

(21) Flaxman, S. R.; Bourne, R. R. A.; Resnikoff, S.; Ackland, P.; Braithwaite, T.; Cicinelli, M. V; Das, A.; Jonas, J. B.; Keeffe, J.; Kempen, J. H. Global Causes of Blindness and Distance Vision Impairment 1990–2020: A Systematic Review and Meta-Analysis. *Lancet Glob. Heal.* **2017**, *5* (12), e1221–e1234.

(22) Zheng, Y.; He, M.; Congdon, N. The Worldwide Epidemic of Diabetic Retinopathy. *Indian J. Ophthalmol.* **2012**, *60* (5), 428–431. https://doi.org/10.4103/0301-4738.100542.

(23) The 4 Stages of Diabetic Retinopathy: What You Can Expect | Griswold.

(24) Diabetic Retinopathy: An Eye Disease with 4 Stages - Topcon Healthcare Solutions.

(25) Zhang, K.; Zhang, L.; Weinreb, R. N. Ophthalmic Drug Discovery: Novel Targets and Mechanisms for Retinal Diseases and Glaucoma. *Nat. Rev. Drug Discov.* **2012**, *11* (7), 541–559. https://doi.org/10.1038/nrd3745.

(26) Marmor, D. J.; Marmor, M. F. Simulating Vision With and Without Macular Disease. *Arch. Ophthalmol.* **2010**, *128* (1), 117–125. https://doi.org/10.1001/archophthalmol.2009.366.

(27) What Is Age-Related Macular Degeneration?

(28) Arnold, J. Age Related Macular Degeneration. *Clinical evidence*. 2006, pp 877–888.

(29) de Jong, E. K.; Geerlings, M. J.; den Hollander, A. I. Chapter 10 - Age-Related Macular Degeneration. In *Genetics and Genomics of Eye Disease*; Gao, X. R., Ed.; Academic Press, 2020; pp 155–180. https://doi.org/https://doi.org/10.1016/B978-0-12-816222-4.00010-1.

(30) Lim, L. S.; Mitchell, P.; Seddon, J. M.; Holz, F. G.; Wong, T. Y. Age-Related Macular Degeneration. *Lancet* **2012**, *379* (9827), 1728–1738.

(31) Berdeaux, G. H.; Nordmann, J.-P.; Colin, E.; Arnould, B. Vision-Related Quality of Life in Patients Suffering from Age-Related Macular Degeneration. *Am. J. Ophthalmol.* **2005**, *139* (2), 271–279.

(32) Avery, R. L.; Pieramici, D. J.; Rabena, M. D.; Castellarin, A. A.; Nasir, M. A.; Giust, M. J. Intravitreal Bevacizumab (Avastin) for Neovascular Age-Related

Macular Degeneration. *Ophthalmology* **2006**, *113* (3), 363-372.e5. https://doi.org/https://doi.org/10.1016/j.ophtha.2005.11.019.

(33) Jyothi, S.; Chowdhury, H.; Elagouz, M.; Sivaprasad, S. Intravitreal Bevacizumab (Avastin) for Age-Related Macular Degeneration: A Critical Analysis of Literature. *Eye* **2010**, *24* (5), 816–824.

(34) Rosenfeld, P. J.; Brown, D. M.; Heier, J. S.; Boyer, D. S.; Kaiser, P. K.; Chung, C. Y.; Kim, R. Y. Ranibizumab for Neovascular Age-Related Macular Degeneration. *N. Engl. J. Med.* **2006**, *355* (14), 1419–1431.

(35) Blick, S. K. A.; Keating, G. M.; Wagstaff, A. J. Ranibizumab. *Drugs* **2007**, *67* (8), 1199–1206.

(36) Heier, J. S.; Brown, D. M.; Chong, V.; Korobelnik, J.-F.; Kaiser, P. K.; Nguyen, Q. D.; Kirchhof, B.; Ho, A.; Ogura, Y.; Yancopoulos, G. D.; et al. Intravitreal Aflibercept (VEGF Trap-Eye) in Wet Age-Related Macular Degeneration. *Ophthalmology* **2012**, *119* (12), 2537–2548. https://doi.org/https://doi.org/10.1016/j.ophtha.2012.09.006.

(37) Trichonas, G.; Kaiser, P. K. Aflibercept for the Treatment of Age-Related Macular Degeneration. *Ophthalmol. Ther.* **2013**, *2* (2), 89–98.

(38) Dugel, P. U.; Koh, A.; Ogura, Y.; Jaffe, G. J.; Schmidt-Erfurth, U.; Brown, D. M.; Gomes, A. V; Warburton, J.; Weichselberger, A.; Holz, F. G. HAWK and HARRIER: Phase 3, Multicenter, Randomized, Double-Masked Trials of Brolucizumab for Neovascular Age-Related Macular Degeneration. *Ophthalmology* **2020**, *127* (1), 72–84.

(39) Sharma, A.; Kumar, N.; Parachuri, N.; Sharma, R.; Bandello, F.; Kuppermann, B. D.; Loewenstein, A. Brolucizumab and Immunogenicity. *Eye* **2020**, *34* (10), 1726–1728.

(40) Gaudreault, J.; Gunde, T.; Floyd, H. S.; Ellis, J.; Tietz, J.; Binggeli, D.; Keller, B.; Schmidt, A.; Escher, D. Preclinical Pharmacology and Safety of ESBA1008, a Single-Chain Antibody Fragment, Investigated as Potential Treatment for Age Related Macular Degeneration. *Invest. Ophthalmol. Vis. Sci.* **2012**, *53* (14), 3025.

(41) Nimz, E. L.; Van't Land, C. W.; Yáñez, J. A.; Chastain, J. E. Intraocular and

Systemic Pharmacokinetics of Brolucizumab (RTH258) in Nonhuman Primates. *Invest. Ophthalmol. Vis. Sci.* **2016**, *57* (12), 4996.

(42) Ren, X.; Bu, S.; Zhang, X.; Jiang, Y.; Tan, L.; Zhang, H.; Li, X. Safety and Efficacy of Intravitreal Conbercept Injection after Vitrectomy for the Treatment of Proliferative Diabetic Retinopathy. *Eye* **2019**, *33* (7), 1177–1183.

(43) Li, X.; Xu, G.; Wang, Y.; Xu, X.; Liu, X.; Tang, S.; Zhang, F.; Zhang, J.; Tang, L.; Wu, Q. Safety and Efficacy of Conbercept in Neovascular Age-Related Macular Degeneration: Results from a 12-Month Randomized Phase 2 Study: AURORA Study. *Ophthalmology* **2014**, *121* (9), 1740–1747.

(44) Cui, J.; Sun, D.; Lu, H.; Dai, R.; Xing, L.; Dong, H.; Wang, L.; Wei, D.; Jiang, B.; Jiao, Y. Comparison of Effectiveness and Safety between Conbercept and Ranibizumab for Treatment of Neovascular Age-Related Macular Degeneration. A Retrospective Case-Controlled Non-Inferiority Multiple Center Study. *Eye* **2018**, *32* (2), 391–399.

(45) Panahi, Y.; Hosseini, M. S.; Khalili, N.; Naimi, E.; Majeed, M.; Sahebkar, A. Antioxidant and Anti-Inflammatory Effects of Curcuminoid-Piperine Combination in Subjects with Metabolic Syndrome: A Randomized Controlled Trial and an Updated Meta-Analysis. *Clin. Nutr.* **2015**, *34* (6), 1101–1108. https://doi.org/https://doi.org/10.1016/j.clnu.2014.12.019.

(46) Fazel Nabavi, S.; Thiagarajan, R.; Rastrelli, L.; Daglia, M.; Sobarzo-Sanchez, E.; Alinezhad, H.; Mohammad Nabavi, S. Curcumin: A Natural Product for Diabetes and Its Complications. *Curr. Top. Med. Chem.* **2015**, *15* (23), 2445–2455.

(47) Mrudula, T.; Suryanarayana, P.; Srinivas, P. N. B. S.; Reddy, G. B. Effect of Curcumin on Hyperglycemia-Induced Vascular Endothelial Growth Factor Expression in Streptozotocin-Induced Diabetic Rat Retina. *Biochem. Biophys. Res. Commun.* **2007**, *361* (2), 528–532. https://doi.org/https://doi.org/10.1016/j.bbrc.2007.07.059.

(48) Keating, G. M.; Croom, K. F. Fenofibrate. *Drugs* **2007**, *67* (1), 121–153.

(49) Qiu, F.; Matlock, G.; Chen, Q.; Zhou, K.; Du, Y.; Wang, X.; Ma, J.-X. Therapeutic Effects of PPARα Agonist on Ocular Neovascularization in Models Recapitulating

Neovascular Age-Related Macular Degeneration. *Invest. Ophthalmol. Vis. Sci.* **2017**, *58* (12), 5065–5075.

(50) Chen, X. R.; Besson, V. C.; Palmier, B.; Garcia, Y.; Plotkine, M.; Marchand-Leroux, C. Neurological Recovery-Promoting, Anti-Inflammatory, and Anti-Oxidative Effects Afforded by Fenofibrate, a PPAR Alpha Agonist, in Traumatic Brain Injury. *J. Neurotrauma* **2007**, *24* (7), 1119–1131. https://doi.org/10.1089/neu.2006.0216.

(51) Dugel, P. U.; Jaffe, G. J.; Sallstig, P.; Warburton, J.; Weichselberger, A.; Wieland, M.; Singerman, L. Brolucizumab versus Aflibercept in Participants with Neovascular Age-Related Macular Degeneration: A Randomized Trial. *Ophthalmology* **2017**, *124* (9), 1296–1304.

(52) Tietz, J.; Spohn, G.; Schmid, G.; Konrad, J.; Jampen, S.; Maurer, P.; Schmidt, A.; Escher, D. Affinity and Potency of RTH258 (ESBA1008), a Novel Inhibitor of Vascular Endothelial Growth Factor a for the Treatment of Retinal Disorders. *Invest. Ophthalmol. Vis. Sci.* **2015**, *56* (7), 1501.

(53) Lu, X.; Sun, X. Profile of Conbercept in the Treatment of Neovascular Age-Related Macular Degeneration. *Drug Des. Devel. Ther.* **2015**, *9*, 2311.

(54) Li, H.; Lei, N.; Zhang, M.; Li, Y.; Xiao, H.; Hao, X. Pharmacokinetics of a Long-Lasting Anti-VEGF Fusion Protein in Rabbit. *Exp. Eye Res.* **2012**, *97* (1), 154–159.

(55) Sinapis, C. I.; Routsias, J. G.; Sinapis, A. I.; Sinapis, D. I.; Agrogiannis, G. D.; Pantopoulou, A.; Theocharis, S. E.; Baltatzis, S.; Patsouris, E.; Perrea, D. Pharmacokinetics of Intravitreal Bevacizumab (Avastin®) in Rabbits. *Clin. Ophthalmol. (Auckland, NZ)* **2011**, *5*, 697.

(56) Gao, L.; Tao, Y.; Liu, M.; Li, L.; Zhang, P.; Wang, H.; Zhang, L. Different Conbercept Injection Strategies for the Treatment of Exudative Age-Related Macular Degeneration: A Retrospective Cohort Study. *Medicine (Baltimore).* **2020**, *99* (7).

(57) Bai, Y.; Nie, H.; Wei, S.; Lu, X.; Ke, X.; Ouyang, X.; Feng, S. Efficacy of Intravitreal Conbercept Injection in the Treatment of Retinopathy of Prematurity.

Br. J. Ophthalmol. **2019**, *103* (4), 494–498.

(58) Kim, D.; Maharjan, P.; Jin, M.; Park, T.; Maharjan, A. Potential Albumin-Based Antioxidant Nanoformulations for Ocular Protection against Oxidative Stress.

(59) Degeneration, A. M.; Qiu, F.; Matlock, G.; Chen, Q.; Zhou, K.; Du, Y.; Wang, X.; Ma, J. Therapeutic Effects of PPAR a Agonist on Ocular Neovascularization in Models Recapitulating Neovascular. **2017**. https://doi.org/10.1167/iovs.17-22091.

(60) Holz, F. G.; Schmitz-Valckenberg, S.; Fleckenstein, M. Recent Developments in the Treatment of Age-Related Macular Degeneration. *J. Clin. Invest.* **2014**, *124* (4), 1430–1438. https://doi.org/10.1172/JCI71029.

(61) Bachu, R. D.; Chowdhury, P.; Al-Saedi, Z. H. F.; Karla, P. K.; Boddu, S. H. S. Ocular Drug Delivery Barriers—Role of Nanocarriers in the Treatment of Anterior Segment Ocular Diseases. *Pharmaceutics*. 2018. https://doi.org/10.3390/pharmaceutics10010028.

(62) Nayak, K.; Misra, M. A Review on Recent Drug Delivery Systems for Posterior Segment of Eye. *Biomed. Pharmacother.* **2018**, *107*, 1564–1582. https://doi.org/https://doi.org/10.1016/j.biopha.2018.08.138.

(63) Patel, A. Ocular Drug Delivery Systems: An Overview. *World J. Pharmacol.* **2013**. https://doi.org/10.5497/wjp.v2.i2.47.

(64) Rodrigues, G. A.; Lutz, D.; Shen, J.; Yuan, X.; Shen, H.; Cunningham, J.; Rivers, H. M. Topical Drug Delivery to the Posterior Segment of the Eye: Addressing the Challenge of Preclinical to Clinical Translation. *Pharm. Res.* **2018**, *35* (12), 245. https://doi.org/10.1007/s11095-018-2519-x.

(65) Yadav, D.; Varma, L. T.; Yadav, K. Drug Delivery to Posterior Segment of the Eye: Conventional Delivery Strategies, Their Barriers, and Restrictions. In *Drug Delivery for the Retina and Posterior Segment Disease*; Springer, 2018; pp 51–67.

(66) Maurice, D. M.; Mishima, S. Ocular Pharmacokinetics. In *Pharmacology of the Eye*; Springer, 1984; pp 19–116.

(67) Nettey, H.; Darko, Y.; Bamiro, O. A.; Addo, R. T. Ocular Barriers. In *Ocular Drug Delivery: Advances, Challenges and Applications*; Addo, R. T., Ed.; Springer International Publishing: Cham, 2016; pp 27–36. https://doi.org/10.1007/978-3-

319-47691-9_3.

(68) Subrizi, A.; del Amo, E. M.; Korzhikov-Vlakh, V.; Tennikova, T.; Ruponen, M.; Urtti, A. Design Principles of Ocular Drug Delivery Systems: Importance of Drug Payload, Release Rate, and Material Properties. *Drug Discovery Today*. 2019. https://doi.org/10.1016/j.drudis.2019.02.001.

(69) Tsai, C. H.; Wang, P. Y.; Lin, I. C.; Huang, H.; Liu, G. S.; Tseng, C. L. Ocular Drug Delivery: Role of Degradable Polymeric Nanocarriers for Ophthalmic Application. *International Journal of Molecular Sciences*. 2018. https://doi.org/10.3390/ijms19092830.

(70) Sunkara, G.; Kompella, U. B. Membrane Transport Processes in the Eye. In *Ophthalmic drug delivery systems*; CRC Press, 2003; pp 34–79.

(71) Ripal, G.; Hari, K. A.; Ashwin, P.; Ashim, K. M. Ocular Drug Delivery. *AAPS J* **2010**, *12*, 348–360.

(72) Gaudana, R.; Ananthula, H. K.; Parenky, A.; Mitra, A. K. Ocular Drug Delivery. *The AAPS journal*. 2010. https://doi.org/10.1208/s12248-010-9183-3.

(73) Chrai, S. S.; Patton, T. F.; Mehta, A.; Robinson, J. R. Lacrimal and Instilled Fluid Dynamics in Rabbit Eyes. *J. Pharm. Sci.* **1973**, *62* (7), 1112–1121.

(74) Laursen, S. østergaard; Bjerrum, P. Timolol Eyedrop-induced Severe Bronchospasm. *Acta Med. Scand.* **1982**, *211* (6), 505–506.

(75) Yu, A.; Shi, H.; Liu, H.; Bao, Z.; Dai, M.; Lin, D.; Lin, D.; Xu, X.; Li, X.; Wang, Y. Mucoadhesive Dexamethasone-Glycol Chitosan Nanoparticles for Ophthalmic Drug Delivery. *Int. J. Pharm.* **2020**, *575*, 118943. https://doi.org/https://doi.org/10.1016/j.ijpharm.2019.118943.

(76) Ludwig, A. The Use of Mucoadhesive Polymers in Ocular Drug Delivery. *Advanced Drug Delivery Reviews*. 2005. https://doi.org/10.1016/j.addr.2005.07.005.

(77) Mansuri, S.; Kesharwani, P.; Jain, K.; Tekade, R. K.; Jain, N. K. Mucoadhesion: A Promising Approach in Drug Delivery System. *React. Funct. Polym.* **2016**, *100*, 151–172.

(78) Shastri, D.; Shelat, P.; Shukla, A.; Patel, P. Ophthalmic Drug Delivery System:

Challenges and Approaches. *Syst. Rev. Pharm.* **2010**. https://doi.org/10.4103/0975-8453.75042.

(79) Urtti, A.; Pipkin, J. D.; Rork, G.; Sendo, T.; Finne, U.; Repta, A. J. Controlled Drug Delivery Devices for Experimental Ocular Studies with Timolol 2. Ocular and Systemic Absorption in Rabbits. *Int. J. Pharm.* **1990**. https://doi.org/10.1016/0378-5173(90)90215-P.

(80) Cholkar, K.; Gilger, B. C.; Mitra, A. K. Topical, Aqueous, Clear Cyclosporine Formulation Design for Anterior and Posterior Ocular Delivery. *Transl. Vis. Sci. Technol.* **2015**, *4* (3), 1. https://doi.org/10.1167/tvst.4.3.1.

(81) Hayakawa, E.; Chien, D.-S.; Inagaki, K.; Yamamoto, A.; Wang, W.; Lee, V. H. L. Conjunctival Penetration of Insulin and Peptide Drugs in the Albino Rabbit. *Pharm. Res.* **1992**, *9* (6), 769–775. https://doi.org/10.1023/A:1015803605621.

(82) Ranta, V.-P.; Mannermaa, E.; Lummepuro, K.; Subrizi, A.; Laukkanen, A.; Antopolsky, M.; Murtomäki, L.; Hornof, M.; Urtti, A. Barrier Analysis of Periocular Drug Delivery to the Posterior Segment. *J. Control. Release* **2010**, *148* (1), 42–48. https://doi.org/https://doi.org/10.1016/j.jconrel.2010.08.028.

(83) TÖRNQUIST, P. Capillary Permeability in Cat Choroid, Studied with the Single Injection Technique (II). *Acta Physiol. Scand.* **1979**, *106* (4), 425–430. https://doi.org/10.1111/j.1748-1716.1979.tb06421.x.

(84) Misra, G. P.; Singh, R. S. J.; Aleman, T. S.; Jacobson, S. G.; Gardner, T. W.; Lowe, T. L. Subconjunctivally Implantable Hydrogels with Degradable and Thermoresponsive Properties for Sustained Release of Insulin to the Retina. *Biomaterials* **2009**, *30* (33), 6541–6547.

(85) Wong, C. W.; Czarny, B.; Metselaar, J. M.; Ho, C.; Ng, S. R.; Barathi, A. V.; Storm, G.; Wong, T. T. Evaluation of Subconjunctival Liposomal Steroids for the Treatment of Experimental Uveitis. *Sci. Rep.* **2018**, *8* (1), 6604.

(86) Myles, M. E.; Neumann, D. M.; Hill, J. M. Recent Progress in Ocular Drug Delivery for Posterior Segment Disease: Emphasis on Transscleral Iontophoresis. *Adv. Drug Deliv. Rev.* **2005**, *57* (14), 2063–2079. https://doi.org/https://doi.org/10.1016/j.addr.2005.08.006.

(87) Atchison, E. A.; Omar, A. F.; Iezzi, R.; Barkmeier, A. J.; Bakri, S. J. OUTCOMES OF AN INTRAVITREAL INJECTION CLINIC. *RETINA* **2017**, *37* (7).

(88) Seah, I.; Zhao, X.; Lin, Q.; Liu, Z.; Su, S. Z. Z.; Yuen, Y. Sen; Hunziker, W.; Lingam, G.; Loh, X. J.; Su, X. Use of Biomaterials for Sustained Delivery of Anti-VEGF to Treat Retinal Diseases. *Eye (Basingstoke)*. 2020. https://doi.org/10.1038/s41433-020-0770-y.

(89) Le Goff, M. M.; Bishop, P. N. Adult Vitreous Structure and Postnatal Changes. *Eye* **2008**, *22* (10), 1214–1222. https://doi.org/10.1038/eye.2008.21.

(90) Thakur, S. S.; Barnett, N. L.; Donaldson, M. J.; Parekh, H. S. Intravitreal Drug Delivery in Retinal Disease: Are We out of Our Depth? *Expert Opin. Drug Deliv.* **2014**, *11* (10), 1575–1590. https://doi.org/10.1517/17425247.2014.927864.

(91) Mitra, A. K.; Anand, B. S.; Duvvuri, S. Drug Delivery to the Eye. *Adv. Organ Biol.* **2005**, *10*, 307–351.

(92) Marsh, D. A. Selection of Drug Delivery Approaches for the Back of the Eye: Opportunities and Unmet Needs. In *Drug product development for the back of the eye*; Springer, 2011; pp 1–20.

(93) Maroñas, O.; García-Quintanilla, L.; Luaces-Rodríguez, A.; Fernández-Ferreiro, A.; Latorre-Pellicer, A.; Abraldes, M. J.; Lamas, M. J.; Carracedo, A. Anti-VEGF Treatment and Response in Age-Related Macular Degeneration: Disease's Susceptibility, Pharmacogenetics and Pharmacokinetics. *Curr. Med. Chem.* **2020**, *27* (4), 549–569.

(94) Wang, R.; Gao, Y.; Liu, A.; Zhai, G. A Review of Nanocarrier-Mediated Drug Delivery Systems for Posterior Segment Eye Disease: Challenges Analysis and Recent Advances. *J. Drug Target.* **2021**, *29* (7), 687–702. https://doi.org/10.1080/1061186X.2021.1878366.

(95) Li, Q.; Qian, X.; Li, H. Y.; Lai, K. L.; Gao, Q.; Lee, W. Y. T. Safety Assessment of Polymeric Micelles as an Ophthalmic Drug Delivery System for Intravitreal Administration of Dasatinib. *Int. J. Pharm.* **2021**, *596*, 120226.

(96) Shen, J.; Gao, H.; Chen, L.; Jiang, Y.; Li, S.; Chao, Y.; Liu, N.; Wang, Y.; Wei, T.; Liu, Y. Eyedrop-Based Macromolecular Ophthalmic Drug Delivery for Ocular

Fundus Disease Treatment. *Sci. Adv.* **2023**, *9* (4), eabq3104.

(97) Naderan, M. Ocular Changes during Pregnancy. *J. Curr. Ophthalmol.* **2018**, *30* (3), 202–210.

(98) Ali, Y.; Lehmussaari, K. Industrial Perspective in Ocular Drug Delivery. *Adv. Drug Deliv. Rev.* **2006**, *58* (11), 1258–1268.

(99) Prosperi-Porta, G.; Kedzior, S.; Muirhead, B.; Sheardown, H. Phenylboronic-Acid-Based Polymeric Micelles for Mucoadhesive Anterior Segment Ocular Drug Delivery. *Biomacromolecules* **2016**, *17* (4), 1449–1457. https://doi.org/10.1021/acs.biomac.6b00054.

(100) Soliman, K. A.; Ullah, K.; Shah, A.; Jones, D. S.; Singh, T. R. R. Poloxamer-Based in Situ Gelling Thermoresponsive Systems for Ocular Drug Delivery Applications. *Drug Discov. Today* **2019**, *24* (8), 1575–1586. https://doi.org/https://doi.org/10.1016/j.drudis.2019.05.036.

(101) Jimenez, J.; Sakthivel, M.; Nischal, K. K.; Fedorchak, M. V. Drug Delivery Systems and Novel Formulations to Improve Treatment of Rare Corneal Disease. *Drug Discov. Today* **2019**, *24* (8), 1564–1574. https://doi.org/https://doi.org/10.1016/j.drudis.2019.03.005.

(102) Meng, T.; Kulkarni, V.; Simmers, R.; Brar, V.; Xu, Q. Therapeutic Implications of Nanomedicine for Ocular Drug Delivery. *Drug Discov. Today* **2019**, *24* (8), 1524–1538. https://doi.org/https://doi.org/10.1016/j.drudis.2019.05.006.

(103) Agban, Y.; Thakur, S. S.; Mugisho, O. O.; Rupenthal, I. D. Depot Formulations to Sustain Periocular Drug Delivery to the Posterior Eye Segment. *Drug Discovery Today*. 2019. https://doi.org/10.1016/j.drudis.2019.03.023.

(104) Nicolson, P. C.; Vogt, J. Soft Contact Lens Polymers: An Evolution. *Biomaterials* **2001**, *22* (24), 3273–3283.

(105) Shah, C.; Raj, C. V; Foulks, G. N. The Evolution in Therapeutic Contact Lenses. *Ophthalmol. Clin. North Am.* **2003**, *16* (1), 95–101.

(106) Alvarez-Lorenzo, C.; Hiratani, H.; Concheiro, A. Contact Lenses for Drug Delivery. *Am. J. Drug Deliv.* **2006**, *4* (3), 131–151.

(107) Ward, M. A.; Georgiou, T. K. Thermoresponsive Polymers for Biomedical

Applications. *Polymers (Basel).* **2011**, *3* (3), 1215–1242.

(108) Ciolino, J. B.; Hoare, T. R.; Iwata, N. G.; Behlau, I.; Dohlman, C. H.; Langer, R.; Kohane, D. S. A Drug-Eluting Contact Lens. *Invest. Ophthalmol. Vis. Sci.* **2009**, *50* (7), 3346–3352. https://doi.org/10.1167/iovs.08-2826.

(109) Vandervoort, J.; Ludwig, A. Ocular Drug Delivery: Nanomedicine Applications. *Nanomedicine* **2007**, *2* (1), 11–21. https://doi.org/10.2217/17435889.2.1.11.

(110) Zhang, Z.; He, Z.; Liang, R.; Ma, Y.; Huang, W.; Jiang, R.; Shi, S.; Chen, H.; Li, X. Fabrication of a Micellar Supramolecular Hydrogel for Ocular Drug Delivery. *Biomacromolecules* **2016**, *17* (3), 798–807.

(111) Kapoor, Y.; Chauhan, A. Ophthalmic Delivery of Cyclosporine A from Brij-97 Microemulsion and Surfactant-Laden p-HEMA Hydrogels. *Int. J. Pharm.* **2008**, *361* (1–2), 222–229.

(112) Ahmed, E. M. Hydrogel: Preparation, Characterization, and Applications: A Review. *J. Adv. Res.* **2015**, *6* (2), 105–121.

(113) Lim, H. L.; Hwang, Y.; Kar, M.; Varghese, S. Smart Hydrogels as Functional Biomimetic Systems. *Biomater. Sci.* **2014**, *2* (5), 603–618. https://doi.org/10.1039/C3BM60288E.

(114) Zhang, Z.; Yu, J.; Zhou, Y.; Zhang, R.; Song, Q.; Lei, L.; Li, X. Supramolecular Nanofibers of Dexamethasone Derivatives to Form Hydrogel for Topical Ocular Drug Delivery. *Colloids Surfaces B Biointerfaces* **2018**, *164*, 436–443. https://doi.org/https://doi.org/10.1016/j.colsurfb.2018.01.051.

(115) Mandal, A.; Bisht, R.; Rupenthal, I. D.; Mitra, A. K. Polymeric Micelles for Ocular Drug Delivery: From Structural Frameworks to Recent Preclinical Studies. *Journal of Controlled Release*. 2017. https://doi.org/10.1016/j.jconrel.2017.01.012.

(116) Owen, S. C.; Chan, D. P. Y.; Shoichet, M. S. Polymeric Micelle Stability. *Nano Today* **2012**, *7* (1), 53–65. https://doi.org/https://doi.org/10.1016/j.nantod.2012.01.002.

(117) Güngör, S.; Kahraman, E.; Ozsoy, Y. Polymeric Micelles for Cutaneous Drug Delivery; 2015; pp 369–387. https://doi.org/10.5599/obp.8.14.

(118) Lu, Y.; Yue, Z.; Xie, J.; Wang, W.; Zhu, H.; Zhang, E.; Cao, Z. Micelles with

Ultralow Critical Micelle Concentration as Carriers for Drug Delivery. *Nat. Biomed. Eng.* **2018**, *2* (5), 318–325.

(119) Cholkar, K.; Patel, A.; Mitra, A. D. V. and A. K. Novel Nanomicellar Formulation Approaches for Anterior and Posterior Segment Ocular Drug Delivery. *Recent Patents on Nanomedicine (Discontinued)*. 2012, pp 82–95. https://doi.org/http://dx.doi.org/10.2174/1877912311202020082.

(120) Mandal, A.; Bisht, R.; Rupenthal, I. D.; Mitra, A. K. Polymeric Micelles for Ocular Drug Delivery: From Structural Frameworks to Recent Preclinical Studies. *J. Control. Release* **2017**, *248*, 96–116.

(121) Di Tommaso, C.; Bourges, J.-L.; Valamanesh, F.; Trubitsyn, G.; Torriglia, A.; Jeanny, J.-C.; Behar-Cohen, F.; Gurny, R.; Möller, M. Novel Micelle Carriers for Cyclosporin A Topical Ocular Delivery: In Vivo Cornea Penetration, Ocular Distribution and Efficacy Studies. *Eur. J. Pharm. Biopharm.* **2012**, *81* (2), 257–264. https://doi.org/https://doi.org/10.1016/j.ejpb.2012.02.014.

(122) Xu, X.; Sun, L.; Zhou, L.; Cheng, Y.; Cao, F. Functional Chitosan Oligosaccharide Nanomicelles for Topical Ocular Drug Delivery of Dexamethasone. *Carbohydr. Polym.* **2020**, *227*, 115356. https://doi.org/https://doi.org/10.1016/j.carbpol.2019.115356.

(123) Gukasyan, H. J.; Hailu, S.; Karami, T. K.; Graham, R. Ocular Biopharmaceutics: Impact of Modeling and Simulation on Topical Ophthalmic Formulation Development. *Drug Discov. Today* **2019**, *24* (8), 1587–1597. https://doi.org/https://doi.org/10.1016/j.drudis.2019.04.002.

(124) HS Boddu, S.; Gupta, H.; Patel, S. Drug Delivery to the Back of the Eye Following Topical Administration: An Update on Research and Patenting Activity. *Recent Pat. Drug Deliv. Formul.* **2014**, *8* (1), 27–36.

(125) Luo, L.; Tam, J.; Maysinger, D.; Eisenberg, A. Cellular Internalization of Poly(Ethylene Oxide)-b-Poly(ε-Caprolactone) Diblock Copolymer Micelles. *Bioconjug. Chem.* **2002**, *13* (6), 1259–1265. https://doi.org/10.1021/bc025524y.

(126) Savić, R.; Luo, L.; Eisenberg, A.; Maysinger, D. Micellar Nanocontainers Distribute to Defined Cytoplasmic Organelles. *Science (80-.).* **2003**, *300* (5619),

615 LP – 618. https://doi.org/10.1126/science.1078192.

(127) Seidi, F.; Jenjob, R.; Crespy, D. Designing Smart Polymer Conjugates for Controlled Release of Payloads. *Chem. Rev.* **2018**, *118* (7), 3965–4036.

(128) Klahan, B.; Seidi, F.; Crespy, D. Oligo(Thioether-Ester)s Blocks in Polyurethanes for Slowly Releasing Active Payloads. *Macromol. Chem. Phys.* **2018**, *219* (23), 1–9. https://doi.org/10.1002/macp.201800392.

(129) Pepic, I.; Lovric, J.; Filipovic-Grcic, J. Polymeric Micelles in Ocular Drug Delivery: Rationale, Strategies and Challenges. *Chem. Biochem. Eng. Q.* **2012**, *26* (4), 365–377.

(130) Wang, W.; Zhao, B.; Meng, X.; She, P.; Zhang, P.; Cao, Y.; Zhang, X. Preparation of Dual-Drug Conjugated Polymeric Micelles with Synergistic Anti-Cancer Efficacy in Vitro. *J. Drug Deliv. Sci. Technol.* **2018**, *43*, 388–396. https://doi.org/https://doi.org/10.1016/j.jddst.2017.11.007.

(131) Kwon, G.; Suwa, S.; Yokoyama, M.; Okano, T.; Sakurai, Y.; Kataoka, K. Enhanced Tumor Accumulation and Prolonged Circulation Times of Micelle-Forming Poly (Ethylene Oxide-Aspartate) Block Copolymer-Adriamycin Conjugates. *J. Control. Release* **1994**, *29* (1), 17–23. https://doi.org/https://doi.org/10.1016/0168-3659(94)90118-X.

(132) Masayuki, Y.; Kwon, G. S.; Teruo, O.; Yasuhisa, S.; Mayumi, N.; Kazunori, K. Influencing Factors on in Vitro Micelle Stability of Adriamycin-Block Copolymer Conjugates. *J. Control. Release* **1994**, *28* (1), 59–65. https://doi.org/https://doi.org/10.1016/0168-3659(94)90153-8.

(133) Kwon, G. S.; Yokoyama, M.; Okano, T.; Sakurai, Y.; Kataoka, K. Biodistribution of Micelle-Forming Polymer–Drug Conjugates. *Pharm. Res.* **1993**, *10* (7), 970–974.

(134) Yokoyama, M.; Sugiyama, T.; Okano, T.; Sakurai, Y.; Naito, M.; Kataoka, K. Analysis of Micelle Formation of an Adriamycin-Conjugated Poly (Ethylene Glycol)–Poly (Aspartic Acid) Block Copolymer by Gel Permeation Chromatography. *Pharm. Res.* **1993**, *10* (6), 895–899.

(135) Yokoyama, M.; Miyauchi, M.; Yamada, N.; Okano, T.; Sakurai, Y.; Kataoka, K.;

Inoue, S. Characterization and Anticancer Activity of the Micelle-Forming Polymeric Anticancer Drug Adriamycin-Conjugated Poly (Ethylene Glycol)-Poly (Aspartic Acid) Block Copolymer. *Cancer Res.* **1990**, *50* (6), 1693–1700.

(136) Zhang, H.; Li, H.; Cao, Z.; Du, J.; Yan, L.; Wang, J. Investigation of the in Vivo Integrity of Polymeric Micelles via Large Stokes Shift Fluorophore-Based FRET. *J. Control. Release* **2020**, *324*, 47–54. https://doi.org/https://doi.org/10.1016/j.jconrel.2020.04.046.

(137) Durgun, M. E.; Güngör, S.; Özsoy, Y. Micelles: Promising Ocular Drug Carriers for Anterior and Posterior Segment Diseases. *J. Ocul. Pharmacol. Ther.* **2020**. https://doi.org/10.1089/jop.2019.0109.

(138) Sang, X.; Yang, Q.; Wen, Q.; Zhang, L.; Ni, C. Preparation and Controlled Drug Release Ability of the Poly[N-Isopropylacryamide-Co-Allyl Poly(Ethylene Glycol)]-b-Poly(γ-Benzyl-l-Glutamate) Polymeric Micelles. *Mater. Sci. Eng. C* **2019**, *98*, 910–917. https://doi.org/https://doi.org/10.1016/j.msec.2019.01.056.

(139) Park, J.-R.; Sarwat, M.; Bolle, E. C. L.; De Laat, M. A.; Van Guyse, J. F. R.; Podevyn, A.; Hoogenboom, R.; Dargaville, T. R. Drug–Polymer Conjugates with Dynamic Cloud Point Temperatures Based on Poly (2-Oxazoline) Copolymers. *Polym. Chem.* **2020**, *11* (32), 5191–5199.

(140) Vuong, M. D. Le; Haouas, M.; Ural, M. S.; Desmaële, D.; Martineau-Corcos, C.; Gref, R. Degradation of Polymer-Drug Conjugate Nanoparticles Based on Lactic and Itaconic Acid. *Int. J. Mol. Sci.* **2022**, *23* (22), 14461.

(141) Yamamoto, T.; Yokoyama, M.; Opanasopit, P.; Hayama, A.; Kawano, K.; Maitani, Y. What Are Determining Factors for Stable Drug Incorporation into Polymeric Micelle Carriers? Consideration on Physical and Chemical Characters of the Micelle Inner Core. *J. Control. release* **2007**, *123* (1), 11–18.

(142) Opanasopit, P.; Yokoyama, M.; Watanabe, M.; Kawano, K.; Maitani, Y.; Okano, T. Block Copolymer Design for Camptothecin Incorporation into Polymeric Micelles for Passive Tumor Targeting. *Pharm. Res.* **2004**, *21* (11), 2001–2008.

(143) Yokoyama, M. Polymeric Micelles as a New Drug Carrier System and Their Required Considerations for Clinical Trials. *Expert Opin. Drug Deliv.* **2010**, *7* (2),

145–158. https://doi.org/10.1517/17425240903436479.

(144) Aliabadi, H. M.; Lavasanifar, A. Polymeric Micelles for Drug Delivery. *Expert Opin. Drug Deliv.* **2006**, *3* (1), 139–162. https://doi.org/10.1517/17425247.3.1.139.

(145) Civiale, C.; Licciardi, M.; Cavallaro, G.; Giammona, G.; Mazzone, M. G. Polyhydroxyethylaspartamide-Based Micelles for Ocular Drug Delivery. *Int. J. Pharm.* **2009**, *378* (1–2), 177–186. https://doi.org/10.1016/j.ijpharm.2009.05.028.

(146) Pepić, I.; Hafner, A.; Lovrić, J.; Pirkić, B.; Filipović-Grčić, J. A Nonionic Surfactant/Chitosan Micelle System in an Innovative Eye Drop Formulation. *J. Pharm. Sci.* **2010**, *99* (10), 4317–4325. https://doi.org/https://doi.org/10.1002/jps.22137.

(147) Terreni, E.; Chetoni, P.; Tampucci, S.; Burgalassi, S.; Al-Kinani, A. A.; Alany, R. G.; Monti, D. Assembling Surfactants-Mucoadhesive Polymer Nanomicelles (ASMP-Nano) for Ocular Delivery of Cyclosporine-A. *Pharmaceutics* **2020**, *12* (3), 253.

(148) Wang, Y.; Khan, A.; Liu, Y.; Feng, J.; Dai, L.; Wang, G.; Alam, N.; Tong, L.; Ni, Y. Chitosan Oligosaccharide-Based Dual PH Responsive Nano-Micelles for Targeted Delivery of Hydrophobic Drugs. *Carbohydr. Polym.* **2019**, *223*, 115061.

(149) Djordjevic, J.; Michniak, B.; Uhrich, K. E. Amphiphilic Star-like Macromolecules as Novel Carriers for Topical Delivery of Nonsteroidal Anti-Inflammatory Drugs. *AAPS PharmSci* **2003**, *5* (4), 1–12. https://doi.org/10.1208/ps050426.

(150) Kataoka, K.; Matsumoto, T.; Yokoyama, M.; Okano, T.; Sakurai, Y.; Fukushima, S.; Okamoto, K.; Kwon, G. S. Doxorubicin-Loaded Poly(Ethylene Glycol)–Poly(β-Benzyl-l-Aspartate) Copolymer Micelles: Their Pharmaceutical Characteristics and Biological Significance. *J. Control. Release* **2000**, *64* (1), 143–153. https://doi.org/https://doi.org/10.1016/S0168-3659(99)00133-9.

(151) Liu, D.; Wu, Q.; Chen, W.; Lin, H.; Zhu, Y.; Liu, Y.; Liang, H.; Zhu, F. M. A Novel FK506 Loaded Nanomicelles Consisting of Amino-Terminated Poly(Ethylene Glycol)-Block-Poly(D,L)-Lactic Acid and Hydroxypropyl Methylcellulose for Ocular Drug Delivery. *Int. J. Pharm.* **2019**, *562* (December

2018), 1–10. https://doi.org/10.1016/j.ijpharm.2019.03.022.

(152) Wang, L.-L.; He, D.-D.; Wang, S.-X.; Dai, Y.-H.; Ju, J.-M.; Zhao, C.-L. Preparation and Evaluation of Curcumin-Loaded Self-Assembled Micelles. *Drug Dev. Ind. Pharm.* **2018**, *44* (4), 563–569. https://doi.org/10.1080/03639045.2017.1405431.

(153) Mehra, N.; Aqil, M.; Sultana, Y. A Grafted Copolymer-Based Nanomicelles for Topical Ocular Delivery of Everolimus: Formulation, Characterization, Ex-Vivo Permeation, in-Vitro Ocular Toxicity, and Stability Study. *Eur. J. Pharm. Sci.* **2021**, *159*, 105735. https://doi.org/https://doi.org/10.1016/j.ejps.2021.105735.

(154) Song, R.; Zhou, Y.; Li, Y.; Yang, Z.; Li, F.; Huang, Q.; Shi, T.; Zhang, G. Preparation and Characterization of m PEG-g-α-zein Biohybrid Micelles as a Nano-carrier. *J. Appl. Polym. Sci.* **2015**, *132* (38).

(155) Shuai, X.; Ai, H.; Nasongkla, N.; Kim, S.; Gao, J. Micellar Carriers Based on Block Copolymers of Poly(ε-Caprolactone) and Poly(Ethylene Glycol) for Doxorubicin Delivery. *J. Control. Release* **2004**, *98* (3), 415–426. https://doi.org/https://doi.org/10.1016/j.jconrel.2004.06.003.

(156) Safwat, M. A.; Mansour, H. F.; Hussein, A. K.; Abdelwahab, S.; Soliman, G. M. Polymeric Micelles for the Ocular Delivery of Triamcinolone Acetonide: Preparation and in Vivo Evaluation in a Rabbit Ocular Inflammatory Model. *Drug Deliv.* **2020**, *27* (1), 1115–1124. https://doi.org/10.1080/10717544.2020.1797241.

(157) Le Garrec, D.; Gori, S.; Luo, L.; Lessard, D.; Smith, D. C.; Yessine, M.-A.; Ranger, M.; Leroux, J.-C. Poly(N-Vinylpyrrolidone)-Block-Poly(d,l-Lactide) as a New Polymeric Solubilizer for Hydrophobic Anticancer Drugs: In Vitro and in Vivo Evaluation. *J. Control. Release* **2004**, *99* (1), 83–101. https://doi.org/https://doi.org/10.1016/j.jconrel.2004.06.018.

(158) Ghezzi, M.; Ferraboschi, I.; Delledonne, A.; Pescina, S.; Padula, C.; Santi, P.; Sissa, C.; Terenziani, F.; Nicoli, S. Cyclosporine-Loaded Micelles for Ocular Delivery: Investigating the Penetration Mechanisms. *J. Control. Release* **2022**, *349*, 744–755. https://doi.org/https://doi.org/10.1016/j.jconrel.2022.07.019.

(159) Özsoy, Y.; Güngör, S.; Kahraman, E.; Ezgi Durgun, M. *Polymeric Micelles as a*

Novel Carrier for Ocular Drug Delivery; 2019. https://doi.org/10.1016/B978-0-12-816200-2.00005-0.

(160) Rabinovich-Guilatt, L.; Couvreur, P.; Lambert, G.; Dubernet, C. Cationic Vectors in Ocular Drug Delivery. *J. Drug Target.* **2004**, *12* (9–10), 623–633.

(161) Liu, S.; Jones, L.; Gu, F. X. Nanomaterials for Ocular Drug Delivery. *Macromol. Biosci.* **2012**, *12* (5), 608–620. https://doi.org/10.1002/mabi.201100419.

(162) Mahmood, A.; Lanthaler, M.; Laffleur, F.; Huck, C. W.; Bernkop-Schnürch, A. Thiolated Chitosan Micelles: Highly Mucoadhesive Drug Carriers. *Carbohydr. Polym.* **2017**, *167*, 250–258. https://doi.org/https://doi.org/10.1016/j.carbpol.2017.03.019.

(163) Li, J.; Li, Z.; Zhou, T.; Zhang, J.; Xia, H.; Li, H.; He, J.; He, S.; Wang, L. Positively Charged Micelles Based on a Triblock Copolymer Demonstrate Enhanced Corneal Penetration. *Int. J. Nanomedicine* **2015**, *10*, 6027–6037. https://doi.org/10.2147/IJN.S90347.

(164) Yuan, X.; Harada, A.; Yamasaki, Y.; Kataoka, K. Stabilization of Lysozyme-Incorporated Polyion Complex Micelles by the ω-End Derivatization of Poly(Ethylene Glycol)−Poly(α,β-Aspartic Acid) Block Copolymers with Hydrophobic Groups. *Langmuir* **2005**, *21* (7), 2668–2674. https://doi.org/10.1021/la0488811.

(165) Groups, H. Stabilization of Lysozyme-Incorporated Polyion Complex Micelles by The. **2005**, No. 5, 2668–2674.

(166) Wakebayashi, D.; Nishiyama, N.; Itaka, K.; Miyata, K.; Yamasaki, Y.; Harada, A.; Koyama, H.; Nagasaki, Y.; Kataoka, K. Polyion Complex Micelles of PDNA with Acetal-Poly(Ethylene Glycol)-Poly(2-(Dimethylamino)Ethyl Methacrylate) Block Copolymer as the Gene Carrier System: Physicochemical Properties of Micelles Relevant to Gene Transfection Efficacy. *Biomacromolecules* **2004**, *5* (6), 2128–2136. https://doi.org/10.1021/bm040009j.

(167) Ren, J.; Zhang, Y.; Zhang, J.; Gao, H.; Liu, G.; Ma, R.; An, Y.; Kong, D.; Shi, L. PH/Sugar Dual Responsive Core-Cross-Linked PIC Micelles for Enhanced Intracellular Protein Delivery. *Biomacromolecules* **2013**, *14* (10), 3434–3443.

https://doi.org/10.1021/bm4007387.

(168) Yu, N.; Li, G.; Gao, Y.; Jiang, H.; Tao, Q. Thermo-Sensitive Complex Micelles from Sodium Alginate-Graft-Poly(N-Isopropylacrylamide) for Drug Release. *Int. J. Biol. Macromol.* **2016**, *86*, 296–301. https://doi.org/10.1016/j.ijbiomac.2016.01.066.

(169) Kuwada, K.; Kurinomaru, T.; Tomita, S.; Shiraki, K. Noncovalent PEGylation-Based Enzyme Switch in Physiological Saline Conditions Using Quaternized Polyamines. *Colloid Polym. Sci.* **2016**, *294* (10), 1551–1556. https://doi.org/10.1007/s00396-016-3916-5.

(170) Yokoyama, M. Polymeric Micelles as Drug Carriers: Their Lights and Shadows. *J. Drug Target.* **2014**, *22* (7), 576–583. https://doi.org/10.3109/1061186X.2014.934688.

(171) Xu, H.; Yang, P.; Ma, H.; Yin, W.; Wu, X.; Wang, H.; Xu, D.; Zhang, X. Amphiphilic Block Copolymers-Based Mixed Micelles for Noninvasive Drug Delivery. *Drug Deliv.* **2016**, *23* (8), 3063–3071.

(172) McClements, D. J. Nanoemulsions versus Microemulsions: Terminology, Differences, and Similarities. *Soft Matter* **2012**, *8* (6), 1719–1729. https://doi.org/10.1039/C2SM06903B.

(173) Ying, L.; Tahara, K.; Takeuchi, H. Drug Delivery to the Ocular Posterior Segment Using Lipid Emulsion via Eye Drop Administration: Effect of Emulsion Formulations and Surface Modification. *Int. J. Pharm.* **2013**, *453* (2), 329–335. https://doi.org/10.1016/j.ijpharm.2013.06.024.

(174) Mahboobian, M. M.; Seyfoddin, A.; Rupenthal, I. D.; Aboofazeli, R.; Foroutan, S. M. Formulation Development and Evaluation of the Therapeutic Efficacy of Brinzolamide Containing Nanoemulsions. *Iran. J. Pharm. Res.* **2017**, *16* (3), 847–857. https://doi.org/10.22037/ijpr.2017.2080.

(175) Gohil, R.; Patel, A.; Pandya, T.; Dharamsi, A. Optimization of Brinzolamide Loaded Microemulsion Using Formulation by Design Approach: Characterization and <l>In-Vitro</i> Evaluation. *Curr. Drug ther.* **2019**, *15* (1), 37–52. https://doi.org/10.2174/1574885514666190104115802.

(176) Jeng, B. H. Recent Updates in Inflammatory Ocular Diseases. *US Ophthalmic Rev.* **2018**, *11* (1), 19. https://doi.org/10.17925/usor.2018.11.1.19.

(177) Gupta, A.; Nayak, K.; Misra, M. Cow Ghee Fortified Ocular Topical Microemulsion; in Vitro, Ex Vivo, and in Vivo Evaluation. *J. Microencapsul.* **2019**, *36* (7), 603–621. https://doi.org/10.1080/02652048.2019.1662121.

(178) Guo, D.; Li, Q.; Sun, Y.; Guo, J.; Zhao, Q.; Yin, X.; Wei, H.; Wu, S.; Bi, H. Evaluation of Controlled-Release Triamcinolone Acetonide-Loaded MPEG-PLGA Nanoparticles in Treating Experimental Autoimmune Uveitis. *Nanotechnology* **2019**, *30* (16), 165702. https://doi.org/10.1088/1361-6528/aafe36.

(179) Alvarez-Trabado, J.; López-García, A.; Martín-Pastor, M.; Diebold, Y.; Sanchez, A. Sorbitan Ester Nanoparticles (SENS) as a Novel Topical Ocular Drug Delivery System: Design, Optimization, and in Vitro/Ex Vivo Evaluation. *Int. J. Pharm.* **2018**, *546* (1–2), 20–30. https://doi.org/10.1016/j.ijpharm.2018.05.015.

(180) Zhou, J.; Ritter, H. Cyclodextrin Functionalized Polymers as Drug Delivery Systems. **2010**, No. October 2001, 1552–1559. https://doi.org/10.1039/c0py00219d.

(181) Tang, P.; Yang, H.; Tang, B.; Wu, D.; Du, Q.; Xu, K.; Li, H. Dimethyl-β-Cyclodextrin/Salazosulfapyridine Inclusion Complex-Loaded Chitosan Nanoparticles for Sustained Release. *Carbohydr. Polym.* **2017**, *156*, 215–222. https://doi.org/10.1016/j.carbpol.2016.09.038.

(182) Zheng, K.; Huang, Z.; Huang, J.; Liu, X.; Ban, J.; Huang, X.; Luo, H.; Chen, Z.; Xie, Q.; Chen, Y. Effect of a 2-HP-β-Cyclodextrin Formulation on the Biological Transport and Delivery of Chemotherapeutic PLGA Nanoparticles. *Drug Des. Devel. Ther.* **2021**, 2605–2618.

(183) Fahmy, S. A.; Mahdy, N. K.; Al Mulla, H.; ElMeshad, A. N.; Issa, M. Y.; Azzazy, H. M. E.-S. PLGA/PEG Nanoparticles Loaded with Cyclodextrin-Peganum Harmala Alkaloid Complex and Ascorbic Acid with Promising Antimicrobial Activities. *Pharmaceutics* **2022**, *14* (1), 142.

(184) Jiang, G.; Jia, H.; Qiu, J.; Mo, Z.; Wen, Y.; Zhang, Y.; Wen, Y.; Xie, Q.; Ban, J.;

Lu, Z. PLGA Nanoparticle Platform for Trans-Ocular Barrier to Enhance Drug Delivery: A Comparative Study Based on the Application of Oligosaccharides in the Outer Membrane of Carriers. *Int. J. Nanomedicine* **2020**, 9373–9387.

(185) Qin, Z.; Li, B.; Deng, Q.; Wen, Y.; Feng, S.; Duan, C.; Zhao, B.; Li, H.; Gao, Y.; Ban, J. Polymer Nanoparticles with 2-HP-β-Cyclodextrin for Enhanced Retention of Uptake into HCE-T Cells. *Molecules* **2024**, *29* (3), 658.

(186) Guo, B.; Xu, D.; Liu, X.; Liao, C.; Li, S.; Huang, Z.; Li, X.; Yi, J. Characterization and Cytotoxicity of PLGA Nanoparticles Loaded with Formononetin Cyclodextrin Complex. *J. Drug Deliv. Sci. Technol.* **2017**, *41*, 375–383. https://doi.org/10.1016/j.jddst.2017.08.010.

(187) Bíró, T.; Aigner, Z. Current Approaches to Use Cyclodextrins and Mucoadhesive Polymers in Ocular Drug Delivery-a Mini-Review. *Sci. Pharm.* **2019**, *87* (3). https://doi.org/10.3390/scipharm87030015.

(188) Shinde, U. A.; Joshi, P. N.; Jain, D. D.; Singh, K. Preparation and Evaluation of N-Trimethyl Chitosan Nanoparticles of Flurbiprofen for Ocular Delivery. *Curr. Eye Res.* **2019**, *44* (5), 575–582. https://doi.org/10.1080/02713683.2019.1567793.

(189) Lorenzo-Veiga, B.; Sigurdsson, H. H.; Loftsson, T. Nepafenac-Loaded Cyclodextrin/Polymer Nanoaggregates: A New Approach to Eye Drop Formulation. *Materials (Basel).* **2019**, *12* (2). https://doi.org/10.3390/ma12020229.

(190) Nanda, A.; Sahoo, R. N.; Pramanik, A.; Mohapatra, R.; Pradhan, S. K.; Thirumurugan, A.; Das, D.; Mallick, S. Drug-in-Mucoadhesive Type Film for Ocular Anti-Inflammatory Potential of Amlodipine: Effect of Sulphobutyl-Ether-Beta-Cyclodextrin on Permeation and Molecular Docking Characterization. *Colloids Surfaces B Biointerfaces* **2018**, *172*, 555–564. https://doi.org/10.1016/j.colsurfb.2018.09.011.

(191) Mazet, R.; Choisnard, L.; Levilly, D.; Wouessidjewe, D.; Gèze, A. Investigation of Combined Cyclodextrin and Hydrogel Formulation for Ocular Delivery of Dexamethasone Acetate by Means of Experimental Designs. *Pharmaceutics* **2018**, *10* (4). https://doi.org/10.3390/pharmaceutics10040249.

(192) Nabih Maria, D.; R Mishra, S.; Wang, L.; Helmy Abd-Elgawad, A.-E.; Abd-Elazeem Soliman, O.; Salah El-Dahan, M.; M Jablonski, M. Water-Soluble Complex of Curcumin with Cyclodextrins: Enhanced Physical Properties for Ocular Drug Delivery. *Curr. Drug Deliv.* **2017**, *14* (6), 875–886.

(193) Lorenzo-Veiga, B.; Sigurdsson, H. H.; Loftsson, T.; Alvarez-Lorenzo, C. Cyclodextrin–Amphiphilic Copolymer Supramolecular Assemblies for the Ocular Delivery of Natamycin. *Nanomaterials* **2019**, *9* (5), 745.

(194) Sayed, S.; Elsayed, I.; Ismail, M. M. Optimization of β-Cyclodextrin Consolidated Micellar Dispersion for Promoting the Transcorneal Permeation of a Practically Insoluble Drug. *Int. J. Pharm.* **2018**, *549* (1–2), 249–260. https://doi.org/10.1016/j.ijpharm.2018.08.001.

(195) Gorantla, S.; Rapalli, V. K.; Waghule, T.; Singh, P. P.; Dubey, S. K.; Saha, R. N.; Singhvi, G. Nanocarriers for Ocular Drug Delivery: Current Status and Translational Opportunity. *RSC Adv.* **2020**, *10* (46), 27835–27855.

(196) Terreni, E.; Zucchetti, E.; Tampucci, S.; Burgalassi, S.; Monti, D.; Chetoni, P. Combination of Nanomicellar Technology and in Situ Gelling Polymer as Ocular Drug Delivery System (ODDS) for Cyclosporine-A. *Pharmaceutics* **2021**, *13* (2), 192.

(197) Kianersi, S.; Solouk, A.; Saber-Samandari, S.; Keshel, S. H.; Pasbakhsh, P. Alginate Nanoparticles as Ocular Drug Delivery Carriers. *J. Drug Deliv. Sci. Technol.* **2021**, *66*, 102889.

(198) Yang, Y.; Lockwood, A. Topical Ocular Drug Delivery Systems: Innovations for an Unmet Need. *Exp. Eye Res.* **2022**, *218*, 109006.

(199) Wang, J.; Liu, Q.; Yang, L.; Xia, X.; Zhu, R.; Chen, S.; Wang, M.; Cheng, L.; Wu, X.; Wang, S. Curcumin-Loaded TPGS/F127/P123 Mixed Polymeric Micelles for Cervical Cancer Therapy: Formulation, Characterization, and in Vitro and in Vivo Evaluation. *J. Biomed. Nanotechnol.* **2017**, *13* (12), 1631–1646.

(200) Koummich, S. A.; Zoukh, I. M.; Gorachinov, F.; Geskovski, N.; Makreski, P.; Dodov, M. G.; Goracinova, K. Design of Ophthalmic Micelles Loaded with Diclofenac Sodium: Effect of Chitosan and Temperature on the Block-Copolymer

Micellization Behaviour. *Drug Deliv. Transl. Res.* **2021**, 1–20.

(201) Thapa, R. K.; Cazzador, F.; Grønlien, K. G.; Tønnesen, H. H. Effect of Curcumin and Cosolvents on the Micellization of Pluronic F127 in Aqueous Solution. *Colloids Surfaces B Biointerfaces* **2020**, *195* (July 2020). https://doi.org/10.1016/j.colsurfb.2020.111250.

(202) Dehvari, K.; Chen, Y.; Tsai, Y.-H.; Tseng, S.-H.; Lin, K.-S. Superparamagnetic Iron Oxide Nanorod Carriers for Paclitaxel Delivery in the Treatment and Imaging of Colon Cancer in Mice. *J. Biomed. Nanotechnol.* **2016**, *12* (9), 1734–1745.

(203) Bao, Z.; Zhou, Y.; Lei, L.; Zhang, R.; Song, Q.; Li, X.; Wang, Y. A Facile Strategy to Generate High Drug Payload Celecoxib Micelles for Enhanced Corneal Permeability. *J. Biomed. Nanotechnol.* **2019**, *15* (4), 822–829.

(204) Akhlaghi, N.; Riahi, S. Salinity Effect on the Surfactant Critical Micelle Concentration through Surface Tension Measurement. *Iran. J. Oil Gas Sci. Technol.* **2019**, *8* (4), 50–63.

(205) Barba, A. A.; d'Amore, M.; Grassi, M.; Chirico, S.; Lamberti, G.; Titomanlio, G. Investigation of Pluronic© F127–Water Solutions Phase Transitions by DSC and Dielectric Spectroscopy. *J. Appl. Polym. Sci.* **2009**, *114* (2), 688–695.

(206) Hsu, C.-T.; Shao, M.-J.; Lin, S.-Y. Adsorption Kinetics of C12E4 at the Air− Water Interface: Adsorption onto a Fresh Interface. *Langmuir* **2000**, *16* (7), 3187–3194.

(207) Mata, J. P.; Majhi, P. R.; Guo, C.; Liu, H. Z.; Bahadur, P. Concentration, Temperature, and Salt-Induced Micellization of a Triblock Copolymer Pluronic L64 in Aqueous Media. *J. Colloid Interface Sci.* **2005**, *292* (2), 548–556. https://doi.org/10.1016/j.jcis.2005.06.013.

(208) Sajid, M.; Akash, H.; Rehman, K.; Chen, S.; Sajid, M.; Akash, H.; Rehman, K.; Chen, S.; Rehman, K.; Chen, S. Pluronic F127-Based Thermosensitive Gels for Delivery of Therapeutic Proteins and Peptides Pluronic F127-Based Thermosensitive Gels for Delivery of Therapeutic Proteins and Peptides. **2017**, *3724* (October). https://doi.org/10.1080/15583724.2014.927885.

(209) Akash, M. S. H.; Rehman, K.; Chen, S. Pluronic F127-Based Thermosensitive

Gels for Delivery of Therapeutic Proteins and Peptides. *Polym. Rev.* **2014**, *54* (4), 573–597. https://doi.org/10.1080/15583724.2014.927885.

(210) Fusco, S.; Borzacchiello, A.; Netti, P. A. Perspectives on: PEO-PPO-PEO Triblock Copolymers and Their Biomedical Applications. *J. Bioact. Compat. Polym.* **2006**, *21* (2), 149–164.

(211) He, C.; Kim, S. W.; Lee, D. S. In Situ Gelling Stimuli-Sensitive Block Copolymer Hydrogels for Drug Delivery. *J. Control. release* **2008**, *127* (3), 189–207.

(212) Jeong, B.; Kim, S. W.; Bae, Y. H. Thermosensitive Sol–Gel Reversible Hydrogels. *Adv. Drug Deliv. Rev.* **2012**, *64*, 154–162.

(213) Moreno, E.; Schwartz, J.; Larrañeta, E.; Nguewa, P. A.; Sanmartín, C.; Agüeros, M.; Irache, J. M.; Espuelas, S. Thermosensitive Hydrogels of Poly (Methyl Vinyl Ether-Co-Maleic Anhydride)–Pluronic® F127 Copolymers for Controlled Protein Release. *Int. J. Pharm.* **2014**, *459* (1–2), 1–9.

(214) Pepić, I.; Jalšenjak, N.; Jalšenjak, I. Micellar Solutions of Triblock Copolymer Surfactants with Pilocarpine. *Int. J. Pharm.* **2004**, *272* (1–2), 57–64. https://doi.org/10.1016/j.ijpharm.2003.11.032.

(215) Gyulai, G.; Magyar, A.; Rohonczy, J.; Orosz, J.; Yamasaki, M.; Bősze, S.; Kiss, É. Preparation and Characterization of Cationic Pluronic for Surface Modification and Functionalization of Polymeric Drug Delivery Nanoparticles. *Express Polym. Lett.* **2016**, *10* (3), 216.

(216) Farkouh, A.; Frigo, P.; Czejka, M. Systemic Side Effects of Eye Drops: A Pharmacokinetic Perspective. *Clin. Ophthalmol.* **2016**, *10*, 2433–2441. https://doi.org/10.2147/OPTH.S118409.

(217) Alambiaga-Caravaca, A. M.; Calatayud-Pascual, M. A.; Rodilla, V.; Concheiro, A.; López-Castellano, A.; Alvarez-Lorenzo, C. Micelles of Progesterone for Topical Eye Administration: Interspecies and Intertissues Differences in Ex Vivo Ocular Permeability. *Pharmaceutics*. 2020. https://doi.org/10.3390/pharmaceutics12080702.

(218) Uchegbu, I. F.; Breznikar, J.; Zaffalon, A.; Odunze, U.; Schätzlein, A. G. Polymeric Micelles for the Enhanced Deposition of Hydrophobic Drugs into

Ocular Tissues, without Plasma Exposure. *Pharmaceutics* **2021**, *13* (5), 744.

(219) Alexandridis, P.; Holzwarth, J. F.; Hatton, T. A. Micellization of Poly (Ethylene Oxide)-Poly (Propylene Oxide)-Poly (Ethylene Oxide) Triblock Copolymers in Aqueous Solutions: Thermodynamics of Copolymer Association. *Macromolecules* **1994**, *27* (9), 2414–2425.

(220) Khan, I.; Umapathi, R.; Neves, M. C.; Coutinho, J. A. P.; Venkatesu, P. Structural Insights into the Effect of Cholinium-Based Ionic Liquids on the Critical Micellization Temperature of Aqueous Triblock Copolymers. *Phys. Chem. Chem. Phys.* **2016**, *18* (12), 8342–8351.

(221) Šarac, B.; Bešter-Rogač, M.; Lah, J. Thermodynamics of Micellization from Heat-Capacity Measurements. *ChemPhysChem* **2014**, *15* (9), 1827–1833. https://doi.org/10.1002/cphc.201400096.

(222) Turabee, M. H.; Jeong, T. H.; Ramalingam, P.; Kang, J. H.; Ko, Y. T. N, N, N-Trimethyl Chitosan Embedded in Situ Pluronic F127 Hydrogel for the Treatment of Brain Tumor. *Carbohydr. Polym.* **2019**, *203*, 302–309.

(223) Tripathi, N.; Singhvi, G.; Roy, A.; Kuperkar, K.; Bahadur, P. Nanoscale Pluronic® Micellar Templates with Varying% EO Content for Controlled Drug Release and Cytotoxicity. *J. Mol. Liq.* **2023**, 122215.

(224) Alexandridis, P.; Athanassiou, V.; Fukuda, S.; Hatton, T. A. Surface Activity of Poly(Ethylene Oxide)-Block-Poly(Propylene Oxide)-Block-Poly(Ethylene Oxide) Copolymers. *Langmuir* **1994**, *10* (8), 2604–2612. https://doi.org/10.1021/la00020a019.

(225) Song, K.; Xin, M.; Yu, H.; Zheng, Z.; Li, J.; Li, M.; Guo, H.; Tan, Y.; Wu, X. Novel Ultra-Small Micelles Based on Rebaudioside A: A Potential Nanoplatform for Ocular Drug Delivery. *Int. J. Pharm.* **2018**, *552* (1–2), 265–276.

(226) Li, M.; Lan, J.; Li, X.; Xin, M.; Wang, H.; Zhang, F.; Lu, X.; Zhuang, Z.; Wu, X. Novel Ultra-Small Micelles Based on Ginsenoside Rb1: A Potential Nanoplatform for Ocular Drug Delivery. *Drug Deliv.* **2019**, *26* (1), 481–489.

(227) Song, K.; Xin, M.; Zhang, F.; Xie, W.; Sun, M.; Wu, X. Novel Ultrasmall Nanomicelles Based on Rebaudioside A: A Potential Nanoplatform for the Ocular

Delivery of Pterostilbene. *Int. J. Pharm.* **2020**, *577* (January), 119035. https://doi.org/10.1016/j.ijpharm.2020.119035.

(228) Durgun, M. E.; Kahraman, E.; Hacıoğlu, M.; Güngör, S.; Özsoy, Y. Posaconazole Micelles for Ocular Delivery: In Vitro Permeation, Ocular Irritation and Antifungal Activity Studies. *Drug Deliv. Transl. Res.* **2022**, 1–14.

(229) Lin, X.; Yang, H.; Su, L.; Yang, Z.; Tang, X. Effect of Size on the in Vitro/in Vivo Drug Release and Degradation of Exenatide-Loaded PLGA Microspheres. *J. Drug Deliv. Sci. Technol.* **2018**, *45*, 346–356. https://doi.org/https://doi.org/10.1016/j.jddst.2018.03.024.

(230) Pepić, I.; Lovrić, J.; Hafner, A.; Filipović-Grčić, J. Powder Form and Stability of Pluronic Mixed Micelle Dispersions for Drug Delivery Applications. *Drug Dev. Ind. Pharm.* **2014**, *40* (7), 944–951.

(231) Ojha, T.; Hu, Q.; Colombo, C.; Wit, J.; van Geijn, M.; van Steenbergen, M. J.; Bagheri, M.; Königs-Werner, H.; Buhl, E. M.; Bansal, R.; et al. Lyophilization Stabilizes Clinical-Stage Core-Crosslinked Polymeric Micelles to Overcome Cold Chain Supply Challenges. *Biotechnol. J.* **2021**, *16* (6), e2000212. https://doi.org/10.1002/biot.202000212.

(232) Liu, L. L.; Wang, Y. The Influence of Surfactant on the Size Control and Shape of Nano Materials. *J. Chang. Norm. Univ* **2014**, *33*, 62–64.

(233) González, F. G.; Vilchez, M. A. C.; Hidalgo-Alvarez, R. Adsorption of Anionic Surfactants on Positively Charged Polystyrene Particles II. *Colloid Polym. Sci.* **1991**, *269* (4), 406–411. https://doi.org/10.1007/BF00654587.

(234) Varshosaz, J.; Taymouri, S.; Hassanzadeh, F.; Haghjooy Javanmard, S.; Rostami, M. Folated Synperonic-Cholesteryl Hemisuccinate Polymeric Micelles for the Targeted Delivery of Docetaxel in Melanoma. *Biomed Res. Int.* **2015**, *2015*.

(235) Zhao, J.; Pispas, S.; Zhang, G. Effect of Sonication on Polymeric Aggregates Formed by Poly(Ethylene Oxide)-Based Amphiphilic Block Copolymers. *Macromol. Chem. Phys.* **2009**, *210* (12), 1026–1032. https://doi.org/10.1002/macp.200900161.

(236) Yokoyama, M.; Satoh, A.; Sakurai, Y.; Okano, T.; Matsumura, Y.; Kakizoe, T.;

Kataoka, K. Incorporation of Water-Insoluble Anticancer Drug into Polymeric Micelles and Control of Their Particle Size. *J. Control. Release* **1998**, *55* (2–3), 219–229. https://doi.org/10.1016/s0168-3659(98)00054-6.

(237) Pescina, S.; Grolli Lucca, L.; Govoni, P.; Padula, C.; Del Favero, E.; Cantù, L.; Santi, P.; Nicoli, S. Ex Vivo Conjunctival Retention and Transconjunctival Transport of Poorly Soluble Drugs Using Polymeric Micelles. *Pharmaceutics* **2019**, *11* (9), 476.

(238) Li, M.; Zhang, L.; Li, R.; Yan, M. New Resveratrol Micelle Formulation for Ocular Delivery: Characterization and in Vitro/in Vivo Evaluation. *Drug Dev. Ind. Pharm.* **2020**, *46* (12), 1960–1970.

(239) Sundar Dhilip Kumar, S.; Houreld, N. N.; Abrahamse, H. Therapeutic Potential and Recent Advances of Curcumin in the Treatment of Aging-Associated Diseases. *Molecules* **2018**, *23* (4), 835.

(240) Dinte, E.; Vostinaru, O.; Samoila, O.; Sevastre, B.; Bodoki, E. Ophthalmic Nanosystems with Antioxidants for the Prevention and Treatment of Eye Diseases. *Coatings* **2020**, *10* (1), 36.

(241) de Andrade, Â. G. L. L.; Sangaletti, P.; Ricken, Y. S.; da Costa, J. S.; de Lima, I. S.; Parize, A. L.; Marin, C. F. F.; Gerola, A. P.; Fajardo, A. R.; da Silva Filho, E. C. Controlled Release of Curcumin from Hydrogels: Biomedical Applications with a Focus on Neurodegenerative Diseases. In *Curcumin and Neurodegenerative Diseases: From Traditional to Translational Medicines*; Springer, 2024; pp 403–436.

(242) Abdelkader, H.; Wertheim, D.; Pierscionek, B.; Alany, R. G. Curcumin in Situ Gelling Polymeric Insert with Enhanced Ocular Performance. *Pharmaceutics* **2020**, *12* (12), 1158.

(243) Akbar, M. U.; Zia, K. M.; Nazir, A.; Iqbal, J.; Ejaz, S. A.; Akash, M. S. H. Pluronic-Based Mixed Polymeric Micelles Enhance the Therapeutic Potential of Curcumin. *AAPS PharmSciTech* **2018**, *19* (6), 2719–2739. https://doi.org/10.1208/s12249-018-1098-9.

(244) Suresh, K.; Nangia, A. Curcumin: Pharmaceutical Solids as a Platform to Improve

Solubility and Bioavailability. *CrystEngComm* **2018**, *20* (24), 3277–3296.

(245) Li, M.; Xin, M.; Guo, C.; Lin, G.; Wu, X. New Nanomicelle Curcumin Formulation for Ocular Delivery: Improved Stability, Solubility, and Ocular Anti-Inflammatory Treatment. *Drug Dev. Ind. Pharm.* **2017**, *43* (11), 1846–1857.

(246) Gote, V.; Mandal, A.; Alshamrani, M.; Pal, D. Self-Assembling Tacrolimus Nanomicelles for Retinal Drug Delivery. *Pharmaceutics* **2020**, *12* (11), 1072.

(247) Anirudhan, T. S.; Varghese, S.; Manjusha, V. Hyaluronic Acid Coated Pluronic F127/Pluronic P123 Mixed Micelle for Targeted Delivery of Paclitaxel and Curcumin. *Int. J. Biol. Macromol.* **2021**, *192*, 950–957.

(248) Vaidya, F. U.; Sharma, R.; Shaikh, S.; Ray, D.; Aswal, V. K.; Pathak, C. Pluronic Micelles Encapsulated Curcumin Manifests Apoptotic Cell Death and Inhibits Pro-Inflammatory Cytokines in Human Breast Adenocarcinoma Cells. *Cancer reports (Hoboken, N.J.)* **2019**, *2* (1), e1133. https://doi.org/10.1002/cnr2.1133.

(249) Chung, C. K.; García-Couce, J.; Campos, Y.; Kralisch, D.; Bierau, K.; Chan, A.; Ossendorp, F.; Cruz, L. J. Doxorubicin Loaded Poloxamer Thermosensitive Hydrogels: Chemical, Pharmacological and Biological Evaluation. *Molecules* **2020**, *25* (9). https://doi.org/10.3390/molecules25092219.

(250) Gerardos, A. M.; Balafouti, A.; Pispas, S. Mixed Hyperbranched/Triblock Copolymer Micelle Assemblies: Physicochemical Properties and Potential for Drug Encapsulation. *Macromol. Chem. Phys.* **2023**, *224* (17), 2300109.

(251) Wang, H.; He, Y.; Hou, Y.; Geng, Y.; Wu, X. Novel Self-Nanomicellizing Formulation Based on Rebaudioside A: A Potential Nanoplatform for Oral Delivery of Naringenin. *Mater. Sci. Eng. C* **2020**, *112*, 557–571. https://doi.org/10.1016/j.msec.2020.110926.

(252) Sahu, A.; Kasoju, N.; Goswami, P.; Bora, U. Encapsulation of Curcumin in Pluronic Block Copolymer Micelles for Drug Delivery Applications. *J. Biomater. Appl.* **2011**, *25* (6), 619–639. https://doi.org/10.1177/0885328209357110.

(253) Alshamrani, M.; Sikder, S.; Coulibaly, F.; Mandal, A.; Pal, D.; Mitra, A. K. Self-Assembling Topical Nanomicellar Formulation to Improve Curcumin Absorption Across Ocular Tissues. *AAPS PharmSciTech* **2019**, *20* (7), 1–16.

https://doi.org/10.1208/s12249-019-1404-1.

(254) Gou, M.; Men, K.; Shi, H.; Xiang, M.; Zhang, J.; Song, J.; Long, J.; Wan, Y.; Luo, F.; Zhao, X. Curcumin-Loaded Biodegradable Polymeric Micelles for Colon Cancer Therapy in Vitro and in Vivo. *Nanoscale* **2011**, *3* (4), 1558–1567.

(255) Ma, Z.; Haddadi, A.; Molavi, O.; Lavasanifar, A.; Lai, R.; Samuel, J. Micelles of Poly(Ethylene Oxide)-b-Poly(Epsilon-Caprolactone) as Vehicles for the Solubilization, Stabilization, and Controlled Delivery of Curcumin. *J. Biomed. Mater. Res. A* **2008**, *86* (2), 300–310. https://doi.org/10.1002/jbm.a.31584.

(256) Pescina, S.; Govoni, P.; Potenza, A.; Padula, C.; Santi, P.; Nicoli, S. Development of a Convenient Ex Vivo Model for the Study of the Transcorneal Permeation of Drugs: Histological and Permeability Evaluation. *J. Pharm. Sci.* **2015**, *104* (1), 63–71. https://doi.org/10.1002/jps.24231.

(257) Baidya, D.; Kushwaha, J.; Mahadik, K.; Patil, S. Chrysin-Loaded Folate Conjugated PF127-F68 Mixed Micelles with Enhanced Oral Bioavailability and Anticancer Activity against Human Breast Cancer Cells. *Drug Dev. Ind. Pharm.* **2019**, *45* (5), 852–860.

(258) Hernández-Giottonini, K. Y.; Rodríguez-Córdova, R. J.; Gutiérrez-Valenzuela, C. A.; Peñuñuri-Miranda, O.; Zavala-Rivera, P.; Guerrero-Germán, P.; Lucero-Acuña, A. PLGA Nanoparticle Preparations by Emulsification and Nanoprecipitation Techniques: Effects of Formulation Parameters. *Rsc Adv.* **2020**, *10* (8), 4218–4231.

(259) Weng, J.; Tong, H. H. Y.; Chow, S. F. In Vitro Release Study of the Polymeric Drug Nanoparticles: Development and Validation of a Novel Method. *Pharmaceutics* **2020**, *12* (8), 732.

(260) Lin, H. R.; Chang, P. C. Novel Pluronic-Chitosan Micelle as an Ocular Delivery System. *J. Biomed. Mater. Res. - Part B Appl. Biomater.* **2013**, *101 B* (5), 689–699. https://doi.org/10.1002/jbm.b.32871.

(261) Shearer, S. A.; Hudson, J. R. Fluid Mechanics: Stokes' Law and Viscosity. *Meas. Lab.* **2008**, *3*.

(262) Cheng, P. Y.; Schachman, H. K. Studies on the Validity of the Einstein Viscosity

Law and Stokes' Law of Sedimentation. *J. Polym. Sci.* **1955**, *16* (81), 19–30.

(263) Oshima, K.; Nakamura, K.; Guo, H.; Smith Jr, R. L. Mini-Review on Application of Analytical Centrifugation, Ultracentrifugation and Centrifugal Devices to Phase Equilibria and Separation Processes. *Fluid Phase Equilib.* **2022**, *558*, 113457.

(264) Mahajan, H. S.; Patil, P. H. Central Composite Design-Based Optimization of Lopinavir Vitamin E-TPGS Micelle: In Vitro Characterization and in Vivo Pharmacokinetic Study. *Colloids Surfaces B Biointerfaces* **2020**, *194*, 111149.

(265) Kumari, P.; Swami, M. O.; Nadipalli, S. K.; Myneni, S.; Ghosh, B.; Biswas, S. Curcumin Delivery by Poly(Lactide)-Based Co-Polymeric Micelles: An In Vitro Anticancer Study. *Pharm. Res.* **2016**, *33* (4), 826–841. https://doi.org/10.1007/s11095-015-1830-z.

(266) El-Banna, F. S.; Hanafy, N. A. N.; Mahfouz, M. E.; El-Kemary, M. Hollow Spherical Curcumin Nanomicelles CUR@PLA@PF127: A New Trial on Breast Cancer Cells. *Biotechnol. Bioprocess Eng.* **2023**, *28* (5), 842–852. https://doi.org/10.1007/s12257-023-0075-7.

(267) Song, L.; Shen, Y.; Hou, J.; Lei, L.; Guo, S.; Qian, C. Polymeric Micelles for Parenteral Delivery of Curcumin: Preparation, Characterization and in Vitro Evaluation. *Colloids Surfaces A Physicochem. Eng. Asp.* **2011**, *390* (1–3), 25–32.

(268) Liang, N.; Sun, S.; Gong, X.; Li, Q.; Yan, P.; Cui, F. Polymeric Micelles Based on Modified Glycol Chitosan for Paclitaxel Delivery: Preparation, Characterization and Evaluation. *Int. J. Mol. Sci.* **2018**, *19* (6), 1550.

(269) Lu, Y.; Zhang, E.; Yang, J.; Cao, Z. Strategies to Improve Micelle Stability for Drug Delivery. *Nano Res.* **2018**, *11* (10), 4985–4998. https://doi.org/10.1007/s12274-018-2152-3.

(270) Gupta, A.; Costa, A. P.; Xu, X.; Lee, S.-L.; Cruz, C. N.; Bao, Q.; Burgess, D. J. Formulation and Characterization of Curcumin Loaded Polymeric Micelles Produced via Continuous Processing. *Int. J. Pharm.* **2020**, *583*, 119340. https://doi.org/10.1016/j.ijpharm.2020.119340.

(271) Rasoulianboroujeni, M.; Repp, L.; Lee, H. J.; Kwon, G. S. Production of Paclitaxel-Loaded PEG-b-PLA Micelles Using PEG for Drug Loading and Freeze-

Drying. *J. Control. Release* **2022**, *350*, 350–359.

(272) Luo, W.-C.; Beringhs, A. O.; Kim, R.; Zhang, W.; Patel, S. M.; Bogner, R. H.; Lu, X. Impact of Formulation on the Quality and Stability of Freeze-Dried Nanoparticles. *Eur. J. Pharm. Biopharm.* **2021**, *169*, 256–267.

(273) Vorobiova, I. G.; Mirgorod, Y. A.; Chekadanov, A. S. Ultrasound Effect on Molecules of Sodium Dodecyl Sulphate as Systems of Nanoparticles. *J. Nano-and Electron. Phys.* **2018**, *10* (6).

(274) Schulnies, F.; Höhme, L.; Kleinschmidt, T. Ultrasonication of Micellar Casein Concentrate to Reduce Viscosity—Role of Undissolved Material. *Foods* **2023**, *12* (24), 4519.

(275) Mohamed, E. A.; Hashim, I. I. A.; Yusif, R. M.; Suddek, G. M.; Shaaban, A. A. A.; Badria, F. A. E. Enhanced in Vitro Cytotoxicity and Anti-Tumor Activity of Vorinostat-Loaded Pluronic Micelles with Prolonged Release and Reduced Hepatic and Renal Toxicities. *Eur. J. Pharm. Sci.* **2017**, *96*, 232–242.

(276) Patil, P. H.; Mahajan, H. S. Mixed Micelles for Bioavailability Enhancement of Nelfinavir Mesylate: In Vitro Characterisation and In Vivo Pharmacokinetic Study. *Mater. Technol.* **2018**, *33* (12), 793–802.

(277) Ding, Y.; Wang, C.; Wang, Y.; Xu, Y.; Zhao, J.; Gao, M.; Ding, Y.; Peng, J.; Li, L. Development and Evaluation of a Novel Drug Delivery: Soluplus(®)/TPGS Mixed Micelles Loaded with Piperine in Vitro and in Vivo. *Drug Dev. Ind. Pharm.* **2018**, *44* (9), 1409–1416. https://doi.org/10.1080/03639045.2018.1472277.

(278) Yang, M.; Fazio, S.; Munch, D.; Drumm, P. Impact of Methanol and Acetonitrile on Separations Based on π–π Interactions with a Reversed-Phase Phenyl Column. *J. Chromatogr. A* **2005**, *1097* (1–2), 124–129.

(279) Alarjah, M. A.; Shahin, M. H.; Al-Azzah, F.; Alarjah, A. A.; Omran, Z. H. Concomitant Analysis of Dasatinib and Curcuminoids in a Pluronic-Based Nanoparticle Formulation Using a Novel HPLC Method. *Chromatographia* **2020**, *83*, 1355–1370.

(280) ROWLAND, S. J.; Rook, J. A. F. Analytical Methods. *Int. J. Dairy Technol.* **1961**, *14* (3), 112–114. https://doi.org/10.1111/j.1471-0307.1961.tb00962.x.

(281) Wu, P.; Jia, Y.; Qu, F.; Sun, Y.; Wang, P.; Zhang, K.; Xu, C.; Liu, Q.; Wang, X. Ultrasound-Responsive Polymeric Micelles for Sonoporation-Assisted Site-Specific Therapeutic Action. *ACS Appl. Mater. Interfaces* **2017**, *9* (31), 25706–25716.

(282) Patil, S.; Choudhary, B.; Rathore, A.; Roy, K.; Mahadik, K. Enhanced Oral Bioavailability and Anticancer Activity of Novel Curcumin Loaded Mixed Micelles in Human Lung Cancer Cells. *Phytomedicine* **2015**, *22* (12), 1103–1111. https://doi.org/https://doi.org/10.1016/j.phymed.2015.08.006.

(283) Chen, L.; Yue, B.; Liu, Z.; Luo, Y.; Ni, L.; Zhou, Z.; Ge, X. Study on the Preparation, Characterization, and Stability of Freeze-Dried Curcumin-Loaded Cochleates. *Foods* . 2022. https://doi.org/10.3390/foods11050710.

(284) Cheng, M.; Liu, Q.; Gan, T.; Fang, Y.; Yue, P.; Sun, Y.; Jin, Y.; Feng, J.; Tu, L. Nanocrystal-Loaded Micelles for the Enhanced in Vivo Circulation of Docetaxel. *Molecules* **2021**, *26* (15), 4481.

(285) Durgun, M. E.; Kahraman, E.; Güngör, S.; Özsoy, Y. Optimization and Characterization of Aqueous Micellar Formulations for Ocular Delivery of an Antifungal Drug, Posaconazole. *Curr. Pharm. Des.* **2020**, *26* (14), 1543–1555.

(286) Dahanayake, R.; Dormidontova, E. E. Molecular Structure and Co-Solvent Distribution in PPO–PEO and Pluronic Micelles. *Macromolecules* **2022**, *55* (23), 10439–10449.

(287) Gökçe Kocabay, Ö.; Ismail, O. Preparation and Optimization of Biodegradable Self-Assembled PCL-PEG-PCL Nano-Sized Micelles for Drug Delivery Systems. *Int. J. Polym. Mater. Polym. Biomater.* **2021**, *70* (5), 328–337.

(288) Khoshneviszadeh, R.; Bazzaz, B. S. F.; Housaindokht, M. R.; Ebrahim-Habibi, A.; Rajabi, O. A Comparison of Explanation Methods of Encapsulation Efficacy of Hydroquinone in a Liposomal System. *Arch. Adv. Biosci.* **2016**, *7* (2), 23–28.

(289) Gaikwad, V. L.; Choudhari, P. B.; Bhatia, N. M.; Bhatia, M. S. Chapter 2 - Characterization of Pharmaceutical Nanocarriers: In Vitro and in Vivo Studies; Grumezescu, A. M. B. T.-N. for D. D. and T., Ed.; William Andrew Publishing, 2019; pp 33–58. https://doi.org/https://doi.org/10.1016/B978-0-12-816505-

8.00016-3.

(290) Ardhi, A.; Schreiner, M. Evaluation of Extraction and Entrapment Efficiency of Black Seed Oil-Containing Emulsion as a Delivery System for Thymoquinone. *J. Food Meas. Charact.* **2024**, *18* (1), 393–401.

(291) Bhuptani, R. S.; Jain, A. S.; Makhija, D. T.; Jagtap, A. G.; Hassan, P. A. R.; Nagarsenker, M. S. Soluplus Based Polymeric Micelles and Mixed Micelles of Lornoxicam: Design, Characterization and In Vivo Efficacy Studies in Rats. *Indian J. Pharm. Educ. Res.* **2016**, *50* (2), 277–286.

(292) Garms, B. C.; Poli, H.; Baggley, D.; Han, F. Y.; Whittaker, A. K.; Anitha, A.; Grøndahl, L. Evaluating the Effect of Synthesis, Isolation, and Characterisation Variables on Reported Particle Size and Dispersity of Drug Loaded PLGA Nanoparticles. *Mater. Adv.* **2021**, *2* (17), 5657–5671.

(293) Zhang, F.; Chen, H.; Lan, J.; Song, K.; Wu, X. Preparation and in Vitro/in Vivo Evaluations of Novel Ocular Micelle Formulations of Hesperetin with Glycyrrhizin as a Nanocarrier. *Exp. Eye Res.* **2021**, *202*, 108313.

(294) Arukkunakorn, W.; Sajomsang, W.; Ovatlarnporn, C. Resveratrol Enhance Loading Capacity and Solubility of Dimethylcurcumin in Pluronic F-127 Nanomicelles. *Eur. Chem. Bull.* **2023**.

(295) Dalgakiran, E. A.; Ergin, A. D.; Kacar, G. Properties of Pluronic F68 and F127 Micelles Interacting Furosemide from Coarse-Grained Molecular Simulations as Validated by Experiments. *Colloids Surfaces A Physicochem. Eng. Asp.* **2023**, *666*, 131352.

(296) Phan, C.-M.; Ross, M.; Fahmy, K.; McEwen, B.; Hofmann, I.; Chan, V. W. Y.; Clark-Baba, C.; Jones, L. Evaluating Viscosity and Tear Breakup Time of Contemporary Commercial Ocular Lubricants on an In Vitro Eye Model. *Transl. Vis. Sci. Technol.* **2023**, *12* (6), 29. https://doi.org/10.1167/tvst.12.6.29.

(297) Singh, M.; Bharadwaj, S.; Lee, K. E.; Kang, S. G. Therapeutic Nanoemulsions in Ophthalmic Drug Administration: Concept in Formulations and Characterization Techniques for Ocular Drug Delivery. *J. Control. Release* **2020**, *328*, 895–916.

(298) Arif, F. A. C.; Hilmi, M. R.; Kamal, K. M.; Ithnin, M. H. Evaluation of 18 Artificial

Tears Based on Viscosity and PH. *Malaysian J. Ophthalmol.* **2020**, *2* (2), 96–111.

(299) Kassem, A. A.; Salama, A.; Mohsen, A. M. Formulation and Optimization of Cationic Nanoemulsions for Enhanced Ocular Delivery of Dorzolamide Hydrochloride Using Box-Behnken Design: In Vitro and in Vivo Assessments. *J. Drug Deliv. Sci. Technol.* **2022**, *68*, 103047.

(300) Grassiri, B.; Zambito, Y.; Bernkop-Schnürch, A. Strategies to Prolong the Residence Time of Drug Delivery Systems on Ocular Surface. *Adv. Colloid Interface Sci.* **2021**, *288*, 102342.

(301) Bagheri, M.; Fens, M. H.; Kleijn, T. G.; Capomaccio, R. B.; Mehn, D.; Krawczyk, P. M.; Scutigliani, E. M.; Gurinov, A.; Baldus, M.; van Kronenburg, N. C. H. In Vitro and in Vivo Studies on HPMA-Based Polymeric Micelles Loaded with Curcumin. *Mol. Pharm.* **2021**, *18* (3), 1247–1263.

(302) Nikzamir, M.; Akbarzadeh, A.; Panahi, Y. An Overview on Nanoparticles Used in Biomedicine and Their Cytotoxicity. *J. Drug Deliv. Sci. Technol.* **2021**, *61*, 102316.

(303) Gupta, T.; Singh, J.; Kaur, S.; Sandhu, S.; Singh, G.; Kaur, I. P. Enhancing Bioavailability and Stability of Curcumin Using Solid Lipid Nanoparticles (CLEN): A Covenant for Its Effectiveness. *Front. Bioeng. Biotechnol.* **2020**, *8*, 879. https://doi.org/10.3389/fbioe.2020.00879.

(304) Naksuriya, O.; van Steenbergen, M. J.; Torano, J. S.; Okonogi, S.; Hennink, W. E. A Kinetic Degradation Study of Curcumin in Its Free Form and Loaded in Polymeric Micelles. *AAPS J.* **2016**, *18* (3), 777–787.

(305) Bose, A.; Roy Burman, D.; Sikdar, B.; Patra, P. Nanomicelles: Types, Properties and Applications in Drug Delivery. *IET nanobiotechnology* **2021**, *15* (1), 19–27. https://doi.org/10.1049/nbt2.12018.

(306) Xu, X.; Sun, L.; Zhou, L.; Cheng, Y.; Cao, F. Functional Chitosan Oligosaccharide Nanomicelles for Topical Ocular Drug Delivery of Dexamethasone. *Carbohydr. Polym.* **2020**, *227*, 115356. https://doi.org/https://doi.org/10.1016/j.carbpol.2019.115356.

(307) Siddiqui, N. A. Evaluation of Thermo Sensitivity of Curcumin and Quantification

of Ferulic Acid and Vanillin as Degradation Products by a Validated HPTLC Method. *Pak. J. Pharm. Sci* **2015**, *28* (1), 299–305.

(308) Slavova-Kazakova, A. K.; Koleva, L.; Kancheva, V. D.; Delogu, G. Comparative Study of Antioxidant Potential of Curcumin and Its Degradation Products–Vanillin, Ferulic Acid and Dehydrozingerone. *ИНИЦИАТИВА „БАН ПРЕДСТАВЯ СВОИТЕ ИНСТИТУТИ "ИНСТИТУТ ПО ОРГАНИЧНА ХИМИЯ С ЦЕНТЪР ПО ФИТОХИМИЯ* **2018**, 54.

(309) Peram, M. R.; Jalalpure, S. S.; Palkar, M. B.; Diwan, P. V. Stability Studies of Pure and Mixture Form of Curcuminoids by Reverse Phase-HPLC Method under Various Experimental Stress Conditions. *Food Sci. Biotechnol.* **2017**, *26* (3), 591–602.

(310) Ibáñez, C.; Acuña, T.; Quintanilla, M. E.; Pérez-Reytor, D.; Morales, P.; Karahanian, E. Fenofibrate Decreases Ethanol-Induced Neuroinflammation and Oxidative Stress and Reduces Alcohol Relapse in Rats by a PPAR-α-Dependent Mechanism. *Antioxidants (Basel, Switzerland)* **2023**, *12* (9). https://doi.org/10.3390/antiox12091758.

(311) Hsu, Y.-J.; Lin, C.-W.; Cho, S.-L.; Yang, W.-S.; Yang, C.-M.; Yang, C.-H. Protective Effect of Fenofibrate on Oxidative Stress-Induced Apoptosis in Retinal–Choroidal Vascular Endothelial Cells: Implication for Diabetic Retinopathy Treatment. *Antioxidants* **2020**, *9* (8), 712.

(312) Kumar, R. Solubility and Bioavailability of Fenofibrate Nanoformulations. *ChemistrySelect* **2020**, *5* (4), 1478–1490.

(313) Lee, H. W.; Kang, W. Y.; Jung, W.; Gwon, M.-R.; Cho, K.; Yang, D. H.; Yoon, Y.-R.; Seong, S. J. Evaluation of the Pharmacokinetic Drug–Drug Interaction between Micronized Fenofibrate and Pitavastatin in Healthy Volunteers. *Pharmaceutics* **2020**, *12* (9), 869.

(314) Pandit, J.; Chaudhary, N.; Emad, N. A.; Ahmad, S.; Solanki, P.; Aqil, M.; Sultana, Y.; Solanki, P. Fenofibrate Loaded Nanofibers Based Thermo-Responsive Gel for Ocular Delivery: Formulation Development, Characterization and in Vitro Toxicity Study. *J. Drug Deliv. Sci. Technol.* **2023**, *89*, 104935.

(315) Hanaguri, J.; Nagai, N.; Yokota, H.; Kushiyama, A.; Watanabe, M.; Yamagami, S.; Nagaoka, T. Fenofibrate Nano-Eyedrops Ameliorate Retinal Blood Flow Dysregulation and Neurovascular Coupling in Type 2 Diabetic Mice. *Pharmaceutics* **2022**, *14* (2), 384.

(316) Huang, L.; Liang, W.; Zhou, K.; Wassel, R. A.; Ridge, Z. D.; Ma, J.-X.; Wang, B. Therapeutic Effects of Fenofibrate Nano-Emulsion Eye Drops on Retinal Vascular Leakage and Neovascularization. *Biology (Basel).* **2021**, *10* (12), 1328.

(317) Khin, S. Y.; Soe, H. M. S. H.; Chansriniyom, C.; Pornputtapong, N.; Asasutjarit, R.; Loftsson, T.; Jansook, P. Development of Fenofibrate/Randomly Methylated β-Cyclodextrin-Loaded Eudragit® RL 100 Nanoparticles for Ocular Delivery. *Molecules* **2022**, *27* (15), 4755.

(318) States, U. Feno Fi Brate-Loaded Biodegradable Nanoparticles for the Treatment of Experimental Diabetic Retinopathy and Neovascular Age-Related Macular Degeneration. **2019**. https://doi.org/10.1021/acs.molpharmaceut.8b01319.

(319) Elsaid, N.; Jackson, T. L.; Elsaid, Z.; Alqathama, A.; Somavarapu, S. PLGA Microparticles Entrapping Chitosan-Based Nanoparticles for the Ocular Delivery of Ranibizumab. *Mol. Pharm.* **2016**, *13* (9), 2923–2940. https://doi.org/10.1021/acs.molpharmaceut.6b00335.

(320) Sousa, F.; Cruz, A.; Fonte, P.; Pinto, I. M.; Neves-Petersen, M. T.; Sarmento, B. A New Paradigm for Antiangiogenic Therapy through Controlled Release of Bevacizumab from PLGA Nanoparticles. *Sci. Rep.* **2017**, *7* (1), 1–13.

(321) Kelly, S. J.; Hirani, A.; Shahidadpury, V.; Solanki, A.; Halasz, K.; Varghese Gupta, S.; Madow, B.; Sutariya, V. Aflibercept Nanoformulation Inhibits VEGF Expression in Ocular in Vitro Model: A Preliminary Report. *Biomedicines* **2018**, *6* (3), 92.

(322) Mahesh, M. B.; Shrikrushna, A. S.; Ganesh, S. T. Enhancement of Solubility and Dissolution Rate of Fenofibrate Using β-Cyclodextrin. *Innov. Pharm. Pharmacother.* **2020**, *8* (3).

(323) Nedelcu, A.; Olteanu, A.-A.; Constantinescu, I. C.; Florea, M.; Stănescu, L.-M.; Bărbuceanu, Ş. F.; Aramă, C.-C. Studies on the Effects of Inclusion Complexation

of Fenofibrate with EPI-NS vs. β-CD and Some of Its Substituted Derivatives. *Farmacia* **2022**, *70* (5).

(324) Lorenzo-Veiga, B.; Sigurdsson, H. H.; Loftsson, T.; Alvarez-Lorenzo, C. Cyclodextrin–Amphiphilic Copolymer Supramolecular Assemblies for the Ocular Delivery of Natamycin. *Nanomaterials* **2019**, *9* (5). https://doi.org/10.3390/nano9050745.

(325) Pignatello, R.; Corsaro, R.; Bonaccorso, A.; Zingale, E.; Carbone, C.; Musumeci, T. Soluplus® Polymeric Nanomicelles Improve Solubility of BCS-Class II Drugs. *Drug Deliv. Transl. Res.* **2022**, *12* (8), 1991–2006.

(326) Feng, X.; Chen, Y.; Li, L.; Zhang, Y.; Zhang, L.; Zhang, Z. Preparation, Evaluation and Metabolites Study in Rats of Novel Amentoflavone-Loaded TPGS/Soluplus Mixed Nanomicelles. *Drug Deliv.* **2020**, *27* (1), 137–150.

(327) Alvarez-Rivera, F.; Fernández-Villanueva, D.; Concheiro, A.; Alvarez-Lorenzo, C. α-Lipoic Acid in Soluplus® Polymeric Nanomicelles for Ocular Treatment of Diabetes-Associated Corneal Diseases. *J. Pharm. Sci.* **2016**, *105* (9), 2855–2863. https://doi.org/10.1016/j.xphs.2016.03.006.

(328) Arnaoutova, I.; George, J.; Kleinman, H. K.; Benton, G. The Endothelial Cell Tube Formation Assay on Basement Membrane Turns 20: State of the Science and the Art. *Angiogenesis* **2009**, *12* (3), 267–274. https://doi.org/10.1007/s10456-009-9146-4.

(329) Shi, F.; Chen, L.; Wang, Y.; Liu, J.; Adu-Frimpong, M.; Ji, H.; Toreniyazov, E.; Wang, Q.; Yu, J.; Xu, X. Enhancement of Oral Bioavailability and Anti-Hyperuricemic Activity of Aloe Emodin via Novel Soluplus®—Glycyrrhizic Acid Mixed Micelle System. *Drug Deliv. Transl. Res.* **2022**, 1–12.

(330) Kamenova, K.; Grancharov, G.; Kortenova, V.; Petrov, P. D. Redox-Responsive Crosslinked Mixed Micelles for Controllable Release of Caffeic Acid Phenethyl Ester. *Pharmaceutics* **2022**, *14* (3), 679.

(331) Mishra, A. K.; Lim, J.; Lee, J.; Park, S.; Seo, Y.; Hwang, H.; Kim, J. K. Control Drug Release Behavior by Highly Stable and PH Sensitive Poly (N-Vinylpyrrolidone)-Block-Poly (4-Vinylpyridine) Copolymer Micelles. *Polymer*

(Guildf). **2021**, *213*, 123329.

(332) Lynnerup, J. T.; Eriksen, J. B.; Bauer-Brandl, A.; Holsæter, A. M.; Brandl, M. Insight into the Mechanism behind Oral Bioavailability-Enhancement by Nanosuspensions through Combined Dissolution/Permeation Studies. *Eur. J. Pharm. Sci.* **2023**, *184*, 106417.

(333) Abedin Zadeh, M.; Alany, R. G.; Satarian, L.; Shavandi, A.; Abdullah Almousa, M.; Brocchini, S.; Khoder, M. Maillard Reaction Crosslinked Alginate-Albumin Scaffolds for Enhanced Fenofibrate Delivery to the Retina: A Promising Strategy to Treat RPE-Related Dysfunction. *Pharmaceutics* **2023**, *15* (5), 1330.

(334) Varela-Garcia, A.; Concheiro, A.; Alvarez-Lorenzo, C. Soluplus Micelles for Acyclovir Ocular Delivery: Formulation and Cornea and Sclera Permeability. *Int. J. Pharm.* **2018**, *552* (1), 39–47. https://doi.org/https://doi.org/10.1016/j.ijpharm.2018.09.053.

(335) Saokham, P.; Muankaew, C.; Jansook, P.; Loftsson, T. Solubility of Cyclodextrins and Drug/Cyclodextrin Complexes. *Molecules* **2018**, *23* (5), 1161.

(336) Schönbeck, C.; Madsen, T. L.; Peters, G. H.; Holm, R.; Loftsson, T. Soluble 1:1 Complexes and Insoluble 3:2 Complexes - Understanding the Phase-Solubility Diagram of Hydrocortisone and γ-Cyclodextrin. *Int. J. Pharm.* **2017**, *531* (2), 504–511. https://doi.org/10.1016/j.ijpharm.2017.05.024.

(337) Jansook, P.; Ogawa, N.; Loftsson, T. Cyclodextrins: Structure, Physicochemical Properties and Pharmaceutical Applications. *Int. J. Pharm.* **2018**, *535* (1), 272–284. https://doi.org/https://doi.org/10.1016/j.ijpharm.2017.11.018.

(338) Wong, J. W.; Yuen, K. H. Inclusion Complexation of Artemisinin with Alpha-, Beta-, and Gamma-Cyclodextrins. *Drug Dev. Ind. Pharm.* **2003**, *29* (9), 1035–1044. https://doi.org/10.1081/ddc-120025460.

(339) Jagdale, S. K.; Dehghan, M. H.; Paul, N. S. Enhancement of Dissolution of Fenofibrate Using Complexation with Hydroxy Propyl β-Cyclodextrin. *Turkish J. Pharm. Sci.* **2019**, *16* (1), 48–53. https://doi.org/10.4274/tjps.60490.

(340) Yousaf, A. M.; Kim, D. W.; Oh, Y.-K.; Yong, C. S.; Kim, J. O.; Choi, H.-G. Enhanced Oral Bioavailability of Fenofibrate Using Polymeric Nanoparticulated

Systems: Physicochemical Characterization and in Vivo Investigation. *Int. J. Nanomedicine* **2015**, *10*, 1819–1830. https://doi.org/10.2147/IJN.S78895.

(341) Loftsson, T.; Jarho, P.; Másson, M.; Järvinen, T. Cyclodextrins in Drug Delivery. *Expert Opin. Drug Deliv.* **2005**, *2* (2), 335–351. https://doi.org/10.1517/17425247.2.1.335.

(342) Agency, E. M. Background Review for Cyclodextrins Used as Excipients. EMA London, UK 2014.

(343) Sun, C.; Li, W.; Ma, P.; Li, Y.; Zhu, Y.; Zhang, H.; Adu-Frimpong, M.; Deng, W.; Yu, J.; Xu, X. Development of TPGS/F127/F68 Mixed Polymeric Micelles: Enhanced Oral Bioavailability and Hepatoprotection of Syringic Acid against Carbon Tetrachloride-Induced Hepatotoxicity. *Food Chem. Toxicol.* **2020**, *137*, 111126.

(344) Krawczyk-Santos, A. P.; Marreto, R. N.; Concheiro, A.; Alvarez-Lorenzo, C.; Taveira, S. F. Poly (Pseudo) Rotaxanes Formed by Mixed Micelles and α-Cyclodextrin Enhance Terbinafine Nail Permeation to Deeper Layers. *Int. J. Pharm. X* **2022**, *4*, 100118.

(345) Öztürk, K.; Arslan, F. B.; Öztürk, S. C.; Çalış, S. Mixed Micelles Formulation for Carvedilol Delivery: In-Vitro Characterization and in-Vivo Evaluation. *Int. J. Pharm.* **2022**, *611*, 121294.

(346) Jansook, P.; Loftsson, T. Self-Assembled γ-Cyclodextrin as Nanocarriers for Enhanced Ocular Drug Bioavailability. *Int. J. Pharm.* **2022**, *618*, 121654.

(347) Simões, S. M. N.; Veiga, F.; Ribeiro, A. C. F.; Figueiras, A. R.; Taboada, P.; Concheiro, A.; Alvarez-Lorenzo, C. Supramolecular Gels of Poly-α-Cyclodextrin and PEO-Based Copolymers for Controlled Drug Release. *Eur. J. Pharm. Biopharm.* **2014**, *87* (3), 579–588.

(348) Fenyvesi, F.; Nguyen, T. L. P.; Haimhoffer, Á.; Rusznyák, Á.; Vasvári, G.; Bácskay, I.; Vecsernyés, M.; Ignat, S.-R.; Dinescu, S.; Costache, M. Cyclodextrin Complexation Improves the Solubility and Caco-2 Permeability of Chrysin. *Materials (Basel).* **2020**, *13* (16), 3618.

(349) Alopaeus, J. F.; Göbel, A.; Breitkreutz, J.; Sande, S. A.; Tho, I. Investigation of

Hydroxypropyl-β-Cyclodextrin Inclusion Complexation of Two Poorly Soluble Model Drugs and Their Taste-Sensation-Effect of Electrolytes, Freeze-Drying and Incorporation into Oral Film Formulations. *J. Drug Deliv. Sci. Technol.* **2021**, *61*, 102245.

(350) Yang, B.; Yang, L.-J.; Lin, J.; Chen, Y.; Liu, Y. Binding Behaviors of Scutellarin with α-, β-, γ-Cyclodextrins and Their Derivatives. *J. Incl. Phenom. Macrocycl. Chem.* **2009**, *64*, 149–155.

(351) Shaikhullina, M.; Khaliullina, A.; Gimatdinov, R.; Butakov, A.; Chernov, V.; Filippov, A. NMR Relaxation and Self-Diffusion in Aqueous Micellar Gels of Pluronic F-127. *J. Mol. Liq.* **2020**, *306*, 112898.

(352) del Amo, E. M.; Rimpelä, A.-K.; Heikkinen, E.; Kari, O. K.; Ramsay, E.; Lajunen, T.; Schmitt, M.; Pelkonen, L.; Bhattacharya, M.; Richardson, D.; et al. Pharmacokinetic Aspects of Retinal Drug Delivery. *Prog. Retin. Eye Res.* **2017**, *57*, 134–185. https://doi.org/https://doi.org/10.1016/j.preteyeres.2016.12.001.

(353) Patil, A.; Lakhani, P.; Taskar, P.; Wu, K.-W.; Sweeney, C.; Avula, B.; Wang, Y.-H.; Khan, I. A.; Majumdar, S. Formulation Development, Optimization, and in Vitro–in Vivo Characterization of Natamycin-Loaded Pegylated Nano-Lipid Carriers for Ocular Applications. *J. Pharm. Sci.* **2018**, *107* (8), 2160–2171.

(354) Christensen, G.; Urimi, D.; Lorenzo-Soler, L.; Schipper, N.; Paquet-Durand, F. Ocular Permeability, Intraocular Biodistribution of Lipid Nanocapsule Formulation Intended for Retinal Drug Delivery. *Eur. J. Pharm. Biopharm.* **2023**, *187*, 175–183. https://doi.org/https://doi.org/10.1016/j.ejpb.2023.04.012.

(355) Gunwal, D.; Dutt, B. B.; Choudhary, M. A Comprehensive Review on the Drug: Fenofibrate. *IJRPS* **2021**, *12* (3), 2164–2172.

(356) Catapano, J.; Luty, M.; Wróbel, T.; Pudełek, M.; Piwowarczyk, K.; Kędracka-Krok, S.; Siedlar, M.; Madeja, Z.; Czyż, J. Acquired Drug Resistance Interferes with the Susceptibility of Prostate Cancer Cells to Metabolic Stress. *Cell. Mol. Biol. Lett.* **2022**, *27* (1), 100.

(357) Luty, M.; Piwowarczyk, K.; Łabędź-Masłowska, A.; Wróbel, T.; Szczygieł, M.; Catapano, J.; Drabik, G.; Ryszawy, D.; Kędracka-Krok, S.; Madeja, Z. Fenofibrate

Augments the Sensitivity of Drug-Resistant Prostate Cancer Cells to Docetaxel. *Cancers (Basel).* **2019**, *11* (1), 77.

(358) German, C.; Chen, Z.; Przekwas, A.; Walenga, R.; Babiskin, A.; Zhao, L.; Fan, J.; Tan, M. L. Computational Model of In Vivo Corneal Pharmacokinetics and Pharmacodynamics of Topically Administered Ophthalmic Drug Products. *Pharm. Res.* **2023**, *40* (4), 961–975. https://doi.org/10.1007/s11095-023-03480-6.

(359) Worakul, N.; Robinson, J. R. Ocular Pharmacokinetics/Pharmacodynamics. *Eur. J. Pharm. Biopharm.* **1997**, *44* (1), 71–83.

(360) Agrahari, V.; Mandal, A.; Agrahari, V.; Trinh, H. M.; Joseph, M.; Ray, A.; Hadji, H.; Mitra, R.; Pal, D.; Mitra, A. K. A Comprehensive Insight on Ocular Pharmacokinetics. *Drug Deliv. Transl. Res.* **2016**, *6* (6), 735–754. https://doi.org/10.1007/s13346-016-0339-2.

(361) Setapa, A.; Ahmad, N.; Mohd Mahali, S.; Mohd Amin, M. C. I. Mathematical Model for Estimating Parameters of Swelling Drug Delivery Devices in a Two-Phase Release. *Polymers (Basel).* **2020**, *12* (12), 2921.

(362) Veit, J. G. S.; Birru, B.; Singh, R.; Arrigali, E. M.; Serban, M. A. An In Vitro Model for Characterization of Drug Permeability across the Tympanic Membrane. *Pharmaceuticals (Basel).* **2022**, *15* (9). https://doi.org/10.3390/ph15091114.

(363) Toffoletto, N.; Saramago, B.; Serro, A. P.; Chauhan, A. A Physiology-Based Mathematical Model to Understand Drug Delivery from Contact Lenses to the Back of the Eye. *Pharm. Res.* **2023**, *40* (8), 1939–1951.

(364) Lorenzo Veiga, B. Cyclodextrin Nanostructures and Ocular Drug Delivery. **2020**.

(365) Pescina, S.; Sonvico, F.; Clementino, A.; Padula, C.; Santi, P.; Nicoli, S. Preliminary Investigation on Simvastatin-Loaded Polymeric Micelles in View of the Treatment of the Back of the Eye. *Pharmaceutics* . 2021. https://doi.org/10.3390/pharmaceutics13060855.

(366) Rasoanirina, B. N. V.; Lassoued, M. A.; Kamoun, A.; Bahloul, B.; Miladi, K.; Sfar, S. Voriconazole-Loaded Self-Nanoemulsifying Drug Delivery System (SNEDDS) to Improve Transcorneal Permeability. *Pharm. Dev. Technol.* **2020**, *25* (6), 694–703.

(367) Elmowafy, E.; Gad, H.; Biondo, F.; Casettari, L.; Soliman, M. E. Exploring Optimized Methoxy Poly(Ethylene Glycol)-Block-Poly(ε-Caprolactone) Crystalline Cored Micelles in Anti-Glaucoma Pharmacotherapy. *Int. J. Pharm.* **2019**, *566*, 573–584. https://doi.org/https://doi.org/10.1016/j.ijpharm.2019.06.011.

(368) Ch, S.; Padaga, S. G.; Ghosh, B.; Roy, S.; Biswas, S. Chitosan-Poly (Lactide-Co-Glycolide)/Poloxamer Mixed Micelles as a Mucoadhesive Thermo-Responsive Moxifloxacin Eye Drop to Improve Treatment Efficacy in Bacterial Keratitis. *Carbohydr. Polym.* **2023**, *312*, 120822.

(369) Modi, D.; Mohammad; Warsi, M. H.; Garg, V.; Bhatia, M.; Kesharwani, P.; Jain, G. K. Formulation Development, Optimization, and in Vitro Assessment of Thermoresponsive Ophthalmic Pluronic F127-Chitosan in Situ Tacrolimus Gel. *J. Biomater. Sci. Polym. Ed.* **2021**, *32* (13), 1678–1702.

(370) Burhan, A. M.; Klahan, B.; Cummins, W.; Andrés-Guerrero, V.; Byrne, M. E.; O'reilly, N. J.; Chauhan, A.; Fitzhenry, L.; Hughes, H. Posterior Segment Ophthalmic Drug Delivery: Role of Muco-Adhesion with a Special Focus on Chitosan. *Pharmaceutics* **2021**, *13* (10), 1685.

(371) Padaga, S. G.; Ch, S.; Paul, M.; Wable, B. D.; Ghosh, B.; Biswas, S. Chitosan Oligosaccharide/Pluronic F127 Micelles Exhibiting Anti-Biofilm Effect to Treat Bacterial Keratitis. *Carbohydr. Polym.* **2024**, *330*, 121818.

(372) Concheiro, A. Surfactant Interactions in Aqueous Media Part I : Nonionic Surfactants. **2003**, *258*, 165–177. https://doi.org/10.1016/S0378-5173(03)00181-9.

(373) Singh, M.; Sachar, S.; Yoshimura, T.; Esumi, K. Association Behavior of Poly (Ethylene Oxide)– Poly (Propylene Oxide)– Poly (Ethylene Oxide) Block Copolymers with Cationic Surfactants in Aqueous Solution. **2004**, *278*, 224–233. https://doi.org/10.1016/j.jcis.2004.05.025.

(374) Vinceković, M.; Bujan, M.; Šmit, I.; Filipović-Vinceković, N. Phase Behavior in Mixtures of Cationic Surfactant and Anionic Polyelectrolytes. *Colloids Surfaces A Physicochem. Eng. Asp.* **2005**, *255* (1–3), 181–191.

(375) Zhang, W.; Gilstrap, K.; Wu, L.; Remant Bahadur, K. C.; Moss, M. A.; Wang, Q.; Lu, X.; He, X. Synthesis and Characterization of Thermally Responsive Pluronic F127-Chitosan Nanocapsules for Controlled Release and Intracellular Delivery of Small Molecules. *ACS Nano* **2010**, *4* (11), 6747–6759. https://doi.org/10.1021/nn101617n.

(376) KC, R. B.; Lee, S. M.; Yoo, E. S.; Choi, J. H.; Do Ghim, H. Glycoconjugated Chitosan Stabilized Iron Oxide Nanoparticles as a Multifunctional Nanoprobe. *Mater. Sci. Eng. C* **2009**, *29* (5), 1668–1673.

(377) Heacock, R. A.; Marion, L. The Infrared Spectra of Secondary Amines and Their Salts. *Can. J. Chem.* **1956**, *34* (12), 1782–1795.

Appendices

Table S1: Absorbance values of degradation products obtained from forced degradation studies of CUR by UV spectrophotometry (n=3).

Time (h)	Absorbance value					
	At 420 nm (CUR)		At 260 nm (Vanillic acid)		At 280 nm (Vanillin)	
	By thermal	By photo	By thermal	By photo	By thermal	By photo
Start	1.50	1.52	0.25	0.35	0.15	0.22
6	1.27	1.52	0.32	0.34	0.23	0.21
18	1.30	1.49	0.34	0.34	0.27	0.21
24	0.79	1.52	0.45	0.35	0.40	0.22

Table S2: Standard and observed KBr-FTIR transmittance peak positions for PF127, CH, physical mixture of PF127 and CH and mixed PF127/CH micelles in DI water and PBS solutions.

Structural bond	Associated components	Standard peak position from reference (cm^{-1})	Measured peak position (cm^{-1})						
			Raw materials			Formulations			
			PF127	CH	Physical mixture	PF127 (14 %(w/v))		PF127 (14 %(w/v))/ CH (0.12 %(w/v))	
						DI water	PBS	DI water	PBS
C-H stretching	PF127	2880	2885	-	2885	2883	2888	2883	2888
C-O-C stretching	PF127	1100	1086	-	1110	1105	1109	1103	1109
O-H stretching	CH	3460	-	3440	3475	-	-	3477	3437
CONH stretching of amide I	CH	1657	-	1650	1650	-	-	1645	1641
N-H bending	CH	1530	-	1583	1567	-	-	-	-

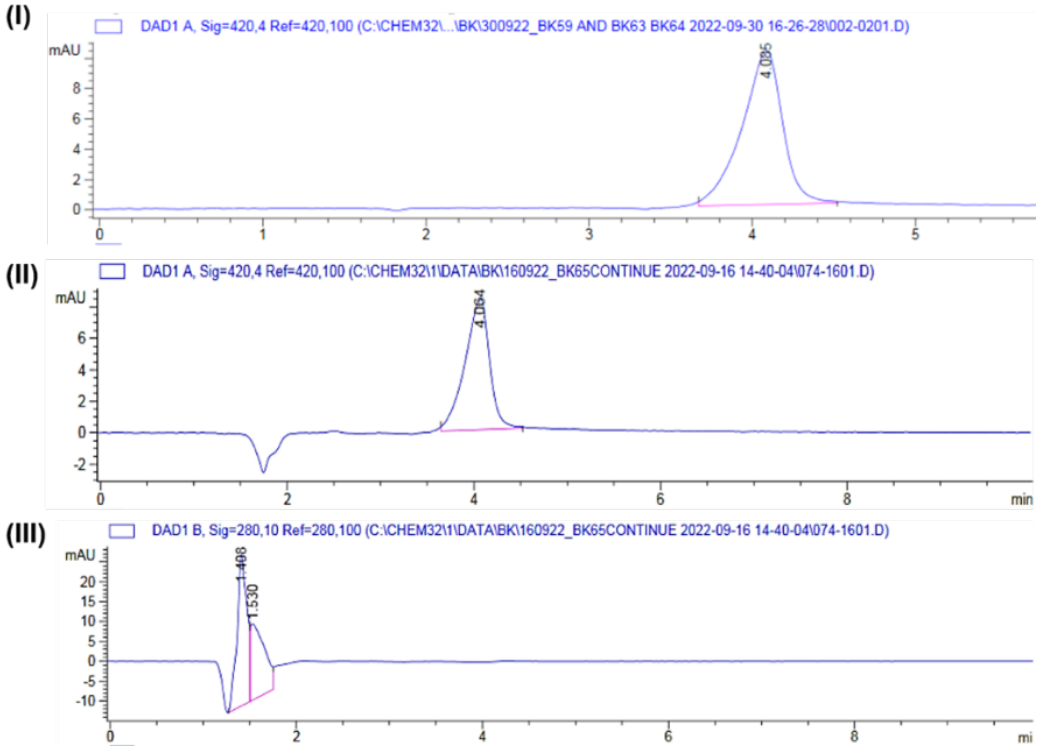

Figure S1: A schematic represents an example of the CUR peak observed by the HPLC chromatogram of (I) the CUR/MeOH standard compared to the CUR sample from thermal degradation detected at wavelengths (II) 420 nm and (III) 280 nm at 24 h.

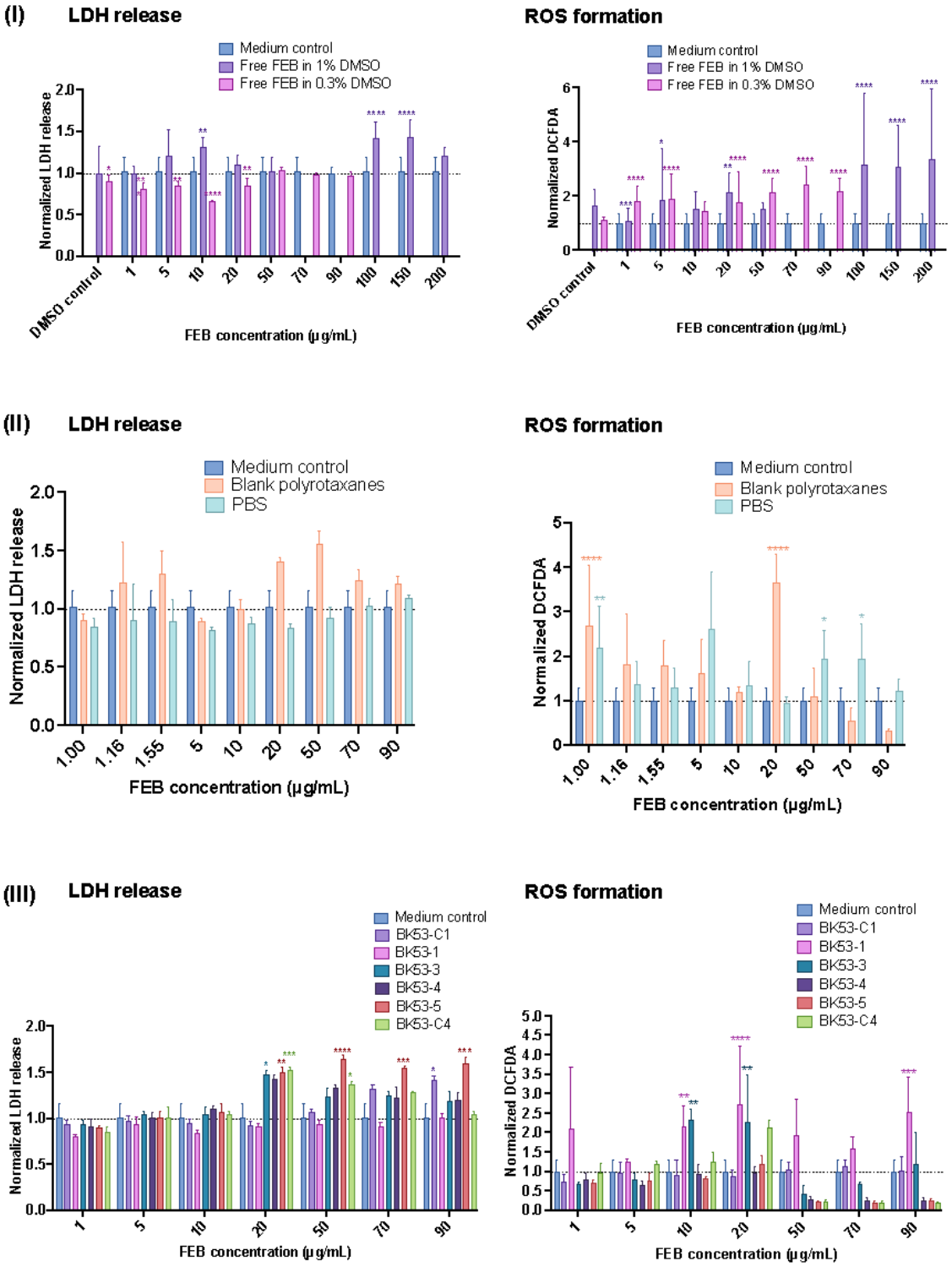

Figure S2: Assessment of LDH release (left) and ROS formation (right) treated with I) free FEB at 1% and 0.3% DMSO), (II) blank PPRs and PBS, and (III) FEB formulations from Table 4.1 at FEB

concentration of 1–90 µg/mL for 24 h. *p<0.05, **p<0.01, ***p<0.001 and ****p<0.0001 compared to the mean values of the medium control condition analyzed by the One-way ANOVA followed by Dunnett's multiple comparisons. Data are normalized to the medium control condition. Data are presented as mean ± SD of three experiments for (I) (n=3) and two experiments for (II) and (III) (n=3 and n=2, each experiment by the mean of its three technical replicates).